

# Mathematical model of the mucosal immune response to study inflammatory bowel diseases and their treatments

---

Sabine Stübler

Dissertation

zur Erlangung des akademischen Grades

“doctor rerum naturalium” (Dr. rer. nat.)

in der Wissenschaftsdisziplin “Systembiologie”

eingereicht an der

Mathematisch-Naturwissenschaftlichen Fakultät

Institut für Biochemie und Biologie

der Universität Potsdam



März 2023



Unless otherwise indicated, this work is licensed under a Creative Commons License Attribution 4.0 International.

This does not apply to quoted content and works based on other permissions.

To view a copy of this licence visit:

<https://creativecommons.org/licenses/by/4.0>

### **Sabine Stübler**

*Mathematical model of the mucosal immune response to study inflammatory bowel diseases and their treatments*

Dissertation zur Erlangung des akademischen Grades

*doctor rerum naturalium* (Dr. rer. nat.)

Reviewers: Prof. Dr. Wilhelm Huisinga, Prof. Dr. Oliver Pabst, Prof. Dr. Ursula Kummer

Supervisors: Prof. Dr. Wilhelm Huisinga, Prof. Dr. Charlotte Kloft

### **Universität Potsdam**

Mathematische Modellierung und Systembiologie

Institut für Biochemie und Biologie

Mathematisch-Naturwissenschaftliche Fakultät

Karl-Liebknecht-Str. 24/25

14476 Potsdam

Published online on the

Publication Server of the University of Potsdam:

<https://doi.org/10.25932/publishup-61230>

<https://nbn-resolving.org/urn:nbn:de:kobv:517-opus4-612301>



## Summary

Inflammatory bowel diseases (IBD), characterised by a chronic inflammation of the gut wall, develop as consequence of an overreacting immune response to commensal bacteria, caused by a combination of genetic and environmental conditions. Large inter-individual differences in the outcome of currently available therapies complicate the decision for the best option for an individual patient. Predicting the prospects of therapeutic success for an individual patient is currently only possible to a limited extent; for this, a better understanding of possible differences between responders and non-responders is needed.

In this thesis, we have developed a mathematical model describing the most important processes of the gut mucosal immune system on the cellular level. The model is based on literature data, which were on the one hand used (qualitatively) to choose which cell types and processes to incorporate and to derive the model structure, and on the other hand (quantitatively) to derive the parameter values. Using ordinary differential equations, it describes the concentration-time course of neutrophils, macrophages, dendritic cells, T cells and bacteria, each subdivided into different cell types and activation states, in the lamina propria and mesenteric lymph nodes. We evaluate the model by means of simulations of the healthy immune response to salmonella infection and mucosal injury.

A virtual population includes IBD patients, which we define through their initially asymptomatic, but after a trigger chronically inflamed gut wall. We demonstrate the model's usefulness in different analyses: (i) The comparison of virtual IBD patients with virtual healthy individuals shows that the disease is elicited by many small or fewer large changes, and allows to make hypotheses about dispositions relevant for development of the disease. (ii) We simulate the effects of different therapeutic targets and make predictions about the therapeutic outcome based on the pre-treatment state. (iii) From the analysis of differences between virtual responders and non-responders, we derive hypotheses about reasons for the inter-individual variability in treatment outcome. (iv) For the example of anti-TNF- $\alpha$  therapy, we analyse, which alternative therapies are most promising in case of therapeutic failure, and which therapies are most suited for combination therapies: For drugs also directly targeting the cytokine levels or inhibiting the recruitment of innate immune cells, we predict a low probability of success when used as alternative treatment, but a large gain when used in a combination treatment. For drugs with direct effects on T cells, via modulation of the sphingosine-1-phosphate receptor or inhibition of T cell proliferation, we predict a considerably larger probability of success when used as alternative treatment, but only a small additional gain when used in a combination therapy.



---

# Zusammenfassung

Chronisch-entzündliche Darmerkrankungen (CED), charakterisiert durch chronische Entzündung der Darmwand, entstehen durch eine Überreaktion der Immunantwort auf kommensale Bakterien, ausgelöst durch eine Kombination an genetischen und Umwelteinflüssen. Große inter-individuelle Unterschiede im Behandlungserfolg mit den verfügbaren Medikamenten erschweren die Wahl der für den jeweiligen Patienten besten Therapieoption. Eine Vorhersage der Erfolgsaussichten einer Behandlung für einen Patienten ist zum jetzigen Zeitpunkt nur sehr bedingt möglich; dafür wird ein besseres Verständnis möglicher Unterschiede zwischen sogenannten Respondern und Non-Respondern (Patienten, die gut bzw. schlecht auf ein Medikament ansprechen) benötigt.

In der Dissertation haben wir ein mathematisches Modell entwickelt, das die wichtigsten Prozesse des mukosalen Immunsystems des Darms auf zellulärer Ebene beschreibt. Das Modell basiert auf Literaturdaten, die einerseits (qualitativ) zur Auswahl der zu betrachtenden Zelltypen und Prozesse und zur Herleitung der Modellstruktur und andererseits (quantitativ) zur Herleitung der Parameterwerte verwendet wurden. Mithilfe gewöhnlicher Differentialgleichungen wird der Konzentrations-Zeit-Verlauf von Neutrophilen, Makrophagen, dendritischen Zellen, T-Zellen und Bakterien, jeweils unterteilt in unterschiedliche Zelltypen und Aktivierungszustände, in der Lamina propria und den mesenterischen Lymphknoten, beschrieben. Wir evaluieren das Modells anhand von Simulationen der gesunden Immunantwort auf Salmonelleninfektion und Verletzung der Darmbarriere.

Eine virtuelle Population beinhaltet CED-Patienten, die wir durch ein zunächst asymptomatisches, aber nach einem Auslöser chronisch entzündetes Darmgewebe definieren. Wir zeigen den Nutzen des Modells anhand verschiedener Analysen: (i) Der Vergleich von virtuellen CED-Patienten und virtuellen gesunden Individuen zeigt, dass die Krankheit durch viele kleine oder wenige große Veränderungen ausgelöst werden kann, und erlaubt, Hypothesen über krankheitsauslösende Veränderungen aufzustellen. (ii) Wir simulieren verschiedene Therapiemechanismen und treffen, basierend auf dem Zustand vor Behandlungsstart, Vorhersagen über den Therapieerfolg. (iii) Durch Analyse der Unterschiede zwischen virtuellen Respondern und Non-Respondern leiten wir Hypothesen über Ursachen für die inter-individuelle Variabilität im Therapieerfolg her. (iv) Am Beispiel von TNF- $\alpha$ -Antikörpern untersuchen wir, welche alternativen Therapien bei Therapieversagen am vielversprechendsten sind und welche Therapien sich besonders für Kombinationstherapien eignen: Für Medikamente, die auch direkt die Zytokinlevel beeinflussen oder die Rekrutierung von Zellen der natürlichen Immunantwort inhibieren, sagen wir eine geringe Erfolgswahrscheinlichkeit bei Nutzung als Alternativtherapie, aber einen großen Gewinn durch Nutzung in einer Kombinationstherapie vorher. Für Medikamente mit direkten Effekten auf T-Zellen, durch Modulation des Sphingosin-1-Phosphat-Rezeptors oder Inhibierung der T-Zellproliferation, sagen wir eine deutlich größere Erfolgswahrscheinlichkeit bei Nutzung als Alternativtherapie, aber nur einen geringen zusätzlichen Effekt bei Nutzung in einer Kombinationstherapie vorher.





# Acknowledgements

First of all, I would like to thank my supervisor, Prof. Wilhelm Huisinga for the great supervision and support, for always having time for intense discussions, and for his enthusiasm and perfectionism. I am also grateful to my co-supervisor Prof. Charlotte Kloft, for the good discussions, helpful tips and new ideas from the clinical perspective.

In addition, I want to acknowledge the great academic modules of the PharMetrX program: Thanks for putting together these dense and well-prepared lessons and teaching with so much enthusiasm!

Furthermore, I would like to thank my mentor Jens Borghardt, for regular discussions on the industry perspective of my work, and a very good preparation for the life after PhD in industry.

Different people contributed by giving feedback and discussing my work and ideas, including the Pharmacometrics group at AbbVie in Ludwigshafen, the Computational DMPK group at Boehringer Ingelheim in Biberach, Prof. Oliver Pabst from RWTH Aachen and his group (special thanks to Dr. Vuk Cerovic for extensive discussions about dendritic cell migration), and, most importantly, my colleagues from the Mathematical and Systems Biology group and the PharMetrX program.

An important part of my PhD journey was an internship at the Pharmacometrics group at AbbVie in Ludwigshafen. Thank you very much, Peter Nörtersheuser and Sathej Gopalakrishnan, for having me and making this internship such a great experience!

Last but not least, when I think about my PhD, it's not only about work—it's especially also the great times that I spent with my amazing colleagues in Potsdam and Berlin: Thanks a lot for all our coffee, lunch or ice-cream breaks, and the fun we had together at conferences.



# Contents

<b>1</b>	<b>Introduction</b>	<b>1</b>
1.1	Inflammatory bowel diseases . . . . .	1
1.2	Treatment of inflammatory bowel diseases . . . . .	2
1.3	Systems biology in disease modelling . . . . .	3
1.4	Aim of this work . . . . .	3
<b>2</b>	<b>Systems biology model of the mucosal immune system</b>	<b>5</b>
2.1	Previous modelling efforts . . . . .	8
2.2	Overview . . . . .	9
2.3	Volume correction factors for transfer between compartments . . . . .	12
2.4	Bacterial dynamics in intestinal lumen . . . . .	13
2.5	Epithelial barrier, mucus layer and tissue . . . . .	14
2.6	Elimination of bacteria from the tissue . . . . .	17
2.7	Neutrophils . . . . .	19
2.8	Macrophages . . . . .	24
2.9	Dendritic cells . . . . .	34
2.10	Antigen presentation to T cells . . . . .	39
2.11	T cell receptor (TCR) stimulation and T cell proliferation . . . . .	42
2.12	Effector T cell subsets . . . . .	48
2.13	Regulatory T cells . . . . .	52
2.14	Cytokine-mediated interactions . . . . .	56
2.15	Resolution of inflammation . . . . .	62
2.16	B cells and antibodies . . . . .	63
2.17	Healthy steady state . . . . .	64
2.18	Inflammation scenarios . . . . .	65
	2.18.1 Infection with generic extracellular pathogen . . . . .	65
	2.18.2 Infection with <i>Salmonella</i> Typhimurium ( <i>S. Typhimurium</i> ) . . . . .	68
	2.18.3 Immune response to mucosal injury . . . . .	74
2.19	Conclusion . . . . .	77
<b>3</b>	<b>Model evaluation</b>	<b>81</b>
3.1	Knockout scenarios . . . . .	81
	3.1.1 T cell knockout . . . . .	81
	3.1.2 T helper cell knockout . . . . .	82
	3.1.3 Regulatory T cell knockout . . . . .	82
	3.1.4 Commensal bacteria knockout . . . . .	83
	3.1.5 Neutrophil knockout . . . . .	83
3.2	Local sensitivity analysis . . . . .	84
3.3	Input-response indices . . . . .	86
3.4	Conclusion . . . . .	89

<b>4</b>	<b>Simulation and analysis of IBD using a virtual population</b>	<b>91</b>
4.1	Generation of a virtual population . . . . .	92
4.2	Evaluation of the model representation of IBD by comparison with literature	93
4.3	Comparison of parameters to detect inflammatory bowel disease (IBD) pre-dispositions . . . . .	96
4.4	Disease-relevant parameter changes for IBD . . . . .	98
4.5	Comparison of the pre-trigger steady state to detect early biomarkers for IBD . . . . .	101
4.6	Prediction of IBD based on selected parameters and pre-trigger state variables	102
4.7	Subclasses of IBD individuals based on required trigger extent . . . . .	106
4.8	Conclusion . . . . .	110
<b>5</b>	<b>Implementation and analysis of different treatment effects</b>	<b>113</b>
5.1	Virtual study simulation . . . . .	113
5.2	Implementation of treatment effects . . . . .	114
5.3	Monoclonal antibodies targeting cytokines/cytokine production . . . . .	115
5.4	Anti-cell adhesion molecules . . . . .	119
5.5	Sphingosine-1-phosphate receptor modulators . . . . .	121
5.6	Orally administered phosphatidylcholine . . . . .	121
5.7	Faecal microbial transplant . . . . .	122
5.8	T cell proliferation inhibitors . . . . .	122
5.9	Antibiotics . . . . .	122
5.10	Comparison of parameters between responders and non-responders . . . . .	123
5.11	Influence of disease-relevant parameter changes on response to treatment .	124
5.12	Comparison of the pre-treatment steady state between responders and non-responders . . . . .	126
5.13	Prediction of individual patients' responsiveness based on the pre-treatment steady state . . . . .	127
5.14	Correlation of treatment response with IBD type . . . . .	129
5.15	Prediction of (immediate) relapse post-treatment . . . . .	129
5.16	Conclusion . . . . .	131
<b>6</b>	<b>Model-guided choice of second-line treatments and combination therapies</b>	<b>135</b>
6.1	Correlations between responsiveness to different treatments . . . . .	135
6.2	Combination treatments . . . . .	137
<b>7</b>	<b>Discussion</b>	<b>141</b>
7.1	Summary . . . . .	141
7.2	Setting our work in context . . . . .	141
7.3	Limitations . . . . .	142
7.4	Main findings . . . . .	143
7.5	Further research questions . . . . .	144
7.6	Potential applications of the novel systems biology model . . . . .	145
<b>8</b>	<b>References</b>	<b>153</b>

---

<b>9</b>	<b>Appendix</b>	<b>169</b>
9.1	ODEs of the model . . . . .	169
9.2	Parameters of the model . . . . .	177
9.3	Full model scheme . . . . .	179
9.4	Knockout simulations . . . . .	181
9.5	Classification of the virtual population . . . . .	187
9.6	Derivation of disease-relevant parameter changes for IBD . . . . .	187
9.7	$h_{\text{pro,deact,M}}$ , the most frequent parameter among the disease-relevant parameter changes . . . . .	188
9.8	Classification and feature selection . . . . .	189
9.9	Subclasses of IBD individuals based on required trigger extent . . . . .	192
9.10	Virtual Crohn's disease endoscopic index of severity (CDEIS) analog . . . . .	193



---

# 1 Introduction

## 1.1 Inflammatory bowel diseases

Inflammatory bowel diseases (IBDs) are chronic diseases characterised by chronic inflammation of various parts of the gastrointestinal tract. They severely decrease the quality of life of affected patients, often resulting in life-threatening complications [1]. Approximately 0.3% of western populations are affected, with increasing prevalence [2].

*Pathogenesis.* The pathogenesis of IBD is not fully understood. The disease is characterised by an over-reaction of the mucosal immune system (especially T cell responses) to commensal bacteria in the gut, resulting in increased cellular recruitment, overexpression of pro-inflammatory cytokines and decreased levels of anti-inflammatory cytokines [3]. Many different genetic and environmental stimuli have been found as risk factors for the disease, where a lot of different combinations of those accumulated risk factors appear to be able to lead to the outbreak of disease. Genome-wide association studies have identified many different genetic loci and susceptibility genes, and revealed that especially defective intracellular bacterial killing and deregulated adaptive immune responses are linked to the development of IBD [3–5]. The exact trigger leading to the outbreak of the disease is not completely known. Many literature sources, however, discuss environmental factors that perturb the mucosal barrier, alter the balance of gut microbiota, as well as abnormally stimulate the immune system of the gut, as triggers for the onset of disease [4, 6, 7].

*Symptoms.* Common symptoms of IBD include rectal bleeding, diarrhoea, abdominal cramping pain, fatigue, weight loss and fever [8]. As the mucosal immune system is highly connected to the rest of the body, however, a wide variety of extraintestinal symptoms can occur, affecting e.g. the skin, muscles or joints [8, 9]. IBD is mainly diagnosed via endoscopy and histology [8]. The disease is characterised by a relapsing behaviour, i.e. phases of active disease (flares) alternating with phases of quiescent disease [10].

*Crohn's disease and Ulcerative colitis.* The two main subtypes of IBD are Crohn's disease (CD) and Ulcerative colitis (UC), which, despite a large overlap, differ in the location of the inflammation, in symptoms and in associated risk factors. In addition,  $\approx 5\text{--}10\%$  of IBD patients can not be classified into CD or UC; the disease is then called indeterminate colitis [8]. Characteristic for CD is an inflammation that is (i) transmural, i.e. affecting the full thickness of the gut wall and (ii) patchy and discontinuous, i.e. appearing anywhere in the gastrointestinal tract (but most often in terminal ileum and ascending colon), with inflamed areas alternating with normal areas [3, 8, 11]. In contrast, in UC patients the inflammation is restricted to the mucosa and the colon [8, 11].

In summary, IBD patients are a very heterogeneous patient population regarding both the course of the disease and the underlying genetic and environmental stimuli.

## 1.2 Treatment of inflammatory bowel diseases

At present, IBD can not be cured. The aims of treatment are to control the inflammation, reduce symptoms, achieve clinical remission or even mucosal healing [8]. Several different treatment options are in use, and many more are in clinical development.

Small molecule drugs used in the treatment of IBD include glucocorticoids, which are immunosuppressors that have inhibitory effects on many pro-inflammatory pathways. They result in complete remission in  $> 50\%$  of patients, but their use is limited to acute flares due to severe side effects [12]. In addition, different immunomodulators are in use: (i) 6-mercaptopurine and its prodrug azathioprine, inhibiting T cell proliferation and inducing T cell apoptosis [12], and (ii) methotrexate, whose mechanism of action is not clear (it possibly suppresses inflammatory functions of neutrophils, macrophages, dendritic cells and lymphocytes [13]). Especially in UC, 5-aminosalicylic acid is frequently used as first-line treatment; its mechanism of action is also unclear (it probably inhibits several pro-inflammatory processes in the mucosa) [10]. In addition, antibiotics are in use as adjuvant therapy [8].

More recently, additional small molecule drugs targeting specific pathways emerged, including (among others) JAK inhibitors inhibiting the JAK-STAT pathway important in production of multiple cytokines and S1PR modulators inhibiting the sphingosine-1-phosphate receptor type 1 (S1PR1) mediating T cells' migration from the lymph nodes into the tissue [14].

The first monoclonal antibody approved for the treatment of IBD targeted the pro-inflammatory cytokine tumour necrosis factor (TNF)- $\alpha$  and was viewed as important milestone [14]. TNF- $\alpha$  (both in soluble and receptor-bound form) is increased in IBD patients and acts as an important pro-inflammatory cytokine [14]. Since then, several other pathways and processes have successfully been targeted by monoclonal antibodies, including e.g. interleukin (IL)-23 (involved in T helper cell differentiation), IL-6 (having multiple pro-inflammatory effects) and integrins (important for adhesion of immune cells to endothelial cells and therefore required for migration into tissue) [14].

Other treatment concepts include orally administered phosphatidylcholine (directly targeting the destructed mucosal barrier) and faecal microbial transplant (FMT) (modifying the microbiota) [14]. Despite the variety of drug treatment options, in many cases only surgical intervention remains as a last option.

*Problems in treatment of inflammatory bowel diseases.* As described above, a wide variety of treatment options for IBD are available. However, the clinical response rates are highly variable, and typically do not exceed 70% (e.g. anti-TNF- $\alpha$  monoclonal antibodies: up to  $\approx 70\%$  [15], integrin inhibitor vedolizumab:  $\approx 50\%$  [16], S1PR1 modulator ozanimod: 41% [17], orally administered phosphatidylcholine:  $\approx 50\%$  in Phase II, although Phase III recently stopped [14, 18], FMT:  $\approx 50\%$  [14], where the reported response rates naturally also depend on the clinical trial and the score used to measure response). Consequently, a large fraction of patients, the so-called non-responders, do not respond to the treatment they receive, and have to change treatments frequently until a successful treatment option is eventually found. This causes large personal suffering and high costs.

Reasons for non-response can be due to both the pharmacokinetics and the pharmacodynamics of the drugs [19, 20]. Non-response caused by pharmacokinetics (i.e. the distribution of the drug in the body) means that the drug exposure is insufficient, which



can e.g. be due to an increased clearance of the drug due to high inflammation, or, in the case of monoclonal antibodies, due to the emergence of anti-drug antibodies [19, 20]. Non-response caused by pharmacodynamics (i.e. the effect of the drug on the body) means that either the drug is not able to suppress the target sufficiently, or that not the target of the drug is the driving factor for the disease, but another molecule or process that is not targeted [19, 20]. This can e.g. be seen for monoclonal antibodies targeting TNF- $\alpha$ , where the response is higher in patients with higher numbers of cells with membrane-bound TNF- $\alpha$  [21].

### 1.3 Systems biology in disease modelling

*Systems biology models.* A systems biology model is a computational model that summarises experimental knowledge about a biological system using a mathematical language. Models can be quantitative or qualitative, and can be developed at different levels, e.g. a cell, an organism, or virus-host interactions, where every model is developed for a specific purpose and typically only represents specific aspects of the respective biological system. Systems biology models can then be used to test hypotheses, make quantitative predictions or analyse properties of the respective systems. The main types of systems biology models are (i) network-based models, where model compounds (e.g. genes or molecules) are described by state variables representing their amount or activity, and which comprise ordinary differential equation (ODE)-based models (the most frequent type of systems biology models; also used in the work), stochastic reaction networks and boolean models; (ii) agent-based models, where states are updated based on sets of rules; and (iii) statistical models, which describe relations between measured data, e.g. linear regression. [22]

*Disease modelling and quantitative systems pharmacology.* For many diseases, systems biology models have been applied to describe (parts of) the complex biological interactions underlying the disease. Using such a computational disease model can give insights into the disease that are not feasible based on *in vivo* or *in vitro* experiments alone. The term “quantitative systems pharmacology” is often used when such a disease model includes treatment effects and is used in the development or optimisation of drug treatment. Computational disease models have successfully been applied in many different fields [23]. For IBD, a few disease models describing different aspects of the disease have previously been published (e.g. [24–28]), see Sections 2.1 and 7.2 for a detailed evaluation thereof.

### 1.4 Aim of this work

As described above, with regard to IBD and its treatment options, there is a strong need to better understand

- the disease etiology, i.e. which factors contribute how to the development and outbreak of the disease;
- the mechanisms of the different treatment options in clinical use and development;
- reasons for non-response to different treatments.

All these can be supported by *in silico* studies (not replacing, but in addition to *in vitro*, *in vivo* and clinical studies). Therefore, the aim of this thesis was to develop a mathematical model describing the mucosal immune response, including disruption of the healthy immune response resulting in IBD and the effects of different treatment options, and to use it to help analyse the unmet needs identified above.

---

## 2 Systems biology model of the mucosal immune system

The main part of this work, and the prerequisite for the following chapters, was the development of a systems biology model describing the healthy mucosal immune response on a cellular level. This chapter gives a description of the developed systems biology model, including the biological background of the processes included in the model, the mathematical equations constituting the model, and a detailed derivation and explanation of these equations.

*Aim of the model.* The aim of this work was to develop a mathematical model of the mucosal immune response as a tool for the analysis of IBD pathogenesis, for finding possible reasons for non-responsiveness to treatment, and as help in the development of new treatment targets and combination therapies. For this, the model must be able to describe the chronic inflammation of the mucosal immune system in IBD. Although there are differences between the two major forms of IBD, CD and UC (concerning genetic dispositions, cell and protein concentrations, spatial location of the inflammation, and symptoms), we did not differentiate between them, as those differences are mostly on a level beyond the complexity of the model we intended to develop. In addition, the model must be able to describe the response of a heterogeneous population of virtual IBD patients to various treatment options. In this virtual population of IBD patients, every virtual individual is defined by a set of parameters. By comparing resulting time courses and underlying parameter sets between healthy and diseased individuals and between responders and non-responders to treatment, we will generate hypotheses about pathogenicity and causes for the high inter-individual differences between IBD patients in response to treatment.

As basis for simulation of chronic inflammation and treatment, however, we need a model that as accurately as possible describes the healthy mucosal immune response. Only when the healthy mucosal immune response can convincingly be described by the model, the simulation of the pathological state, chronic inflammation as in IBD, can be credible.

For this, the model must fulfil several requirements: On the one hand, it must be able to describe the overall characteristics of a healthy immune response, which we test and show by simulating the immune response to intracellular and extracellular pathogens and mucosal injury. These characteristics include a significant increase of inflammatory cell types in response to the stimulus, the elimination of the inflowing pathogenic or commensal bacteria, and a timely return to the healthy steady state. On the other hand, for every of the included cell types and processes, qualitative and quantitative expectations on their dynamics on the cellular level, which are derived from the literature, must be fulfilled. This large set of cellular-level requirements includes e.g. steady state concentrations, quantitative relations between concentrations and concentration changes, the chronological order of effects, and qualitative characteristics of the dynamics.

*Approach.* The mucosal immune system is highly complex, and therefore every model will be a simplification. However, a model can still be useful, in that it can serve as a systematic integration of available knowledge, which can be used to generate hypotheses that can again be a starting point for further experimental studies. We focused on the cellular level, i.e. modelling the concentrations of different cell types over time, without explicitly simulating intracellular processes. Intracellular processes were only implicitly implemented: the concentration change of a specific cell as result of the sum of interactions with other cells. As it was, naturally, not possible to account for all processes of the mucosal immune system, we focused on those processes that we found, and judged, based on our literature research, to be most important for the simulations of infection and IBD. This means that processes or cell types that may be very important for the mucosal immune system, but which are either (more or less) constant during an infection or chronic inflammation, or do not have a significant impact on the course of infection or chronic inflammation, were not explicitly considered in the model, but were still implicitly part of the model's environment.

From the literature we obtained data from studies in human, mouse, rat or other organisms as well as from *in vitro* and *in silico* studies. These data can be of qualitative or quantitative nature, giving knowledge about processes of the mucosal immune system or providing directly or indirectly parameter values, respectively. We combined the knowledge gained from the literature into a mathematical model consisting of ordinary differential equations (ODEs). The structure of this model was based on the qualitative literature data, where we translated the knowledge about processes into mathematical equations that mechanistically mimic the physiological behaviour. The parameterisation of the model was then mainly based on quantitative literature data, but also taking into account qualitative observations. The model describes different cell types, each of which can switch between different states and/or spatial locations. During the modelling process, we first implemented the different cell types or processes separately, as submodels, making sure the submodels described the respective physiological processes appropriately, and then combined them into the full model. We considered two general types of interactions between different cell types: cell-cell contacts, e.g. T cell receptor stimulation by antigen-presenting cells, and interactions via cytokines (pro-inflammatory, anti-inflammatory, pro-resolving). As the data are from several different studies in different organisms and settings, the results of the model simulations are naturally intended more qualitative than quantitative. During the modelling process, we analysed, which processes, cell types and interactions had to be included into the model, in order to reproduce our expectations, which were also generated from literature.

To ensure and demonstrate the functional capability of our virtual mucosal immune system, we simulated infection with extra- and intracellular bacteria and the response to mucosal injury. We used the (qualitative) knowledge about the expected time course of a healthy immune response to these triggers to implement and parameterise the model. Therefore, these simulations (described in detail in Section 2.18) are no external validation.

*Very short overview of the mucosal immune response in the gut.* The main function of the immune system is to protect the host from potentially harmful pathogens (e.g. bacteria or viruses). In the case of bacterial infection of the gut tissue, the focus of our systems biology model, the intact epithelial barrier and the mucus layer secreted by it largely prevent bacterial invasion into the tissue. Only in the case of epithelial destruction

or infection with pathogenic bacteria can a significant amount of bacterial cells overcome this barrier. Then bacteria reach the uppermost layer of the gut wall, the lamina propria, where a large variety of immune cells are ready to fight inflowing bacteria: Innate immune cells, such as neutrophils, macrophages and dendritic cells engulf and kill bacterial cells. In addition, dendritic cells migrate to the draining lymph nodes in the mesenterium and present bacterial antigen to T cells, which are part of the adaptive immune response, and, once activated by stimulation with their cognate antigen, proliferate and differentiate into effector T cells, migrate back to the lamina propria and further recruit and activate innate immune cells to help them fight the pathogens. [29]

The mucosal immune response in the gut differs from the immune response in other tissues: In most tissues, every bacterial stimulus will elicit an immune response, with the aim to eliminate the source. In the gut, the constant encounter of bacterial antigen originating from the commensal bacteria must not result in a state of active inflammation, as inflammation also destroys the tissue. However, the immune system must still be able to eliminate pathogenic bacteria via an effective immune response. The solution is that there is a constant low level of inflammation that keeps the commensal bacteria at bay without destroying the host tissue. In the case of an infection with pathogenic bacteria resulting in much higher levels of bacterial antigen in the tissue, a full immune response is elicited. [29]

*Cell-level modelling using ordinary differential equations and mass action kinetics.* Our mathematical model of the mucosal immune system consists of ordinary differential equations (ODEs), implying mass action kinetics. The law of mass action states that the rate of a reaction is proportional to the product of the concentrations of the reactants [22]. This law was derived for chemical reactions, i.e. on a molecular level. It has, however, already in many cases successfully been applied also on a higher level such as the cellular level we chose for our systems biology model, for example in the fields of HIV modelling [30, 31] or epidemiology [32]. Here, we treat cells as the basic entities of the model (model species/ state variables), reactions (e.g. inflow, outflow or transition between state variables) change the concentrations of the cells, with reaction rates proportional to the reaction educt cell concentrations.

The model is given by a system of ODEs

$$\frac{d}{dt}\mathbf{x}(t) = f(\mathbf{x}(t)),$$

where  $\mathbf{x}(t) = (x_1(t), \dots, x_N(t))$  is the vector of  $N$  state variables of the model. The ODEs are obtained by multiplication of the stoichiometric matrix with the vector of reaction rates. The stoichiometric matrix  $\nu \in \mathbb{R}^{N \times M}$  contains the change in numbers of molecules per reaction for each state variable  $n$  ( $n = 1, \dots, N$ ) and each reaction  $m$  ( $m = 1, \dots, M$ ). The vector of reaction rates  $\mathbf{a}(\mathbf{x}(t)) = (a_1(\mathbf{x}(t)), \dots, a_M(\mathbf{x}(t)))$  describes the reaction rate of each of the  $M$  reactions depending on a given state  $\mathbf{x}(t)$ . Then the model state  $\mathbf{x}(t)$  at time point  $t$  is defined by the ODE system and the vector of initial state values  $\mathbf{x}_0(t)$ . As complex ODE systems such as our systems biology model cannot be solved analytically, the solution needs to be approximated numerically.

The quasi-steady state (QSS) approximation is a useful approach of model order reduction, i.e. to reduce the number of required state variables. It can be applied if the response times of the state variables are on different time scales; then the “fast state

variables” can be assumed to be in QSS, i.e. to follow the “slow state variables”, and can directly be calculated from their concentrations [22]. An important example for the application of the QSS approximation is the Michaelis-Menten equation, which describes the approximation of the rate  $V$  of an enzyme-catalysed reaction as

$$V = \frac{V_{\max} \cdot S}{K_m + S},$$

where  $S$  is the substrate concentration,  $V_{\max}$  is the maximal reaction rate and the Michaelis-Menten constant  $K_m$  is the substrate concentration for which the reaction rate is half-maximal [22]. Through that, state variables for enzyme and enzyme-substrate complexes are not needed. The reaction rate is limited by the (constant) total concentration of enzyme. When cooperativity between different binding sites of the enzyme plays a role, the Hill equation can be used instead:

$$V = \frac{V_{\max} \cdot S^h}{K_m^h + S^h},$$

where  $h$  is the Hill coefficient, describing positive ( $h > 1$ ) or negative ( $0 < h < 1$ ) cooperativity [22, 33]. We used these concepts from enzyme kinetics for cytokine-mediated reactions, where the reaction rate is limited by the cell’s maximal velocity to change its state or location.

## 2.1 Previous modelling efforts

There have been several publications of mathematical models of IBD over the last few years, with different aims.

In 2010, Wendelsdorf et al. [24] presented a “model of colonic inflammation”, a system of 29 ODEs, describing different cell types of the mucosal immune system in three different compartments (intestinal lumen, lamina propria and mesenteric lymph nodes): (naive, central memory, effector memory, helper and induced and natural regulatory) T cells, (immature, stimulatory and tolerogenic) dendritic cells, macrophages (type M0, M1 and M2), epithelial cells, bacteria and (activating and deactivating) cytokines. Using their model they simulated bacterial infection and IBD. For the infection scenario they considered commensal and foreign bacteria, where commensal bacteria activated the (anti-inflammatory) tolerogenic dendritic cells and M2 macrophages, and foreign bacteria activated the (pro-inflammatory) stimulatory dendritic cells and M1 macrophages. For the IBD scenario they assumed a constant fraction of commensal bacteria to activate the (pro-inflammatory) stimulatory dendritic cells and M1 macrophages, leading to a new steady state. In the analysis of this model we observed several physiological inconsistencies, of which the most obvious one was the missing volume correction coefficients for cellular migration between the different tissues, leading to a predicted drop of the luminal bacterial concentration by about one third in infection and by more than 90% in IBD, and the most serious one was the assumption that there were no pro-inflammatory cells such as M1 macrophages or T helper cells in the healthy tissue (in strong contrast to the continuous low-level inflammation in the gut tissue described in literature [29]).

The partial differential equation model by Lo et al. (2013) [25] focused on T helper cells type 1 and 2 and regulatory T cells, and their development and interactions via

transcription factors and cytokines. Other cells were not explicitly included in the model, antigen-presenting cells such as dendritic cells and macrophages were only accounted for by their secretion of cytokines.

Dwivedi et al. (2014) [26] developed a mathematical model with the aim to study therapeutics targeting IL-6 or its receptor. Therefore, their model focused on IL-6, IL-6 receptor and the corresponding intracellular signalling pathway. Two different organs (gut and liver) were included in the model, but both consisted only of one cell type. For drug treatment, a PK model for monoclonal antibodies targeting IL-6 or its receptor was included.

Balbas-Martinez et al. (2018) [27] provided a Boolean network model consisting of 43 nodes (accounting for cells, signalling molecules and receptors) and almost 300 qualitative interactions between them, implemented as boolean functions. Those boolean functions define for each of the states whether it is active or inactive, dependent on other states. The authors validated their model by comparison of upregulated nodes in simulation of IBD with upregulated cells or signalling molecules in clinical studies of IBD, and by comparing the results of simulated clinical trials with reported clinical trials.

In conclusion, the models by Wendelsdorf et al. [24] and Balbas-Martinez et al. [27] are the most detailed regarding different cell types and processes, whereas we assess the models by Lo et al. [25] and Dwivedi et al. [26] to be too specialised for our purpose. Due to the physiological inconsistencies in the ODE model by Wendelsdorf et al. [24] and the non-quantitative behaviour of the boolean network model by Balbas-Martinez et al. [27], however, we decided that the development of a novel, ODE-based systems biology model of the mucosal immune system was required with regard to our research aims. We considered the model by Wendelsdorf et al. [24] a good starting point regarding the physiological compartments to consider and the relevant cell types and processes. For our research aims, however, we at the same time aimed for a more physiological representation of the mucosal immune response in health and disease.

After research for this thesis was completed (February 2020), Rogers et al. (2020) [28, 34] published a systems pharmacology model of IBD that also aimed at analysing treatment effects using a virtual IBD population, but with differences both in the underlying model structure describing the mucosal immune response and the generation of the virtual population of healthy and diseased individuals. A more detailed comparison of the two models, including the resulting conclusions drawn with respect to different treatments, will be given in the Discussion (Section 7.2).

## 2.2 Overview

The gastrointestinal tract is composed of mouth, pharynx, oesophagus, stomach, small intestine (duodenum, jejunum, ileum) and large intestine (caecum, colon, rectum, anal canal) [35]. All of those parts can be inflamed in Crohn's disease, whereas ulcerative colitis is restricted to the colon [11]. Therefore, we focused on the colon (more specifically sigmoidal colon, if data were available and different for different parts of the colon) and the developed systems biology model is intended to describe the time course of cell concentrations in the colon. The general principles and processes are similar, but the concentrations of the immune cells vary between the different parts of the intestine. The gut-associated lymphoid tissue (GALT) (comprising Peyer's patches and isolated lymphoid follicles) was not explicitly included in our model (see Section 2.16).

As proposed by Wendelsdorf et al. [24], we considered three different spatial compartments where the relevant processes of the mucosal immune system take place:

- i) the intestinal lumen, where commensal (and pathogenic) bacteria reside in healthy individuals;
- ii) the lamina propria (LP), which is the uppermost layer of the gut wall, separated from the intestinal lumen by a single layer of epithelial cells. Here bacteria breaching the epithelial barrier encounter cells of the innate and adaptive immune system; and
- iii) the mesenteric lymph node (LN), where the adaptive immune system is activated.

The model describes the time course of 55 state variables (healthy, no infection with pathogenic bacteria) using ODEs that describe the rate of change of each state variable over time. The majority of state variables represent concentrations of different cell types in LN and LP. State variables describing the barrier function and bacteria in the intestinal lumen were implemented as unitless values describing their fractional functional capabilities.

In this chapter, we describe the healthy mucosal immune system of one individual, which we call the reference individual. Variability in the parameter values then defined a virtual population of different individuals, as described in Chapter 4.

Figure 1 gives an overview of the processes we considered in the model. It shows a simplified model scheme, showing the different cell types, their spatial location and their interactions. It also shows the sections that describe the different submodels (cell types or processes), where more detailed model schemes and the detailed derivation and explanation of the ODEs describing the submodels, together with a short introduction into the physiological background to the respective cell types and processes, are given.

*Infection.* The intent of the developed model is to describe the healthy mucosal immune system in response to mucosal injury and infection with pathogenic bacteria, as basis for subsequent simulations of chronic inflammation by variations in the parameter values (as described in Chapter 4). Therefore, we show the characteristics of the different submodels (cell types and processes) that are described in the next sections (Section 2.4 - 2.15) via the time course of the cell types in the two scenarios of infection with *S. Typhimurium* and mucosal injury. A more detailed description of these two, and another scenario of infection with an extracellular pathogen, are given in Section 2.18. In short, *S. Typhimurium* is an extracellular bacterium that is able to invade the gut tissue. Its pathogenicity lies mainly in its ability to cross the epithelial barrier and to evade destruction by macrophages and instead being able to proliferate intracellularly [29]. Macrophages need help from T helper cells to efficiently eliminate the intracellular salmonellae [36]. By mucosal injury we denote a scenario where external stimuli such as physical injury, chemicals or drugs lead to a partial destruction of the epithelial barrier and tissue, allowing for an inflow of commensal bacteria into the tissue that elicits an immune response. The figures show the steady state concentrations before and the time course after a stimulus (*S. Typhimurium* in the gut lumen or partial destruction of epithelium and tissue for salmonella infection or mucosal injury, respectively) at time point  $t = 0$ , until the system goes back to steady state.

The model can be adjusted to include different bacterial species. In case of more than one bacterial species (e.g. commensal and pathogenic bacteria), several cell types



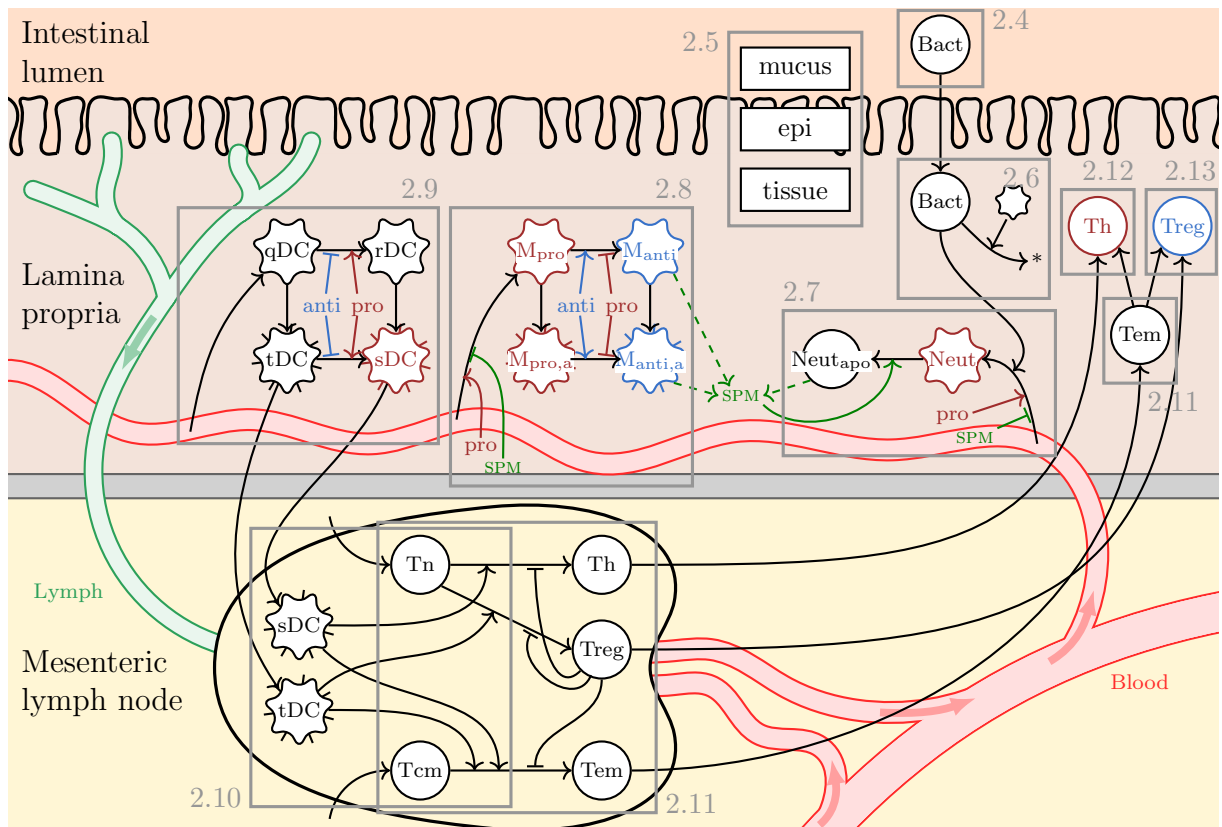




Figure 1: **Simplified model scheme.** Overview of the cell types that we included into the model, and their interactions. White circles/shapes represent cell types (model species). Arrows between model species represent transition or migration. Arrows targeting on arrows indicate a stimulating ( $\longrightarrow$ ) or inhibiting ( $\longrightarrow$ ) influence on this reaction. Pro- and anti-inflammatory cytokines are produced by the respective colour-coded cell types. Dashed arrows show production of cytokines by a model species. For detailed description of the implementation of the different processes/cell types in grey boxes see text in the sections indicated by grey numbers.

Legend:

pro	pro-inflammatory cytokines
anti	anti-inflammatory cytokines
SPM	specialised pro-resolving mediators
Bact	bacteria
qDC, rDC, tDC, sDC	quiescent, responsive, tolerogenic, stimulatory dendritic cells
$M_{pro}$ , $M_{anti}$	pro-/anti-inflammatory macrophages
$M_{pro,a}$ , $M_{anti,a}$	antigen-experienced pro-/anti-inflammatory macrophages
Neut, $Neut_{apo}$	neutrophils, apoptotic neutrophils
Tn	naive CD4+ T cells
Tcm, Tem	central/effector memory T cells
Th	T helper cells
Treg	regulatory T cells
	phagocytic cell
	antigen-presenting cell

are modelled specific to the different bacteria. These cell types (in the following called “bacteria-specific species”) include the bacteria themselves, antigen-presenting innate immune cells, which are modelled to present antigen of either type of bacteria, and adaptive immune cells with receptors specific for either type of bacteria. For a given number  $N_{\text{Bact}}$  of different bacterial species, those cell types are modelled as  $N_{\text{Bact}}$  different state variables in the model, each specific for one type of bacteria. In the following, we summarise all commensal bacteria as one bacterial species.

A complete mathematical description of the model can be found in the Appendix: Section 9.1 for the full system of ODEs, Section 9.3/Figure 49 for the complete model scheme and Section 9.2/Table 10 for the parameter values.

The model was implemented in Matlab 2018b. ODEs were solved using the ode15s solver. Figures of simulations were made using Matlab and the matlab2tikz toolbox [37] (with small modifications). All other figures were made using TikZ.

Matlab code of the model implementation and all simulations shown in this thesis can be found online: <https://zenodo.org/record/7614716#.Y-IZfOLMKwo>.

### 2.3 Volume correction factors for transfer between compartments

The developed systems biology model describes the time course of cellular concentrations in different tissues, including migration of cells between different spatial compartments (mesenteric LN and LP). In a migration reaction from one compartment to another, the number of cells leaving the first compartment equals the number of cells arriving in the target tissue, however, the concentration decrease in the leaving compartment does not equal the concentration increase in the target compartment, because of the different volumes of the compartments. To get the change of concentration in the target compartment corresponding to this reaction, the reaction rate needs to be multiplied by a volume correction coefficient (volume of the leaving tissue divided by volume of the target tissue).

The total volume of mesenteric LNs in an adult was reported to be approximately 11 mL [38]. Naive and memory T cells circulate through LNs, where they may encounter dendritic cells presenting their cognate antigen. This takes place in a specific area of the LN, the T cell zone (paracortex) [29], which we assume to be approximately one half of the total LN volume. Thus, the total volume of mesenteric LN T cell zones is  $V_{\text{LN}} = 5.5$  mL. This volume corresponds to the total amount of mesenteric LNs draining the small and large intestine; we did not have information on the fraction of mesenteric LNs draining the different parts of the intestine. Therefore we assumed the ratio of LP volume and draining LN volume to be constant throughout the intestine, i.e. volume correction coefficients independent of the part of the intestine. Thus, to calculate the volume correction coefficients, we needed the total volume of LP of small and large intestine. Helander et al. (2014) [39] calculated the surface area of the small and large intestine using the length and diameter of the intestine and the relative surface amplification due to plicae, villi and microvilli. In contrast to Helander et al., we were not interested in the surface area of the epithelium, but in the tissue area as basis for the volume calculation (compare the black line of the epithelium representing the surface and the grey bar of lower LP boundary representing the width of the shown tissue in Figure 1). Therefore we repeated

the calculation without accounting for surface amplification due to villi or microvilli, i.e.  $\text{area} = \text{length} \cdot \text{diameter} \cdot \pi \cdot \text{amplification by plicae}$ , resulting in a total area of  $6453 \text{ cm}^2$  for small and large intestine. Dhesi et al. (1984) [40] reported the height of the LP to be  $1.35 \cdot 10^{-2} \text{ cm}$ , resulting in the LP volume  $V_{\text{LP}} = 87 \text{ mL}$ . The resulting volume correction coefficients were  $\frac{V_{\text{LP}}}{V_{\text{LN}}}$  for migration from LP to LN and  $\frac{V_{\text{LN}}}{V_{\text{LP}}}$  for migration from LN to LP.

We did not model the model species in the intestinal lumen (commensal and pathogenic bacteria) in concentrations, as the luminal contents (faeces) are not fluid and the concentration of bacteria is not uniform. Instead, we modelled those species as unitless values describing their fractional functional capabilities (see Section 2.4). Therefore we did not have to take the volume of the intestinal lumen into account.

For cell types that are present in more than one spatial compartment, we include the location as subscript in the state variables' names. For cell types that are only present in one spatial compartment, we did not include the location in the names, to keep the names short.

## 2.4 Bacterial dynamics in intestinal lumen

The intestinal lumen hosts a large variety of bacteria, which live in symbiosis with the human body, called commensal bacteria. These commensal bacteria provide nutrients, prevent pathogens from colonisation by competition for nutrients, and stimulate the mucosal immune system and epithelial barrier, preparing it for pathogenic infection [29]. Commensal bacteria reside in the intestinal lumen and the upper layer of the mucus layer [41], but can not breach the intact epithelial barrier to get into the tissue in a significant amount in healthy conditions. Bacteria that can breach the epithelial barrier, damage host tissue und thereby cause disease, are called pathogenic bacteria.

We considered the following differences between commensal and pathogenic bacteria:

- (i) Survival in lumen is impaired in pathogenic compared to commensal bacteria, because commensal bacteria are better adapted to this niche and outcompete the pathogenic bacteria in the competition for space and nutrients [29].
- (ii) In contrast to commensal bacteria, pathogenic bacteria are able to penetrate the epithelium and thereby invade the gut LP, through the use of specific toxins, e.g. enterotoxins [42].
- (iii) Extracellular pathogenic bacteria are better able to evade phagocytosis by innate immune cells in the LP than commensal bacteria [42] (see Section 2.6).
- (iv) Intracellular pathogenic bacteria are able to survive inside specific innate immune cells after phagocytosis by evading intracellular elimination [29] (see Section 2.18.2).

In the model we differentiated between commensal bacteria (a combination of many different bacterial strains) and pathogenic bacteria (one exemplary pathogenic strain). Bacteria in the lumen ( $\text{Bact}_{\text{Lu},b}$ , subscript  $b$  indicates the bacterial species) were modelled as fraction of the steady-state concentration of commensal bacteria. In addition, to account for the competition between commensal and pathogenic bacteria, nutrients were modelled as fraction of their steady-state concentration, with a constant inflow  $\lambda_{\text{nutrients}}$  and a consumption by proliferating bacteria with rate constant  $p_{\text{Bact,Lu}}$ .

$$\frac{d}{dt} \text{nutrients} = \lambda_{\text{nutrients}} - \sum_b p_{\text{Bact,Lu},b} \cdot \text{Bact}_{\text{Lu},b} \cdot \text{nutrients}$$

Bacteria proliferate dependent on the available nutrients with rate constant  $p_{\text{Bact,Lu}}$  and die with rate constant  $\mu_{\text{Bact,Lu}}$ .

$$\frac{d}{dt}\text{Bact}_{\text{Lu},b} = p_{\text{Bact,Lu},b} \cdot \text{Bact}_{\text{Lu},b} \cdot \text{nutrients} - \mu_{\text{Bact,Lu}} \cdot \text{Bact}_{\text{Lu},b}$$

for each bacterial species  $b$ . Throughout this thesis, we considered three different types of bacterial species: commensal bacteria, a generic extracellular pathogen, and salmonellae, i.e.  $b = \{\text{commensal}, \text{extracellular}, \text{salmonellae}\}$ . The structure of the ODEs for  $\text{Bact}_{\text{Lu},b}$  is the same for each bacterial species  $b$  in lumen, but the (bacteria-specific) proliferation rate constant  $p_{\text{Bact,Lu},b}$  is higher for commensal than pathogenic bacteria. From our definition of  $\text{Bact}_{\text{Lu},\text{commensal}}$  and nutrients, modelling the relative change from their unknown baseline, follows that both are 1 in steady state (without pathogen). From this follows that  $\lambda_{\text{nutrients}} = p_{\text{Bact,Lu},\text{commensal}} = \mu_{\text{Bact,Lu}}$ , which was set to  $\frac{1}{24} \frac{1}{\text{h}}$ , assuming a mean life time of 1 d for the bacteria (including death and removal from the intestine by excretion). For pathogenic bacteria, the proliferation rate constant was decreased by 0.8 to account for the slightly decreased adaptation to the environment compared to commensal bacteria,  $p_{\text{Bact,Lu},\text{extracellular}} = p_{\text{Bact,Lu},\text{salmonellae}} = 0.8 \cdot p_{\text{Bact,Lu},\text{commensal}}$ . This led to extinction of pathogenic bacteria from the gut lumen after approximately one week, if no further inflow of pathogenic bacteria was considered.

## 2.5 Epithelial barrier, mucus layer and tissue

The intestinal epithelium, a single layer of epithelial cells, separates the lumen from the uppermost layer of the gut wall, the lamina propria (LP) [43]. Its function is to allow for the transport of nutrients from the intestinal content to the blood circulation while preventing inflow of potentially harmful luminal contents such as bacteria. Absorption of nutrients is carried out by enterocytes, the main cell type of the intestinal epithelium [44]. Other cells are mainly secretory, such as goblet cells and Paneth cells, which produce mucins and a variety of antimicrobial peptides (AMPs) released into the lumen [44]. In addition, secretory immunoglobulin A (SIgA) is transported from the LP into the lumen by intestinal epithelial cells via transcytosis [45]. The mucins, mainly MUC2, form the gel-like mucus containing AMPs and SIgA. SIgA binding to antigens on bacterial cells prevents them from reaching the epithelium by trapping them in the mucus via their secretory component binding to mucins, by steric prevention from binding to receptors and by direct neutralisation of toxins [46]. AMPs directly attack conserved bacterial features such as membranes and cell walls [44]. In the colon, the mucus consists of a sterile dense inner layer and a loose outer layer, where bacteria reside [47], and provides defence against commensal and pathogenic bacteria to prevent them from contact with the epithelial barrier. Intestinal epithelial cells are connected by tight junctions and thereby also form a physical barrier [43]. The underlying tissue, the LP, is composed of intestinal stromal cells (mainly myofibroblasts and fibroblasts), stromal stem cells, cells of the innate and adaptive immune system, and small blood and lymph vessels [48]. The non-cellular content of the tissue is called the extracellular matrix (ECM). It ensures mechanic stability of the tissue and acts as a reservoir of signalling molecules [49]. Both epithelium and tissue can be damaged by pro-inflammatory cytokines. When pathogenic bacteria cross the epithelium, they do so using specific toxins that make the

epithelium penetrable, allowing the pathogens access into the tissue [50]. Consequently, the epithelium gets impaired during this process. Tissue remodelling is the complex physiological response ensuring tissue repair and wound healing, which depends on the interplay of proteases (e.g. matrix metalloproteinases (MMPs)) and their inhibitors [51]. Gut-resident anti-inflammatory macrophages and T helper cells type 2 play an important role in tissue remodelling [52, 53]. Insufficient tissue repair results in the formation of ulcers, whereas excessive tissue repair results in fibrosis; both are frequent problems in IBD [54].

We modelled tissue, mucus and epithelial layer as unitless state variables representing their relative functional capability. For the mucus and epithelial barriers, the values (between 0 and 1) represent their capability to prevent bacteria from getting through, where 0 means the barrier is completely permeable and 1 means the barrier is impermeable. For tissue, the value represents the intactness of the tissue, and its ability to enable the build-up of epithelium. The tissue value can be larger than 1, representing fibrosis.

*Tissue.* The state variable tissue represents the ECM and stromal cells, and models their relative intactness. We implemented a zero-order synthesis and first-order degradation rate with rate constants  $\lambda_{\text{tis}}$  and  $\mu_{\text{tis}}$ , respectively. As, by definition, tissue = 1 in steady state,  $\lambda_{\text{tis}} = \mu_{\text{tis}}$ . A rough estimate of the half-life of tissue components is 6 d [38], resulting in  $\mu_{\text{tis}} = \frac{\ln(2)}{6 \text{ d}} = 0.0048 \frac{1}{\text{h}}$ . We accounted for destructing influence by pro-inflammatory cytokines  $\text{cyto}_{\text{destr,tis}}$  and tissue remodelling effects by cytokines from anti-inflammatory macrophages and T helper cells type 2  $\text{cyto}_{\text{remod,tis}}$  (details on the derivation of cytokine concentrations in Section 2.14). Tissue destruction by cytokines was implemented by multiplying the degradation rate with  $(1 + \frac{F_{\text{max,tis}} \cdot \text{cyto}_{\text{destr,tis}}}{1 + \text{cyto}_{\text{destr,tis}}})$ , where  $\text{cyto}_{\text{destr,tis}}$  is a unitless description of the cytokine concentration, resulting in half-maximal effect for  $\text{cyto}_{\text{destr,tis}} = 1$  (see Section 2.14), describing a saturable increase of the degradation rate of maximally  $(F_{\text{max,tis}} + 1)$ -fold. This factor was set to  $F_{\text{max,tis}} = 1$ , to limit the degradation rate to two times the steady state degradation rate. Tissue remodelling effects of cytokines were implemented accordingly, by multiplying the synthesis rate with  $(1 + \frac{F_{\text{max,tis}} \cdot \text{cyto}_{\text{remod,tis}}}{1 + \text{cyto}_{\text{remod,tis}}})$ . The resulting ODE for tissue is

$$\frac{d}{dt} \text{tissue} = \lambda_{\text{tis}} \cdot \left( 1 + \frac{F_{\text{max,tis}} \cdot \text{cyto}_{\text{remod,tis}}}{1 + \text{cyto}_{\text{remod,tis}}} \right) - \mu_{\text{tis}} \cdot \text{tissue} \cdot \left( 1 + \frac{F_{\text{max,tis}} \cdot \text{cyto}_{\text{destr,tis}}}{1 + \text{cyto}_{\text{destr,tis}}} \right).$$

*Epithelial barrier.* The state variable epi represents the gut epithelium, and models its functional capability. Synthesis of epi depends on the intactness of the tissue: for fully intact tissue (tissue = 1) synthesis is zero order with rate constant  $\lambda_{\text{epi}}$ ; for (partially) destroyed tissue, the synthesis rate is accordingly lower. In case of fibrosis (tissue > 1) we assumed the same synthesis rate as for fully intact tissue. The first-order degradation rate is  $\mu_{\text{epi}} = 0.0096 \frac{1}{\text{h}}$ , corresponding to a half-life of epithelium of 3 d [38]. As, by definition, epi = 1 and tissue = 1 in steady state,  $\lambda_{\text{epi}} = \mu_{\text{epi}}$ . Destruction of epithelium by pro-inflammatory cytokines  $\text{cyto}_{\text{destr,epi}}$  was implemented similarly to destruction of tissue, i.e. by multiplication of the degradation rate with  $(1 + \frac{F_{\text{max,epi}} \cdot \text{cyto}_{\text{destr,epi}}}{1 + \text{cyto}_{\text{destr,epi}}})$ , with  $F_{\text{max,epi}} = 1$ . Destruction of epithelium by inflowing pathogenic bacteria using toxins was implemented dependent on the rate of bacterial inflow with toxin (as described in paragraph *Bacterial*

*inflow*), multiplied by a factor set to  $\mu_{\text{epi,Bact}} = 1 \cdot 10^{-10} \text{mL}$ . The resulting ODE for epi is

$$\begin{aligned} \frac{d}{dt} \text{epi} = & \lambda_{\text{epi}} \cdot \min(\text{tissue}, 1) - \mu_{\text{epi}} \cdot \text{epi} \cdot \left( 1 + \frac{F_{\text{max,epi}} \cdot \text{cyto}_{\text{destr,epi}}}{1 + \text{cyto}_{\text{destr,epi}}} \right) \\ & - \mu_{\text{epi,Bact}} \cdot \sum_b \epsilon_{\text{Bact},2,b} \cdot (1 - \text{mucus}) \cdot \text{epi} \cdot \text{Bact}_{\text{Lu}}, \end{aligned}$$

where  $\sum_b \epsilon_{\text{Bact},2,b} \cdot (1 - \text{mucus}) \cdot \text{epi} \cdot \text{Bact}_{\text{Lu}}$  is the inflow rate of bacteria using toxins, described in paragraph *Bacterial inflow*.

*Mucus layer.* The state variable mucus represents the mucus layer, including antimicrobial peptides (AMPs) and secretory immunoglobulin A (SIgA). As described in Section 2.16, because of the high cross-reactivity between antibodies specific to commensal and pathogenic antigens, we assume antibodies of the gut to bind to commensal and pathogenic bacteria with similar affinities, and to be present at constant levels. Therefore we did not explicitly account for SIgA specificities, but included them into the mucus layer value. As mucins, AMPs and SIgA are secreted by epithelial cells [44], we implemented the synthesis of mucus dependent on the relative capability of the epithelium (epi) with rate constant  $\lambda_{\text{mucus}}$ . We assumed  $\text{mucus} = 0.9$  in steady state (i.e. for  $\text{epi} = 1$  and  $\text{tissue} = 1$ ), as the mucus layer is not as effective as the epithelial barrier in preventing bacterial inflow, resulting in  $\lambda_{\text{mucus}} = 0.9 \cdot \mu_{\text{mucus}}$ . The first-order degradation rate of mucus is  $\mu_{\text{mucus}} = 0.46 \frac{1}{\text{h}}$ , corresponding to a half-life of 1.5 h [41]. The resulting ODE for mucus is

$$\frac{d}{dt} \text{mucus} = \lambda_{\text{mucus}} \cdot \text{epi} - \mu_{\text{mucus}} \cdot \text{mucus}.$$

The resulting time course of the tissue, epi and mucus state variables for the two scenarios of infection with salmonellae and mucosal injury is shown in Figure 2. Due to the influence of cytokines on synthesis and degradation of tissue and epi, the resulting healthy steady state is not exactly 1.

*Bacterial inflow.* The inflow rate of bacteria into LP is dependent on the epithelial and mucus barrier. It consists of two parts: (i) the inflow through permeable barriers and (ii) the forced invasion via toxins by pathogens. (i) The inflow through permeable barriers depends on the permeability of the two barriers, i.e.  $(1 - \text{mucus})$  and  $(1 - \text{epi})$ , with rate constant  $\epsilon_{\text{Bact},1}$ , i.e. inflow without toxin =  $\epsilon_{\text{Bact},1} \cdot (1 - \text{mucus}) \cdot (1 - \text{epi}) \cdot \text{Bact}_{\text{Lu},b}$ . The rate constant was set to  $\epsilon_{\text{Bact},1} = 3 \cdot 10^8 \frac{1}{\text{mL}\cdot\text{h}}$  based on the resulting time course, representing the maximal inflow rate of bacteria without toxins in the case of total destruction of the barrier. (ii) The inflow via toxins depends on the permeability of the mucus layer  $(1 - \text{mucus})$ , and the relative intactness of the epithelial barrier (epi), as it describes the inflow rate through the epithelial cells, with the bacteria-specific rate constant  $\epsilon_{\text{Bact},2,b}$ , i.e. inflow with toxin =  $\epsilon_{\text{Bact},2,b} \cdot (1 - \text{mucus}) \cdot \text{epi} \cdot \text{Bact}_{\text{Lu},b}$  for the different bacterial species  $b$ . The rate constant was set to  $\epsilon_{\text{Bact},2,\text{commensal}} = 0 \frac{1}{\text{mL}\cdot\text{h}}$ , as commensal bacteria are defined as not having those toxins; and to  $\epsilon_{\text{Bact},2,\text{salmonellae}} = 1 \cdot 10^{10} \frac{1}{\text{mL}\cdot\text{h}}$  and  $\epsilon_{\text{Bact},2,\text{extracellular}} = 1 \cdot 10^{11} \frac{1}{\text{mL}\cdot\text{h}}$  based on the resulting time course, representing the maximal inflow rate of bacteria with toxins in the case of a fully impermeable epithelial barrier. The resulting bacterial inflow rate is

$$\text{bacterial inflow}_b = \epsilon_{\text{Bact},1} \cdot (1 - \text{mucus}) \cdot (1 - \text{epi}) \cdot \text{Bact}_{\text{Lu},b}$$

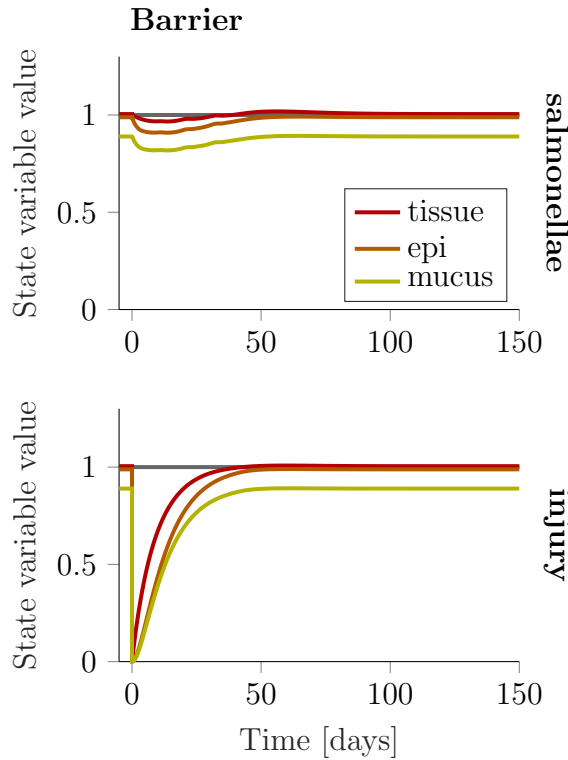


Figure 2: **Barrier dynamics.** Tissue, epithelium and mucus state variables over time. The state variables represent the relative intactness/capability of the tissue layer, epithelial barrier and mucus barrier, where tissue = 1, epi = 1 and mucus = 0.9 is the theoretical steady state representing a healthy barrier. For salmonella infection, the trigger is a stimulus of salmonellae in the lumen ( $\text{Bact}_{\text{Lu},\text{salmonellae}}$ ) at  $t = 0$ , whereas the trigger for the mucosal injury scenario is a complete destruction of the barrier and tissue, implemented by setting tissue = epi = mucus = 0 at  $t = 0$ .

$$+ \epsilon_{\text{Bact},2,b} \cdot (1 - \text{mucus}) \cdot \text{epi} \cdot \text{Bact}_{\text{Lu},b}$$

for each bacterial species  $b$ .

## 2.6 Elimination of bacteria from the tissue

In infections with pathogenic bacteria or chronic inflammation of the mucosal tissue, as in IBD, large amounts of bacterial cells enter the tissue, and also in healthy steady state there is a significant, although comparably low, inflow of bacteria [55]. In the tissue, bacterial cells are fought by phagocytic cells, such as neutrophils, macrophages and dendritic cells via phagocytosis, antimicrobial peptides or neutrophil extracellular traps [56], among which phagocytosis is the most important route of elimination for most pathogens [57]. Once phagocytosed, bacteria are destroyed using degradative enzymes and other antimicrobial substances [29]. Phagocytosis is also important to eliminate apoptotic cells from the tissue, mainly by macrophages. This process is called efferocytosis, and further described in Sections 2.8 and 2.15.

We focused on elimination of bacteria via phagocytosis. Li et al. (2004) [58] measured bacterial growth of *Staphylococcus epidermidis* (*S. epidermidis*) over time in fibrin gels

(representing tissue) in the presence of neutrophils, for different combinations of bacterial and neutrophil concentrations. Using these *in vitro* experiments they determined the critical neutrophil concentrations for different concentrations of bacteria, i.e. the required concentration of neutrophils to prevent growth of the bacteria. For this, they assumed bacterial dynamics to be a result of bacterial growth and bacterial killing by neutrophils,

$$b = b_0 \cdot e^{-(kp-g)t},$$

where  $b$  was the bacterial concentration at time point  $t$ ,  $b_0$  was the initial bacterial concentration at  $t = 0$ ,  $p$  was the neutrophil concentration (constant over time), and  $k$  and  $g$  were the rate constants for killing (second-order) and growth (first-order), respectively. For each initial bacterial concentration  $b_0$  they estimated  $k$  and  $g$  from their data, and observed that the growth rate constant  $g$  was constant over the range of bacterial concentrations, whereas the killing rate constant  $k$  decreased with higher bacterial concentrations. The critical neutrophil concentration (for each  $b_0$ ) was then calculated as  $\text{CNC} = \frac{g}{k}$ , so that  $b = b_0$  for  $p = \text{CNC}$ ,  $b$  increasing over time for  $p < \text{CNC}$  and  $b$  decreasing for  $p > \text{CNC}$ . The authors indicated that the decreasing killing rate constant over initial bacterial concentrations could be due to saturation of phagocytosis by neutrophils.

To get a continuous function of killing over all concentrations of bacteria and neutrophils, we transformed the second-order killing reaction proposed by Li et al. [58] (killing =  $k \cdot p \cdot b$ , with  $k$  dependent on  $b_0$ ) into a saturable reaction with maximal killing rate per neutrophil  $V_{\max, \text{Phago}}$  and bacterial concentration for half-maximal killing rate  $\text{Km}_{\text{Phago}}$ , so that

$$\text{killing rate} = \frac{V_{\max, \text{Phago}} \cdot b}{\text{Km}_{\text{Phago}} + b} \cdot p.$$

For this, we calculated the killing rate per neutrophil for each initial bacterial concentration  $b_0$ , and used these data of killing rate over  $b_0$  to estimate the parameters  $V_{\max, \text{Phago}} = 22.2 \frac{1}{\text{h}}$  and  $\text{Km}_{\text{Phago}} = 3.7 \cdot 10^7 \frac{1}{\text{mL}}$  using least squares approximation.

For inclusion into our model of the mucosal immune system, where we also accounted for the phagocytic activity of macrophages and dendritic cells, we calculated a weighted sum of those phagocytic cells that represented their phagocytic activity normalised to neutrophils, which we called the neutrophil equivalent concentration (NEC). Due to lack of other information, we assumed all dendritic cells and anti-inflammatory macrophages (macrophage population P4, see Section 2.8) to have the same phagocytic capacity as neutrophils. Pro-inflammatory macrophages have been reported to have lower phagocytic capacities than anti-inflammatory macrophages by factors  $w_{\text{phago}, \text{P1}} = 0.034$ ,  $w_{\text{phago}, \text{P2}} = 0.12$  and  $w_{\text{phago}, \text{P3}} = 0.31$ , for macrophage populations P1, P2 and P3, respectively [59].

In addition to elimination, bacterial growth in LP was included with rate constant  $p_{\text{Bact}, \text{LP}, b} = 0.72 \frac{1}{\text{h}}$  (for commensal and extracellular bacteria), which equaled the growth rate constant  $g$  estimated by Li et al. [58]. As intracellular bacteria mainly proliferate inside cells, the extracellular growth rate constant was set to  $p_{\text{Bact}, \text{LP}, \text{salmonellae}} = 0$ . To avoid infinite growth of bacteria in our model simulations, we limited the concentration of bacteria to  $C_{\max, \text{Bact}} = 10^{10} \frac{1}{\text{mL}}$ . (The exact value of this parameter does only have an influence in the case of chronic infection, which was not the intention of our work.)

Commensal bacteria, such as *S. epidermidis* as used by Li et al. [58], can readily be recognised by phagocytic cells. Some pathogenic bacteria, however, can evade this



recognition, e.g. by having a polysaccharide capsule [29]. To account for this we included the bacteria-specific parameter  $R_{\text{phago},b}$  that describes the relative ability of phagocytic cells to recognise this bacterial species. For commensal bacteria and intracellular bacteria this parameter is set to  $R_{\text{phago,commensal}} = R_{\text{phago,salmonellae}} = 1$ ; for extracellular bacteria we set  $R_{\text{phago,extracellular}} = 0.1$ .

The resulting ODE for the concentration of bacteria in LP is

$$\begin{aligned} \frac{d}{dt} \text{Bact}_{\text{LP},b} = & \text{bacterial inflow}_b + p_{\text{Bact,LP},b} \cdot \left( 1 - \frac{\sum_b \text{Bact}_{\text{LP},b}}{C_{\text{max,Bact}}} \right) \cdot \text{Bact}_{\text{LP},b} \\ & - \frac{V_{\text{max,Phago}} \cdot \text{Bact}_{\text{LP},b}}{\frac{K_{\text{mPhago}}}{R_{\text{phago},b}} + \sum_b \text{Bact}_{\text{LP},b}} \cdot \text{NEC}_{\text{LP}} \end{aligned}$$

for  $b$ . The (bacteria-specific) bacterial inflow rate into the tissue has been defined in the previous section (Section 2.5). Note that the killing rate of a bacterial species depends on the bacteria-specific concentration (in the numerator), but is saturated by the total concentration of bacteria (in the denominator).

We calculated the critical NEC, i.e. the concentration of phagocytic cells (normalised by their phagocytic capacity to neutrophils) that is required to prevent bacterial growth for a given concentration of bacteria (in the absence of further bacterial inflow), according to the calculation of the critical neutrophil concentration by Li et al. [58]. For the different bacterial species  $b$ , the critical NEC (cNEC) is given by

$$\text{cNEC}_b = p_{\text{Bact,LP},b} \cdot \left( 1 - \frac{\sum_b \text{Bact}_{\text{LP},b}}{C_{\text{max,Bact}}} \right) \cdot \frac{\frac{K_{\text{mPhago}}}{R_{\text{phago},b}} + \sum_b \text{Bact}_{\text{LP},b}}{V_{\text{max,Phago}}}. \quad (*^1)$$

For commensal bacteria, the critical NEC dependent on the bacterial concentration is given in Figure 3. If  $\text{NEC}_{\text{LP}} > \text{cNEC}$ , bacteria are eliminated from the tissue, if  $\text{NEC}_{\text{LP}} < \text{cNEC}$ , bacterial growth can not be controlled by phagocytic cells. In healthy steady state, the model predicts  $\text{NEC}_{\text{LP}} = 2.1 \cdot 10^7 \frac{1}{\text{mL}}$  and  $\text{Bact}_{\text{LP}} = 2.7 \cdot 10^4 \frac{1}{\text{mL}}$  (indicated by the violet cross in Figure 3), which results in elimination of bacteria, as can be seen in Figure 3, indicating that the innate immune system is perfectly able to control the bacteria in the tissue. Only for very high bacterial concentrations ( $\text{Bact}_{\text{LP}} > 7 \cdot 10^8$ ), the steady state NEC would not suffice. Such high bacterial concentrations will, however, trigger an extensive recruitment of innate immune cells (see Sections 2.7 and 2.8). This also implies a substantial margin, so that a slight decrease in phagocytic cells can be well tolerated.

## 2.7 Neutrophils

Neutrophils are the most abundant leukocyte population in blood [56]. In healthy tissue they are, however, not detectable [29]. During an infection, neutrophils are the first immune cells to enter the tissue after bacterial inflow [29]. They are recruited by cytokines and chemokines (mainly produced or induced by T helper cells type 17 and macrophages, but also by neutrophils themselves) and bacterial products (directly and via endothelial and epithelial cells) [52, 56, 60, 61]. Neutrophils are highly phagocytic and efficiently recruit macrophages to the tissue [62]. The very fast recruitment after infection is followed

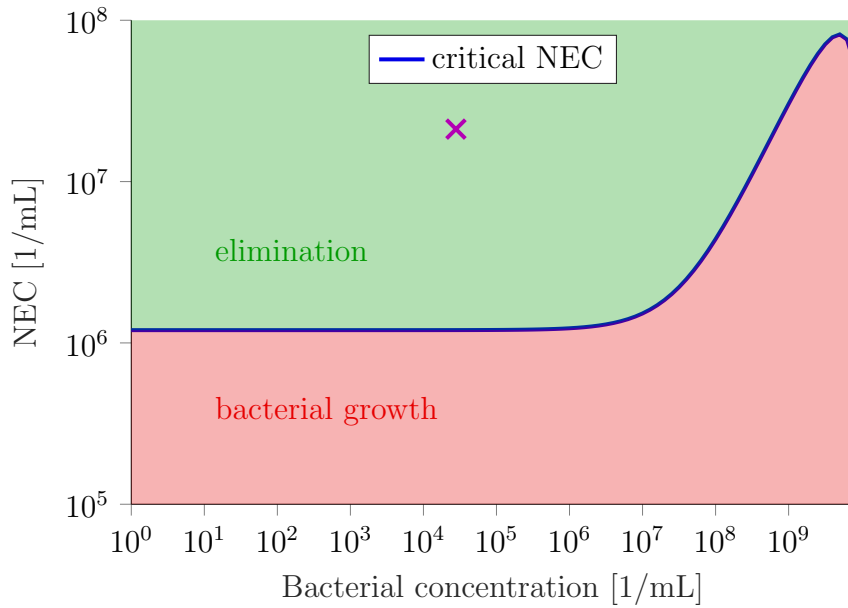


Figure 3: **Critical neutrophil equivalent concentration**  $cNEC$ , for different bacterial concentrations, calculated using Equation ( $*^1$ ). Growth (red) or elimination (green) of commensal bacteria dependent on the concentrations of bacteria and neutrophil equivalents. If  $NEC_{LP} > cNEC$ , bacterial elimination is larger than bacterial growth, resulting in net elimination (green), if  $NEC_{LP} < cNEC$ , bacterial growth is larger than bacterial elimination, resulting in net growth (red). The violet cross indicates the steady-state values.

by a fast decrease in tissue neutrophil concentrations [56]. This second phase is induced by a lipid-mediator class switch: First, pro-inflammatory lipid mediators (cytokines) are produced; at apoptosis, the lipid mediator class switch induces the production of so-called specialised pro-resolving mediators (SPM) instead [63]. Those SPM further stimulate neutrophil apoptosis and inhibit innate immune cell recruitment into the tissue [63]. In addition, phagocytosis of bacteria induces neutrophil apoptosis [60]. Pro-inflammatory cytokines delay neutrophil apoptosis [60], however, pro-apoptotic stimuli mostly override apoptosis-delaying stimuli [64]. Neutrophil apoptosis is the first—and crucial—step to resolution of the inflammation [60]: Apoptotic neutrophils are eliminated from the tissue via phagocytosis by macrophages; this process is called efferocytosis [65]. This process induces SPM production in the efferocytosing macrophages, in even much larger amounts than by the apoptotic neutrophils [66]. The resolution of inflammation via SPM is described in more detail in Section 2.15.

An overview of the neutrophil submodel, including involved state variables and all reactions, is shown in Figure 4.

*Recruitment.* Neutrophils are recruited to the tissue in response to pro-inflammatory cytokines, chemokines and bacterial stimuli [56, 61]. In healthy steady state, neutrophils are not detectable in the LP [29], i.e. the recruitment must be very low in spite of the present (low) levels of pro-inflammatory cytokines. To react fast in the case of an inflammation, neutrophils must be very sensitive to bacterial stimuli. Therefore, we need an implementation of neutrophil recruitment that ensures that the recruitment rate is very low for

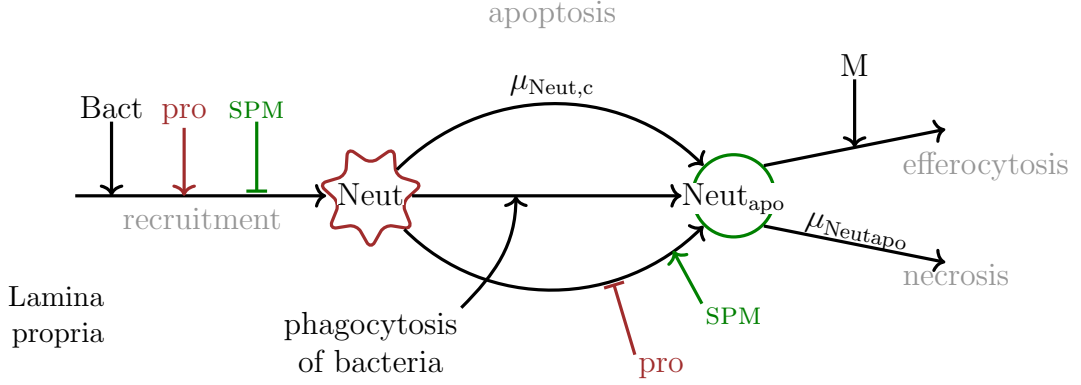
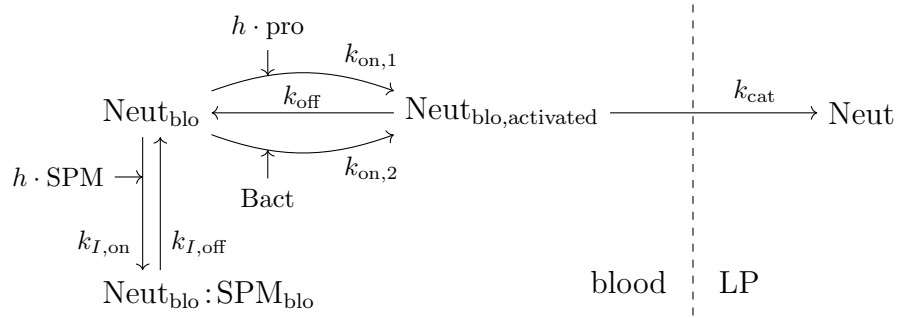


Figure 4: **Neutrophil submodel.** Two state variables, neutrophils  $\text{Neut}$  and apoptotic neutrophils  $\text{Neut}_{\text{apo}}$  represent neutrophils in the model. Arrows indicate inflow, outflow and transitions between states, with rate constants on the arrows or rates given in the text for the reactions labeled in grey. Arrows targeting on arrows mean stimulating ( $\longrightarrow$ ) or inhibiting ( $\dashrightarrow$ ) influence on this reaction. pro: pro-inflammatory cytokines  $\text{cyto}_{\text{rec,Neut}}$ , SPM: specialised pro-resolving mediators, M: macrophages.

low pro-inflammatory cytokine concentrations, high for high pro-inflammatory cytokine concentrations, and high even for low bacterial concentrations. This can be achieved by including a Hill coefficient on the recruitment by pro-inflammatory cytokines, but not on the recruitment by bacteria. Neutrophil recruitment is inhibited by SPM [63]. To ensure that SPM effects are able to override pro-inflammatory cytokine effects, we included the same Hill coefficient also on SPM inhibition of recruitment. We described the recruitment process of neutrophils from blood into LP by competitive binding of pro-inflammatory cytokines and bacterial products versus SPM: Binding of pro-inflammatory cytokines or bacterial products results in a switch of the neutrophil towards an activated state in which it is likely to enter the tissue, and binding of SPM results in a switch towards a state in which it is not able to react to pro-inflammatory cytokines or bacterial stimuli. Both states last only for a specific time, then the neutrophil reverts to its initial state:



Assuming  $\text{Neut}_{\text{blo}}$ ,  $\text{Neut}_{\text{blo,activated}}$  and  $\text{Neut}_{\text{blo}}:\text{SPM}_{\text{blo}}$  to be in quasi-steady state (applying principles of enzyme kinetics), the recruitment rate can be simplified to

$$\text{recruitment rate} = \frac{k_{\text{cat}} \cdot \text{Neut}_{\text{blo,tot}} \cdot \frac{\text{pro}^h + \frac{k_{\text{on},1} \cdot \text{Bact}}{k_{\text{on},2}}}{\text{Km}}}{1 + \frac{\text{SPM}^h}{K_I} + \frac{\text{pro}^h + \frac{k_{\text{on},1} \cdot \text{Bact}}{k_{\text{on},2}}}{\text{Km}}},$$

with  $\text{Km} = \frac{k_{\text{off}} + k_{\text{cat}}}{k_{\text{on}}}$ ,  $K_I = \frac{k_{I,\text{off}}}{k_{I,\text{on}}}$  and  $\text{Neut}_{\text{blo,tot}} = \text{Neut}_{\text{blo}} + \text{Neut}_{\text{blo}}:\text{SPM}_{\text{blo}} + \text{Neut}_{\text{blo,activated}}$ .

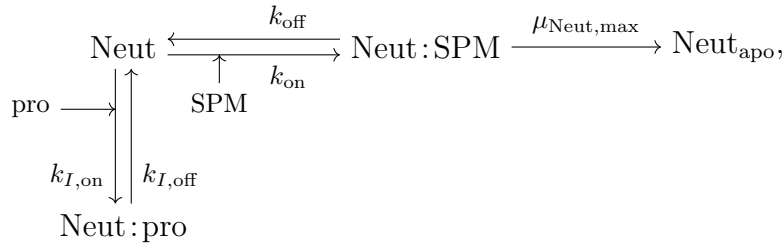
We simplified further, normalising the pro-inflammatory cytokine and SPM concentrations by  $K_m$  and  $K_I$ :  $\text{cyto}_{\text{rec,Neut}} = \frac{\text{pro}}{\sqrt[3]{K_m}}$  and  $\text{SPM} = \frac{\widetilde{\text{SPM}}}{\sqrt[3]{K_I}}$ . The maximal neutrophil recruitment rate is described by  $\lambda_{\text{Neut,max}} = k_{\text{cat}} \cdot \text{Neut}_{\text{blo,tot}}$ . The parameter describing the relative contribution of bacteria and pro-inflammatory cytokines is  $w_{\text{pro,Bact}} = \frac{k_{\text{on},1}}{k_{\text{on},2}}$ . All different bacterial species  $\sum_b \text{Bact}_{\text{LP}}$  are similarly taken into account. This results in

$$\text{recruitment rate} = \frac{\lambda_{\text{Neut,max}} \cdot ((\text{cyto}_{\text{rec,Neut}})^{h_{\text{rec,Neut}}} + w_{\text{pro,Bact}} \cdot \sum_b \text{Bact}_{\text{LP}})}{1 + \text{SPM}^{h_{\text{rec,Neut}}} + (\text{cyto}_{\text{rec,Neut}})^{h_{\text{rec,Neut}}} + w_{\text{pro,Bact}} \cdot \sum_b \text{Bact}_{\text{LP}}},$$

with  $h_{\text{rec,Neut}} = h$ .

Parameter values were set to  $w_{\text{pro,Bact}} = 1 \cdot 10^{-6}$ ,  $h_{\text{rec,Neut}} = 2$  and  $\lambda_{\text{Neut,max}} = 1 \cdot 10^8 \frac{1}{\text{mL} \cdot \text{h}}$ , ensuring the previously stated requirements on neutrophil recruitment. For details on the cytokine concentration, see Section 2.14.

*Apoptosis.* We included three different forms of apoptosis: (i) A constant cell death rate constant  $\mu_{\text{Neut,c}} = \frac{1}{7} \frac{1}{\text{d}}$  represents the maximal life span of a neutrophil in tissue of 7 d [67]. (ii) Neutrophils die with the rate  $\mu_{\text{Neut,Phago}} \cdot \text{phagocytosis rate of neutrophils}$ , where  $1/\mu_{\text{Neut,Phago}} = 50$  represents the average number of bacteria each neutrophil can eliminate before going into apoptosis [68]. (iii) Apoptosis is stimulated by SPM, but inhibited by pro-inflammatory cytokines, which we implemented using competitive binding of SPM and pro-inflammatory cytokines to neutrophils, where apoptosis can only be induced in neutrophils bound to SPM:



resulting in

$$\text{induced apoptosis rate} = \frac{\mu_{\text{Neut,max}} \cdot \text{Neut} \cdot \frac{\widetilde{\text{SPM}}}{K_m}}{1 + \frac{\text{pro}}{K_I} + \frac{\widetilde{\text{SPM}}}{K_m}},$$

with the maximal induced apoptosis rate constant set to  $\mu_{\text{Neut,max}} = 0.35 \frac{1}{\text{h}}$ . Again, we included the  $K_m$  and  $K_I$  in the weighted sums representing pro-inflammatory cytokines and SPM, and used the same cytokines as for neutrophil recruitment:  $\text{cyto}_{\text{rec,Neut}} = \frac{\text{pro}}{K_I}$  and  $\text{SPM} = \frac{\widetilde{\text{SPM}}}{K_m}$ , so that

$$\text{induced apoptosis rate} = \frac{\mu_{\text{Neut,max}} \cdot \text{Neut} \cdot \text{SPM}}{1 + \text{cyto}_{\text{rec,Neut}} + \text{SPM}}.$$

Thus, the total neutrophil apoptosis rate is

$$\text{apoptosis rate} = \mu_{\text{Neut,c}} \cdot \text{Neut}$$

$$\begin{aligned}
& + \mu_{\text{Neut,Phago}} \cdot \sum_b \left( \frac{V_{\text{max,Phago}} \cdot \text{Bact}_{\text{LP},b}}{\frac{\text{Km}_{\text{Phago}}}{R_{\text{phago},b}} + \sum_b \text{Bact}_{\text{LP},b}} \right) \cdot \text{Neut} \\
& + \frac{\mu_{\text{Neut,max}} \cdot \text{Neut} \cdot \text{SPM}}{1 + \text{cyto}_{\text{rec,Neut}} + \text{SPM}}.
\end{aligned}$$

*Elimination of apoptotic neutrophils.* Apoptotic neutrophils are mainly eliminated from the tissue by macrophages (efferocytosis). We implemented this form of phagocytosis similar to the phagocytosis of bacteria:

$$\text{efferocytosis rate} = \frac{V_{\text{max,Phago}} \cdot \text{Neut}_{\text{apo}}}{\text{Km}_{\text{Phago}} + \text{Neut}_{\text{apo}}} \cdot \text{NEC}_{\text{M,LP}},$$

assuming the same maximal phagocytosis rate  $V_{\text{max,Phago}}$  and concentration for half-maximal phagocytosis  $\text{Km}_{\text{Phago}}$ .  $\text{NEC}_{\text{M,LP}}$  represents the concentration of macrophages, normalised by their phagocytic activity to neutrophils, i.e. the subset of  $\text{NEC}_{\text{LP}}$  corresponding to macrophages, as described in Section 2.6. In addition, we included a low macrophage-independent elimination rate of apoptotic neutrophils  $\mu_{\text{Neut,apo}} = \frac{1}{48} \frac{1}{\text{h}}$ , accounting for necrosis. Efferocytosis of apoptotic neutrophils by macrophages influences the activation state of the macrophages, which we call efferocytosis-type macrophages ( $M_{\text{effero}}$ ). This is described in more detail in Section 2.8 (paragraph *Efferocytosis*). Apoptotic neutrophils, and, to a much higher extent, efferocytosis-type macrophages, produce specialised pro-resolving mediators (SPM), which have an important role in the resolution of inflammation, in detail described in Section 2.15.

The resulting ODEs for neutrophils and apoptotic neutrophils are

$$\begin{aligned}
\frac{d}{dt} \text{Neut} &= \frac{\lambda_{\text{Neut,max}} \cdot ((\text{cyto}_{\text{rec,Neut}})^{h_{\text{rec,Neut}}} + w_{\text{pro,Bact}} \cdot \sum_b \text{Bact}_{\text{LP}})}{1 + \text{SPM}^{h_{\text{rec,Neut}}} + (\text{cyto}_{\text{rec,Neut}})^{h_{\text{rec,Neut}}} + w_{\text{pro,Bact}} \cdot \sum_b \text{Bact}_{\text{LP}}} \\
&\quad - \mu_{\text{Neut,c}} \cdot \text{Neut} \\
&\quad - \mu_{\text{Neut,Phago}} \cdot \sum_b \left( \frac{V_{\text{max,Phago}} \cdot \text{Bact}_{\text{LP},b}}{\frac{\text{Km}_{\text{Phago}}}{R_{\text{phago},b}} + \sum_b \text{Bact}_{\text{LP},b}} \right) \cdot \text{Neut} \\
&\quad - \frac{\mu_{\text{Neut,max}} \cdot \text{Neut} \cdot \text{SPM}}{1 + \text{cyto}_{\text{rec,Neut}} + \text{SPM}} \\
\frac{d}{dt} \text{Neut}_{\text{apo}} &= \mu_{\text{Neut,c}} \cdot \text{Neut} \\
&\quad + \mu_{\text{Neut,Phago}} \cdot \sum_b \left( \frac{V_{\text{max,Phago}} \cdot \text{Bact}_{\text{LP},b}}{\frac{\text{Km}_{\text{Phago}}}{R_{\text{phago},b}} + \sum_b \text{Bact}_{\text{LP},b}} \right) \cdot \text{Neut} \\
&\quad + \frac{\mu_{\text{Neut,max}} \cdot \text{Neut} \cdot \text{SPM}}{1 + \text{cyto}_{\text{rec,Neut}} + \text{SPM}} \\
&\quad - \frac{V_{\text{max,Phago}} \cdot \text{Neut}_{\text{apo}}}{\text{Km}_{\text{Phago}} + \text{Neut}_{\text{apo}}} \cdot \text{NEC}_{\text{M,LP}} \\
&\quad - \mu_{\text{Neut,apo}} \cdot \text{Neut}_{\text{apo}}.
\end{aligned}$$

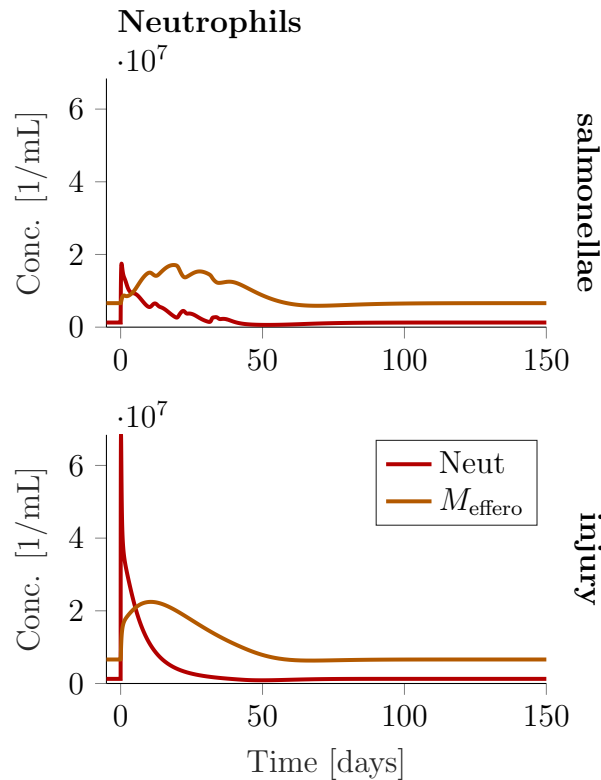


Figure 5: **Neutrophil dynamics.** Concentrations of neutrophils and efferocytosis-type macrophages over time for the two inflammation scenarios of salmonella infection and mucosal injury.

The resulting time courses of neutrophils and efferocytosis-type macrophages are shown in Figure 5. The predicted neutrophil concentration peaks 19.5 h after salmonellae infection and 1.7 h after mucosal injury. In both cases, the peak is earlier than reported in literature (peak at 24 – 48 h after infection or inflammatory stimuli [56]). Reasons for this very early predicted peak (1.7 h) after mucosal injury could be the immediacy of this stimulus in our simulation. Compared to an infection or stimulation with a pro-inflammatory substance, where the bacteria or molecules have to reach the tissue before neutrophils are recruited, our simulation of mucosal injury starts with a very high inflow of bacteria at  $t = 0$ , leading directly to a high recruitment of neutrophils and the immediate start of the immune response.

## 2.8 Macrophages

The main functions of macrophages in LP are elimination of bacteria, clearance of apoptotic cells, tissue remodelling and production of many different cytokines [52]. In particular the production of the anti-inflammatory cytokine IL-10 is important for the maintenance of the regulatory T cell population in LP [69]. In addition, they play an important role in the resolution of the inflammation [70], further described in Section 2.15. Macrophages are recruited as monocytes from the blood; proliferation in the gut LP is negligible [71]. In contrast to most other tissues, in the gut, macrophages can not be divided into M1 and M2 macrophages [72], and most gut-resident macrophages do not secrete pro-

inflammatory cytokines in response to encounter of bacterial antigen [71]. Bain et al. (2013) [59] showed in mouse colon that macrophages are recruited into the LP in a pro-inflammatory state, i.e. the same state as the monocytes in the blood, and then gradually turn into an anti-inflammatory state, mediated by the local anti-inflammatory cytokine milieu. They were able to identify four different states, which the macrophages transit through [59]. In inflammation, the transit through those states is delayed, resulting in an accumulation of more pro-inflammatory macrophages [59]. Macrophages can take up antigen and present it on MHCII, however, their importance in antigen presentation to T cells is controversial, especially because of their inability to migrate to LNs [73]. In case of an infection, the antigen stems mainly from bacteria that have invaded the LP. In addition, macrophages and/or dendritic cells extend dendrites through the epithelium to sample antigen from the lumen, which is probably also transferred between macrophages and dendritic cells [52, 73].

An overview of the macrophage submodel, including involved state variables and all reactions, is shown in Figure 6.

*Recruitment.* We calculated the steady state concentration of macrophages in the LP from the steady state concentration of dendritic cells (derivation in Section 2.9) and the reported ratio of macrophages to dendritic cells in LP of 3.5 (mouse small intestine) [74] to be  $M_{\text{tot,ss}} = 1.98 \cdot 10^7 \frac{1}{\text{mL}}$ . For determination of the death rate constant  $\mu_M = 0.0031 \frac{1}{\text{h}}$  see next paragraph (*Deactivation*, based on data by Bain et al. (2013) [59]). This death rate constant results in an expected life time of 13.3 d of macrophages in the tissue. Based on death rate and steady state concentration, we calculated the rate constant of steady state inflow to be  $\lambda_{M,c} = \mu_M \cdot M_{\text{tot,ss}} = 6.2 \cdot 10^4 \frac{1}{\text{mL}}$ . In inflammation there is much higher recruitment of macrophages into tissue, which we implemented by an additional recruitment rate dependent on pro-inflammatory cytokines (see Section 2.14), inhibited by SPM. This cytokine-dependent recruitment rate is structurally similar to the neutrophil recruitment rate, with two differences: (i) Bacteria do not directly influence macrophage recruitment. (ii) As the inhibiting role of SPM on macrophage recruitment is not as clear as on neutrophil recruitment, we implemented SPM binding to blood monocytes without Hill factor, ensuring that pro-inflammatory cytokine effects can override SPM effects. This led to

$$\text{M recruitment rate} = \lambda_{M,c} + \frac{\lambda_{M,\text{max}} \cdot (\text{cyto}_{\text{rec},M})^{h_{\text{rec},M}}}{1 + \text{SPM} + (\text{cyto}_{\text{rec},M})^{h_{\text{rec},M}}},$$

where the first summand describes the constant recruitment rate and the second summand describes the additional recruitment rate in response to inflammation, analogous to the neutrophil recruitment rate. Parameter values were set to  $h_{\text{rec},M} = 2$  and  $\lambda_{M,\text{max}} = 1 \cdot 10^6 \frac{1}{\text{mL} \cdot \text{h}}$ , ensuring a reasonable macrophage inflow in the tested inflammation scenarios. For details on the cytokine concentration, see Section 2.14.

*Deactivation.* Bain et al. (2013) [59] described the step-wise transition from newly recruited pro-inflammatory macrophages to the main gut-resident population of anti-inflammatory macrophages. We call this transition deactivation; this does, however, not refer to the general capability of cytokine production or other functions such as phagocytosis. Bain et al. (2013) [59] described four different main populations of macrophages, called P1 to P4, where P1 macrophages are identical to blood monocytes, P4 macrophages represent the major population in healthy steady state, and P2 and P3 macrophages are

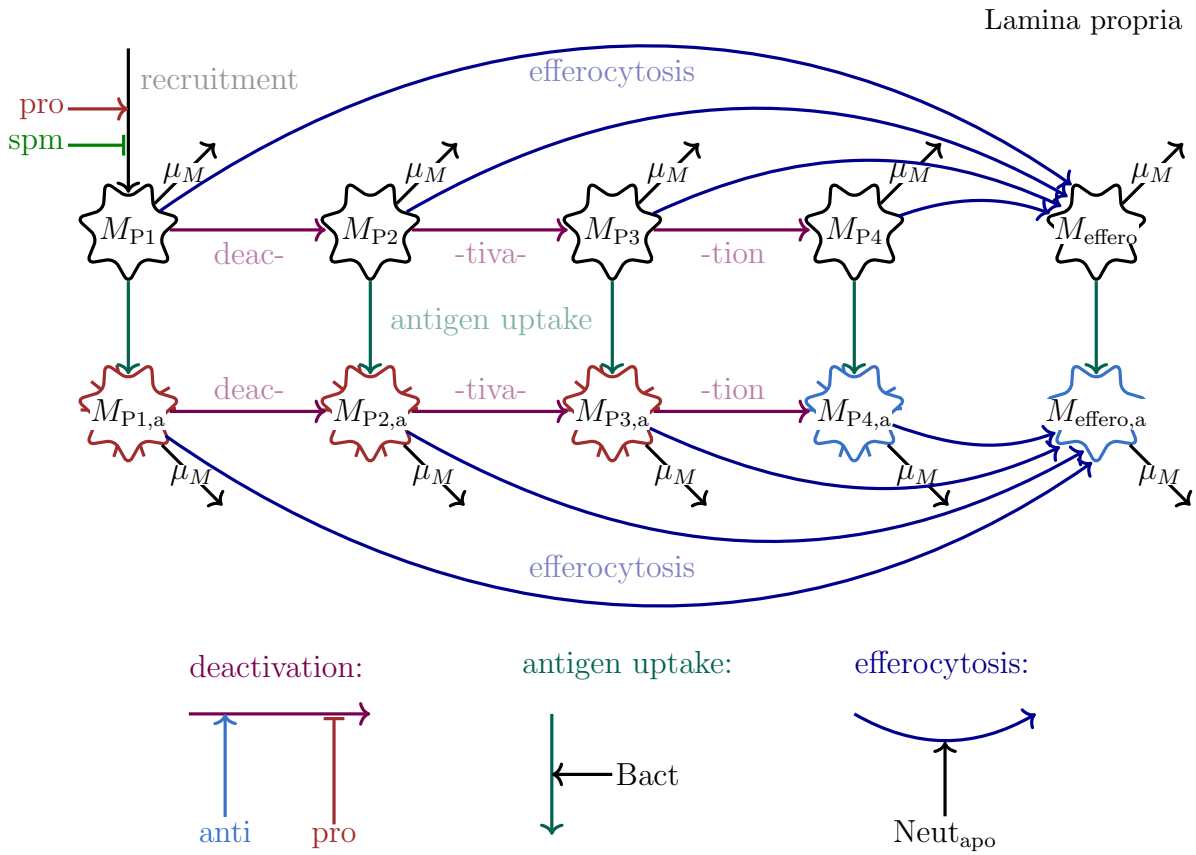


Figure 6: **Macrophage submodel.** Macrophages in the LP were implemented as different state variables for the four different populations P1 to P4 and efferocytosis-type, before ( $M_{P_i}$ ) and after ( $M_{P_i,a}$ ) encounter with bacterial antigen. Additional macrophage state variables will be described in Section 2.13 and 2.18.2. Arrows indicate inflow, death and transitions between states, with rate constants on the arrows or rates given in the text for the reactions labeled in grey/light colours. Arrows targeting on arrows mean stimulating ( $\longrightarrow$ ) or inhibiting ( $\longleftarrow$ ) influence on this reaction. pro: pro-inflammatory cytokines  $\text{cyto}_{\text{rec},M}$  or  $\text{cyto}_{\text{pro,deact},M}$ , anti: anti-inflammatory cytokines  $\text{cyto}_{\text{anti,deact},M}$ , SPM: specialised pro-resolving mediators.

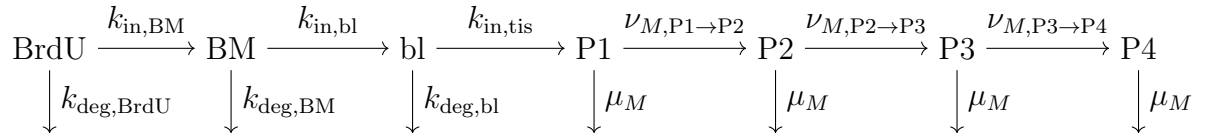
transitional states in between. All subsets contain pro-inflammatory cytokine-producing and anti-inflammatory cytokine-producing cells, with decreasing and increasing fractions from P1 to P4, respectively. For simplification, we regarded P1 to P3 as pro-inflammatory cells producing pro-inflammatory cytokines, and P4, the resident population, as anti-inflammatory cells producing anti-inflammatory cytokines. In addition, the populations differ in their phagocytic activity, which increases for P1 to P4 (see Section 2.6).

We used data from different experiments by Bain et al. [59]: (i) Supplementary Figure 1a + 1g [59] give the steady state fractions of P1 to P3 from  $\text{CX3CR1}^{\text{int}}$  cells, the fraction of  $\text{CX3CR1}^{\text{int}}$  cells from  $\text{CD45}^+$  cells, and the fraction of P4 (all  $\text{CX3CR1}^{\text{high}}$  cells) from  $\text{CD45}^+$  cells, from which we calculated the steady state concentrations of P1 to P4 in the unit fraction of  $\text{CD45}^+$  cells in colon LP. (ii) Figure 2b + 2c [59] show the results of a bromodeoxyuridine (BrdU) pulse-chase experiment, where they injected mice with BrdU (a thymidine analog that is incorporated into newly synthesised DNA and can then be detected by antibodies) at time point 0. They derived the percentage of



BrdU-containing monocytes in bone marrow (BM) and blood at 3 h and 12 h, and in LP, separately for the four different macrophage populations P1 to P4, at 3 h, 12 h, 24 h and 48 h after the BrdU pulse. BrdU incorporation is assumed only to take place in BM, as monocytes/macrophages do not proliferate in the periphery, and thus the experiment is used to follow those BrdU<sup>+</sup> cells from BM through blood and the different LP macrophage populations. The data [59] are given in % BrdU for each cell compartment. We transformed the data for P1 to P4 into the unit fraction BrdU<sup>+</sup> cells of CD45<sup>+</sup> cells, using the fractions of P1 to P4 from CD45<sup>+</sup> cells. Through that we ensured that the concentrations of P1 to P4 were in the same unit, so that we could model the transit through those compartments. The transformed data are shown in Figure 7.

We fitted the following macrophage transition submodel to the transformed data:



The corresponding system of ODEs is:

$$\begin{aligned}
 \frac{d}{dt}\text{BrdU} &= -\hat{k}_{\text{deg,BrdU}} \cdot \text{BrdU} \\
 \frac{d}{dt}\text{BM} &= k_{\text{in,BM}} \cdot \text{BrdU} - \hat{k}_{\text{deg,BM}} \cdot \text{BM} \\
 \frac{d}{dt}\text{bl} &= k_{\text{in,bl}} \cdot \text{BM} - \hat{k}_{\text{deg,bl}} \cdot \text{bl} \\
 \frac{d}{dt}\text{P1} &= k_{\text{in,tis}} \cdot \text{bl} - (\nu_{M,\text{P1}\rightarrow\text{P2}} + \mu_M) \cdot \text{P1} \\
 \frac{d}{dt}\text{P2} &= \nu_{M,\text{P1}\rightarrow\text{P2}} \cdot \text{P1} - (\nu_{M,\text{P2}\rightarrow\text{P3}} + \mu_M) \cdot \text{P2} \\
 \frac{d}{dt}\text{P3} &= \nu_{M,\text{P2}\rightarrow\text{P3}} \cdot \text{P2} - (\nu_{M,\text{P3}\rightarrow\text{P4}} + \mu_M) \cdot \text{P3} \\
 \frac{d}{dt}\text{P4} &= \nu_{M,\text{P3}\rightarrow\text{P4}} \cdot \text{P3} - \mu_M \cdot \text{P4}
 \end{aligned}$$

with  $\hat{k}_{\text{deg,BrdU}} = k_{\text{deg,BrdU}} + k_{\text{in,BM}}$ ,  $\hat{k}_{\text{deg,BM}} = k_{\text{deg,BM}} + k_{\text{in,bl}}$  and  $\hat{k}_{\text{deg,bl}} = k_{\text{deg,bl}} + k_{\text{in,tis}}$ . Using the given steady state concentrations of P1 to P4 (transformed data, see above) and using bl = 1, the parameters  $\nu_{M,\text{P1}\rightarrow\text{P2}}$ ,  $\nu_{M,\text{P2}\rightarrow\text{P3}}$ ,  $\nu_{M,\text{P3}\rightarrow\text{P4}}$  and  $\mu_M$  were given as a function of  $k_{\text{in,tis}}$  by setting  $\frac{d}{dt}\text{P1} = 0$ ,  $\frac{d}{dt}\text{P2} = 0$ ,  $\frac{d}{dt}\text{P3} = 0$  and  $\frac{d}{dt}\text{P4} = 0$ , using bl = 1 for steady state and solving for the parameters:

$$\begin{aligned}
 \nu_{M,\text{P1}\rightarrow\text{P2}} &= \frac{k_{\text{in,tis}}}{\text{P1}_{\text{ss}} + \text{P2}_{\text{ss}} + \text{P3}_{\text{ss}} + \text{P4}_{\text{ss}}} \cdot \frac{\text{P2}_{\text{ss}} + \text{P3}_{\text{ss}} + \text{P4}_{\text{ss}}}{\text{P1}_{\text{ss}}} \\
 \nu_{M,\text{P2}\rightarrow\text{P3}} &= \frac{k_{\text{in,tis}}}{\text{P1}_{\text{ss}} + \text{P2}_{\text{ss}} + \text{P3}_{\text{ss}} + \text{P4}_{\text{ss}}} \cdot \frac{\text{P3}_{\text{ss}} + \text{P4}_{\text{ss}}}{\text{P2}_{\text{ss}}} \\
 \nu_{M,\text{P3}\rightarrow\text{P4}} &= \frac{k_{\text{in,tis}}}{\text{P1}_{\text{ss}} + \text{P2}_{\text{ss}} + \text{P3}_{\text{ss}} + \text{P4}_{\text{ss}}} \cdot \frac{\text{P4}_{\text{ss}}}{\text{P3}_{\text{ss}}} \\
 \mu_M &= \frac{k_{\text{in,tis}}}{\text{P1}_{\text{ss}} + \text{P2}_{\text{ss}} + \text{P3}_{\text{ss}} + \text{P4}_{\text{ss}}}
 \end{aligned}$$

Then we used the data from the BrdU experiment ([59], transformed as described above, see Figure 7) to estimate the remaining parameters above using least squares estimation. Due to the different scales, the squared differences of P1 to P3 predictions from observations were weighted with factor 1000. Data for P4 were not used, because they are inexplicably high already at very early time points, which is not in accordance with the proposed mechanism of transit through the different populations (see Figure 7, right, violet dots). We assumed that this arose from measurement errors, as the original data (in % BrdU<sup>+</sup> cells) at early time points are on similar low levels for P1 to P4, but because of the higher steady state concentrations of P4, the same % BrdU<sup>+</sup> cells transforms to much higher concentrations in the unit of fraction BrdU<sup>+</sup> cells of CD45<sup>+</sup> cells. The resulting parameter values are given in Table 1. Figure 7 shows the data taken from Bain et al. [59, Fig. 2b + 2c], together with the predicted time course by the above macrophage transition submodel using the estimated parameter values.

Table 1: **Macrophage parameter estimates.** Parameters of the macrophage transition submodel, estimated based on data from Bain et al. (2013) [59], Figure 2 b and c and Supplementary Figure 1 a and g.

Parameter	Value	Unit
$\hat{k}_{\text{deg,BrdU}}$	$5.68 \cdot 10^{-2}$	$\frac{1}{\text{h}}$
$k_{\text{in,BM}}$	$9.80 \cdot 10^{-2}$	$\frac{\text{fraction BrdU}^+ \text{ cells}}{\text{h}}$
$\hat{k}_{\text{deg,BM}}$	$5.68 \cdot 10^{-2}$	$\frac{1}{\text{h}}$
$k_{\text{in,bl}}$	$1.14 \cdot 10^{-1}$	$\frac{\text{fraction BrdU}^+ \text{ cells}}{\text{h}}$
$\hat{k}_{\text{deg,bl}}$	$1.38 \cdot 10^{-1}$	$\frac{1}{\text{h}}$
$k_{\text{in,tis}}$	$6.24 \cdot 10^{-4}$	$\frac{\text{fraction BrdU}^+ \text{ cells of CD45}^+ \text{ cells}}{\text{h}}$
$\nu_{M,P1 \rightarrow P2}$	$4.88 \cdot 10^{-2}$	$\frac{1}{\text{h}}$
$\nu_{M,P2 \rightarrow P3}$	$7.88 \cdot 10^{-2}$	$\frac{1}{\text{h}}$
$\nu_{M,P3 \rightarrow P4}$	$2.21 \cdot 10^{-2}$	$\frac{1}{\text{h}}$
$\mu_M$	$3.12 \cdot 10^{-3}$	$\frac{1}{\text{h}}$

We used the resulting parameters values for  $\nu_{M,P1 \rightarrow P2}$ ,  $\nu_{M,P2 \rightarrow P3}$ ,  $\nu_{M,P3 \rightarrow P4}$  (with a modification to account for the impact of cytokines as described in the next paragraph, *Influence of inflammation on deactivation*) and  $\mu_M$  in our systems biology model (as shown in Figure 6). Those first-order parameters can easily be used in models with state variables in different units (fraction BrdU<sup>+</sup> cells of CD45<sup>+</sup> cells vs  $\frac{1}{\text{mL}}$ ). As the zero-order parameter for macrophage inflow into the tissue is in unit fraction BrdU<sup>+</sup> cells of CD45<sup>+</sup> cells, we could not directly use this parameter in our systems biology model. Instead, we calculated the steady state inflow rate constant  $\lambda_{M,c}$  based on the death rate constant  $\mu_M$  and the steady state concentration of total macrophages, as described in the previous paragraph (*Recruitment*).

In our systems biology model we accounted for those four different LP macrophage populations, which were renamed  $M_{P1,\text{tot}}$ ,  $M_{P2,\text{tot}}$ ,  $M_{P3,\text{tot}}$ ,  $M_{P4,\text{tot}}$ . The subscript “tot” was used as they were each further divided into subpopulations (see next paragraphs).

*Influence of inflammation on deactivation.* Bain et al. (2013) [59] examined the influence of inflammation on the macrophage populations in mice with dextran sodium sulfate (DSS)-induced colitis (DSS is a frequently used substance to induce epithelial cell injury

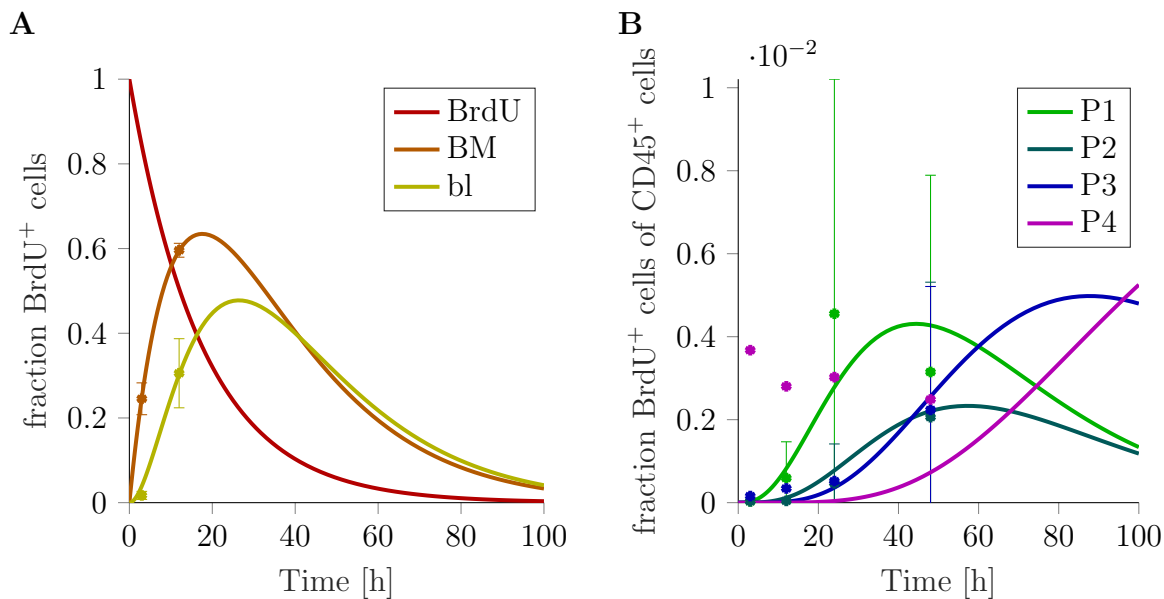
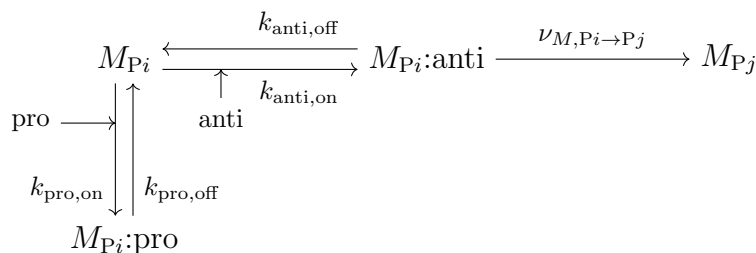


Figure 7: **Macrophage submodel fit.** Data from Bain et al. (2013) [59] together with the corresponding predicted time course using the macrophage submodel described in the text with estimated parameters given in Table 1. BrdU is given as fraction of initial concentration; macrophages in bone marrow (BM) and blood (bl) are given as fractions of BrdU<sup>+</sup> macrophages from total macrophages; and the macrophage populations P1 to P4 in LP are given as fractions of BrdU<sup>+</sup> macrophages of this population from all CD45<sup>+</sup> cells in LP. Data are given as mean and standard deviation (if available). For P1 to P4, we calculated the data by multiplication of different reported values (see text), where we calculated the mean  $E[Y]$  and standard deviation  $\sqrt{\text{Var}[Y]}$  of the resulting data by multiplication of independent normally distributed random variables  $Y = X_1 \cdot \dots \cdot X_n$ :  $E[Y] = \prod_{i=1}^n E[X_i]$  and  $\text{Var}[Y] = \prod_{i=1}^n (\text{Var}[X_i] + (E[X_i])^2) - \prod_{i=1}^n (E[X_i])^2$ . Data for P4 were not used for parameter estimation (see text).

and thereby intestinal inflammation in mice [75], see also Section 2.18.3). Apart from an overall increase of macrophages in the colon, they observed an accumulation of P1, P2 and (to a lower extent) P3 cells, while the numbers of P4 cells decreased. After adoptive transfer of monocytes, they observed a much slower local differentiation through populations P1 to P4 in inflamed than in healthy mice, strongly suggesting that the deactivation of pro-inflammatory monocyte-like macrophages to anti-inflammatory resident macrophages is disrupted in inflammation [59].

We implemented this into our system biology model by assuming the stepwise deactivation from P1 to P4 to be dependent on anti-inflammatory cytokines and inhibited by pro-inflammatory cytokines, according to the following scheme:



for  $(i, j) = (1, 2), (2, 3), (3, 4)$ . Using the quasi-steady state approximation, this results in a transition rate of

$$\text{transition rate } M_{P_{i(a)}} \rightarrow M_{P_{j(a)}} = \frac{\nu_{M, P_i \rightarrow P_j} \cdot \text{cyto}_{\text{anti, deact, M}}^{h_{\text{anti, deact, M}}}}{1 + \text{cyto}_{\text{anti, deact, M}}^{h_{\text{anti, deact, M}}} + \text{cyto}_{\text{pro, deact, M}}^{h_{\text{pro, deact, M}}}} \cdot M_{P_{i(a)}},$$

for  $(i, j) = (1, 2), (2, 3), (3, 4)$ , where  $\text{cyto}_{\text{anti, deact, M}} = \text{anti}$ ,  $\text{cyto}_{\text{pro, deact, M}} = \text{pro}$ , the cytokine concentrations (see Section 2.14) are normalised by the corresponding  $K_m$  or  $K_I$ , and the Hill factors are set to 1 for the reference individual. Subscript “a” refers to antigen experience, described in paragraph *Antigen uptake*, and is included here to show that the transition rate is similar for antigen-experienced and antigen-unexperienced macrophages.

As the parameters described in the previous paragraph (*Deactivation*) refer to the healthy steady state, but healthy steady state includes a low level of inflammation, we multiplied  $\nu_{M, P_i \rightarrow P_j}$  with factor 1.25 to counteract the inhibiting influence of the present pro-inflammatory cytokines and ensure the right steady state fractions of the different populations (as measured by Bain et al. [59]). I.e.  $\nu_{M, P_1 \rightarrow P_2} = 6.10 \cdot 10^{-2} \frac{1}{h}$ ,  $\nu_{M, P_2 \rightarrow P_3} = 9.85 \cdot 10^{-2} \frac{1}{h}$  and  $\nu_{M, P_3 \rightarrow P_4} = 2.76 \cdot 10^{-2} \frac{1}{h}$ .

Figure 8 shows (analogous to Figure 4f in Bain et al. (2013) [59]) the distributions of macrophage populations P1 to P4 before an inflammatory stimulus and at day 4 and 6 of inflammation. The additional population  $M_{\text{effero, tot}}$  (described in paragraph *Efferocytosis*) corresponds also to P4. The figure shows that the simulated distribution of macrophage populations in healthy steady state (day 0) is very similar to the resting distribution reported in Bain et al. (2013) [59]. Slight differences are due to the approximate factor of 1.25 to counteract the inhibiting influence of steady state low-level inflammation and the efferocytosis reaction. The macrophage populations in the simulation of mucosal injury show much less inflammation than in the experimental colitis by Bain et al., but the extent of inflammation seen in the macrophage populations in the simulation of salmonella infection are comparable to the experimental colitis (e.g. day 6 salmonellae vs experimental colitis). This confirms that our implementation of the inhibition of macrophage deactivation by pro-inflammatory cytokines qualitatively reflects the experimental results by Bain et al., as the resulting changes in macrophage populations are of the same order of magnitude.

*Efferocytosis.* The role of macrophages in the resolution of the inflammation is described in more detail in Section 2.15, especially the phagocytosis of apoptotic neutrophils, called efferocytosis. Phagocytosis of apoptotic neutrophils leads to a change of the state of the phagocytosing macrophage [66]. We called this state efferocytosis-type macrophage and included it as an additional population to the macrophage populations P1 to P4, assuming it similar to P4 macrophages (concerning phagocytic activity and production of anti-inflammatory cytokines), but in addition able to produce SPM (see Section 2.15). As described in Section 2.7, we implemented efferocytosis similar to phagocytosis of bacterial cells, using the same parameter values. A fraction  $p_{\text{effero}}$  of the macrophages phagocytosing apoptotic neutrophils become efferocytosis-type macrophages, i.e. the expected number of apoptotic neutrophils a macrophage has to phagocytose before becoming an efferocytosis-type macrophage is  $1/p_{\text{effero}}$ . For lack of knowledge we set the probability to  $p_{\text{effero}} = 0.1$ , resulting in plausible macrophage distributions over time. The efferocytosis rate is, similar to the phagocytosis rate, different for the macrophage populations P1 to P4, with relative

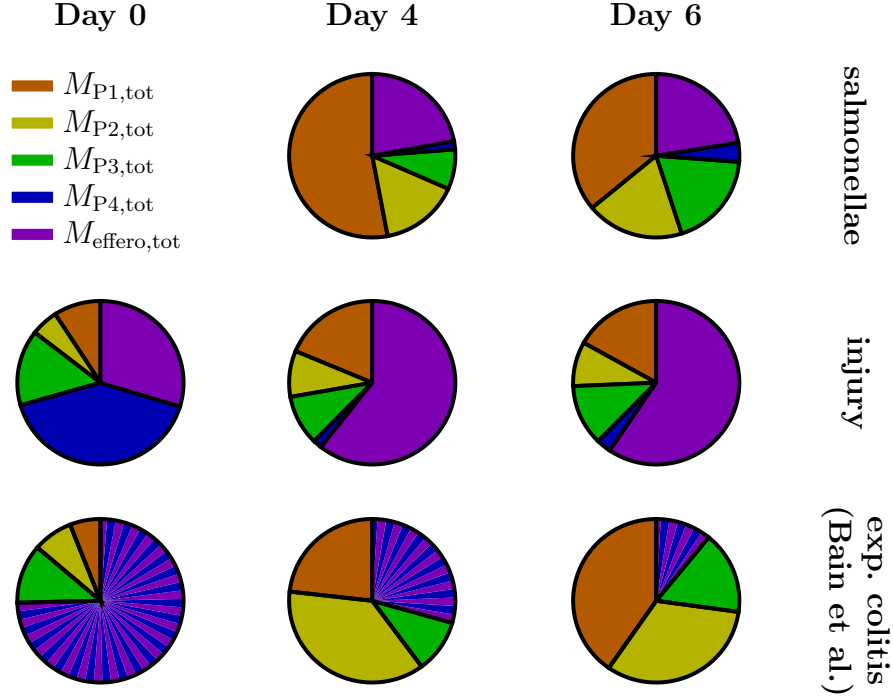


Figure 8: **Macrophage populations in inflammation.** Distribution of macrophage populations P1 to P4 at different time points before/after an inflammatory stimulus, for the two simulated inflammation scenarios (salmonella infection, mucosal injury) and experimental colitis in Bain et al. (2013) [59]. Data for experimental colitis are taken from Bain et al. [59], Figure 4e. Day 0 is the same for salmonellae and mucosal injury as it describes the state before the inflammatory stimulus.  $M_{P4,tot}$  and  $M_{effero,tot}$  together correspond to  $M_{P4,tot}$  in experimental colitis data by Bain et al. (2013) [59]. For description of  $M_{effero,tot}$  see paragraph *Efferocytosis*.

weights  $w_{phago,P1} = 0.034$ ,  $w_{phago,P2} = 0.12$ ,  $w_{phago,P3} = 0.31$  and  $w_{phago,P4} = 1$ , respectively [59]. Thus the efferocytosis rate of any macrophage population P1 to P4, independent if antigen-experienced or not, is

$$M_{P_{i(a)}} \text{ efferocytosis rate} = p_{effero} \cdot \frac{V_{\max,Phago} \cdot Neut_{apo}}{K_{mPhago} + Neut_{apo}} \cdot M_{P_{i(a)}} \cdot w_{phago,P_i},$$

describing the transition from state variable  $M_{P_{i(a)}}$  to  $M_{effero(i,a)}$ .

Figure 9 (left column) shows the time course of the different macrophage populations P1 to P4 and efferocytosis-type over time for the two different inflammation scenarios (salmonella infection and mucosal injury).

*Antigen uptake.* Macrophages can take up antigen and present it on MHCII. Their importance in antigen presentation to T cells, however, is controversial, especially because of their inability to migrate to LNs [73]. Therefore, a direct role in activation of naive and central memory T cells is not plausible, but presentation of antigen to and activation of effector memory T cells and effector T cells seems possible (described in detail in Section 2.11. paragraph *Effector memory T cells (LP)*).

We implemented antigen uptake by all macrophages populations (P1 to P4 and efferocytosis-

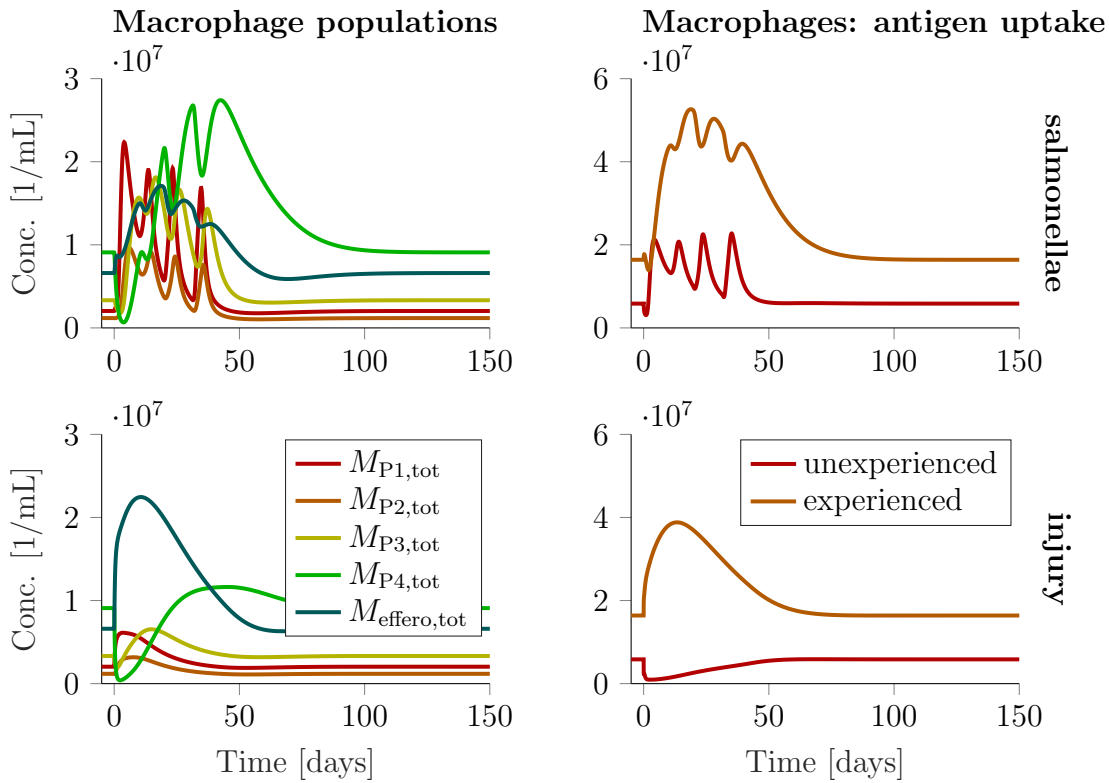


Figure 9: **Macrophage dynamics.** Concentrations in LP of different macrophage subsets over time for the two inflammation scenarios of salmonella infection and mucosal injury. Left column: Time course of the different macrophage populations (P1 to P4 and efferocytosis-type); for each population the sum of antigen-unexperienced, antigen-experienced, pMHCII-depleted (see Section 2.13) and salmonella-infected (see Section 2.18.2) macrophages is shown. Right column: Time course of antigen-unexperienced and antigen-experienced macrophages; antigen-experienced macrophages include pMHCII-depleted (see Section 2.13) and salmonella-infected (see Section 2.18.2) macrophages; the sum over the macrophage populations (P1 to P4 and efferocytosis-type) is shown.

type) dependent on their specific phagocytosis rate. We only considered bacterial antigens; uptake of food or other antigens was neglected. Phagocytosis of a bacterial cell by an antigen-unexperienced macrophage leads to transition of this macrophage to an antigen-experienced state. The engulfed bacterial cell determines the bacteria-specificity of the antigen-experienced macrophage. The activation type (P1 to P4 or efferocytosis-type) remains the same. For every macrophage population, separate model species describe antigen-unexperienced ( $M_{P1}$ ,  $M_{P2}$ ,  $M_{P3}$ ,  $M_{P4}$ ,  $M_{effero}$ ) and antigen-experienced ( $M_{P1,a}$ ,  $M_{P2,a}$ ,  $M_{P3,a}$ ,  $M_{P4,a}$ ,  $M_{effero,a}$ ) macrophages, as shown in Figure 6. Deactivation of antigen-experienced macrophages was implemented analogous to deactivation of antigen-unexperienced macrophages. The transition rate from antigen-unexperienced to the respective antigen-experienced state equal the phagocytosis rate of bacteria attributable to the respective antigen-unexperienced state. Phagocytosis of bacteria by already antigen-experienced macrophages does not further influence the state, which is a simplification of the gradual progress of antigen uptake. In addition to phagocytosis of bacteria in LP, we considered a low rate of antigen uptake from the lumen. We assume this antigen uptake

rate constant  $\nu_{\text{ant.upt}} = 0.0144 \frac{1}{\text{h}}$  (corresponding to a half-life of unexperienced dendritic cells/macrophages of 2d in case of no bacteria in LP) to be equal between dendritic cells and the highly phagocytic P4 macrophage population, and lower for P1, P2 and P3 according to their reported lower phagocytic activities by factors  $w_{\text{phago,P1}} = 0.034$ ,  $w_{\text{phago,P2}} = 0.12$  and  $w_{\text{phago,P3}} = 0.31$ , respectively [59, Fig. 1e]. Both antigen uptake rates and the resulting antigen-experienced macrophage populations are bacteria-specific. Thus, the transition rate from an antigen-unexperienced macrophage population  $M_{P_i}$  to the respective antigen-experienced macrophage population  $M_{P_{i,a}}$  is

$$M_{P_i} \text{ antigen uptake rate}_b = \nu_{\text{ant.upt}} \cdot \text{Bact}_{\text{LP},b} \cdot M_{P_i} \cdot w_{\text{phago,P}_i} \\ + \frac{V_{\text{max,Phago}} \cdot \text{Bact}_{\text{LP},b}}{\frac{K_{\text{mPhago}}}{R_{\text{phago},b}} + \sum_b \text{Bact}_{\text{LP},b}} \cdot M_{P_i} \cdot w_{\text{phago,P}_i}$$

for each bacterial species  $b$ .

Figure 9 (right column) shows the time course of total antigen-unexperienced and total antigen-experienced macrophages over time for the two different inflammation scenarios (salmonella infection and mucosal injury). It shows that after mucosal injury, almost all macrophages immediately become antigen-experienced because of the large number of bacteria in LP. In salmonella infection the number of bacteria in LP is lower, and the inflammatory reaction is stronger and prolonged compared to mucosal injury, leading to a larger recruitment of macrophages. The outcome of this is a strong increase of antigen-experienced and a weaker increase of antigen-unexperienced macrophages, showing that the antigen uptake by macrophages is increased, but the recruitment (of antigen-unexperienced macrophages) is increased more.

In accordance with the description of the macrophage subpopulations by Bain et al. [59], after antigen encounter, macrophage populations P1 to P3 produce pro-inflammatory cytokines, and population P4 produces anti-inflammatory cytokines, i.e.  $M_{P_{1,a}}$ ,  $M_{P_{2,a}}$  and  $M_{P_{3,a}}$  produce pro-inflammatory cytokines, and  $M_{P_{4,a}}$  produces anti-inflammatory cytokines. Cytokine production and their effects are described in Section 2.14. In addition, antigen-experienced macrophages present the acquired antigen on their surface, and are able to activate T cells with the specific T cell receptor upon contact, as described in Section 2.10. This antigen presentation ability can be inhibited by regulatory T cells, as described in Section 2.13.

The resulting ODEs for the macrophage state variables are

$$\begin{aligned} \frac{d}{dt} M_{P1} &= \text{M recruitment rate} - \text{transition rate } M_{P1} \rightarrow M_{P2} \\ &\quad - M_{P1} \text{ efferocytosis rate} - M_{P1} \text{ antigen uptake rate} - \mu_M \cdot M_{P1} \\ \frac{d}{dt} M_{P1,a} &= - \text{transition rate } M_{P1,a} \rightarrow M_{P2,a} \\ &\quad - M_{P1,a} \text{ efferocytosis rate} + M_{P1} \text{ antigen uptake rate} - \mu_M \cdot M_{P1,a} \\ \frac{d}{dt} M_{P2} &= \text{transition rate } M_{P1} \rightarrow M_{P2} - \text{transition rate } M_{P2} \rightarrow M_{P3} \\ &\quad - M_{P2} \text{ efferocytosis rate} - M_{P2} \text{ antigen uptake rate} - \mu_M \cdot M_{P2} \\ \frac{d}{dt} M_{P2,a} &= \text{transition rate } M_{P1,a} \rightarrow M_{P2,a} - \text{transition rate } M_{P2,a} \rightarrow M_{P3,a} \end{aligned}$$

$$\begin{aligned}
& - M_{P2,a} \text{ efferocytosis rate} + M_{P2} \text{ antigen uptake rate} - \mu_M \cdot M_{P2,a} \\
\frac{d}{dt} M_{P3} &= \text{transition rate } M_{P2} \rightarrow M_{P3} - \text{transition rate } M_{P3} \rightarrow M_{P4} \\
& - M_{P3} \text{ efferocytosis rate} - M_{P3} \text{ antigen uptake rate} - \mu_M \cdot M_{P3} \\
\frac{d}{dt} M_{P3,a} &= \text{transition rate } M_{P2,a} \rightarrow M_{P3,a} - \text{transition rate } M_{P3,a} \rightarrow M_{P4,a} \\
& - M_{P3,a} \text{ efferocytosis rate} + M_{P3} \text{ antigen uptake rate} - \mu_M \cdot M_{P3,a} \\
\frac{d}{dt} M_{P4} &= \text{transition rate } M_{P3} \rightarrow M_{P4} \\
& - M_{P4} \text{ efferocytosis rate} - M_{P4} \text{ antigen uptake rate} - \mu_M \cdot M_{P4} \\
\frac{d}{dt} M_{P4,a} &= \text{transition rate } M_{P3,a} \rightarrow M_{P4,a} \\
& - M_{P4,a} \text{ efferocytosis rate} + M_{P4} \text{ antigen uptake rate} - \mu_M \cdot M_{P4,a} \\
\frac{d}{dt} M_{\text{effero}} &= M_{P1} \text{ efferocytosis rate} + M_{P2} \text{ efferocytosis rate} \\
& + M_{P3} \text{ efferocytosis rate} + M_{P4} \text{ efferocytosis rate} \\
& - M_{\text{effero}} \text{ antigen uptake rate} - \mu_M \cdot M_{\text{effero}} \\
\frac{d}{dt} M_{\text{effero},a} &= M_{P1,a} \text{ efferocytosis rate} + M_{P2,a} \text{ efferocytosis rate} \\
& + M_{P3,a} \text{ efferocytosis rate} + M_{P4,a} \text{ efferocytosis rate} \\
& + M_{\text{effero}} \text{ antigen uptake rate} - \mu_M \cdot M_{\text{effero},a}
\end{aligned}$$

In Section 2.13, the influence of regulatory T cells on antigen-presenting macrophages is described, with some additional rates to be added to the above ODEs. All antigen-experienced macrophage state variables and corresponding reactions are bacteria-specific (subscript b neglected here for readability).

## 2.9 Dendritic cells

Dendritic cells are another cell type that eliminates pathogens by phagocytosis [29]. Their phenotype is very similar to macrophages, but in contrast to macrophages, dendritic cells are able to migrate to the LN [73]. This is related to their main function: presentation of the antigen from the phagocytosed and degraded pathogen via MHCII on their surface, and thereby activation of T cells, mainly in the LN [29]. Through that, dendritic cells provide the link between the innate and adaptive immune systems [29]. In most tissues, dendritic cells that sense bacterial antigens become activated and subsequently elicit pro-inflammatory T helper cell responses [29]. In contrast, in the LP, dendritic cells that enter the mucosal tissue from blood are kept in a quiescent state by the local cytokine milieu, so that recognition of bacterial antigen does not result in activated dendritic cells that mediate pro-inflammatory T cell responses [29]. Instead, these so-called tolerogenic dendritic cells (antigen-experienced, but not activated) trigger regulatory T cell responses, which are anti-inflammatory [76]. To become activated, dendritic cells in the gut need additional pro-inflammatory stimuli from their environment [29, 77]. This mechanism plays a crucial role in the toleration of commensal bacteria [29].

Dendritic cells can be classified into a variety of different types [77–79]. We sum-



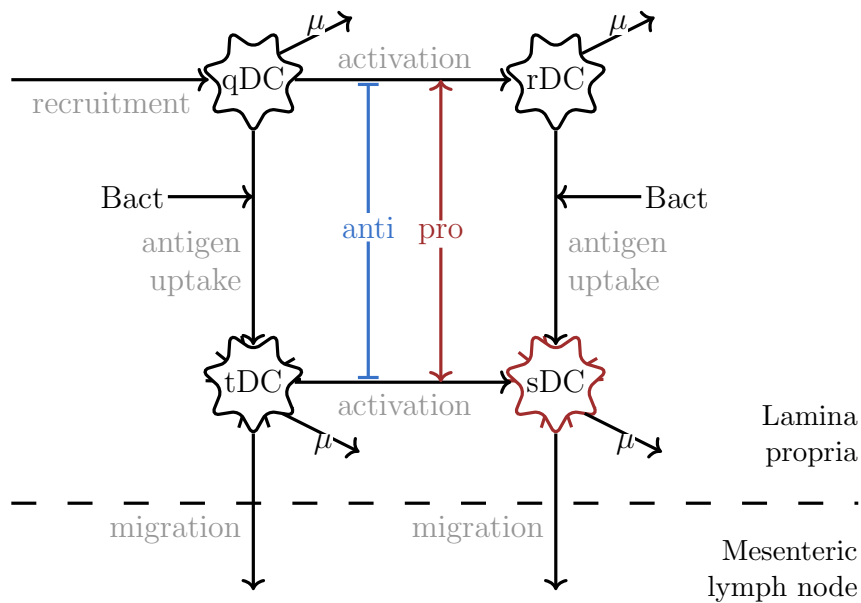


Figure 10: **Dendritic cell submodel.** Dendritic cells in the LP were implemented as four different state variables: quiescent dendritic cells qDC, responsive dendritic cells rDC, tolerogenic dendritic cells tDC and stimulatory dendritic cells sDC. Arrows indicate inflow, death, migration and transition between states, with rate constants on the arrows or rates given in the text for the reactions labeled in grey. Arrows targeting on arrows mean stimulating ( $\longrightarrow$ ) or inhibiting ( $\longrightarrow$ ) influence on this reaction. pro: pro-inflammatory cytokines  $\text{cyto}_{\text{pro,act,DC}}$ ; anti: anti-inflammatory cytokines  $\text{cyto}_{\text{anti,act,DC}}$ .

marised the different types, and only differentiated between four different dendritic cell states, dependent on activation state and antigen uptake: quiescent dendritic cells (qDC; not activated, antigen-unexperienced), tolerogenic dendritic cells (tDC<sub>LP</sub>; not activated, antigen-experienced), responsive dendritic cells (rDC; activated, antigen-unexperienced), stimulatory dendritic cells (sDC<sub>LP</sub>; activated, antigen-experienced). As for macrophages, we only considered antigen from bacterial cells, and did not account for other antigen such as food antigen. Figure 10 shows the four different dendritic cell states in LP and transition rates between them. Figure 11 shows the time course of the implemented four different dendritic cell states in LP in the two simulation scenarios (salmonella infection and mucosal injury).

*Recruitment.* The concentration of dendritic cells in healthy steady state was calculated based on the reported concentration of T cells in colon LP [80] and the fractions of T cells and dendritic cells from mononuclear cells in colon LP [81, 82], resulting in  $\text{DC}_{\text{tot,LP,ss}} = 5.65 \cdot 10^6 \frac{1}{\text{mL}}$ . The half-life of dendritic cells in tissue is 2 d [83–85], yielding a death rate constant of  $\mu_{\text{DC,LP}} = 0.014 \frac{1}{\text{h}}$ . For dendritic cells, no additional recruitment in response to inflammatory stimuli was implemented. The constant recruitment rate constant  $\lambda_{\text{DC}}$  was calculated such that the literature steady state concentrations were ensured in healthy steady state. As this depends not only on the death rate, but also on activation and migration rates, the calculation of this parameter is described at the end of the section (paragraph *Migration to LN*).

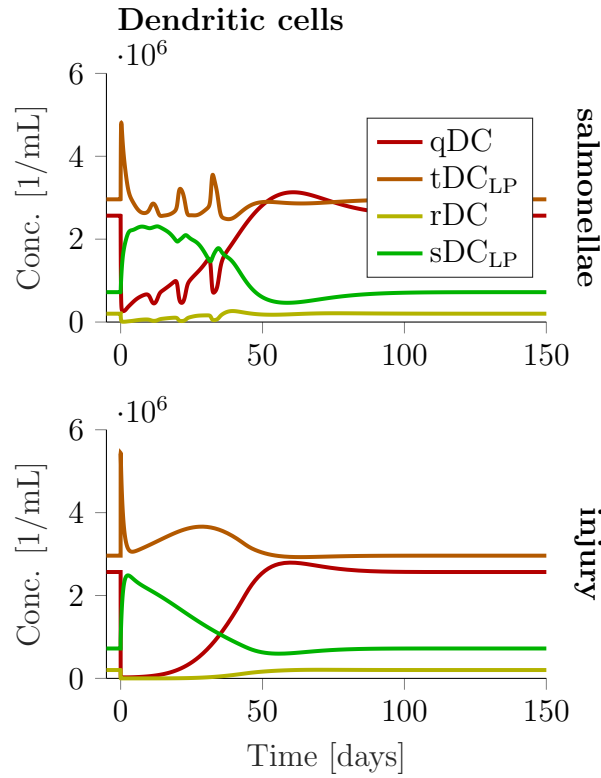
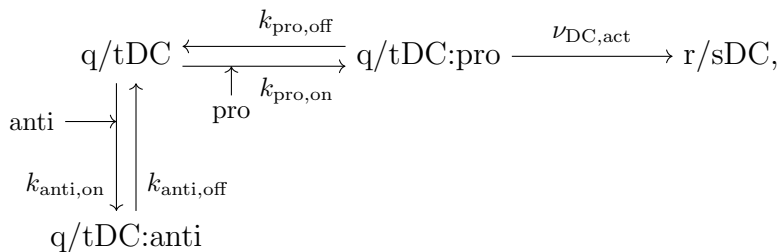


Figure 11: **Dendritic cell dynamics.** Concentrations of quiescent (qDC), tolerogenic (tDC), responsive (rDC) and stimulatory (sDC) dendritic cells in LP over time for the two inflammation scenarios of salmonella infection and mucosal injury. tDC and sDC include also the respective pMHCII-depleted dendritic cells (see Section 2.13).

*Activation.* Dendritic cells enter the tissue as qDC, and, if not activated, become tDC<sub>LP</sub> after antigen uptake (see next paragraph *Antigen uptake*), which induce an anti-inflammatory T cell response in the LN. Only when qDC or tDC<sub>LP</sub> are activated by an inflammatory environment, they become responsive or, if antigen-experienced, stimulatory dendritic cells that can induce a pro-inflammatory T cell response. The term activation here refers to transition from a quiescent or tolerogenic to a responsive or stimulatory state, i.e. the transition from dendritic cells eliciting anti-inflammatory adaptive immune responses to dendritic cells eliciting pro-inflammatory responses. We implemented activation of qDC and tDC<sub>LP</sub> (resulting in rDC and sDC<sub>LP</sub>, respectively) analogous to the deactivation of macrophages (see Section 2.8, paragraph *Deactivation*), with pro-inflammatory cytokines stimulating and anti-inflammatory cytokines inhibiting activation, according to the following scheme:



resulting in the activation rate

$$\text{q/tDC activation rate} = \frac{\nu_{\text{DC,act}} \cdot \text{cyto}_{\text{pro,act,DC}}^{h_{\text{pro,act,DC}}}}{1 + \text{cyto}_{\text{pro,act,DC}}^{h_{\text{pro,act,DC}}} + \text{cyto}_{\text{anti,act,DC}}^{h_{\text{anti,act,DC}}}} \cdot \text{q/tDC},$$

where  $\text{cyto}_{\text{pro,act,DC}} = \text{pro}$ ,  $\text{cyto}_{\text{anti,act,DC}} = \text{anti}$ , the cytokine concentrations are normalised by the corresponding  $K_m$  or  $K_I$ , and the Hill factors are set to 1 for the reference individual. The maximal activation rate was set to  $\nu_{\text{DC,act}} = 0.03 \frac{1}{\text{h}}$ , based on the resulting time course.

*Antigen uptake.* Antigen uptake of dendritic cells was implemented analogous to antigen uptake by macrophages (see Section 2.8, paragraph *Antigen uptake*). The resulting bacteria-specific antigen uptake rate by qDC and rDC (resulting in  $\text{tDC}_{\text{LP}}$  and  $\text{sDC}_{\text{LP}}$ , respectively) is thus

$$\begin{aligned} \text{q/rDC antigen uptake rate} &= \nu_{\text{ant.upt}} \cdot \text{Bact}_{\text{Lu},b} \cdot \text{q/rDC} \\ &+ \frac{V_{\text{max,Phago}} \cdot \text{Bact}_{\text{LP},b}}{\frac{K_{\text{mPhago}}}{R_{\text{phago},b}} + \sum_b \text{Bact}_{\text{LP},b}} \cdot \text{q/rDC} \end{aligned}$$

for each bacterial species  $b$ , where the first summand describes the sampling of bacterial antigen from the lumen, and the second summand describes phagocytosis of bacteria in LP. The antigen uptake rate and the antigen-experienced dendritic cell states  $\text{tDC}_{\text{LP}}$  and  $\text{sDC}_{\text{LP}}$  are bacteria-specific.

*Migration to LN.* Antigen-experienced dendritic cells migrate via the lymph to the draining mesenteric LNs. There they present antigen on their surface via MHCII. In experiments with Dendra-2 photoconvertible mice, 85% of migratory dendritic cells (in contrast to resident dendritic cells, which we did not account for in our model) of the LN were replaced after 24 h (Vuk Cerovic, RWTH Aachen, unpublished observations). Assuming a first-order exit rate from the LN, the rate constant results to be  $\mu_{\text{DC,LN}} = 1.9 \frac{1}{\text{d}}$ . Tentative estimations of a dendritic cell ratio in LP to LN of 10 (Vuk Cerovic, RWTH Aachen, unpublished observations) would yield a rate constant of  $k = 0.19 \frac{1}{\text{d}}$  of the dendritic cells in LP leaving for the LN per day, assuming that all dendritic cells leaving the LP end up in LN and that migration from LP is the only inflow rate of dendritic cells into the LN. As, however, only antigen-experienced dendritic cells ( $\text{tDC}$  and  $\text{sDC}$ ) migrate to the LN, the migration rate constant has to be adapted accordingly.

The rate constants for migration  $\epsilon_{\text{DC}}$  of  $\text{tDC}$  and  $\text{sDC}$  to LN and for recruitment  $\lambda_{\text{DC}}$  of qDC into LP were calculated based on the literature values for the steady state concentrations of dendritic cells and bacterial cells in LP, the derived death rate constant  $\mu_{\text{DC,LP}}$  and the derived rate constant  $k$  of total dendritic cells leaving the LP for the LN per day. The concentration of bacterial cells in healthy colon LP was reported to be  $\text{Bact}_{\text{LP,ss}} = 2.7 \cdot 10^5 \frac{1}{\text{mL}}$  [55]. In the following calculation, we only had to account for commensal bacteria, as the situation refers to the healthy steady state (i.e.  $\text{Bact}_{\text{Lu,commensal}} = 1$  and  $R_{\text{phago,commensal}} = 1$ ). From

$$\frac{d}{dt}(\text{tDC}_{\text{LP}} + \text{sDC}_{\text{LP}}) = \nu \cdot (\text{qDC} + \text{rDC}) - (\mu_{\text{DC,LP}} + \epsilon_{\text{DC}}) \cdot (\text{tDC}_{\text{LP}} + \text{sDC}_{\text{LP}}),$$

with  $\nu = \nu_{\text{ant.upt}} + \frac{V_{\text{max,Phago}} \cdot \text{Bact}_{\text{LP,ss}}}{K_{\text{mPhago}} + \text{Bact}_{\text{LP,ss}}}$  describing the antigen uptake rate per antigen-unexperienced dendritic cell (qDC or rDC), follows for the concentration of antigen-experienced LP dendritic cells

$$\text{tDC}_{\text{LP}} + \text{sDC}_{\text{LP}} = \frac{\nu}{\mu_{\text{DC,LP}} + \nu + \epsilon_{\text{DC}}} \cdot \text{DC}_{\text{tot,LP,ss}}.$$

The total dendritic cell migration rate is

$$k \cdot \text{DC}_{\text{tot,LP,ss}} = \epsilon_{\text{DC}} \cdot (\text{tDC}_{\text{LP}} + \text{sDC}_{\text{LP}}).$$

Using the above derived concentration of antigen-experienced dendritic cells as function of total dendritic cells, results in

$$\epsilon_{\text{DC}} = \frac{k \cdot (\nu + \mu_{\text{DC,LP}})}{\nu - k} = 0.009 \frac{1}{\text{h}}.$$

In steady state, the inflow equals the outflow of dendritic cells, i.e. the recruitment rate equals the sum of the death rate and the migration rate:

$$\lambda_{\text{DC}} = \mu_{\text{DC,LP}} \cdot \text{DC}_{\text{tot,LP,ss}} + k \cdot \text{DC}_{\text{tot,LP,ss}} = 1.26 \cdot 10^5 \frac{1}{\text{mL} \cdot \text{h}}.$$

Due to differences in simulated steady state concentrations of bacteria in LP to the literature value, the resulting simulated steady state concentration of dendritic cells in LP is slightly higher than the calculated literature concentration ( $\text{DC}_{\text{tot,LP,ss}} = 6.45 \cdot 10^6 \frac{1}{\text{mL}}$  compared to  $\text{DC}_{\text{tot,LP,ss}} = 5.65 \cdot 10^6 \frac{1}{\text{mL}}$  as calculated in paragraph *Recruitment* using literature data [80–82]).

The resulting ODEs for the dendritic cell state variables are

$$\begin{aligned} \frac{d}{dt} \text{qDC} &= \lambda_{\text{DC}} - \mu_{\text{DC,LP}} \cdot \text{qDC} - \text{qDC antigen uptake rate} - \text{qDC activation rate} \\ \frac{d}{dt} \text{rDC} &= -\mu_{\text{DC,LP}} \cdot \text{rDC} - \text{rDC antigen uptake rate} + \text{qDC activation rate} \\ \frac{d}{dt} \text{tDC}_{\text{LP}} &= \text{qDC antigen uptake rate} - \text{tDC activation rate} - (\mu_{\text{DC,LP}} + \epsilon_{\text{DC}}) \cdot \text{tDC}_{\text{LP}} \\ \frac{d}{dt} \text{sDC}_{\text{LP}} &= \text{rDC antigen uptake rate} + \text{tDC activation rate} - (\mu_{\text{DC,LP}} + \epsilon_{\text{DC}}) \cdot \text{sDC}_{\text{LP}} \\ \frac{d}{dt} \text{tDC}_{\text{LN}} &= \epsilon_{\text{DC}} \cdot \text{tDC}_{\text{LP}} \cdot \frac{V_{\text{LP}}}{V_{\text{LN}}} - \mu_{\text{DC,LP}} \cdot \text{tDC}_{\text{LN}} \\ \frac{d}{dt} \text{sDC}_{\text{LN}} &= \epsilon_{\text{DC}} \cdot \text{sDC}_{\text{LP}} \cdot \frac{V_{\text{LP}}}{V_{\text{LN}}} - \mu_{\text{DC,LP}} \cdot \text{sDC}_{\text{LN}}. \end{aligned}$$

Note that  $\text{tDC}_{\text{LP}}$ ,  $\text{sDC}_{\text{LP}}$ ,  $\text{tDC}_{\text{LN}}$ ,  $\text{sDC}_{\text{LN}}$  and all corresponding reaction rates are bacteria-specific. In Section 2.13 the influence of regulatory T cells on antigen-presenting dendritic cells is described, with some additional rates to be added in the above ODEs.

## 2.10 Antigen presentation to T cells

In the following sections (Section 2.10 - 2.13) we will describe the implementation of T cell dynamics and effects in our model. T cells are part of the adaptive immune response; they provide targeted effects against pathogens. T cells present T cell receptors (TCRs) on their cell surface, where all TCRs of one T cell are identical, but TCRs of different T cells are different. The TCR binds to a complex of a foreign peptide bound to the cell surface receptor MHCII (peptide:MHCII, pMHCII). Each TCR only binds to very specific peptides. In the case of a bacterial infection, bacterial antigens enter the host tissue, are taken up by antigen-presenting cells (APCs) (dendritic cells and macrophages), and are subsequently presented as small peptides via MHCII on the APC's cell surface. Naive T cells circulate through LNs. Upon encounter of an APC they search its surface for their cognate antigen. Binding of the TCR to its cognate antigen leads to a closer and longer contact between the T cell and the APC, and the T cell receives additional signals from the APC that stimulate the T cell to proliferate and also determine the effector type the T cell will differentiate into. The thus stimulated naive T cells proliferate efficiently for several days, the so-called expansion phase, leading to a large increase in T cell numbers, and then differentiate into effector T cells with specific functions. T cells derived from the same naive T cell have the same TCR. At the end of an infection, when the invading pathogen is cleared, most effector T cells die; this is called the contraction phase. Some effector T cells, however, survive as memory T cells. Memory T cells are long-lived and can, in the case of a renewed infection with the same pathogen, be again activated by an APC presenting their cognate antigen, similar to activation of naive T cells, but with faster and less pronounced proliferation, enabling a faster and more efficient immune response in secondary compared to primary infection. Memory T cells can be divided into two classes: Central memory T cells circulate through LNs (similar to naive T cells) and, when activated, proliferate and differentiate into effector memory T cells. Effector memory T cells circulate through the tissues and, when activated, proliferate and differentiate into effector T cells. The two main T cell populations are distinguishable by the surface proteins CD4 and CD8 and give rise to different effector T cells: CD4<sup>+</sup> T cells differentiate into either regulatory T cells or T helper cells, which play important roles in bacterial infections, parasite infections and allergic reactions. CD8<sup>+</sup> T cells differentiate into cytotoxic T cells, which kill virus-infected or tumour cells [29].

As we focused our model on bacterial infections of the gut LP, we did not account for CD8<sup>+</sup> T cells, but only included CD4<sup>+</sup> T cells, i.e. in the sequel, T cells will refer to CD4<sup>+</sup> T cells. In addition, we simplified memory T cell generation: We did not account for the influence of an acute immune reaction on the memory T cell repertoire, but considered it constant, i.e. with constant fractions of memory T cells for the different bacterial antigens over time. As commensal bacteria are always present, we assumed that memory T cells specific for commensal antigens are existing; for pathogens that have not been encountered before (in our simulations of infection with salmonellae or extracellular pathogens), we assumed the fraction of specific memory T cells to be smaller but still existing due to conserved structures between bacterial strains that allow for cross-reactivity between different bacterial strains [86].

For the induction of a T cell immune response, the naive or memory T cell must encounter its cognate antigen presented by an APC (see Section 2.11). In addition, T helper cells need to be activated by APCs to produce pro-inflammatory cytokines (see Section 2.14), regulatory T cells inhibit antigen presentation by APCs in an antigen-

specific manner (see Section 2.13), and T helper cells type 1 help macrophages presenting their cognate antigen with the elimination of intracellular bacteria (see Section 2.18.2). For the implementation of all of these processes, we therefore need the contact rate between T cells and APCs in LN and LP. We start with the derivation of the concentration of contacts between T cells and dendritic cells, and then adapt for macrophages. Differences between LN and LP are given if applicable.

The contact rates of T cells and dendritic cells in the LN have been estimated via several methods in the literature: Miller et al. (2004) [87] counted the contacts of single fluorescence-labeled dendritic cells with fluorescence-labeled T cells and back-calculated the contact rate using the fraction of labeled T cells, resulting in  $4630 \pm 670$  contacts per h per dendritic cell. Beltman et al. (2007) [88] performed an *in silico* study, simulating T cell and dendritic cell migration in the LN environment, reporting about 2000 contacts per h per dendritic cell or 100 contacts per h per T cell. Mandl et al. (2012) [89] measured transit times of T cells and contact durations and, assuming T cells to be in contact with one dendritic cell at every time point, estimated that each T cell contacts 160-320 dendritic cells per LN transit ( $\approx 12.2$  h), resulting in 13-26 contacts per h per T cell. In contrast to Mandl et al. [89], Beltman et al. [88] and Miller et al. [87] assumed that one T cell can be in contact with multiple dendritic cells at a time. As multiple contacts seemed plausible to us, we included this possibility into the model. Miller et al. [87] measured the cell surface of dendritic cells and T cells to be  $\approx 2400 \mu\text{m}^2$  and  $\approx 140 \mu\text{m}^2$ , respectively, and the contact area to be on average  $\approx 8 \mu\text{m}^2$ . From that, assuming no further sterical hindrance, we calculated the number of binding sites per dendritic cell and T cell to be  $\text{bs}_{\text{perDC}} = 300$  and  $\text{bs}_{\text{perT}} = 17.5$ , respectively. As recently activated T cells (before the first division) stay in close contact to the dendritic cell and have frequent longer contacts with it [90], we assumed that these cells occupy binding sites on the dendritic cells that activated them, and thereby further limit the number of new contacts. We found different contact durations reported in the literature: 3.4 min [87], 1.3 min [88], 3-4 min [89], 2.5 min [91], 1 min [92], and used the mean of those:  $T_{\text{contact}} = 2.3$  min.

Using this information, we propose the following implementation of contact formation between T cells  $T_{\text{tot}}$  and dendritic cells  $\text{DC}_{\text{tot,LP}}$ , assuming similar binding characteristics of all types of T cells (except the recently activated ones) and of all types of dendritic cells:

$$\text{BS}_{\text{T,free}} + \text{BS}_{\text{DC,free}} \frac{k_{\text{on}}}{k_{\text{off}}} \text{contacts},$$

with total concentration of T cell binding sites  $\text{BS}_{\text{T}} = \text{BS}_{\text{T,free}} + \text{contacts} = T_{\text{tot}} \cdot \text{bs}_{\text{perT}}$  and total concentration of dendritic cell binding sites  $\text{BS}_{\text{DC}} = \text{BS}_{\text{DC,free}} + \text{contacts} + \text{BS}_{\text{DC,occ}} = \text{DC}_{\text{tot,LP}} \cdot \text{bs}_{\text{perDC}}$ , where  $\text{BS}_{\text{DC,occ}}$  describes the DC binding sites occupied by recently activated T cells, and  $\text{BS}_{\text{DC,av}} = \text{BS}_{\text{DC}} - \text{BS}_{\text{DC,occ}} = \text{BS}_{\text{DC,free}} + \text{contacts}$  describes the dendritic cell binding sites available for contact formation. As the formation and dissociation of contacts is on a much faster time scale than the change of dendritic cell and T cell concentrations (contact duration in minutes), we used the quasi-steady-state approximation to determine the concentration of contacts:

$$\begin{aligned} \frac{d}{dt} \text{contacts} &= 0 = k_{\text{on}} \cdot \text{BS}_{\text{T,free}} \cdot \text{BS}_{\text{DC,free}} - k_{\text{off}} \cdot \text{contacts} \\ 0 &= (\text{BS}_{\text{T}} - \text{contacts}) \cdot (\text{BS}_{\text{DC,av}} - \text{contacts}) - \frac{k_{\text{off}}}{k_{\text{on}}} \cdot \text{contacts} \end{aligned}$$

$$0 = \text{contacts}^2 - \left( \text{BS}_T + \text{BS}_{\text{DC,av}} + \frac{k_{\text{off}}}{k_{\text{on}}} \right) \cdot \text{contacts} + \text{BS}_T \cdot \text{BS}_{\text{DC,av}}$$

Solving the quadratic equation gives

$$\text{contacts} = \frac{\text{BS}_T + \text{BS}_{\text{DC,av}} + \frac{k_{\text{off}}}{k_{\text{on}}} - \sqrt{(\text{BS}_T + \text{BS}_{\text{DC,av}} + \frac{k_{\text{off}}}{k_{\text{on}}})^2 - 4 \cdot \text{BS}_T \cdot \text{BS}_{\text{DC,av}}}}{2}.$$

The dissociation rate constant  $k_{\text{off}}$  is determined by the contact duration:  $k_{\text{off}} = T_{\text{contact}}^{-1}$ . The association rate constant  $k_{\text{on}}$  is determined by the contact rate constant between T cells and dendritic cells  $k_{\text{T:DC}}$ , corrected for the number of binding sites per T cell and dendritic cell  $k_{\text{on}} = \frac{k_{\text{T:DC,LN}}}{\text{bs}_{\text{perT}} \cdot \text{bs}_{\text{perDC}}}$  in LN and  $k_{\text{on}} = \frac{k_{\text{T:DC,LP}}}{\text{bs}_{\text{perT}} \cdot \text{bs}_{\text{perDC}}}$  in LP, resulting in two different concentrations of contacts in LN and LP ( $\text{contacts}_{\text{LN}}$  and  $\text{contacts}_{\text{LP}}$ ). We chose the contact rate constant  $k_{\text{T:DC,LN}} = 2 \cdot 10^{-5} \frac{\text{mL}}{\text{h}}$  so that the resulting steady state contact rates, 2132 contacts per h per dendritic cell, were in the same order as those reported by Miller et al. [87] and Beltman et al. [88]. This implied that in steady state, in the LN each dendritic cell was on average in contact with 204 T cells at a time, and each T cell was on average in contact with 3 dendritic cells at a time.

As, in contrast to the LN, the environment of the LP is not specialised for T cell - dendritic cell contacts [93], we assumed the contact rate constant to be lower by a factor 10, i.e.  $k_{\text{T:DC,LP}} = 2 \cdot 10^{-6} \frac{\text{mL}}{\text{h}}$ , so that in the steady state LP each dendritic cell was on average in contact with 33 T cells at a time, and each T cell was on average in contact with 0.7 dendritic cells at a time.

In the LP, not only dendritic cells, but also macrophages present antigen on MHCII on their cell surface. Therefore it is assumed that macrophages can, at least to some extent, present antigen to T cells, too. However, the role of macrophages in T cell stimulation is controversial, and surely lower than the role of dendritic cells [73]. Therefore, in the LP, we did not only consider dendritic cells, but also macrophages (together: APCs) as contact partners for T cells. To account for the smaller role of macrophages, we assumed the number of binding sites smaller than for dendritic cells by factor 20:  $\text{bs}_{\text{perM}} = 15$ , while assuming the same binding characteristics. This results in a concentration of available binding sites on APCs

$$\begin{aligned} \text{BS}_{\text{APC,av}} &= \text{BS}_{\text{APC}} - \text{BS}_{\text{APC,occ}} \\ &= \text{DC}_{\text{tot,LP}} \cdot \text{bs}_{\text{perDC}} + M_{\text{tot}} \cdot \text{bs}_{\text{perM}} - \text{BS}_{\text{APC,occ}}, \end{aligned}$$

where  $\text{BS}_{\text{APC,occ}}$  are again the binding sites occupied by recently activated T cells. From this follows that the role of a macrophage in comparison to a dendritic cell in T cell activation is lower by factor  $\frac{\text{bs}_{\text{perM}}}{\text{bs}_{\text{perDC}}} = 1/20$ . In LN we did not have to account for macrophages, as they are not able to migrate from the LP to the LN [73].

In summary, we calculate the concentrations of contacts in LN ( $\text{contacts}_{\text{LN}}$ ) and in LP ( $\text{contacts}_{\text{LP}}$ ) between all present T cells and APCs, replacing in the above equation for contacts  $\text{BS}_{\text{DC,av}}$  with  $\text{BS}_{\text{APC,av}}$ . The applying total concentrations of binding sites on T cells and APCs in LN and LP are

$$\text{BS}_{\text{T,LN}} = \left( \text{Tn} + \text{Tcm} + \sum_b \sum_{i=2}^{N_{\text{T,prol}}} \text{Tn2Teff}_i + \sum_b \sum_{i=2}^{N_{\text{T,prol}}} \text{Tcm2Tem}_i \right) \cdot \text{bs}_{\text{perT}}$$

$$\begin{aligned}
BS_{T,LP} &= \left( \sum_b T_{\text{eff}} + \sum_b T_{\text{em}} + \sum_b \sum_{i=2}^{N_{T,\text{prol}}} T_{\text{em}2T_{\text{eff}_i}} \right) \cdot b_{\text{SperT}} \\
BS_{\text{APC},\text{av},\text{LN}} &= (\text{tDC}_{\text{LN}} + \text{sDC}_{\text{LN}} + \text{tDC}_{\text{dep},\text{LN}} + \text{sDC}_{\text{dep},\text{LN}}) \cdot b_{\text{SperDC}} \\
&\quad - (T_{\text{n}2T_{\text{eff}_1}} + T_{\text{cm}2T_{\text{em}_1}}) \\
BS_{\text{APC},\text{av},\text{LP}} &= (\text{tDC}_{\text{LP}} + \text{sDC}_{\text{LP}} + \text{tDC}_{\text{dep},\text{LP}} + \text{sDC}_{\text{dep},\text{LP}}) \cdot b_{\text{SperDC}} + (M_{\text{P1},\text{a}} + M_{\text{P2},\text{a}} \\
&\quad + M_{\text{P3},\text{a}} + M_{\text{P4},\text{a}} + M_{\text{effero},\text{a}} + M_{\text{P1},\text{a},\text{dep}} + M_{\text{P2},\text{a},\text{dep}} + M_{\text{P3},\text{a},\text{dep}} + M_{\text{P4},\text{a},\text{dep}} \\
&\quad + M_{\text{effero},\text{a},\text{dep}}) \cdot b_{\text{SperM}} - T_{\text{em}2T_{\text{eff}_1}}
\end{aligned}$$

where  $T_{\text{n}}$ ,  $T_{\text{cm}}$  and  $T_{\text{em}}$  are naive, central memory and effector memory T cells,  $T_{\text{n}2T_{\text{eff}_1}}$ ,  $T_{\text{cm}2T_{\text{em}_1}}$  and  $T_{\text{em}2T_{\text{eff}_i}}$  are proliferating T cells (implemented as  $N_{T,\text{prol}}$  transit compartments, where the subscript 1 indicates the cells before first division, i.e. recently activated T cells occupying APC binding sites) and  $T_{\text{eff}}$  are effector T cells, described in the following Section 2.11 and Figure 14; and the subscript “dep” on APCs indicates pMHCII depletion by regulatory T cells, described in Section 2.13. To obtain the concentration of contacts between any specific subset of T cells and any specific subset of APCs, one has to multiply the total concentration of contacts in the respective tissue ( $\text{contacts}_{\text{LN}}$  or  $\text{contacts}_{\text{LP}}$ ) with the fraction of the specific T cell subset from the total T cell concentration ( $T_{\text{tot},\text{LN}}$  or  $T_{\text{tot},\text{LP}}$ ) and the fraction of available binding sites on the specific APC subset from the total available binding sites on APCs ( $BS_{\text{APC},\text{av},\text{LN}}$  or  $BS_{\text{APC},\text{av},\text{LP}}$ ).

## 2.11 TCR stimulation and T cell proliferation

Naive and central memory T cells frequently circulate through LNs [29]. They enter the LN via high endothelial venules, migrate to the T cell zones, and exit via cortical sinuses into the lymph, which brings them via the thoracic duct back into blood [94]. The egress from the LN is mediated via a gradient of sphingosine-1-phosphate (S1P), for which the T cells express the surface receptor S1PR1 [94]. When naive or memory T cells encounter their cognate antigen presented via MHCII by an APC, they become activated to proliferate and differentiate [29]. In the following hours, they first stay close to the stimulating APC, with frequent long contacts; after the first division the T cells only have brief contacts to APCs [90]. Expression of S1PR1 in T cells is downregulated after activation, but is then upregulated again, to an even higher level [95]. Effector T cells that have been activated by dendritic cells derived from the gut LP leave the mesenteric LN and migrate via the blood to the gut LP, a process called gut homing [96].

We first describe the TCR stimulation and differentiation of naive T cells by tolerogenic or stimulatory dendritic cells in the LN. Afterwards we describe the differences that apply in TCR stimulation and proliferation of central memory T cells. Lastly, we describe TCR stimulation and proliferation of effector memory T cells, which takes place in LP.

*Naive T cells (LN).* The mean residence time of naive T cells  $T_{\text{n}}$  in LNs was reported to be 9.6 h [89]. We calculated the concentration of naive T cells in the LN using literature values of the total concentration of CD4+ T cells in lymphoid tissue [97], and the fraction of naive T cells from CD4+ T cells [98] to be  $T_{\text{n,ss}} = 1.9 \cdot 10^8 \frac{1}{\text{mL}}$ . Using these values we calculated the inflow and egress rates of naive T cells in the mesenteric LNs to be  $\lambda_{T_{\text{n}}} = 1.9 \cdot 10^7 \frac{1}{\text{mL}\cdot\text{h}}$  and  $\mu_{T,\text{LN}} = 0.10 \frac{1}{\text{h}}$ , respectively. The resulting ODE for naive T cells



is

$$\frac{d}{dt}T_n = \lambda_{T_n} - \mu_{T,LN} \cdot T_n - T_n \text{ activation rate.}$$

In most cases of contact between a T cell and a dendritic cell, the T cell will not find an antigen matching its TCR. For naive T cells, the probability of a TCR to be specific for a given antigen is  $\approx 10^{-6} = \alpha_{T_n}$  [99, 100]. We assume that each bacterial cell has on average  $\beta = 10$  presentable antigens and each dendritic cell presents only antigen from one bacterial cell, i.e. from that bacterial cell it engulfed in the LP (in the reaction from  $qDC \rightarrow tDC_{LP}$  or  $rDC \rightarrow sDC_{LP}$ ). The activation rate of naive T cells is the dissociation rate (with dissociation rate constant  $T_{\text{contact}}^{-1}$ ) of contacts between naive T cells and APCs ( $\frac{T_n}{T_{\text{tot},LN}} \cdot \text{contacts}_{LN}$ ) multiplied by the probability that the naive T cell encounters its cognate antigen on the APC ( $\alpha_{T_n} \cdot \beta$ ), i.e.

$$T_n \text{ activation rate} = \frac{T_n}{T_{\text{tot},LN}} \cdot \frac{\alpha_{T_n} \cdot \beta}{T_{\text{contact}}} \cdot \text{contacts}_{LN}.$$

(Inhibition of this rate by regulatory T cells is not considered here, but will be described in Section 2.13.)

There are several published models of proliferation and apoptosis of activated T cells. Two of them seemed most accurate to us:

(i) The ‘‘Cyton model’’ described by Hawkins et al. (2007) [101] and consecutive publications [102–104]: It describes T cell growth by two competing times, the time to divide and the time to die, where the shorter one determines a cell’s fate. Those times are drawn from probability distributions for every cell and division cycle. They introduce the term of ‘‘division destiny’’, the division number at which cells stop to divide, which they show to be normally distributed. From the parameters of the normal distribution given by experimental data, they calculate back the so-called ‘‘progressor fraction’’, the fraction of cells that do not stop dividing after a given number of divisions.

(ii) The ‘‘T cell fate decision algorithm’’ by Arias et al. (2014) [105]: It describes T cell growth by competition of two inhibitory intracellular molecules: active Rb, which prevents cell cycle progression, and active Bcl-2, which prevents apoptosis, where the first of those two to drop below a threshold determines a cell’s fate. They reason that the number of cell surface receptors determines the change of those molecules over time. From the initial composition of receptors, which are randomly distributed between the two daughter cells of a dividing cell, they determine if a cell divides or dies. Through that ‘‘dilution’’ of receptors over time after the initial stimulation, the typical profile of initial expansion and subsequent contraction can be simulated.

Both of these models could not be directly implemented in our deterministic model because of their stochastic nature. However, we summarised the main ideas of those models [101, 105] as transition of activated T cells through several rounds of division, where in each division round there is a competition between death and further division, and the probability to stop division increases with higher numbers of division. Those main aspects were implemented in our model as follows (see also Figure 12): We used transit compartments  $T_n2T_{\text{eff}_i}$  ( $i = 1, \dots, N_{T,\text{prol}}$ ) to describe the T cells of different division numbers, with transition rates between them (describing the proliferation) being equal for all division numbers except the first, which is lower, accounting for the longer time to the first division [101]:  $p_{T_n,1} = 0.025 \frac{1}{h}$ ,  $p_{T_n,>1} = 0.11 \frac{1}{h}$ , representing a time to first division of 40 h and time for subsequent divisions of 9 h [101, 106]. As the transition rates

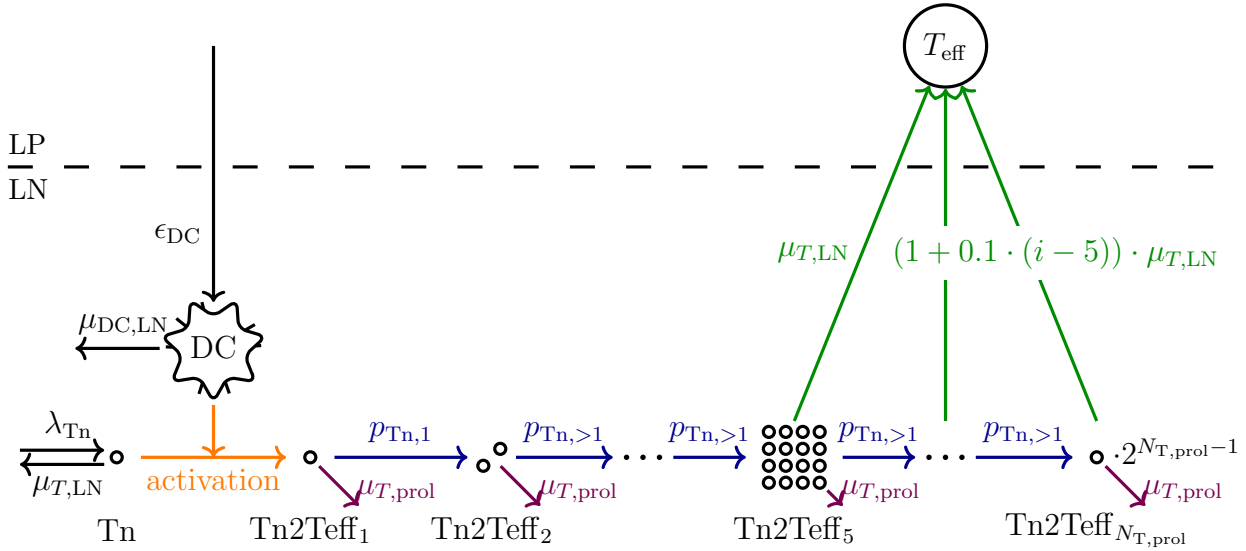


Figure 12: **Submodel of naive T cell stimulation, proliferation and differentiation.** Arrows indicate transitions between states, with rates as indicated by the rate constants on the arrows or given in the text for the  $T_n$  activation rate. Arrows targeting on arrows mean stimulating influence on this reaction. Colours should simplify reading, as they indicate the different processes: **Tn activation**, **proliferation of activated Tn**, **death of proliferating Tn**, **egress of fully differentiated T cells from LN into LP**.

between the transit compartments describe proliferation, we also need a stoichiometric coefficient of 2 for the product state variable, i.e.  $Tn2Teff_i \rightarrow 2 Tn2Teff_{i+1}$ . The transit compartment  $Tn2Teff_i$  consequently describes the proliferating and differentiating T cells that have divided  $i - 1$  times. Death of proliferating T cells was implemented using the rate constant  $\mu_{T,prol} = 0.047 \frac{1}{h}$  [106] independent of the division number. Egress of T cells from the LN is mediated by S1PR1, which is downregulated after activation, so that T cells can not leave the LN, but then upregulated again [95]. Pham et al. (2008) [107] described the egress of activated naive T cells from the LNs to occur only after 4 divisions, and to increase with the division number. We therefore implemented egress rates from the transit compartments  $Tn2Teff_{\geq 5}$  with increasing egress rates for higher division numbers. We assumed a base egress rate constant equal to the egress rate constant of naive T cells  $\mu_{T,LN}$  for  $Tn2Teff_5$ , and an increase by 10% after each additional division, i.e.  $(1 + 0.1 \cdot (i - 5)) \cdot \mu_{T,LN}$  for  $Tn2Teff_i, i > 5$  to mimic the increasing egress rates reported by Pham et al. [107, Fig. 6B]. T cells leaving the  $Tn2Teff$  compartments migrate as fully differentiated effector T cells  $T_{eff}$  to the LP. The number of transit compartments  $N_{T,prol} = 18$  was chosen so that a higher number would not make a significant effect to the simulation (i.e.  $Tn2Teff_{N_{T,prol}} \approx 0$ ). Figure 12 shows the model of naive T cell stimulation, proliferation and differentiation into effector T cells. Figure 13 (left) shows the numbers of proliferating T cells of different division numbers over time per activated naive T cell.

The resulting ODEs for the transit compartments describing proliferating and differ-

entiating T cells are

$$\begin{aligned}\frac{d}{dt}\text{Tn2Teff}_1 &= \text{Tn activation rate} - p_{\text{Tn},1} \cdot \text{Tn2Teff}_1 - \mu_{T,\text{prol}} \cdot \text{Tn2Teff}_1 \\ \frac{d}{dt}\text{Tn2Teff}_2 &= p_{\text{Tn},1} \cdot \text{Tn2Teff}_1 - p_{\text{Tn},>1} \cdot \text{Tn2Teff}_2 - \mu_{T,\text{prol}} \cdot \text{Tn2Teff}_2 \\ \frac{d}{dt}\text{Tn2Teff}_i &= p_{\text{Tn},>1} \cdot \text{Tn2Teff}_{i-1} - p_{\text{Tn},>1} \cdot \text{Tn2Teff}_i - \mu_{T,\text{prol}} \cdot \text{Tn2Teff}_i \\ &\quad - (1 + 0.1 \cdot (i - 5)) \cdot \mu_{T,\text{LN}} \cdot \text{Tn2Teff}_i \cdot \mathbf{1}_{\{i \geq 5\}},\end{aligned}$$

for  $i = 3, \dots, N_{T,\text{prol}}$ , where  $\mathbf{1}_{\{i \geq 5\}} = \begin{cases} 1, & \text{if } i \geq 5 \\ 0, & \text{if } i < 5 \end{cases}$ . Subscripts  $b$  are omitted for readability; all proliferating T cells are bacteria-specific, with identical parameters for all bacterial species (additional details in the following Section 2.12).

*Central memory T cells (LN).* For central memory T cells Tcm, we assumed inflow and egress to be similar to naive T cells, i.e. the same egress rate constant  $\mu_{T,\text{LN}}$  and the inflow rate constant corrected by the ratio of naive and central memory T cells in the blood (implying a first-order inflow rate with same rate constant for both T cell types):  $\lambda_{\text{Tcm}} = \lambda_{\text{Tn}} \cdot \frac{\text{fraction Tcm of CD4+ (bl)}}{\text{fraction Tn of CD4+ (bl)}} = 1.8 \cdot 10^7 \frac{1}{\text{mL}\cdot\text{h}}$  (fractions in blood from [98]). The resulting steady state concentration of central memory T cells in LN was  $\text{Tcm}_{\text{ss}} = 1.2 \cdot 10^8 \frac{1}{\text{mL}}$ , slightly lower than the literature value of  $3.1 \cdot 10^8 \frac{1}{\text{mL}}$  (calculated from the total concentration of CD4+ T cells in lymphoid tissue [97], and the fraction of central memory T cells from CD4+ T cells [98]). The resulting ODE for central memory T cells is

$$\frac{d}{dt}\text{Tcm} = \lambda_{\text{Tcm}} - \mu_{T,\text{LN}} \cdot \text{Tcm} - \text{Tcm activation rate}.$$

The stimulation and proliferation of central memory T cells was implemented largely similar to that of naive T cells, with the following differences: The number of different TCR specificities in naive T cells was reported to be  $\approx 166$  times higher than the number of TCR specificities in memory T cells [108], resulting in a probability of a memory T cell's TCR to be specific for a given antigen of  $\alpha_{\text{Tm},b} = 1.66 \cdot 10^{-4}$  for an antigen that has been encountered before, and  $\alpha_{\text{Tm},b} = 1.66 \cdot 10^{-4} \cdot R_{\text{Tm},b}$  for an antigen that has not been encountered before, where  $0 \leq R_{\text{Tm},b} \leq 1$  describes the degree of partial recognition of bacterial antigens due to conserved structures [86]. We chose  $\alpha_{\text{Tm},\text{commensal}} = 1.66 \cdot 10^{-4}$  (i.e.  $R_{\text{Tm},\text{commensal}} = 1$ ) and  $\alpha_{\text{Tm},\text{extracellular}} = \alpha_{\text{Tm},\text{salmonellae}} = 1.66 \cdot 10^{-4} \cdot 0.7$  (i.e.  $R_{\text{Tm},\text{extracellular}} = R_{\text{Tm},\text{salmonellae}} = 0.7$ ), as commensal bacteria are permanently present and therefore well recognised by the immune system, and the salmonellae and extracellular bacteria in our simulations have not been encountered by the immune system before, but can still be recognised (although to a lower extent). The resulting activation rate of central memory T cells is

$$\text{Tcm activation rate} = \frac{\text{Tcm}}{T_{\text{tot,LN}}} \cdot \frac{\alpha_{\text{Tm},b} \cdot \beta}{T_{\text{contact}}} \cdot \text{contacts}_{\text{LN}}.$$

Transit compartments of proliferating central memory T cells are called Tcm2Tem; T cells leaving the Tcm2Tem compartments migrate to the LP as effector memory T cells Tem. As proliferation of memory T cells is shorter and therefore faster than proliferation of naive T cells, and T cell responses occur shortly after simulation, we used the same

proliferation rate constant  $p_{Tn,>1}$  for all transit compartments but implemented the possibility of egress already before first division, with the same increase in egress rates for higher division numbers as for naive T cells.

$$\begin{aligned} \frac{d}{dt} T_{cm2Tem_1} &= T_{cm} \text{ activation rate} - p_{Tn,>1} \cdot T_{cm2Tem_1} - \mu_{T,prol} \cdot T_{cm2Tem_1} \\ \frac{d}{dt} T_{cm2Tem_i} &= p_{Tn,>1} \cdot T_{cm2Tem_{i-1}} - p_{Tn,>1} \cdot T_{cm2Tem_i} - \mu_{T,prol} \cdot T_{cm2Tem_i} \\ &\quad - (1 + 0.1 \cdot (i - 1)) \cdot \mu_{T,LN} \cdot T_{cm2Tem_i}, \end{aligned}$$

for  $i = 2, \dots, N_{T,prol}$ . Subscripts  $b$  are omitted for readability; all proliferating T cells are bacteria-specific, with identical parameters for all bacterial species except  $\alpha_{Tm,b}$  (additional details in the following Section 2.12).

*Effector memory T cells (LP).* In contrast to naive and central memory T cells, effector memory T cell stimulation and proliferation takes place in LP. We neglected possible loss of T cells during gut homing, i.e. migration from the LN to the LP. Therefore, the inflow of effector memory T cells  $Tem$  into LP is defined by the outflow of fully differentiated  $Tem$  from proliferating  $T_{cm}$  in LN. The lifespan of effector memory T cells is 164 d [109], i.e.  $\mu_{Tem} = 2.5 \cdot 10^{-4} \frac{1}{h}$ .

$$\begin{aligned} \frac{d}{dt} Tem &= \sum_{i=1}^{N_{T,prol}} (1 + 0.1 \cdot (i - 1)) \cdot \mu_{T,LN} \cdot T_{cm2Tem_i} \cdot \frac{V_{LN}}{V_{LP}} \\ &\quad - \mu_{Tem} \cdot Tem - Tem \text{ activation rate} \end{aligned}$$

The stimulation and proliferation of effector memory T cells was implemented similar to that of naive T cells, the only difference are the stimulating APCs, as in LP there are macrophages in addition to dendritic cells. As described in Section 2.10, the role of macrophages in T cell activation is controversial, which is why we implemented their influence lower than that of dendritic cells by factor  $\frac{bs_{perM}}{bs_{perDC}} = 1/20$ . Effector memory T cells can only be activated by the same type of APCs (pro- vs anti-inflammatory) as the original central memory T cell. Consequently, we need to distinguish between two different  $Tem$  activation rates for pro- and anti-inflammatory-stimulated effector memory T cells.

$$Tem_{APCtype} \text{ activation rate} = \frac{Tem_{APCtype}}{T_{tot,LP}} \cdot \frac{BS_{APCtype,av,LP}}{BS_{APC,av,LP}} \cdot \frac{\alpha_{Tm,b} \cdot \beta}{T_{contact}} \cdot contacts_{LP}$$

for the different stimulating APC types that are described in the next Section 2.12.

We implemented the duration of proliferation equal to central memory T cells, but the resulting fully differentiated effector T cells do not leave the tissue, but stay in LP as effector T cells. The resulting ODEs for proliferating effector memory T cells are

$$\begin{aligned} \frac{d}{dt} Tem2Teff_1 &= Tem \text{ activation rate} - p_{Tn,>1} \cdot Tem2Teff_1 - \mu_{T,prol} \cdot Tem2Teff_1 \\ \frac{d}{dt} Tem2Teff_i &= p_{Tn,>1} \cdot Tem2Teff_{i-1} - p_{Tn,>1} \cdot Tem2Teff_i - \mu_{T,prol} \cdot Tem2Teff_i \\ &\quad - (1 + 0.1 \cdot (i - 1)) \cdot \mu_{T,LN} \cdot Tem2Teff_i, \end{aligned}$$

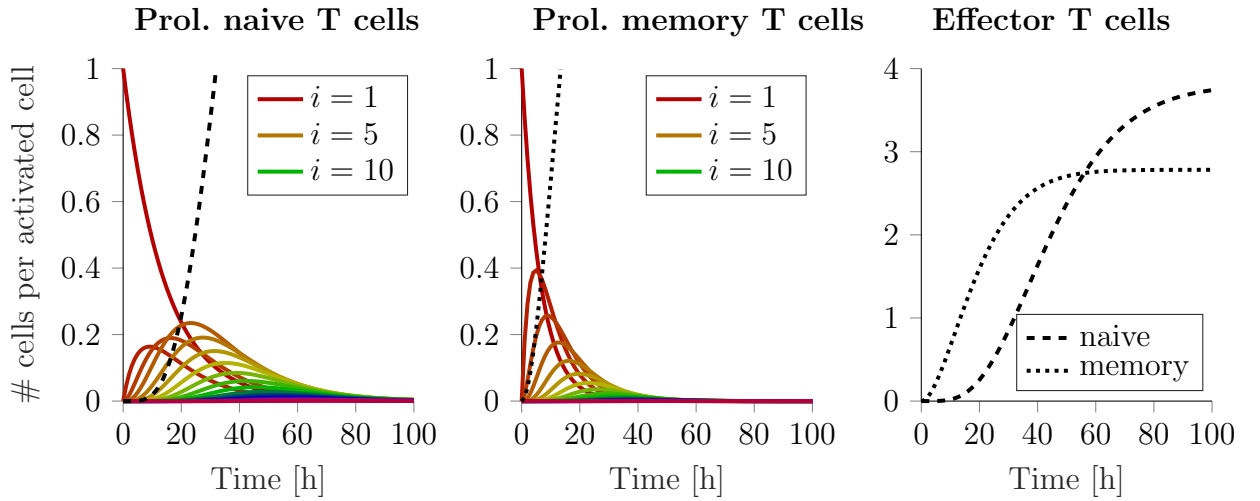


Figure 13: **Dynamics of proliferating T cells.** Proliferating T cells of different division numbers per activated naive or memory T cell. Shown are  $T_{n2Th1_i}$  (left) and  $T_{cm2Tem1_i}$  (middle). For this simulation, the black dashed/dotted lines show the resulting number of effector/effector memory T cells over time, where death of effector/effector memory T cells was neglected. Note the different scales of the y-axis. Dynamics of proliferating central memory and proliferating effector memory T cells are the same; dynamics of proliferating naive/memory T cells differentiating into different T helper cell types are the same.

for  $i = 2, \dots, N_{T, \text{prol}}$ , specific for the T cells activated by the different APC types. Subscripts  $b$  are omitted for readability; all proliferating T cells are bacteria-specific, with identical parameters for all bacterial species except  $\alpha_{T_m, b}$  (additional details in the following Section 2.12). To ensure the same proliferation characteristics as for central memory T cells, we used the rate constant  $\mu_{T, LN}$  for the transition from the transit compartments to the fully differentiated effector T cells.

Figure 13 shows the resulting dynamics of proliferating naive and memory T cells over time. For this simulation, we considered one activated naive or memory T cell (i.e.  $T_{n2Th1_1} = 1$  or  $T_{cm2Tem1} = 1$  at  $t = 0$ ) and observed the resulting numbers of proliferating cells ( $T_{n2Th1_i}$  or  $T_{cm2Tem1_i}$ ) and effector cells over time. We neglected death of effector cells to show the total number of effector cells that result from one activated naive or memory T cell. As expected, the increase in effector T cells after the activation is faster for memory T cells than naive T cells, but naive T cells give rise to more effector cells than memory T cells (3.81 vs 2.78 effector cells per activated naive or memory T cell, respectively). These numbers seem very low compared to the reports of extensive proliferation in literature [29, 110]. They lead, however, to a considerable and plausible increase of T helper cells in our inflammation scenarios (see the concentration of T helper cells over time in Figure 15). This is because of the high number of naive and memory T cells that are activated in the inflammation scenarios, which can be explained by the frequency of cognate antigen encounter ( $\alpha_{T_n}$  and  $\alpha_{T_m}$ ) in relation to the steady state concentrations of naive and central memory T cells and dendritic cells in the LN.

## 2.12 Effector T cell subsets

In the previous section (2.11) we described how activated naive ( $T_n$ ) and memory T cells ( $T_{cm}$  and  $T_{em}$ ) differentiated via  $T_n \rightarrow T_{eff}$ ,  $T_{cm} \rightarrow T_{em}$  and  $T_{em} \rightarrow T_{eff}$  into effector T cells  $T_{eff}$ . In the model, however, we further differentiated between four different types of effector T cells: induced regulatory T cells (iTregs) and T helper cells (Ths) of type 1, 2 and 17 (iTreg, Th1, Th2 and Th17, respectively). Other T helper cell types (such as follicular T helper cells  $T_{FH}$  [111, 112] or Th9 [113, 114]) are neglected.

The type of effector T cell is determined at the time point of stimulation of the naive or central memory T cells in the LN, via signalling molecules secreted by the stimulating dendritic cell [29]. The dendritic cell produces those signalling molecules in response to specific triggers [29], so that specific situations result in specific (distributions of) effector T cells with specific functions that are best adapted to the underlying situations. iTreg is induced by transforming growth factor (TGF)- $\beta$ , when IL-6 and other pro-inflammatory cytokines are absent. TGF- $\beta$  is produced by dendritic cells when they are not (yet) fully activated. The effector functions of iTregs are suppression of inflammation and T cell responses via production of IL-10 and TGF- $\beta$  [29]. Th1 is induced by IL-12 and interferon (IFN)- $\gamma$ . These cytokines are produced by dendritic cells in response to viruses and intracellular bacteria. Th1 effector functions are stimulation of production, recruitment and activation of macrophages via production of granulocyte-macrophage colony-stimulating factor (GM-CSF), IFN- $\gamma$  and lymphotoxin (LT)- $\alpha$  [29]. Th2 is induced by IL-4. This cytokine is probably produced by eosinophils, basophils and mast cells that have been activated by parasites. Th2 effector functions are activation of eosinophils, mast cells and B cells via production of IL-4, IL-5 and IL-13, contributing to allergic reactions, and anti-inflammatory effects via production of IL-10 [29]. Th17 is induced by IL-6 and TGF- $\beta$ , when IL-4 and IL-12 are absent. IL-6, which is crucial in the decision if iTreg or Th17 is induced, is produced by dendritic cells in response to extracellular bacteria and fungi. Th17 effector functions are recruitment of innate immune cells, especially neutrophils, via production of IL-17, TNF- $\alpha$  and CXCL1 [29].

As the effector T cell type is determined at the time of activation, we implemented all following T cell state variables specific to the resulting effector T cell type, i.e. the given activation rates of  $T_n$ ,  $T_{cm}$  and  $T_{em}$  are divided into four activation rates each and all T cell state variables given in Section 2.11 (except  $T_n$  and  $T_{cm}$ ) are divided into four separate state variables. Figure 14 shows the resulting scheme of the T cell proliferation model including all T cell state variables. The above T cell proliferation model (Section 2.11) applies to all four effector T cell types. The only difference is that naive T cells differentiating into regulatory T cells have a lower susceptibility to cell death [115], which we implemented by multiplying the death rate of  $T_n \rightarrow T_{reg}$  by 0.5. In addition, all activated T cells are bacteria-specific, where the bacteria-specificity is determined by the bacteria that the stimulating APC engulfed.

We implemented the partition of the activation rates in two steps, representing the factors that determine the effector T cell type: (i) The distinction between regulatory T cells and T helper cells was implemented as the result of the stimulating APC: We classified APCs into pro-inflammatory (stimulatory dendritic cells and antigen-experienced macrophages of populations P1 to P3) and anti-inflammatory (tolerogenic dendritic cells and antigen-experienced macrophages of population P4 or efferocytosis-type). T cells stimulated by pro-inflammatory APCs become T helper cells and T cells stimulated by anti-inflammatory APCs become regulatory T cells. For this, the activation rates of  $T_n$ ,

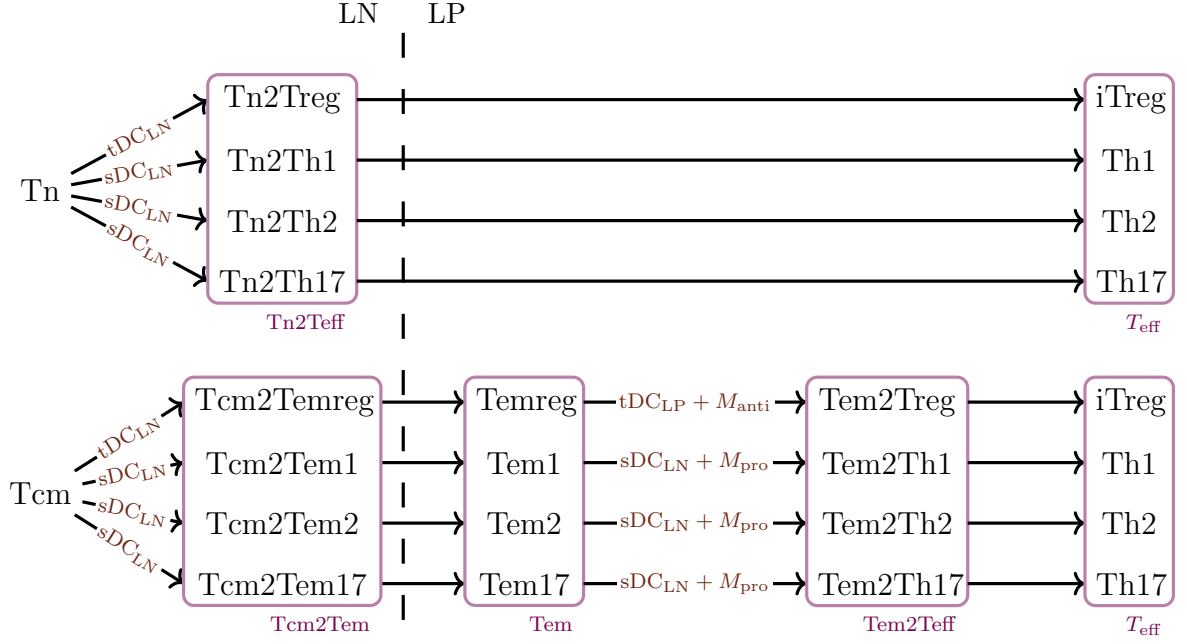


Figure 14: **Submodel of T cell proliferation and differentiation.** Arrows indicate transitions between states, with APCs stimulating the proliferation/differentiation indicated in brown on the arrows.  $M_{pro,a} = M_{P1,a} + M_{P2,a} + M_{P3,a}$ ,  $M_{anti,a} = M_{P4,a} + M_{effero,a}$ . Transit compartments are combined (all state variables with “2” in their names), inflow, outflow and death rates are not shown. All state variables of activated T cells (i.e. all shown state variables except  $T_n$  and  $T_{cm}$ ) are bacteria-specific, where the bacteria-specificity is determined by the stimulating APC. For a more detailed representation of the T cell activation, proliferation and differentiation model for the example of naive T cells, see Figure 12. State variable names in violet show the previously used T cell state variables (from Section 2.11) and their division into four separate state variables according to effector T cell type (e.g.  $T_{n2Teff} = T_{n2Treg} + T_{n2Th1} + T_{n2Th2} + T_{n2Th17}$ ).

$T_{cm}$  and  $T_{em}$  given in Section 2.11 are multiplied by the fraction of available binding sites on pro-inflammatory APCs divided by available binding sites on all APCs of the tissue to give the activation rates into T helper cells and by the fraction of available binding sites on anti-inflammatory APCs divided by available binding sites on all APCs of the tissue to give the activation rates into regulatory T cells. (ii) T helper cells are further divided into type 1, 2 and 17 according to fractions that depend on both the bacterial strain from which the antigen presented by the stimulating dendritic cell is derived and the host. The activation rates resulting in T helper cells (i.e. by stimulation with pro-inflammatory APCs) are multiplied by these fractions to give the activation rates into each of the different T helper cell types.

The fractions determining the distribution of type 1, 2 and 17, dependent on bacterial strain and host, were derived as follows: To implement the bacteria-specific and host-specific influences, we assumed that the host APCs have a specific distribution of receptors (pattern recognition receptors such as e.g. Toll-like receptors [29]) that recognise bacterial antigens and lead to production of signalling molecules stimulating T cells to become specific helper cell types. We group these receptors based on the resulting T helper cell type, i.e.  $R_1$  denotes the concentration of all receptors leading to type 1,  $R_2$  leading to type 2 and  $R_{17}$  leading to type 17. In addition, we assume that each bacterial strain has

a specific distribution of antigens that can be recognised by these receptors; we group bacterial antigens by the receptor groups that recognise them and denote by  $A_1$  the concentration of those antigens recognised by  $R_1$ ,  $A_2$  those recognised by  $R_2$  and  $A_{17}$  those recognised by  $R_{17}$ . Assuming receptor-specific binding and unbinding rate constants  $k_i, k_{-i}$ , the ODE for the concentration of antigen-receptor complex  $R_i:A_i$  ( $i = 1, 2, 17$ ) is

$$\frac{d}{dt}R_i:A_i = k_i \cdot R_i \cdot A_i - k_{-i} \cdot R_i:A_i.$$

Assuming, because of the very fast intracellular dynamics compared to the cellular level of our systems biology model, those complexes to be in quasi-steady state, results in the concentration

$$R_i:A_i = K_i^{-1} \cdot R_i \cdot A_i \quad \text{with } K_i = \frac{k_{-i}}{k_i}$$

We described production of signalling molecules  $S_i$  leading to differentiation of T cells into a specific helper cell type  $i$  ( $i = 1, 2, 17$ ) assuming a specific production rate constant  $p_i$  and degradation rate constant  $k_{\text{deg},i}$  as

$$\frac{d}{dt}S_i = p_i \cdot R_i:A_i - k_{\text{deg},i} \cdot S_i,$$

resulting in a quasi-steady state concentration of

$$S_i = \frac{p_i \cdot R_i \cdot A_i}{K_i \cdot k_{\text{deg},i}} = \frac{A_i}{h_i},$$

where  $h_i = \frac{p_i \cdot R_i}{K_i \cdot k_{\text{deg},i}}$  is a combination of all host-related parameters. The fractions  $f_i$  ( $i = 1, 2, 17$ ) of resulting T helper cell types are finally assumed to be equal to the fractions of the respective signalling molecules, i.e.

$$f_i = \frac{S_i}{S_1 + S_2 + S_{17}} = \frac{A_i/h_i}{A_1/h_1 + A_2/h_2 + A_{17}/h_{17}} = \frac{A_i \cdot H_i}{A_1 \cdot H_1 + A_2 \cdot H_2 + A_{17} \cdot H_{17}},$$

where  $H_i = h_i^{-1}$  for better direct interpretability and comparison of bacteria- and host-specific influences. Due to the normalisation, the absolute values of  $A_i$  and  $H_i$  are irrelevant, only the relative values of  $A_1$  vs  $A_2$  and  $A_{17}$  and accordingly  $H_1$  vs  $H_2$  and  $H_{17}$  impact the resulting fractions  $f_i$ . This implies that we can normalise  $A_i$  to  $\sum A_i = 1$  and  $H_i$  to  $\sum H_i = 1$ , so that  $f_i = A_i$  for host-specific parameters  $H_1 = H_2 = H_{17} = 1/3$  and  $f_i = H_i$  for bacteria-specific parameters  $A_1 = A_2 = A_{17} = 1/3$ . Through that, the three parameters  $A_i$  (or  $H_i$ ) are defined by two parameter values and  $\sum A_i = 1$  (or  $\sum H_i = 1$ ). Interestingly, this corresponds to the logistic-normal distribution, which allows for sampling of parameters for  $A_i$  (or  $H_i$ ) with specified mean  $M = [\mathbb{E}_{\sim\mu}(A_1), \mathbb{E}(A_2), \mathbb{E}(A_{17})]$  (or  $M = [\mathbb{E}(H_1), \mathbb{E}(H_2), \mathbb{E}(H_{17})]$ ) and covariance matrix  $\Sigma$ .

For the inclusion in our systems biology model, it follows that we need three parameter values  $H_1$ ,  $H_2$  and  $H_{17}$  for the host (can be defined by two parameter values and  $\sum H_i = 1$ ). For the reference individual, we choose an equal distribution of T helper cell types, i.e.  $H_1 = H_2 = H_{17} = 1/3$ . In addition, we need three parameter values  $A_{1,b}$ ,  $A_{2,b}$  and  $A_{17,b}$  per bacterial strain. For commensal bacteria, we assume an equal distribution of elicited T helper cell types,  $A_{1,\text{commensal}} = A_{2,\text{commensal}} = A_{17,\text{commensal}} = 1/3$ . Salmonellae mainly elicit Th1 responses [29], therefore  $A_{1,\text{salmonellae}} = 1, A_{2,\text{salmonellae}} =$



$A_{17,\text{salmonellae}} = 0$ . Extracellular bacteria mainly elicit Th17 responses [29], therefore  $A_{1,\text{extracellular}} = A_{2,\text{extracellular}} = 0$ ,  $A_{17,\text{extracellular}} = 1$ . The bacterial strain is defined by the bacteria-specificity of the APC stimulating the T cell (e.g. a stimulatory dendritic cell in LN). In the generation of a virtual population (see Section 4), we sample all parameter values from a distribution around the reference individual. There we do not sample logistic-normal samples, but sample for each individual three host-specific parameters  $H_1, H_2, H_{17}$  and three bacteria-specific parameters  $A_{1,b}, A_{2,b}, A_{17,b}$  per bacterial strain, so that the sums  $\sum H_i$  and  $\sum A_i$  do not necessarily equal 1. Due to the normalisation in the calculation of  $f_i$  this is, however, not of importance, as the influence on the mean is small (zero for  $M = [1/3, 1/3, 1/3]$ ) and we do not aim to control the covariance.

The death rate constant of effector T cells has been reported to be  $\mu_{T,\text{eff}} = 0.5 \frac{1}{\text{d}}$  [116]. The resulting ODEs for the four effector T cell types are

$$\begin{aligned} \frac{d}{dt} \text{iTreg} &= \sum_{i=5}^{N_{T,\text{prol}}} (1 + 0.1 \cdot (i - 5)) \cdot \mu_{T,\text{LN}} \cdot \text{Tn2Treg}_i \cdot \frac{V_{\text{LN}}}{V_{\text{LP}}} \\ &\quad + \sum_{i=1}^{N_{T,\text{prol}}} (1 + 0.1 \cdot (i - 1)) \cdot \mu_{T,\text{LN}} \cdot \text{Tem2Teff}_i - \mu_{T,\text{eff}} \cdot \text{iTreg} \\ \frac{d}{dt} \text{Th1} &= \sum_{i=5}^{N_{T,\text{prol}}} (1 + 0.1 \cdot (i - 5)) \cdot \mu_{T,\text{LN}} \cdot \text{Tn2Th1}_i \cdot \frac{V_{\text{LN}}}{V_{\text{LP}}} \\ &\quad + \sum_{i=1}^{N_{T,\text{prol}}} (1 + 0.1 \cdot (i - 1)) \cdot \mu_{T,\text{LN}} \cdot \text{Tem2Th1}_i - \mu_{T,\text{eff}} \cdot \text{Th1} \\ \frac{d}{dt} \text{Th2} &= \sum_{i=5}^{N_{T,\text{prol}}} (1 + 0.1 \cdot (i - 5)) \cdot \mu_{T,\text{LN}} \cdot \text{Tn2Th2}_i \cdot \frac{V_{\text{LN}}}{V_{\text{LP}}} \\ &\quad + \sum_{i=1}^{N_{T,\text{prol}}} (1 + 0.1 \cdot (i - 1)) \cdot \mu_{T,\text{LN}} \cdot \text{Tem2Th2}_i - \mu_{T,\text{eff}} \cdot \text{Th2} \\ \frac{d}{dt} \text{Th17} &= \sum_{i=5}^{N_{T,\text{prol}}} (1 + 0.1 \cdot (i - 5)) \cdot \mu_{T,\text{LN}} \cdot \text{Tn2Th17}_i \cdot \frac{V_{\text{LN}}}{V_{\text{LP}}} \\ &\quad + \sum_{i=1}^{N_{T,\text{prol}}} (1 + 0.1 \cdot (i - 1)) \cdot \mu_{T,\text{LN}} \cdot \text{Tem2Th17}_i - \mu_{T,\text{eff}} \cdot \text{Th17} \end{aligned}$$

Subscripts  $b$  of the state variables are omitted for readability; all proliferating, effector memory and effector T cells are bacteria-specific.

The implementation of effector functions of iTregs are described in Sections 2.13 (cell contact-dependent effects) and 2.14 (cytokine-mediated effects). The effector functions of Th1, Th2 and Th17 are mainly conducted via cytokines that regulate several processes. Cytokine production and effects are described in detail in Section 2.14. In addition to cytokine production, Th1 help macrophages infected with intracellular bacteria to eliminate those [29], see Section 2.18.2.

### 2.13 Regulatory T cells

Another type of effector T cells that we included in our model are regulatory T cells (Tregs). Two main types of Tregs can be distinguished: Natural regulatory T cells (nTregs) are generated in the thymus, whereas induced regulatory T cells (iTregs) are induced in peripheral lymphoid organs, via stimulation of naive or memory T cells by tolerogenic dendritic cells, as described above [29]. It is assumed that iTregs dominate over nTregs in tissues that are exposed to many different foreign antigens, such as the gut mucosa, where they are constantly induced [117, 118]. As iTregs are induced in the gut by stimulation with bacterial antigen, their resulting TCR repertoire is assumed to be specific for the antigens present in this tissue, whereas the nTreg TCR repertoire is expected to be much less specific [118]. Therefore, we neglected nTregs in our model, and focused on iTregs. Several mechanisms by which Tregs suppress inflammation and T cell proliferation have been reported, such as production of anti-inflammatory cytokines (IL-10 and TGF- $\beta$ ), modulation of dendritic cell activation status or function, reduction of contact formation between dendritic cells and T cells, inhibition of T cell proliferation by reducing the division destiny, inhibition of activated effector and memory T cells, and others [104, 119–121].

We considered two different mechanisms of effect of Treg-mediated inhibition in our model, which seemed, based on literature, most relevant to us: (i) inhibition of T cell proliferation via inhibition of T cell activation by APCs and (ii) effect on the activation status of dendritic cells and macrophages via IL-10 (and other anti-inflammatory cytokines), thereby influencing their cytokine production and T cell activation. For this, we assumed all stimulated Tregs after first division to be equally functional, i.e. the (bacteria-specific) total population of Tregs in LN and LP is

$$\begin{aligned} \text{iTreg}_{\text{tot,LN}} &= \sum_{i=2}^{N_{\text{T,prol}}} \text{Tn2Treg}_i \\ \text{iTreg}_{\text{tot,LP}} &= \text{iTreg} + \text{Temreg} + \sum_{i=2}^{N_{\text{T,prol}}} \text{Tem2Treg}_i. \end{aligned}$$

Figure 15 shows the time course of Tregs compared to T helper cells in LN and LP for the two different inflammation scenarios (salmonella infection and mucosal injury). In healthy steady state, Tregs dominate over T helper cells. In the simulation of infection with salmonellae, especially in LP, a strong increase of the T helper cell concentration and decrease of the Treg concentration leads to almost equal levels of regulatory and T helper cells. In the simulation of mucosal injury this effect is not as pronounced, but the ratio of T helper cells to regulatory T cells also markedly increases during inflammation.

The implementation of IL-10 production and IL-10 effects is described in Section 2.14. The implementation of Treg effects on T cell activation/proliferation is described in the rest of this section:

Although many experiments indicated Tregs to be able to inhibit proliferation in an antigen-unspecific manner (so-called bystander inhibition) [122, 123], Akkaya et al. (2019) [124] very recently showed that bystander suppression could only be observed *in vitro*, but not *in vivo*. They suggested that Tregs inhibit activation of naive T cells of the same

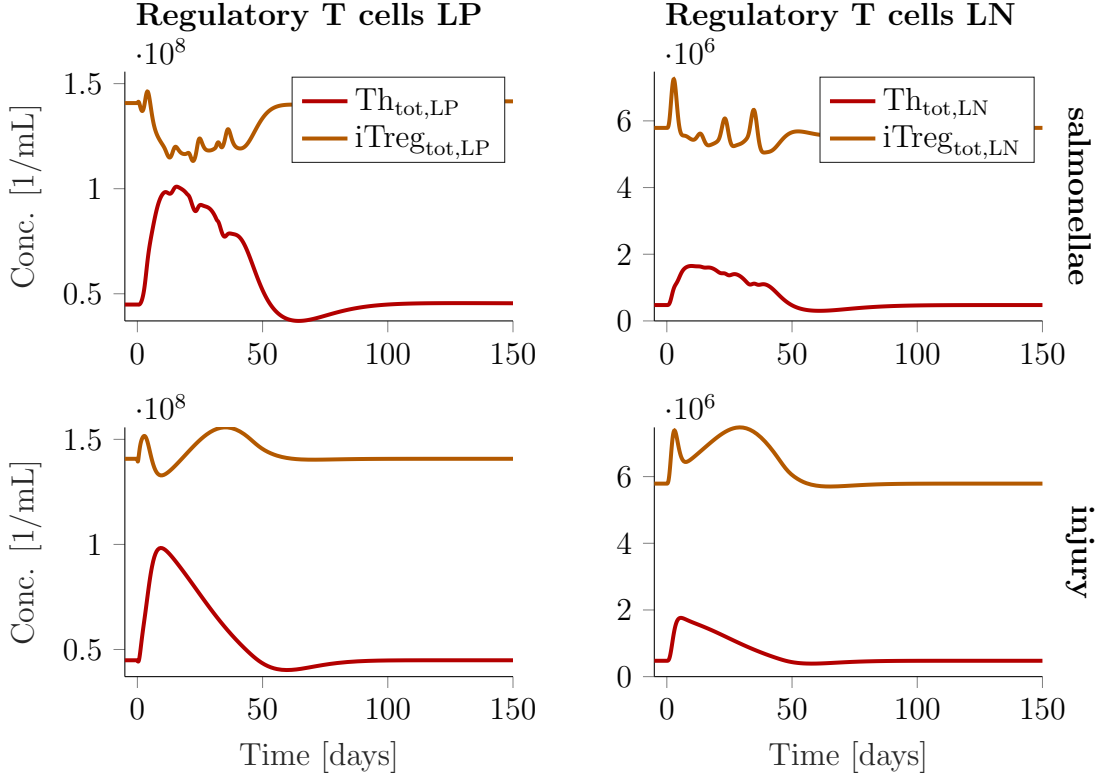


Figure 15: **Regulatory T cell dynamics.** Concentrations of Tregs versus T helper cells in LP and mesenteric LNs.  $Th_{tot,LP} = Th1 + Th2 + Th17 + Tem1 + Tem2 + Tem17 + \sum_{i=2}^{N_{T,prol}} (Tem2Th1_i + Tem2Th2_i + Tem2Th17_i)$ ,  $iTreg_{tot,LP} = iTreg + Temreg + \sum_{i=2}^{N_{T,prol}} Tem2Treg_i$ ,  $Th_{tot,LN} = \sum_{i=2}^{N_{T,prol}} (Tn2Th1_i + Tn2Th2_i + Tn2Th17_i)$ ,  $iTreg_{tot,LN} = \sum_{i=2}^{N_{T,prol}} Tn2Treg_i$  For each state, the sum over all bacteria-specificities is shown.

antigen specificity by removal of pMHCII complexes from the dendritic cell's surface, as they showed the uptake of pMHCII into Tregs, and the diminished ability of dendritic cells pre-incubated with Tregs to stimulate naive T cells of the same antigen specificity, but unchanged ability to stimulate naive T cells specific to other antigens [124].

We implemented this mechanism by adding state variables of pMHCII-depleted APCs. PMHCII depletion is of course fluent and must not necessarily be complete, i.e. it is probable that as a result APCs have lower, but not zero, levels of pMHCII. As this is, however, difficult to implement, we only differentiated between non-depleted (i.e. full pMHCII levels) and fully pMHCII-depleted (i.e. no pMHCII left) APCs. In total, the fractions of non-depleted APCs from all APCs represent the fractions of remaining pMHCII on the surface of all APCs, i.e. the reduction in T cell stimulation potential is the same using this simplification. The resulting new pMHCII-depleted state variables – one for each APC state variable – are  $tDC_{dep,LN}$ ,  $sDC_{dep,LN}$ ,  $tDC_{dep,LP}$ ,  $sDC_{dep,LP}$ ,  $M_{P1,a,dep}$ ,  $M_{P2,a,dep}$ ,  $M_{P3,a,dep}$ ,  $M_{P4,a,dep}$  and  $M_{effero,a,dep}$ . Those pMHCII-depleted APCs are, in contrast to non-depleted APCs, not bacteria-specific, as the only bacteria-specific part of the APCs – the presented peptides – are removed, i.e. pMHCII depletion of an APC of any bacteria-specificity results in the same pMHCII-depleted APC. Apart from that, they behave mostly as their non-depleted counterparts, with the same death and migration (for dendritic cells) rates, and the same activation or deactivation rates as the respective non-depleted APCs. They

also have the same phagocytic activity, but uptake of bacterial antigen leads to transition back to the non-depleted state, as this leads to acquirement of new bacterial antigen that can be presented on the APC's cell surface, i.e. the antigen uptake rate is according to the antigen uptake rate of qDC, rDC,  $M_{P_i}$  ( $i = 1, \dots, 4$ ) and  $M_{\text{effero}}$ . The depletion of pMHCII only affects the potential to stimulate T cells, but does not affect cytokine production, i.e. cytokine production rates are the same for non-depleted and pMHCII-depleted APCs (see Section 2.14).

PMHCII depletion occurs when a Treg encounters its cognate antigen presented on an APC's surface. We used the concentration of contacts between Tregs and the respective APC, calculated from the total concentration of contacts between T cells and dendritic cells derived in Section 2.10. This concentration is bacteria-specific, i.e. the concentration of Tregs specific for one bacterial strain with the respective APCs specific for the same bacterial strain. Then the rate of pMHCII depletion, defined by the concentration of these contacts times the dissociation rate constant ( $T_{\text{contact}}^{-1}$ ) times the probability  $\alpha_{\text{Th}} \cdot \beta$  that the Treg is specific for any antigen presented by the APC, is on the level of binding sites. This follows from the assumption that the Treg searches the full surface of the APC, i.e. is able to find any presented antigen [92], but can only eliminate the pMHCII complexes of the binding site, as it eliminates them via engulfment of the APC's membrane [124]. The probability that a Treg is specific for a given antigen presented by an APC of the same bacteria-specificity is  $\alpha_{\text{Th},b} = \frac{1}{N_{\text{antigen},b}}$ , where  $N_{\text{antigen},b}$  is the number of different bacterial antigens of this bacteria-specificity. As we implemented commensal bacteria as a combination of bacterial strains, the number of antigens is much higher than for a single strain such as salmonellae or the implemented generic extracellular bacteria. We assumed  $N_{\text{antigen,commensal}} = 1000$  different commensal bacterial antigens, accounting for the high number of different strains but also a high level of overlap due to conserved structures. For salmonellae and extracellular bacteria,  $N_{\text{antigen,salmonellae}} = N_{\text{antigen,extracellular}} = \beta = 10$ , as  $\beta$  was earlier (in Section 2.11) defined as the number of different antigens per bacterial cell, which are presented by the APC that take up this bacterial cell via phagocytosis. To translate the pMHCII depletion rate to the level of cells, it is multiplied by  $\text{bs}_{\text{perDC}}^{-1}$  or  $\text{bs}_{\text{perM}}^{-1}$  for dendritic cells or macrophages, respectively. The resulting ODEs for pMHCII-depleted APCs are

$$\begin{aligned} \frac{d}{dt} \text{tDC}_{\text{dep,LN}} &= \epsilon_{\text{DC}} \cdot \text{tDC}_{\text{dep,LP}} \cdot \frac{V_{\text{LP}}}{V_{\text{LN}}} - \mu_{\text{DC,LN}} \cdot \text{tDC}_{\text{dep,LN}} \\ &+ \sum_b \frac{i\text{Treg}_{\text{tot,LN}}}{T_{\text{tot,LN}}} \cdot \frac{\text{tDC}_{\text{LN}} \cdot \text{bs}_{\text{perDC}} - (\text{Tn2Treg}_1 + \text{Tcm2Temreg}_1)}{\text{BS}_{\text{APC,av,LN}}} \\ &\cdot \frac{\alpha_{\text{Th},b} \cdot \beta}{T_{\text{contact}}} \cdot \text{contacts}_{\text{LN}} \cdot \text{bs}_{\text{perDC}}^{-1} \\ \frac{d}{dt} \text{sDC}_{\text{dep,LN}} &= \epsilon_{\text{DC}} \cdot \text{sDC}_{\text{dep,LP}} \cdot \frac{V_{\text{LP}}}{V_{\text{LN}}} - \mu_{\text{DC,LN}} \cdot \text{sDC}_{\text{dep,LN}} \\ &+ \sum_b \frac{i\text{Treg}_{\text{tot,LN}}}{T_{\text{tot,LN}}} \cdot \frac{\text{sDC}_{\text{LN}} \cdot \text{bs}_{\text{perDC}} - (\text{Tn2Th}_1 + \text{Tcm2Temh}_1)}{\text{BS}_{\text{APC,av,LN}}} \\ &\cdot \frac{\alpha_{\text{Th},b} \cdot \beta}{T_{\text{contact}}} \cdot \text{contacts}_{\text{LN}} \cdot \text{bs}_{\text{perDC}}^{-1} \end{aligned}$$

$$\begin{aligned}
\frac{d}{dt}tDC_{\text{dep,LP}} &= \sum_b \frac{iTreg_{\text{tot,LP}}}{T_{\text{tot,LP}}} \cdot \frac{tDC_{\text{LP}} \cdot bs_{\text{perDC}} \cdot \left(1 - \frac{Tem2Treg_1}{tDC_{\text{LP}} \cdot bs_{\text{perDC}} + M_{\text{anti,a}} \cdot bs_{\text{perM}}}\right)}{BS_{\text{APC,av,LP}}} \\
&\quad \cdot \frac{\alpha_{\text{Th,b}} \cdot \beta}{T_{\text{contact}}} \cdot \text{contacts}_{\text{LP}} \cdot bs_{\text{perDC}}^{-1} \\
&\quad - \mu_{\text{DC,LP}} \cdot tDC_{\text{dep,LP}} - \epsilon_{\text{DC}} \cdot tDC_{\text{dep,LP}} \\
&\quad - tDCi \text{ activation rate} - tDCi \text{ antigen uptake rate} \\
\frac{d}{dt}sDC_{\text{dep,LP}} &= \sum_b \frac{iTreg_{\text{tot,LP}}}{T_{\text{tot,LP}}} \cdot \frac{sDC_{\text{LP}} \cdot bs_{\text{perDC}} \cdot \left(1 - \frac{Tem2Th_1}{sDC_{\text{LP}} \cdot bs_{\text{perDC}} + M_{\text{pro,a}} \cdot bs_{\text{perM}}}\right)}{BS_{\text{APC,av,LP}}} \\
&\quad \cdot \frac{\alpha_{\text{Th,b}} \cdot \beta}{T_{\text{contact}}} \cdot \text{contacts}_{\text{LP}} \cdot bs_{\text{perDC}}^{-1} \\
&\quad - \mu_{\text{DC,LP}} \cdot sDC_{\text{dep,LP}} - \epsilon_{\text{DC}} \cdot sDC_{\text{dep,LP}} \\
&\quad + tDCi \text{ activation rate} - sDCi \text{ antigen uptake rate} \\
\frac{d}{dt}M_{\text{P1,a,dep}} &= \sum_b \frac{iTreg_{\text{tot,LP}}}{T_{\text{tot,LP}}} \cdot \frac{M_{\text{P1,a}} \cdot bs_{\text{perM}} \cdot \left(1 - \frac{Tem2Th_1}{sDC_{\text{LP}} \cdot bs_{\text{perDC}} + M_{\text{pro,a}} \cdot bs_{\text{perM}}}\right)}{BS_{\text{APC,av,LP}}} \\
&\quad \cdot \frac{\alpha_{\text{Th,b}} \cdot \beta}{T_{\text{contact}}} \cdot \text{contacts}_{\text{LP}} \cdot bs_{\text{perM}}^{-1} \\
&\quad - \mu_M \cdot M_{\text{P1,a,dep}} - \text{transition rate P1} \rightarrow \text{P2} \\
&\quad - M_{\text{P1,a,dep}} \text{ antigen uptake rate} - M_{\text{P1,a}} \text{ efferocytosis rate} \\
\frac{d}{dt}M_{\text{P2,a,dep}} &= \sum_b \frac{iTreg_{\text{tot,LP}}}{T_{\text{tot,LP}}} \cdot \frac{M_{\text{P2,a}} \cdot bs_{\text{perM}} \cdot \left(1 - \frac{Tem2Th_1}{sDC_{\text{LP}} \cdot bs_{\text{perDC}} + M_{\text{pro,a}} \cdot bs_{\text{perM}}}\right)}{BS_{\text{APC,av,LP}}} \\
&\quad \cdot \frac{\alpha_{\text{Th,b}} \cdot \beta}{T_{\text{contact}}} \cdot \text{contacts}_{\text{LP}} \cdot bs_{\text{perM}}^{-1} \\
&\quad - \mu_M \cdot M_{\text{P2,a,dep}} + \text{transition rate P1} \rightarrow \text{P2} - \text{transition rate P2} \rightarrow \text{P3} \\
&\quad - M_{\text{P2,a,dep}} \text{ antigen uptake rate} - M_{\text{P2,a}} \text{ efferocytosis rate} \\
\frac{d}{dt}M_{\text{P3,a,dep}} &= \sum_b \frac{iTreg_{\text{tot,LP}}}{T_{\text{tot,LP}}} \cdot \frac{M_{\text{P3,a}} \cdot bs_{\text{perM}} \cdot \left(1 - \frac{Tem2Th_1}{sDC_{\text{LP}} \cdot bs_{\text{perDC}} + M_{\text{pro,a}} \cdot bs_{\text{perM}}}\right)}{BS_{\text{APC,av,LP}}} \\
&\quad \cdot \frac{\alpha_{\text{Th,b}} \cdot \beta}{T_{\text{contact}}} \cdot \text{contacts}_{\text{LP}} \cdot bs_{\text{perM}}^{-1} \\
&\quad - \mu_M \cdot M_{\text{P3,a,dep}} + \text{transition rate P2} \rightarrow \text{P3} - \text{transition rate P3} \rightarrow \text{P4} \\
&\quad - M_{\text{P3,a,dep}} \text{ antigen uptake rate} - M_{\text{P3,a}} \text{ efferocytosis rate} \\
\frac{d}{dt}M_{\text{P4,a,dep}} &= \sum_b \frac{iTreg_{\text{tot,LP}}}{T_{\text{tot,LP}}} \cdot \frac{M_{\text{P4,a}} \cdot bs_{\text{perM}} \cdot \left(1 - \frac{Tem2Treg_1}{tDC_{\text{LP}} \cdot bs_{\text{perDC}} + M_{\text{anti,a}} \cdot bs_{\text{perM}}}\right)}{BS_{\text{APC,av,LP}}} \\
&\quad \cdot \frac{\alpha_{\text{Th,b}} \cdot \beta}{T_{\text{contact}}} \cdot \text{contacts}_{\text{LP}} \cdot bs_{\text{perM}}^{-1} \\
&\quad - \mu_M \cdot M_{\text{P4,a,dep}} + \text{transition rate P3} \rightarrow \text{P4}
\end{aligned}$$

$$\begin{aligned}
& - M_{P4,a,dep} \text{ antigen uptake rate} - M_{P4,a} \text{ efferocytosis rate} \\
\frac{d}{dt} M_{\text{effero},a,dep} = & \sum_b \frac{i\text{Treg}_{\text{tot},LP}}{T_{\text{tot},LP}} \cdot \frac{M_{\text{effero},a} \cdot b_{\text{SperM}} \cdot \left(1 - \frac{\text{Tem2Treg}_1}{t\text{DC}_{LP} \cdot b_{\text{SperDC}} + M_{\text{anti},a} \cdot b_{\text{SperM}}}\right)}{\text{BS}_{\text{APC},av,LP}} \\
& \cdot \frac{\alpha_{\text{Th},b} \cdot \beta}{T_{\text{contact}}} \cdot \text{contacts}_{LP} \cdot b_{\text{SperM}}^{-1} \\
& - \mu_M \cdot M_{\text{effero},a,dep} - M_{\text{effero},a,dep} \text{ antigen uptake rate} \\
& + M_{P1,a} \text{ efferocytosis rate} + M_{P2,a} \text{ efferocytosis rate} \\
& + M_{P3,a} \text{ efferocytosis rate} + M_{P4,a} \text{ efferocytosis rate}
\end{aligned}$$

where  $\text{Tn2Th} = \text{Tn2Th1} + \text{Tn2Th2} + \text{Tn2Th17}$  and equivalently for  $\text{Tcm2Temh}$  and  $\text{Tem2Th}$ ;  $M_{\text{pro},a} = M_{P1,a} + M_{P2,a} + M_{P3,a}$  and  $M_{\text{anti},a} = M_{P4,a} + M_{\text{effero},a}$ . Note that we assumed that recently activated T cells occupy binding sites on the dendritic cells that activated them (as described in Section 2.10); therefore these binding sites are also not available for binding of Tregs, and are subtracted in the above terms. The transition rates from and to non-depleted (bacteria-specific) APCs (pMHCII depletion rates and  $M_{P_i,a,dep}$  antigen uptake rates) are added to the respective non-depleted APCs' ODEs derived in Section 2.8 and 2.9.

In the simulated healthy steady state LN, 12.3% of tDC and 15.6% of sDC are pMHCII-depleted, and in the simulated healthy steady state LP, 11.2% of tDC, 14.6% of sDC and 17.7%, 16.4%, 23.4%, 18.2% and 18.9% of antigen-experienced macrophages of populations 1, 2, 3, 4 and efferocytosis-type, respectively, are pMHCII-depleted. The time courses of pMHCII-depleted and non-depleted APCs for the two different inflammation scenarios are shown in Figure 15 for tolerogenic and stimulatory dendritic cells in LN and LP.

As the pMHCII-depleted APCs do not take part in T cell activation, but still bind to APCs and thereby occupy binding sites, the activation rates of Tn, Tcm and Tem are decreased. For example, the Tn activation rate by stimulatory dendritic cells is

$$\begin{aligned}
\text{Tn activation rate by sDC} = & \frac{\text{Tn}}{T_{\text{tot},LN}} \cdot \frac{s\text{DC}_{LN} \cdot b_{\text{SperDC}} - (\text{Tn2Th}_1 + \text{Tcm2Temh}_1)}{\text{BS}_{\text{APC},av,LN}} \\
& \cdot \frac{\alpha_{\text{Tn}} \cdot \beta}{T_{\text{contact}}} \cdot \text{contacts}_{LN}.
\end{aligned}$$

$\text{BS}_{\text{APC},av,LN}$  includes all APCs of the LN ( $t\text{DC}_{LN}$ ,  $s\text{DC}_{LN}$ ,  $t\text{DC}_{dep,LN}$ ,  $s\text{DC}_{dep,LN}$ ) and is therefore independent of the fraction of pMHCII depletion, but the concentration of (non-depleted)  $s\text{DC}_{LN}$  decreases with higher fractions of pMHCII depletion, which linearly translates to the resulting Tn activation rate.

## 2.14 Cytokine-mediated interactions

Cytokines are signalling molecules produced by cells, sensed by the same or other cells via receptors and thereby starting a signalling cascade that leads to specific reactions, e.g. production and secretion of proteins [29].

We did not account for any cytokines as explicit state variables, because of their

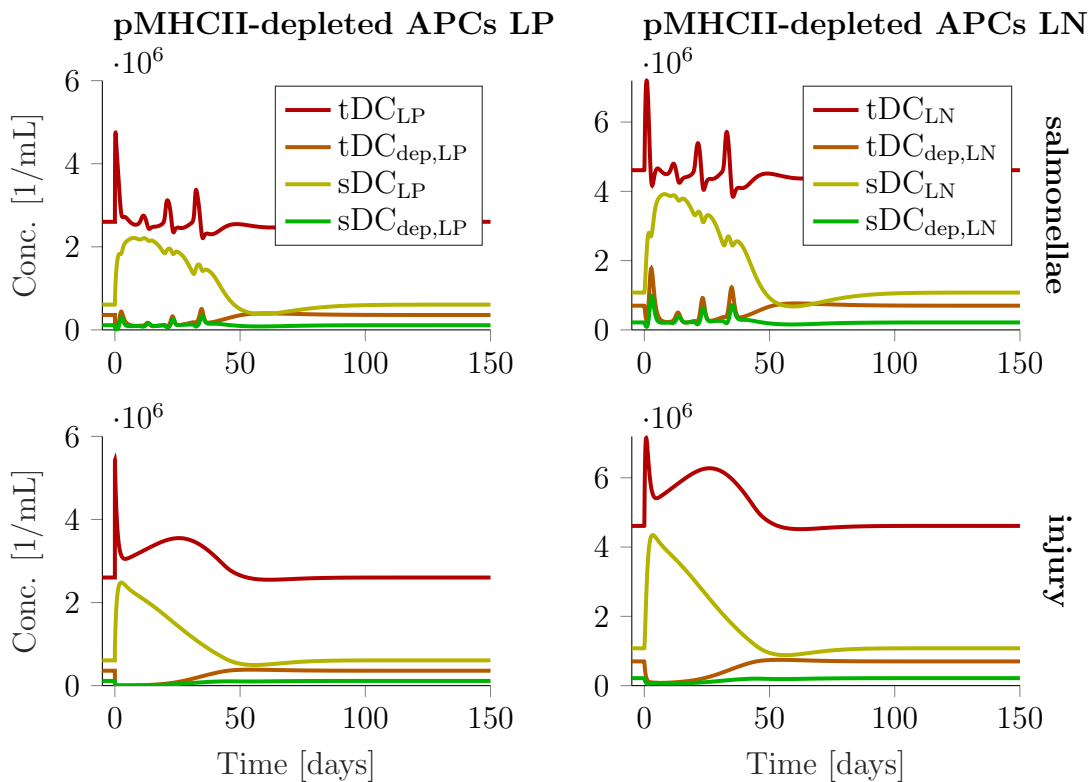


Figure 16: **Dynamics of pMHCII-depleted APCs.** Concentrations of non-depleted vs pMHCII-depleted tolerogenic and stimulatory dendritic cells in LP and LN over time for the two inflammation scenarios of salmonella infection and mucosal injury.

very short half-lives in the order of minutes [125]. On the time scale of the cellular concentrations, which is much slower, the cytokine concentrations would directly follow the cytokine-producing cell concentrations. Applying a quasi-steady state approach yields the cytokine concentration to be a sum of the producing cell concentrations weighted by the specific production rate constants, divided by the degradation rate constant of the cytokine, i.e. a linear combination of the producing cell type concentrations. For any cytokine produced by  $n$  different state variables  $S_i$ ,  $i = 1, \dots, n$ , the concentration can be described as

$$\frac{d}{dt} \text{cytokine} = p_1 \cdot S_1 + \dots + p_n \cdot S_n - k_{\text{deg}} \cdot \text{cytokine}$$

$$\text{cytokine}_{\text{qss}} = \frac{p_1 \cdot S_1 + \dots + p_n \cdot S_n}{k_{\text{deg}}},$$

with production rate constant  $p_i$  of the cytokine by cell type  $S_i$  and degradation rate constant  $k_{\text{deg}}$ . Given the current data situation in literature, it is not feasible to differentiate between the many different cytokines involved in the mucosal immune response, as a quantitative and comparable description of production and effects on target cells for the different cytokines is not available. Therefore, we substantially simplified cytokine production in our model: For each process  $k$  that is influenced by cytokines produced by other cell types, we summarised the effects of all cytokines  $\text{cytokine}_{k,j}$  that are important in this process. Assuming the same degradation rate constant  $k_{\text{deg}}$  for all cytokines, the

concentration of all cytokines important in this process  $k$  can be described by

$$\begin{aligned} \text{cytokines}_k &= \sum_j \text{cytokine}_{k,j} = \sum_j \frac{p_{k,j,1} \cdot S_1 + \dots + p_{k,j,n} \cdot S_n}{k_{\text{deg}}} \\ &= \frac{\sum_j p_{k,j,1} \cdot S_1 + \dots + \sum_j p_{k,j,n} \cdot S_n}{k_{\text{deg}}} \\ &= w'_{k,1} \cdot S_1 + \dots + w'_{k,n} \cdot S_n, \end{aligned}$$

with  $w'_{k,i} = \frac{\sum_j p_{k,j,i}}{k_{\text{deg}}}$ . Thus, the concentration of cytokines acting on a specific process is a weighted sum of the producing cell type concentrations.

As T helper cells only produce cytokines after renewed stimulation by cognate antigen [29], we implemented those cytokine levels dependent on the rate of antigen-specific contacts between T helper cells and APCs. Multiplication of this contact rate with the expected timespan of cytokine production after stimulation gives the concentration of cytokine-producing T helper cells. Therefore, in the above equation, for a T helper cell,  $S_i$  is replaced by the activation rate, which is the rate of antigen-specific contacts over time between the respective T helper cell and any APC (as described in Sections 2.10 and 2.11). The timespan of cytokine production after stimulation  $T_{\text{cytokine production}}$  is included in the respective weights  $w'_i = \frac{\sum_j p_{k,j,i}}{k_{\text{deg}}} \cdot T_{\text{cytokine production}}$ .

As the weights  $w'_{k,i}$  for each producing cell type  $S_i$  are defined separately for each process  $k$ , we included the Michaelis-Menten constants  $K_m$  of the targeted processes in the weights, i.e.  $w_{k,i} = \frac{w'_{k,i}}{K_m}$ , in order to minimise the number of free parameters. The resulting weights (in  $\text{mL} \cdot h$  for T helper cells, and in  $\text{mL}$  for all other cytokine-producing cell types) can be interpreted as the inverse of the concentration of the respective cytokine-producing cell type (or activation rate for T helper cells) that would lead to a half-maximal effect in the respective process.

We determined the weights separately for each process so that the resulting relative influences of the different cell types matched the qualitative descriptions obtained from literature and the total effects resulted in the expected model behaviour in the different infection scenarios. The resulting parameter values for the weights are listed in Table 2. A summary of qualitative literature data on the cytokine-mediated influence of different cell types on the different processes and how we implemented this is given in the paragraphs below, for each of the targeted processes. Figure 17 shows the resulting time courses of the cytokine values in the mucosal injury scenario for the different targeted processes, which are described in detail in the last paragraph of this section, *Cytokine time courses*.

We assumed the production of cytokines by dendritic cells to be quantitatively negligible in comparison to macrophages, as their main function is the antigen presentation to and activation of T cells. Therefore, we neglected dendritic cells in cytokine production. For macrophages, we only considered antigen-experienced macrophages, as macrophages release cytokines in response to the encounter of bacterial antigen [29]. As pMHCII depletion is not related to cytokine production, we assumed macrophage cytokines to be produced by antigen-experienced non-depleted and pMHCII-depleted macrophage state variables to the same extent, but differentiated between pro- (P1 to P3) and anti-inflammatory (P4 and efferocytosis-type) macrophages.

$$M_{\text{pro,a(,dep)}} = M_{\text{P1,a}} + M_{\text{P2,a}} + M_{\text{P3,a}} + M_{\text{P1,a,dep}} + M_{\text{P2,a,dep}} + M_{\text{P3,a,dep}}$$



Table 2: **Cytokine production weights.** Parameter values for the weights  $w_{k,i}$  describing the relative contribution of different cell types  $S_i$  (rows) to the cytokine effects in process  $k$  (columns), here defined by name of the process and the name of the cytokine concentration as used in previous sections. For effector T cells, activation rate is used instead of the cell concentration, see text. Parameter values are in unit  $\text{mL} \cdot h$  for effector T cells, and in  $\text{mL}$  for all other cytokine-producing cell types.

Cell type	Process (pro-inflammatory effect)					
	neutrophil recruitment	macrophage recruitment	macrophage deactivation	dendritic cell activation	damage to epithelium	damage to tissue
	$\text{cyto}_{\text{rec,Neut}}$	$\text{cyto}_{\text{rec,M}}$	$\text{cyto}_{\text{pro,deact,M}}$	$\text{cyto}_{\text{pro,act,DC}}$	$\text{cyto}_{\text{destr,epi}}$	$\text{cyto}_{\text{destr,tis}}$
Th1 <sub>tot</sub>	0	$1 \cdot 10^{-7}$	$2 \cdot 10^{-7}$	$3 \cdot 10^{-8}$	$1 \cdot 10^{-9}$	$1 \cdot 10^{-9}$
Th17 <sub>tot</sub>	$5 \cdot 10^{-8}$	$1 \cdot 10^{-8}$	$2 \cdot 10^{-8}$	$3 \cdot 10^{-9}$	$1 \cdot 10^{-9}$	$1 \cdot 10^{-9}$
Neut	$2 \cdot 10^{-9}$	$2 \cdot 10^{-8}$	$2 \cdot 10^{-8}$	$1 \cdot 10^{-7}$	$5 \cdot 10^{-9}$	$5 \cdot 10^{-9}$
$M_{\text{pro,a,(dep)}}$	$3 \cdot 10^{-8}$	$3 \cdot 10^{-8}$	$3 \cdot 10^{-8}$	$1 \cdot 10^{-7}$	$1 \cdot 10^{-9}$	$1 \cdot 10^{-9}$
Th2 <sub>tot</sub>	0	0	0	0	$2 \cdot 10^{-9}$	$2 \cdot 10^{-9}$

Cell type	Process (anti-inflammatory effect)		
	macrophage deactivation	dendritic cell activation	tissue remodelling
	$\text{cyto}_{\text{anti,deact,M}}$	$\text{cyto}_{\text{anti,act,DC}}$	$\text{cyto}_{\text{remod,tis}}$
iTreg <sub>tot,LP</sub>	$8 \cdot 10^{-9}$	$8 \cdot 10^{-9}$	0
Th2 <sub>tot</sub>	$5 \cdot 10^{-9}$	$5 \cdot 10^{-9}$	$2 \cdot 10^{-9}$
$M_{\text{anti,a,(dep)}}$	$3 \cdot 10^{-8}$	$3 \cdot 10^{-8}$	$1 \cdot 10^{-9}$

$$M_{\text{anti,a,(dep)}} = M_{\text{P4,a}} + M_{\text{effero,a}} + M_{\text{P4,a,dep}} + M_{\text{effero,a,dep}}$$

We implemented cytokine production by all activated T cells, dependent on re-stimulation in the tissue (using the activation rate for T helper cells, as described above):

$$\begin{aligned} \text{iTreg}_{\text{tot,LP}} &= \text{iTreg} + \text{Temreg} + \sum_{i=2}^{N_{\text{T,prol}}} \text{Tem2Treg}_i \\ \text{Th1}_{\text{tot}} &= \text{Th1} + \text{Tem1} + \sum_{i=2}^{N_{\text{T,prol}}} \text{Tem2Th1}_i \\ \text{Th2}_{\text{tot}} &= \text{Th2} + \text{Tem2} + \sum_{i=2}^{N_{\text{T,prol}}} \text{Tem2Th2}_i \\ \text{Th17}_{\text{tot}} &= \text{Th17} + \text{Tem17} + \sum_{i=2}^{N_{\text{T,prol}}} \text{Tem2Th17}_i \end{aligned}$$

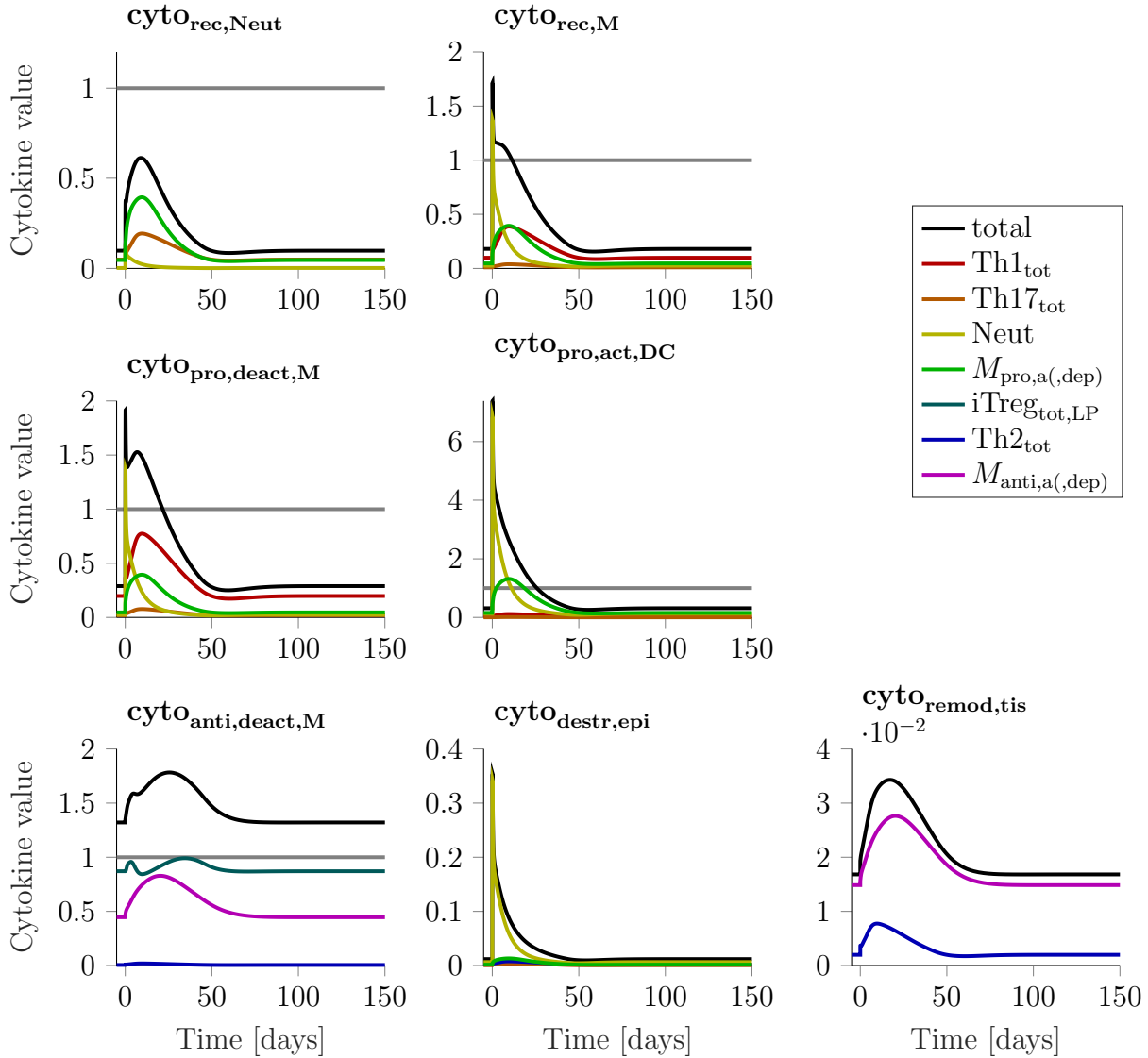


Figure 17: **Cytokine production dynamics.** Shown are the total unitless cytokine values over time for the mucosal injury scenario and the contributions of the different cytokine-producing cell types per affected process. Due to the integration of the  $K_m$  value of the respective process into the cytokine production weights, a resulting cytokine value of 1 (indicated by a grey line) corresponds to a half-maximal effect on the respective process. Note that  $\text{cyto}_{\text{anti,act,DC}} = \text{cyto}_{\text{anti,deact,M}}$  and  $\text{cyto}_{\text{destr,tis}} = \text{cyto}_{\text{destr,epi}}$ .

*Neutrophil recruitment.* The main effect of T helper cells type 17 is to recruit neutrophils to the tissue (see Section 2.12). In comparison, Th1 and Th2 effects on neutrophil recruitment are negligible and therefore not accounted for in the model. We also accounted for pro-inflammatory macrophages producing cytokines and chemokines that are involved in recruitment of neutrophils [52, 60, 61], and neutrophil recruitment by neutrophils themselves [61]. In addition, a direct effect of the bacteria concentration in LP on neutrophil recruitment was implemented, representing both the direct and indirect effect of bacterial products on recruitment of neutrophils [56]. The bacteria concentration is, however, not included in the weighted sum but added as an extra term in the neutrophil recruitment function, because of the different Hill kinetics (see Section 2.7).

*Macrophage recruitment.* As macrophages are constantly present in the LP, we implemented a constant cytokine-independent recruitment rate (see Section 2.8). For the additional recruitment in case of inflammation, which was implemented dependent on cytokines, we accounted especially for the influence of Th1 and neutrophils, both of which are important for macrophage recruitment (see Section 2.12, [29]). In addition, we accounted for production of pro-inflammatory cytokines leading to macrophage recruitment by Th17 and pro-inflammatory macrophages themselves.

*Macrophage deactivation.* Deactivation of macrophages, implemented as a step-wise transition from newly recruited pro-inflammatory to resident anti-inflammatory macrophages, is influenced by the inflammation status of the LP [59], which we implemented by a dependency of the deactivation transition rate on anti-inflammatory cytokines and an inhibition of this rate by pro-inflammatory cytokines (see Section 2.8). Anti-inflammatory cytokines in the LP (mainly IL-10, but also others such as TGF- $\beta$  [119]) are mostly produced by iTreg and anti-inflammatory macrophages, but also by Th2 [126]. As Th1 are specialised on macrophage activation (see Section 2.12), we implemented a high influence of Th1 on inhibition of macrophage deactivation, and a lower influence of the other pro-inflammatory cytokine-producing cell types Th17, neutrophils and pro-inflammatory macrophages.

*Dendritic cell activation.* The influence of pro- and anti-inflammatory cytokines on dendritic cell activation was implemented largely similar to macrophage deactivation, with reversed roles of pro- and anti-inflammatory cytokines; i.e. dendritic cell activation depends on pro-inflammatory cytokines, but is inhibited by anti-inflammatory cytokines (see Section 2.9). We used the same weights for anti-inflammatory cytokine-producing cell types as for macrophage deactivation. For pro-inflammatory cytokines we implemented a higher influence of neutrophils and macrophages than T helper cells, as none of the T helper cell types is specialised on dendritic cell activation in a way that relates to Th1's specialisation on macrophage activation.

*Damage to epithelium/ damage to tissue.* For simplicity, we assumed the same total influence of the different cytokine-producing cell types for the destruction of tissue and epithelium (see Section 2.5). Pro-inflammatory macrophages and neutrophils secrete reactive oxygen species, ECM-degrading enzymes and pro-inflammatory cytokines [54]. Reactive oxygen species are important mediators in the defence against bacterial invasion; however, they also induce local tissue damage [54, 127]. ECM-degrading enzymes, such as MMPs, allow for increased inflow of immune cells into the tissue, but require tight regulation by their inhibitors to limit tissue damage [54]. In addition, transepithelial migration of neutrophils into the gut lumen leads to small gaps between epithelial cells, increasing the permeability of the epithelium [56]. We accounted for the high influence of neutrophils and pro-inflammatory macrophages on tissue and epithelial destruction, and also for a smaller influence of other pro-inflammatory cytokine-producing cell types.

*Tissue remodelling.* Tissue remodelling ensures wound repair (see Section 2.5). It is mainly mediated by cytokines produced by tissue-resident, anti-inflammatory macrophages and Th2 [52, 53].

*Cytokine time courses.* The resulting time courses of the cytokines values in the mucosal injury scenario (Figure 17) show the influence of the different cytokine-producing cell types on the different processes. As the cytokine values are relative to the  $K_m$  values of the targeted process, a cytokine value of 1 corresponds to a half-maximal effect on the targeted process. The chosen parameter values for the cytokine production weights fulfil the qualitative requirements obtained from literature (described in the previous paragraphs): For neutrophil recruitment ( $\text{cyto}_{\text{rec,Neut}}$ ), shortly after the stimulus neutrophils themselves have a very high influence, then the influence of pro-inflammatory macrophages and Th17 becomes stronger. This cytokine value does not reach 1 (for half-maximal effect), as it does not include the additional effect of the bacterial concentration on neutrophil recruitment. Macrophage recruitment ( $\text{cyto}_{\text{rec,M}}$ ) is in the beginning of the inflammation mostly mediated by neutrophils, and later by Th1 and pro-inflammatory macrophages. The relative influences of pro-inflammatory cytokines on macrophage activation ( $\text{cyto}_{\text{pro,deact,M}}$ ) are very similar to macrophage recruitment, but with an even higher influence of Th1. Dendritic cell activation by pro-inflammatory cytokines ( $\text{cyto}_{\text{pro,act,DC}}$ ) is mediated by neutrophils (in the beginning of the inflammation) and pro-inflammatory macrophages (later). The anti-inflammatory environment stimulating macrophage deactivation and inhibiting dendritic cell activation ( $\text{cyto}_{\text{anti,deact,M}}$  and  $\text{cyto}_{\text{anti,act,DC}}$ ) is mainly due to iTreg, and, to a lower extent, anti-inflammatory macrophages. Destruction of tissue and epithelium ( $\text{cyto}_{\text{destr,tis}}$  and  $\text{cyto}_{\text{destr,epi}}$ ) is mainly mediated by neutrophils; tissue remodelling ( $\text{cyto}_{\text{remod,tis}}$ ) is mainly mediated by anti-inflammatory macrophages. Those cytokine values, however, do not reach 1 over the course of the inflammation. This ensures an almost linear effect of those cytokines on the targeted process (as saturation becomes more pronounced only for values higher than 1), and allows for much higher effects on those processes under different inflammation scenarios.

## 2.15 Resolution of inflammation

At the end of an infection, when the pathogens are cleared from the tissue, the immune system should return to its healthy steady state. Otherwise, this results in chronic inflammation, underlying many chronic diseases [128]. This return to healthy steady state is called the resolution phase. Resolution was long thought to be a passive process, resulting from decreasing pro-inflammatory processes, but is now known to be an active process [128]. Crucial to it is the lipid mediator class switch in neutrophils, which happens at apoptosis: The neutrophil switches from production of pro-inflammatory mediators to so-called specialised pro-resolving mediators (SPM) (lipoxins, resolvins, protectins and maresins) [63, 128]. Those SPM stop the production of pro-inflammatory cytokines by the neutrophil, inhibit further neutrophil recruitment, stimulate efferocytosis of the neutrophil by macrophages, and stimulate a pro-resolving phenotype in the efferocytosing macrophage (called “efferocytosis-type macrophage” in our implementation) [63, 70]. Those macrophages produce SPM (in even much higher amounts than apoptotic neutrophils [66]), stimulate tissue repair (see Section 2.14, paragraph *Tissue remodelling*), and are more efficient in phagocytosis of bacteria and efferocytosis of apoptotic cells [63, 128]. Through that, neutrophil apoptosis, and the associated lipid mediator class switch, is the first step to resolution of the inflammation [60], initiated already very early in the infection.

As for pro- and anti-inflammatory cytokines (see Section 2.14), we implemented SPM

as a weighted sum of SPM-producing cells, i.e. apoptotic neutrophils and efferocytosis-type macrophages, normalised by the  $K_I$  value of the inhibited process. The corresponding weights are shown in Table 3. The resulting unitless SPM value is relative to the  $K_I$ , i.e. an SPM value of 1 corresponds to half-maximal inhibition of the targeted process by SPM. Our implementation results in SPM values larger than 1 even at healthy steady state ( $\text{SPM}_{\text{ss}} = 2.5$ ), and increasing in the course of the inflammation. This means that the inflow of neutrophils and macrophages is already strongly controlled by SPM in healthy steady state, but the implementation allows also for much lower inhibition in case of insufficient SPM, leading to impaired resolution of inflammation. The relative production of SPM by macrophages is much higher than by apoptotic neutrophils (factor 430 [66]), so that the contribution of apoptotic neutrophils to SPM levels is negligible and the SPM value is directly proportional to the concentration of efferocytosis-type macrophages. This does, however, not mean that the neutrophils' role in the resolution is smaller; the effect of the apoptotic neutrophils producing SPM is implicitly implemented in the model in the fact that these molecules stimulate the phagocytosing macrophages to become efferocytosis-type macrophages, which produce SPM, participate in tissue repair, and have a higher phagocytosing capacity than pro-inflammatory macrophages. As efferocytosis-type macrophages themselves produce SPM, which increase neutrophil apoptosis and thereby the efferocytosis of apoptotic neutrophils by macrophages leading to a further increase in efferocytosis-type macrophages, the resulting resolution process is self-increasing, i.e. SPM-producing macrophages start to accumulate shortly after the start of the inflammation, until they are sufficient to considerably inhibit further recruitment of neutrophils and pro-inflammatory macrophages, thereby leading to a return of the system back to the healthy steady state.

Table 3: **SPM production weights.** Parameter values for the weights  $w_{\text{SPM},i}$  describing the relative contribution of different cell types  $S_i$  (rows) to SPM production. Parameter values are in unit mL.  $M_{\text{effero,tot}} = M_{\text{effero}} + \sum_b M_{\text{effero,a}} + M_{\text{effero,a,dep}} + M_{\text{effero,inf}}$ .

Cell type	SPM production
Neut <sub>apo</sub>	$1.12 \cdot 10^{-9}$
$M_{\text{effero,tot}}$	$4.8 \cdot 10^{-7}$

## 2.16 B cells and antibodies

B cells are, as T cells, part of the adaptive immune response, i.e. cells that provide antigen-specific help in an immune response. Their B cell receptors (BCRs) are structurally related to TCRs. B cells are activated by  $T_{\text{FH}}$  with the same antigen specificity in secondary lymphoid organs, and subsequently secrete their BCRs as antibodies (immunoglobulins, Ig) that are able to bind the specific antigen. Antibody coating of pathogens directly hinders their function and facilitates recognition and subsequent elimination of the pathogen by innate immune cells [29]. Epithelial cells of the gut mucosa transport IgA via the polymeric Ig receptor (pIgR) into the mucus layer, where it is called secretory immunoglobulin A (SIgA). SIgA coats bacterial cells and sterically hinders them from reaching the epithe-

lium [46, 129].

As commensal bacteria are constantly present in the colon and known to the immune system, we assumed that SIgA specific for commensal bacteria is also constantly present and does not significantly change during inflammation. Benckert et al. (2011) [130] reported that 25% of antigen-producing B cells of the intestine were polyreactive, i.e. binding to diverse self- and non-self antigens, and Keasey et al. (2009) [86] reported extensive cross-reactivity of antibodies to Gram-negative bacteria. From that we concluded that also pathogenic bacteria, even if not encountered by the immune system before, can sufficiently be coated by the available immunoglobulin in LP and SIgA in the mucus layer, and induction of B cells and antibodies specific for the pathogenic antigens does not significantly alter pathogen inflow into LP via the mucus layer or recognition of pathogens in the LP. Therefore we did not explicitly account for B cells or antibodies in our model. However, as we assume their concentrations and therefore their effects to be constant, those are implicitly accounted for, i.e. in the recognition of bacteria by phagocytic cells and as part of the mucus barrier including SIgA.

*Gut-associated lymphoid tissue (GALT).* The GALT of the colon (the part of the intestine that our model focuses on) consists mainly of isolated lymphoid follicles and colonic patches, the colonic counterpart of Peyer's patches in the small intestine. Isolated lymphoid follicles contain mainly B cells. Colonic patches, as Peyer's patches, consist of several B cell follicles and a smaller number of T cells in a defined T cell area. They are localised in the LP with direct contact to the lumen, and their epithelium contains M cells, special epithelial cells that sample antigen from the lumen and transfer it to underlying dendritic cells [29, 131]. As we did not account for B cells in our model, we also neglect isolated lymphoid follicles and colonic patches. The dynamics of T cell activation in colonic patches is qualitatively parallel to LNs, and therefore implicitly accounted for. Antigen sampling of APCs via M cells is implicitly included as part of the LP.

## 2.17 Healthy steady state

An ODE system, especially a complex one such as our systems biology model, can be expected to have several steady states. To determine a steady state corresponding to the healthy state, we simulated the model using the initial values  $x_{0,\text{tissue}} = x_{0,\text{epi}} = x_{0,\text{mucus}} = x_{0,\text{BactLu,commensal}} = 1$  and  $x_{0,i} = 0$  for all other state variables for a long time span, until the relative change over time was  $\frac{d}{dt} \frac{x_i}{x_i} < 1 \cdot 10^{-5}$  for all state variables  $x_i$ . Physiologically, by healthy steady state we denote the state of the mucosal immune system without any additional trigger such as pathogens or injury, corresponding to a healthy patient, i.e. without gut-related disease. Commensal bacteria are, of course, also present in the LP in the healthy steady state. Note that physiologically, there is never a real steady state, i.e. a state where the cell concentrations do not change at all, as there are always changes in the environmental influences (such as food, commensal bacteria composition, inflammation in other parts of the body,...).

The resulting simulated steady state  $\mathbf{x}_{\text{ss}}$  was then used as initial values  $\mathbf{x}_0$  in subsequent simulations of inflammation scenarios (see Section 2.18). In all figures of this chapter showing times courses of the species of the different submodels, the healthy steady state is shown for  $t < 0$ .

In Table 4 we compare the simulated healthy steady state to literature values of healthy steady state, for all model species where we found corresponding literature values. Note that some of the literature data were used to derive model parameters corresponding to the respective model species, i.e. inflow, outflow, death or transition rate constants ( $T_n$ ,  $DC_{\text{tot,LP}}$ ,  $M_{\text{tot}}$ ,  $M_{P_i,\text{tot}}$ ), whereas others were only used to validate the model by comparing if the magnitude approximately corresponds ( $T_{\text{cm}}$ ,  $T_{\text{em}}$ ,  $iT_{\text{reg,tot,LN}}$ ,  $iT_{\text{reg,tot,LP}}$ ,  $\text{Neut}$ ,  $\text{Bact}_{\text{LP}}$ ). The given literature values were calculated from different human studies (with two exceptions, where the data were taken from mouse studies), using mean values over different subjects. Because of high variability between individuals and expected high variability between measurements in different studies, the literature values have to be taken with care. Overall, we evaluate our simulated healthy steady state concentrations compared to the corresponding literature values as appropriate.

## 2.18 Inflammation scenarios

In order to test and show the ability of the developed model to qualitatively reflect the physiological time course of the mucosal immune system in response to bacterial challenge, we considered three different inflammation scenarios: (i) infection with a generic extracellular bacterium (not referring to a specific bacterial strain), (ii) infection with salmonellae (intracellular bacteria), and (iii) mucosal injury leading to an inflow of commensal bacteria into the tissue. Infection with salmonellae and response to mucosal injury were used in the previous sections to illustrate the time course of state variables of the submodels in response to bacterial challenge or injury (Figures 2, 5, 9, 11, 15, 16, 17). For all simulations of inflammation scenarios, we assumed the host to be in healthy steady state, then either added pathogenic (extracellular or intracellular) bacteria to the bacterial lumen or decreased the values of the tissue and epithelium state variables at time point  $t = 0$  (mucosal injury).

Figure 18 shows the time course of bacterial concentrations in LP and total concentrations of neutrophils, macrophages, dendritic cells and T helper cells in LP for the three different inflammation scenarios. Although the amount of inflowing bacteria (note that the total amount of bacteria, i.e. commensal and pathogenic bacteria in LP, is shown) differs highly between the different inflammation scenarios, the time course of immune cells in response to the stimulus, especially their chronological order of increase and decrease, is highly similar between the different simulations. The comparably high concentration of extracellular bacteria in LP is a result of the implemented characteristics of the generic extracellular pathogen: As it is easier eliminated by innate immune cells in the LP than salmonellae, we implemented a higher inflow rate to obtain comparable extents of immune reactions.

### 2.18.1 Infection with generic extracellular pathogen

There are several common extracellular pathogens infecting the human gut. However, most of them mainly infect the stomach (e.g. *Helicobacter pylori* [135]) or small intestine (e.g. *Campylobacter jejuni* [136]), do not invade the tissue (e.g. *Clostridium difficile* [137]), or have special characteristics, such as induction of extensive diarrhoea (e.g. *Clostridium difficile*, *Vibrio cholerae*, diarrhoeagenic *Escherichia coli* [137–139]), that we would have

Table 4: **Healthy steady state: comparison of literature and simulated values.** Healthy steady state concentrations calculated from literature data (green, above, with the corresponding references and details to the measurements) in comparison to simulated healthy steady state concentrations (violet, below), for all model species where we found literature data. All literature values refer to human data, except specified otherwise.

	Conc. [ $\frac{1}{\text{mL}}$ ]	Reference	Measurement details
Tn	$1.9 \cdot 10^8$	[97, 98]	lymphoid tissue/ MLN
	$1.9 \cdot 10^8$		
Tcm	$3.1 \cdot 10^8$	[97, 98]	lymphoid tissue/ MLN
	$1.2 \cdot 10^8$		
Tem	$2.2 \cdot 10^8$	[80, 98]	sigmoid colon/ ascending colon
	$3.1 \cdot 10^7$		
iTreg <sub>tot, LN</sub>	$4.2 \cdot 10^7$	[97, 98, 132, 133]	MLN/ lymphoid tissue/ blood
	$5.8 \cdot 10^6$		
iTreg <sub>tot, LP</sub>	$1.7 \cdot 10^7$	[80, 98, 132, 133]	colon/ sigmoid colon/ ascending colon
	$1.4 \cdot 10^8$		
DC <sub>tot, LP</sub>	$5.6 \cdot 10^6$	[80–82]	sigmoid colon/ colon
	$6.5 \cdot 10^6$		
M <sub>tot</sub>	$2.0 \cdot 10^7$	—, [74]	—, mouse intestine
	$2.2 \cdot 10^7$		
M <sub>P1, tot</sub>	$1.2 \cdot 10^6$	—, [59]	—, mouse colon
	$2.0 \cdot 10^6$		
M <sub>P2, tot</sub>	$7.1 \cdot 10^5$	—	—
	$1.2 \cdot 10^6$		
M <sub>P3, tot</sub>	$2.2 \cdot 10^6$	—	—
	$3.3 \cdot 10^6$		
M <sub>P4, tot</sub>	$1.6 \cdot 10^7$	—	—
	$9.1 \cdot 10^6$		
Neut	$2.0 \cdot 10^6$	[134]	gaster
	$1.3 \cdot 10^6$		
Bact <sub>LP</sub>	$2.7 \cdot 10^5$	[55]	sigmoid colon, total anaerobe count
	$2.7 \cdot 10^4$		



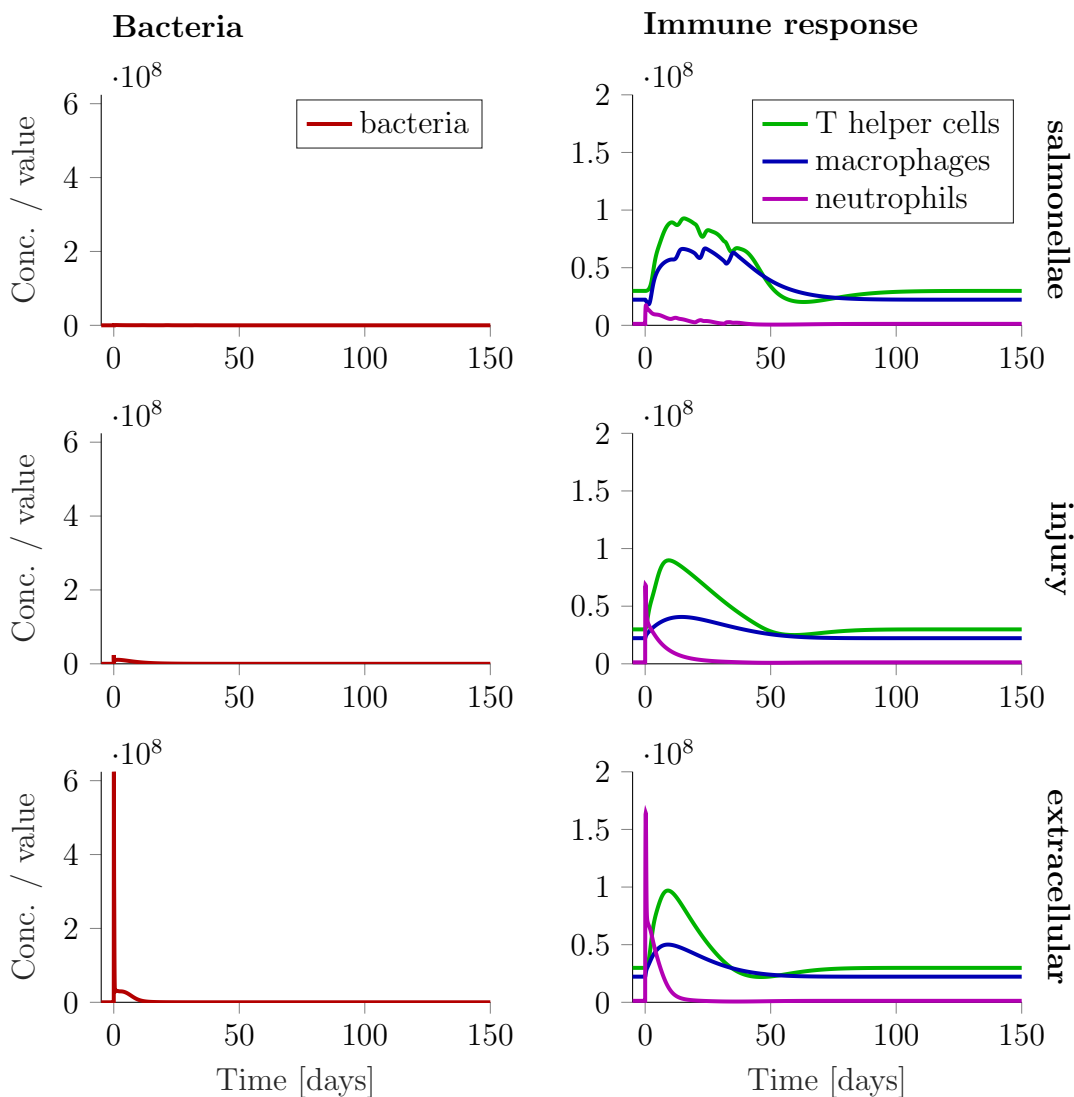


Figure 18: **Time course of inflammation.** Concentrations of bacteria and selected immune cells in LP over time. Bacteria:  $\sum_b \text{Bact}_{\text{LP}}$ , neutrophils:  $\text{Neut}$ , macrophages:  $M_{\text{tot}}$ , dendritic cells:  $\text{DC}_{\text{tot,LP}}$ , T helper cells:  $\text{Th} + \text{Tem1} + \text{Tem2} + \text{Tem17} + \sum_{i=1}^{N_{\text{T,prol}}} \text{Tn2Th}$ . Note the different y-axis for the bacterial concentration in the different inflammation scenarios.

had to account for in our model. Therefore, we implemented a *generic* extracellular pathogen, which does not correspond to a single specific pathogen, but possesses the main characteristics of extracellular pathogens invading the colon LP, i.e. its pathogenicity is defined by its ability to cross the epithelial barrier and evade recognition and phagocytosis by innate immune cells. Potential additional characteristics, such as access to blood or LNs or triggering of diarrhoea, were not considered. Therefore, this simulation should be interpreted with care, as it is only intended to show the characteristics of our model—which aims at the simulation of IBD—and not to analyse infections with extracellular pathogens.

The differences in parameters concerning extracellular pathogenic bacteria compared to commensal bacteria, and thereby defining the modelled generic extracellular pathogen, are the following: Bacterial growth in lumen is lower than for commensal by bacteria by

factor 0.8 (see Section 2.4). Bacterial growth in tissue is similar to commensal bacteria (see Section 2.6). Compared to commensal bacteria, which we implemented as a combination of different strains, we considered only a single strain of extracellular pathogenic bacteria. The pathogenicity is determined by the ability to cross the epithelial barrier, with rate constant  $\epsilon_{\text{Bact},2,\text{extracellular}} = 1 \cdot 10^{11}$  (see Section 2.5) and a decreased recognition and phagocytosis by immune cells by factor 10 compared to commensal bacteria, i.e.  $R_{\text{phago}} = 0.1$  (see Section 2.6). As extracellular pathogens mainly invoke Th17 responses,  $A_{1,\text{extracellular}} = A_{2,\text{extracellular}} = 0, A_{17,\text{extracellular}} = 1$  (see Section 2.12). We simulated a primary infection, i.e. recognition by memory T cells is only due to conserved structures, which we implemented as a decreased probability of antigen recognition by factor  $R_{\text{Tm},\text{extracellular}} = 0.7$  (see Section 2.11, paragraph *Central memory T cells (LN)*).

Figure 19 shows the time course of bacterial concentrations and neutrophils, macrophages and T helper cells in LP in response to different amounts of pathogenic extracellular bacteria. The immune response to the different initial loads differs in the extent of the recruited cells; the general time course and the time to resolution, however, is highly similar.

### 2.18.2 Infection with *Salmonella* Typhimurium (*S. Typhimurium*)

Infection of the gut with salmonellae is a widely used model for gut infection. Their pathogenicity is mediated by proteins encoded in two regions: salmonella pathogenicity islands 1 and 2, mediating engulfment of bacteria, formation of so-called salmonella-containing vacuoles and prevention of reactive oxygen species (ROS) production by macrophages, facilitating intracellular survival [140, 141]. Infected macrophages need help from Th1 to successfully eliminate the intracellular salmonellae [29, 36]. *Salmonella enterica* subspecies *enterica* serovar Typhimurium (*Salmonella* Typhimurium (*S. Typhimurium*)) is responsible for most cases of food poisoning in human [142]. In mice, *S. Typhimurium* does not elicit an inflammatory response in the gut LP. To reproduce an infection behaviour as in human, i.e. invasion of gut LP causing an inflammatory response, a model of streptomycin-pretreated mice was developed [143]: Pre-treatment of the mice with the antibiotic streptomycin, degrading commensal bacteria and thereby favouring *S. Typhimurium*, led to much higher *S. Typhimurium* numbers in faeces and elicitation of colitis, compared to control mice. Using this model system, the main characteristics of human salmonella infection, such as epithelial ulceration and a massive inflow of neutrophils, could be reproduced [143].

We included salmonellae into the model in the following way: As it is a pathogenic bacterium infecting the gut, *S. Typhimurium* is able to cross the epithelial barrier. In contrast to extracellular bacteria, *S. Typhimurium* mainly proliferates intracellularly, mostly in macrophages. Therefore we neglected extracellular growth, assumed that recognition by phagocytic cells is not lower than for commensal bacteria, and implemented infection of macrophages by *S. Typhimurium* based on two published models:

i) Brown et al. (2006) [144] described the distribution of numbers of *S. Typhimurium* per cell in mouse liver sections using different mathematical models. The simplest one uses two parameters, an intracellular growth rate constant and a burst threshold  $N_{\text{burst}}$  of intracellular bacteria in a host cell, at which the host cell dies and releases  $N_{\text{burst}}$  bacteria that directly infect  $N_{\text{burst}}$  new host cells. The rate of intracellular growth, i.e. transition from the state of a cell containing  $n$  bacteria  $M_n$  to the state containing  $n + 1$  bacteria

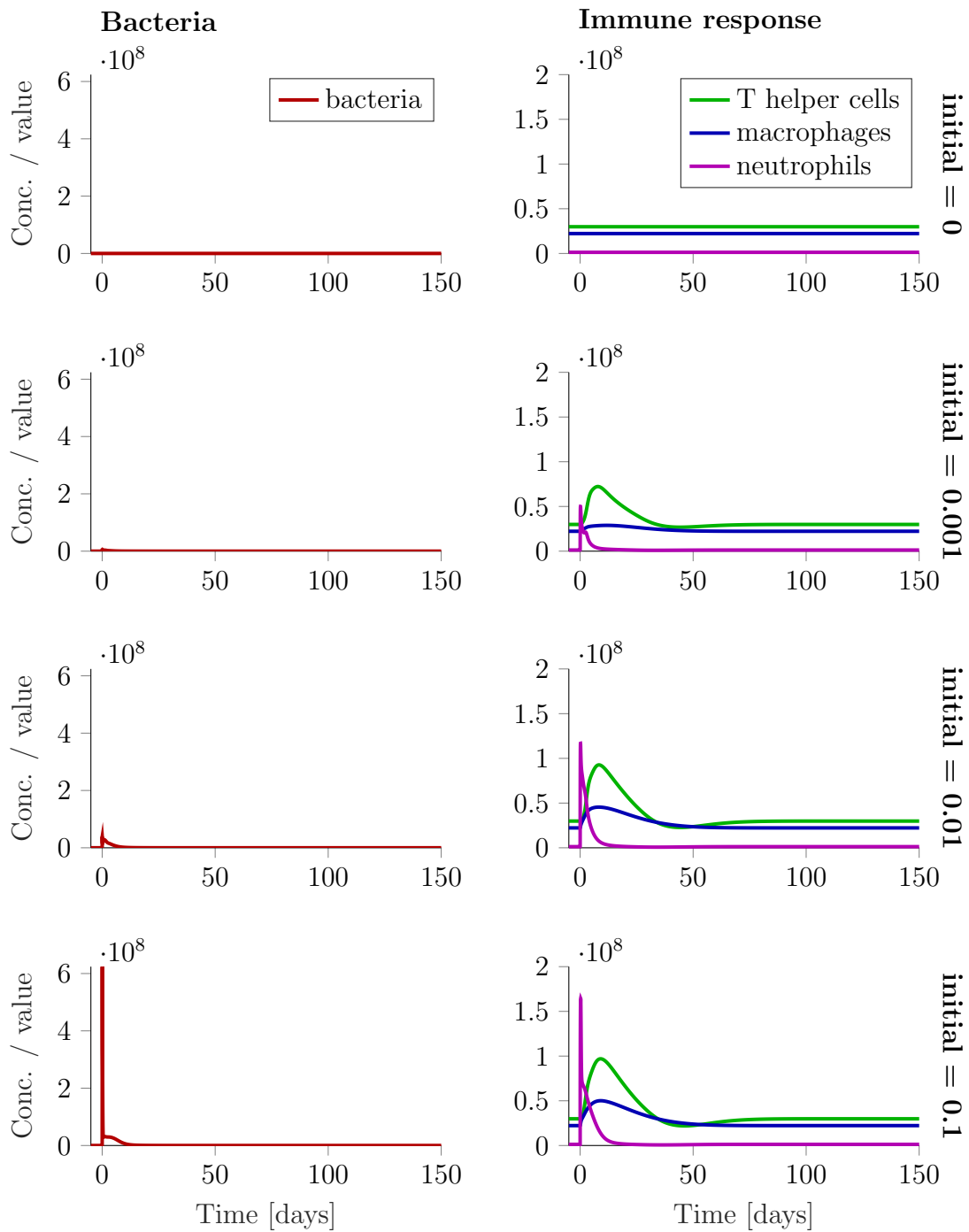


Figure 19: **Time course of infection with generic extracellular pathogen for different initial loads.** Concentrations of bacteria and selected immune cells in LP over time in response to different initial amounts of pathogenic extracellular bacteria at time point  $t = 0$  in lumen. As described in Section 2.4, pathogenic bacteria in the lumen are modelled by a unitless value describing the fraction of pathogenic bacteria from steady state commensal bacteria. i.e. initial = 0.1 corresponds to a pathogen load of 10% of the commensal bacteria in lumen at  $t = 0$ . Bacteria:  $\sum_b \text{Bact}_{\text{LP}}$ , neutrophils: Neut, macrophages:  $M_{\text{tot}}$ , T helper cells: Th + Tem1 + Tem2 + Tem17 +  $\sum_{i=1}^{N_{\text{T,prol}}} \text{Tn2Th}$ .

$M_{n+1}$  is  $n \cdot$  growth rate constant  $\cdot M_n$ . They found that, although the absolute number of infected cells is increasing, the proportion of cells containing  $n$  bacteria is given by  $Q_n = \frac{N_{\text{burst}}}{(N_{\text{burst}}-1) \cdot n \cdot (n+1)}$  (independent of the growth rate constant) [144]. They reported the best fit for the burst threshold to be  $N_{\text{burst}} = 30$ .

ii) Gog et al. (2012) [145] described the early infection dynamics of bone-marrow-derived macrophages with *S. Typhimurium* *in vitro*, i.e. the distribution of numbers of bacteria per cell 10 min after infection for different multiplicities of infection (MOIs) (ratio of bacteria to host cells). Their mathematical model, describing the fractions of macrophages containing 0, 1, ..., 8 or 9 and more bacteria, included an infection rate constant specific for MOI, and a growth rate constant. Death of macrophages was negligible in the given setting. In addition, they showed that reinfection of macrophages already containing at least one bacterial cell was lower than infection of uninfected macrophages (implemented as a relative reinfection constant  $< 1$ ). They fitted a Michaelis-Menten equation to the MOI-specific infection rate constants, giving a maximal infection rate  $V_{\text{max}}$  per macrophage per MOI, and a unitless  $K_M$  value, i.e. the MOI for half-maximal infection rate.

Using the main results and parameters from those two models, we implemented macrophage infection by *S. Typhimurium* as follows: We combined the models by Gog et al. and Brown et al., i.e. we considered infection of macrophages by extracellular *S. Typhimurium*, intracellular growth and burst of the macrophage at the burst threshold, releasing *S. Typhimurium* into the tissue. We neglected reinfection of already infected macrophages, although infected macrophages were able to further eliminate extracellular *S. Typhimurium* but without effect to the number of intracellular bacteria. We used the intracellular growth rate constant  $p_{\text{STm,int}}$  from Gog et al. [145] and the burst threshold  $N_{\text{burst}}$  from Brown et al. [144]. From the Michaelis-Menten parameters for the infection rate per macrophage per MOI by Gog et al. [145] we calculated the Michaelis-Menten parameters for the infection rate per macrophage and *S. Typhimurium* concentrations by dividing  $V_{\text{max}}$  and  $K_M$  by the reported concentration of macrophages in the experimental setting. Those values ( $V_{\text{max}} = 11.9 \frac{1}{\text{h}}$ ,  $K_M = 3.9 \cdot 10^7 \frac{1}{\text{mL}}$ ) are very similar to the  $V_{\text{max}}$  and  $K_M$  values that we derived from Li et al. [58] for the elimination of bacteria from the tissue ( $V_{\text{max}} = 22.2 \frac{1}{\text{h}}$ ,  $K_M = 3.7 \cdot 10^7 \frac{1}{\text{mL}}$ ) in Section 2.6. Therefore, we used the parameters derived from Li et al. [58] for phagocytosis/elimination of all bacteria in the LP, where phagocytosis of *S. Typhimurium* by macrophages resulted in intracellular infection. All different subsets of macrophages in the model (different activation states, antigen-unexperienced/-experienced, efferocytosis-type and pMHCII-depleted; see Sections 2.8 and 2.13) can be infected by *S. Typhimurium*, where the infection rate is slightly different between the subsets (population P1 to P4) depending on the differences in phagocytosis efficiency (see Section 2.8, [59]). All infected macrophages are antigen-experienced, with bacteria-specificity to *S. Typhimurium*, resulting in the five different model species of infected macrophages  $M_{\text{P1,inf}}$ ,  $M_{\text{P2,inf}}$ ,  $M_{\text{P3,inf}}$ ,  $M_{\text{P4,inf}}$  and  $M_{\text{effero,inf}}$ , with rates applying as described in the previous sections (Section 2.8 and 2.13) for the corresponding uninfected macrophage species, an additional rate of macrophage death at bacterial release, and an additional rate for Th1-helped elimination of intracellular bacteria. We calculated the rate of bacterial release according to the model by Brown et al. [144]:

$$\begin{aligned} \text{bacterial release} &= N_{\text{burst}} \cdot (N_{\text{burst}} - 1) \cdot p_{\text{STm,int}} \cdot M_{\text{Pi,inf},N-1} \\ &= N_{\text{burst}} \cdot (N_{\text{burst}} - 1) \cdot p_{\text{STm,int}} \cdot Q_{\text{Pi,inf},N-1} \cdot M_{\text{Pi,inf}} \end{aligned}$$

$$= N_{\text{burst}} \cdot \frac{p_{\text{STm,int}}}{N_{\text{burst}} - 1} \cdot M_{\text{Pi,inf}},$$

where  $M_{\text{Pi,inf},N-1}$  is the concentration of infected macrophages of population  $Pi$  containing exactly  $N - 1$  bacteria,  $Q_{\text{Pi,inf},N-1}$  is the corresponding proportion of macrophages of population  $Pi$  containing  $N - 1$  bacteria, and  $M_{\text{Pi,inf}}$  is the total concentration of infected macrophages of population  $Pi$ . Note that  $M_{\text{Pi,inf},N-1}$  was only used to derive the bacterial release rate as a function of  $M_{\text{Pi,inf}}$ , but was not included as a state variable in the model. The corresponding death rate of macrophages (which die at release of bacterial cells) is

$$\text{macrophage death at bacterial release} = \frac{p_{\text{STm,int}}}{N_{\text{burst}} - 1} \cdot M_{\text{Pi,inf}}.$$

We implemented Th1 help for macrophages in elimination of intracellular bacteria on a cell-contact basis, as described in Section 2.10. Upon the contact of a Th1 specific to *S. Typhimurium* with a salmonella-infected macrophage  $M_{\text{Pi,inf}}$ , the macrophage reverts to an uninfected state, i.e. an antigen-experienced macrophage of the respective population with bacteria-specificity for salmonellae. The rate from  $M_{\text{Pi,inf}}$  to  $M_{\text{Pi,a,salmonellae}}$  is therefore

$$\frac{\text{Th}_{\text{tot,LP,salmonellae}}}{T_{\text{tot,LP}}} \cdot \frac{M_{\text{Pi,inf}} \cdot \text{bs}_{\text{perM}} \cdot \left(1 - \frac{\text{Tem2Treg}_1}{\text{sDC}_{\text{LP}} \cdot \text{bs}_{\text{perDC}} + M_{\text{pro,a}} \cdot \text{bs}_{\text{perM}}}\right)}{\text{BS}_{\text{APC,av,LP}}}$$

for P1 to P3 (pro-inflammatory) and

$$\frac{\text{Th}_{\text{tot,LP,salmonellae}}}{T_{\text{tot,LP}}} \cdot \frac{M_{\text{Pi,inf}} \cdot \text{bs}_{\text{perM}} \cdot \left(1 - \frac{\text{Tem2Treg}_1}{\text{tDC}_{\text{LP}} \cdot \text{bs}_{\text{perDC}} + M_{\text{anti,a}} \cdot \text{bs}_{\text{perM}}}\right)}{\text{BS}_{\text{APC,av,LP}}}$$

for P4 and  $M_{\text{effero}}$  (anti-inflammatory).

Infected macrophages function as APCs and are therefore included in the calculation of available binding sites on APCs  $\text{BS}_{\text{APC,av,LP}}$ . In addition, they produce cytokines to the same extent as the other pro- or anti-inflammatory antigen-experienced macrophage species.

*S. Typhimurium* growth in lumen is aimed to be lower than for commensal by bacteria by factor 0.8 (see Section 2.4). Growth in LP (extracellular) is neglected, i.e.  $p_{\text{Bact,LP,salmonellae}} = 0$ . Recognition and phagocytosis by phagocytic cells is assumed similar to commensal bacteria  $R_{\text{phago,salmonellae}} = R_{\text{phago,commensal}} = 1$ . Compared to commensal bacteria, which we implemented as a combination of different strains, *S. Typhimurium* are implemented as a single strain. The rate constant for crossing the epithelial barrier (with toxin) is  $\epsilon_{\text{Bact,2,salmonellae}} = 1 \cdot 10^{10}$  (see Section 2.5). Note that the inflow rate constant and the initial value of bacterial load in lumen (unitless, given as fraction of steady state commensal bacteria) are highly correlated, i.e. a higher value of *S. Typhimurium* in lumen and a lower inflow rate constant lead to the same concentration in LP as a lower value of *S. Typhimurium* in lumen and a higher inflow rate constant. As intracellular pathogens mainly invoke Th1 responses,  $A_{1,\text{salmonellae}} = 1$ ,  $A_{2,\text{salmonellae}} = A_{17,\text{salmonellae}} = 0$  (see Section 2.12). We simulated a primary infection, i.e. recognition by memory T cells is only due to conserved structures, which we implemented as a decreased probability of antigen recognition by factor  $R_{\text{Tm,salmonellae}} = 0.7$  (see Section 2.11, paragraph *Central memory T cells (LN)*).

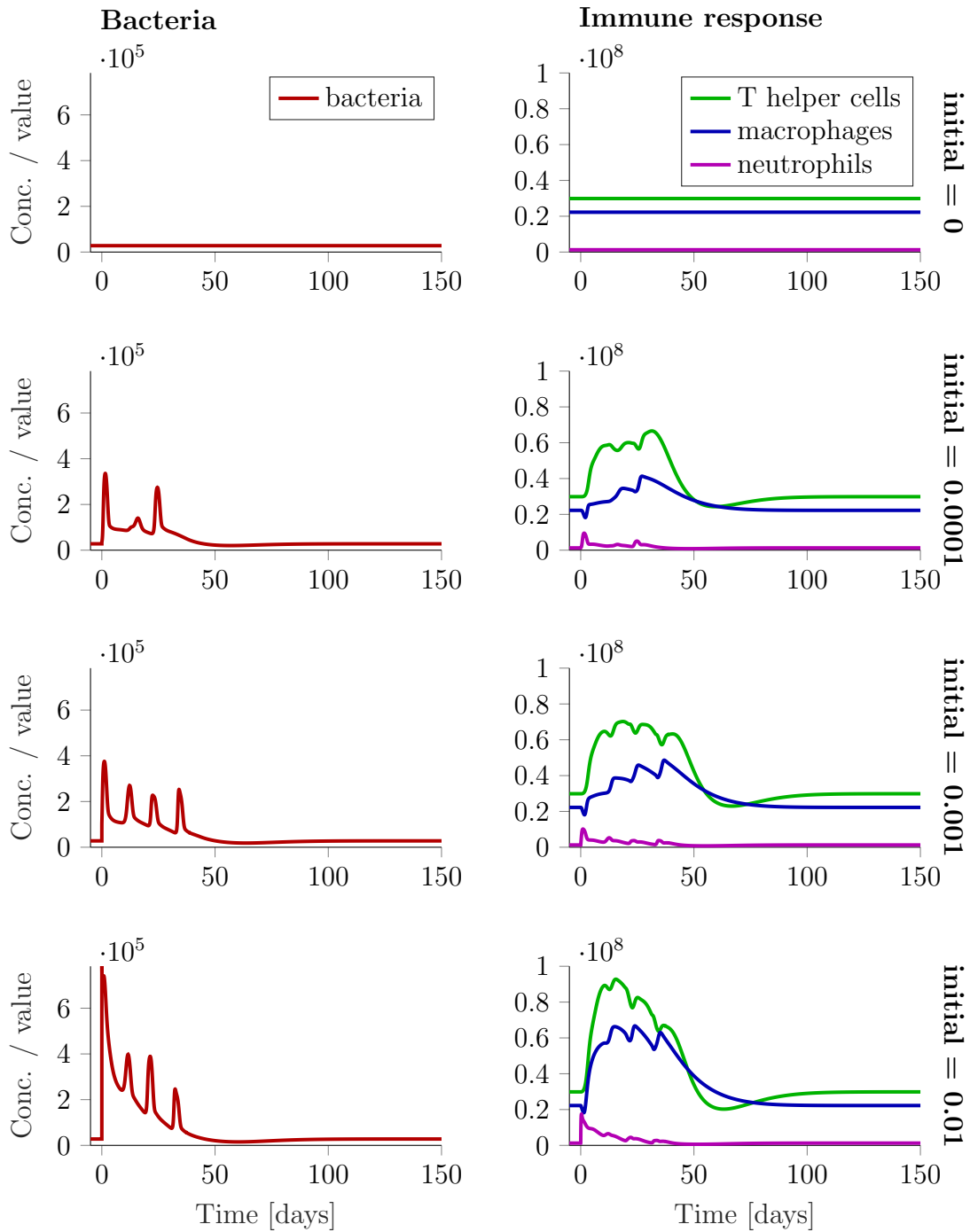


Figure 20: **Time course of *S. Typhimurium* infection for different initial loads.**

Concentrations of bacteria and selected immune cells in LP over time in response to different initial amounts of *S. Typhimurium* at time point  $t = 0$  in lumen. As described in Section 2.4, pathogenic bacteria in the lumen are modelled by a unitless value describing the fraction of pathogenic bacteria from steady state commensal bacteria. i.e. initial = 0.01 corresponds to a pathogen load of 1% of the commensal bacteria in lumen at  $t = 0$ . Bacteria:  $\sum_b \text{Bact}_{LP}$ , neutrophils:  $\text{Neut}$ , macrophages:  $M_{\text{tot}}$ , T helper cells:  $\text{Th} + \text{Tem1} + \text{Tem2} + \text{Tem17} + \sum_{i=1}^{N_{T,\text{prol}}} \text{Tn2Th}$ .

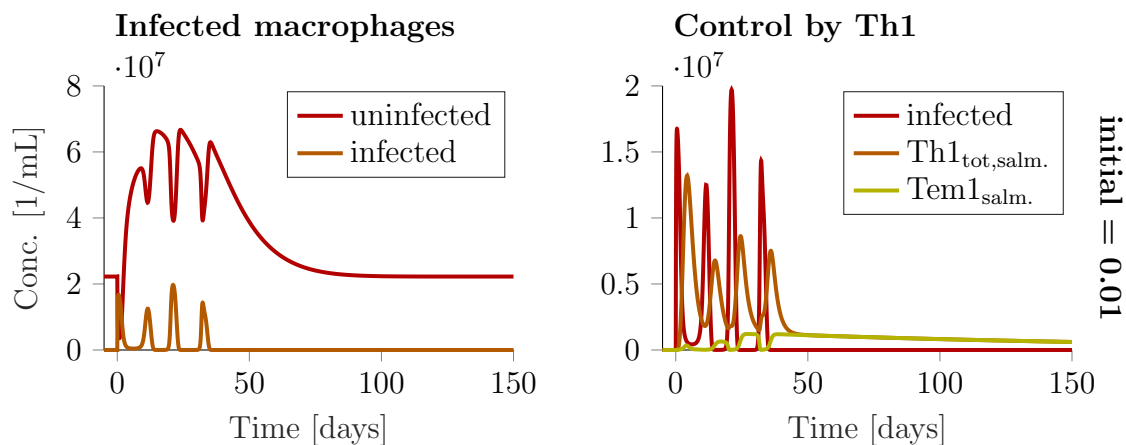


Figure 21: **Infected macrophages by *S. Typhimurium* and their control by Th1 over time.** Infected and uninfected macrophages and salmonella-specific Th1 over the time course of an infection with *S. Typhimurium* (initial amount in lumen of 0.01 of steady state commensal bacteria, corresponding to the last row of Figure 20). Left: Uninfected and infected macrophages over time. Right: Infected macrophages, total effective salmonella-specific Th1  $\text{Th1}_{\text{tot,salmonellae}}$  and salmonella-specific effector memory T cells type 1  $\text{Tem1}_{\text{salmonellae}}$ . Note that  $\text{Tem1}_{\text{salmonellae}}$  is included in  $\text{Th1}_{\text{tot,salmonellae}}$ .

Figure 20 shows the time course of bacterial concentrations and neutrophils, macrophages and T helper cells in LP in response to different initial amounts of *S. Typhimurium*. As in the simulated infection with generic extracellular pathogen, we observed that the immune response to the different initial loads differs in the extent of the recruited cells, but the general time course is highly similar. The recurrent peaks in the LP concentration of bacteria (note that the sum of commensal bacteria and extracellular salmonellae is shown) are due to the control of infected macrophages by Th1 (see Figure 21): The concentration of salmonellae decreases when the salmonella-specific Th1 concentration is high enough to control the infected macrophages, but a decrease in the salmonella concentration also leads to a decrease in salmonella-specific Th1, as they are only induced by salmonella antigens, leading to a recurrent increase in the salmonella concentration when Th1 levels are too low. The increase in effector memory T cells specific for salmonellae is slower but more sustained than the dynamics of fully differentiated Th1; therefore salmonella-specific effector memory T cells accumulate over the course of the infection, allowing for a faster supply of fully differentiated Th1 in response to an outbreak of the salmonella infection. The pattern of recurrent outbreaks of the salmonella infection, followed by increases in the salmonella-specific Th1 concentration, is repeated until the salmonella concentration can be controlled strong and long enough to fully eliminate salmonellae from the LP. In our simulation, all cells of the same type behave identically, whereas in reality there is spatial and stochastic variability and therefore this synchronous behaviour would probably not be visible.

As we use a deterministic approach, the salmonella concentration will never reach zero after an infection, and already a very low concentration will result in a new outbreak once the Th1 concentration returns to normal levels. This does, of course, not reflect the biological behaviour. For very small concentrations of bacteria in the LP, a stochastic approach to analyse the model behaviour would be more appropriate. Such an approach (e.g. using the Gillespie algorithm [146]) could be used to evaluate possible time courses of

very low numbers of salmonellae and infected macrophages, using the probabilities that the different reactions (infection of macrophages leading to production of new pathogens, or elimination of salmonellae) take place in the next infinitesimal time interval (propensities). This approach, in contrast to the deterministic approach, allows for extinction of the pathogen. However, detailed analysis of salmonella infections for very low numbers of bacteria was not the intention of this work. Therefore we did not further consider this problem, but set the concentration of *S. Typhimurium* in LP to zero, if the absolute number of *S. Typhimurium* in the whole gut LP is lower than 1, i.e.  $Bact_{LP,salmonellae} \cdot V_{LP} < 1$ . We note, however, that the developed systems biology model could be used to analyse the behaviour of salmonella infections stochastically, e.g. by applying a hybrid stochastic-deterministic algorithm [147].

In most experiments, the amount of *S. Typhimurium* eliciting the infection was reported as the amount of *S. Typhimurium* orally given [143, 148, 149], whereas the starting point for our simulation is the amount of *S. Typhimurium* in colon lumen, given as the fraction of steady state commensal bacteria. The relation between those two numbers was unknown to us. In addition, we did not account for proliferation of *S. Typhimurium* in lumen or back-transport of *S. Typhimurium* from LP into lumen, as we focused on the dynamics in the tissue and the elicited immune response. In many studies, however, *S. Typhimurium* count in faeces was the main measurement to evaluate the degree of infection [143]. In order to quantitatively compare those experimental results (which are even highly diverse between different experimental studies) to our model simulations, we would have had to adapt our model to the single experiments; as, however, the simulation of *S. Typhimurium* infection was not the intention of our work, but only a means to evaluate our model, we did not pursue these efforts.

On a qualitative level, however, our simulation results reproduce the main characteristics of human salmonella infection and infection of streptomycin-pretreated mice: Most importantly, our virtual immune system is able to timely eliminate the pathogen from the tissue by eliciting an appropriate immune response, i.e. *S. Typhimurium* infection elicits a self-limited inflammation. Thereby, the extent of the immune response, i.e. the increase of the concentration of immune cells, depends on the initial amount of *S. Typhimurium*, but already very low numbers of *S. Typhimurium* lead to an infection and considerable immune response. Lastly, the control of the disease is dependent on the help from Th1. See also Section 3.1.2 for the simulated effect of Th1 knockout on the course of a salmonella infection.

### 2.18.3 Immune response to mucosal injury

Mucosal injury, i.e. injury of the epithelial or tissue layer, resulting in an inflow of commensal bacteria into the tissue, where they elicit an immune response, can occur due to several different reasons: Non-steroidal anti-inflammatory drugs (NSAIDs) (used in treatment of e.g. rheumatoid arthritis or cardiovascular diseases) very frequently lead to injuries mainly in gaster and small intestine [150], but also in colon (in approximately 3% of patients under long-term treatment with NSAIDs [151]). The drug induces damage of mitochondria, leading to an increased production and release of ROS, which in turn destroy intercellular junctions, increasing the barrier permeability. In addition, NSAIDs inhibit cyclooxygenase, which is required in prostaglandin synthesis, thereby leading to decreased levels of prostaglandins, which are important in tissue repair and resolution of



inflammation [150, 152]. Trauma can lead to a decreased epithelial barrier, as the blood flow is redistributed to supply vital organs, leading to ischemia in the intestine, resulting in disruption of tight junctions and increased epithelial cell apoptosis [153]. Another example of mucosal injury is radiation colitis: Radiation therapy targets cellular DNA, which can lead to death, inability to proliferate, or abnormal cell functions in epithelial cells, resulting in a decreased epithelial barrier [154, 155].

Acute DSS colitis is a mouse model for acute colitis due to epithelial damage (in contrast to chronic DSS colitis, which is a widely used mouse model for IBD). Dextran sodium sulfate (DSS), which is administered via drinking water, acts as chemical toxin to colon epithelium, inducing epithelial damage. Consequently, commensal bacteria can enter the colon LP and induce an inflammatory response [75]. Acute DSS colitis is induced by administration of DSS for 6-10 d. The first signs of disease are changes in the expression of tight junction proteins after approximately 1 d, followed by worsening symptoms such as increased intestinal permeability, bleeding and even death [75].

We simulated the immune response to mucosal injury and the resulting inflow of commensal bacteria into the gut LP by reducing the values of epithelium and/or tissue at time point  $t = 0$ , and simulating until the system reached healthy steady state again. As the build-up of the epithelium state variables depends on the tissue state variable, and the build-up of the mucus state variable depends on the epithelium state variable, both decrease of the epithelium and the tissue state variable lead to a decrease of the barrier function and therefore to an inflow of commensal bacteria into LP. Bacteria in LP consequently elicit an immune response. Note that in comparison to physiological causes of mucosal injury, especially to DSS colitis in mice, we simulate mucosal injury as being elicited by an abrupt trigger of epithelial barrier disruption at  $t = 0$ , without any further triggers for  $t > 0$ .

Figure 22 shows the bacterial concentrations and neutrophils, macrophages and T helper cells in LP in response to different combinations of tissue and epithelial destruction. As bacterial inflow depends on the epithelial barrier (and the mucus layer, which strongly follows the epithelial barrier), but not directly on tissue, the peak of the bacterial concentration in LP is higher for pure epithelial damage (2nd row) than for pure tissue damage (3rd row). However, tissue damage leads to a longer-lasting inflow of bacteria and inflammation response (3rd row) than epithelial damage without tissue damage (2nd row), because the epithelium depends on tissue integrity and can only be fully functional when the tissue layer is fully functional.

Nunes et al. (2018) [156] analysed the time course of acute DSS colitis in mice, which is qualitatively widely consistent with our model simulations. Unfortunately, results are only reported for the first 8 d, later time points were not analysed. Note that they induced acute DSS colitis by DSS in drinking water for a time span of 7 d, whereas our simulations assume an abrupt disruption of the epithelial barrier and/or underlying tissue. Despite the additional limitations and unknowns in the translation of the mouse model to human, a qualitative comparison of our simulation results with those experimental results can be used to qualitatively validate our systems biology model. In the acute DSS colitis model, the concentration of macrophages increases up to more than 4-fold during the first 8 d, and the concentrations of T helper cells and regulatory T cells increase up to  $\approx 3$ -fold during the first 8 d [156]. The increase in macrophages and T helper cells can also be seen in our model simulations (right column of Figure 22). The increase in regulatory T cells, however, is much less pronounced in our model simulations (see Figure 15). The severity of the acute DSS colitis, measured by clinical and histological scores, was

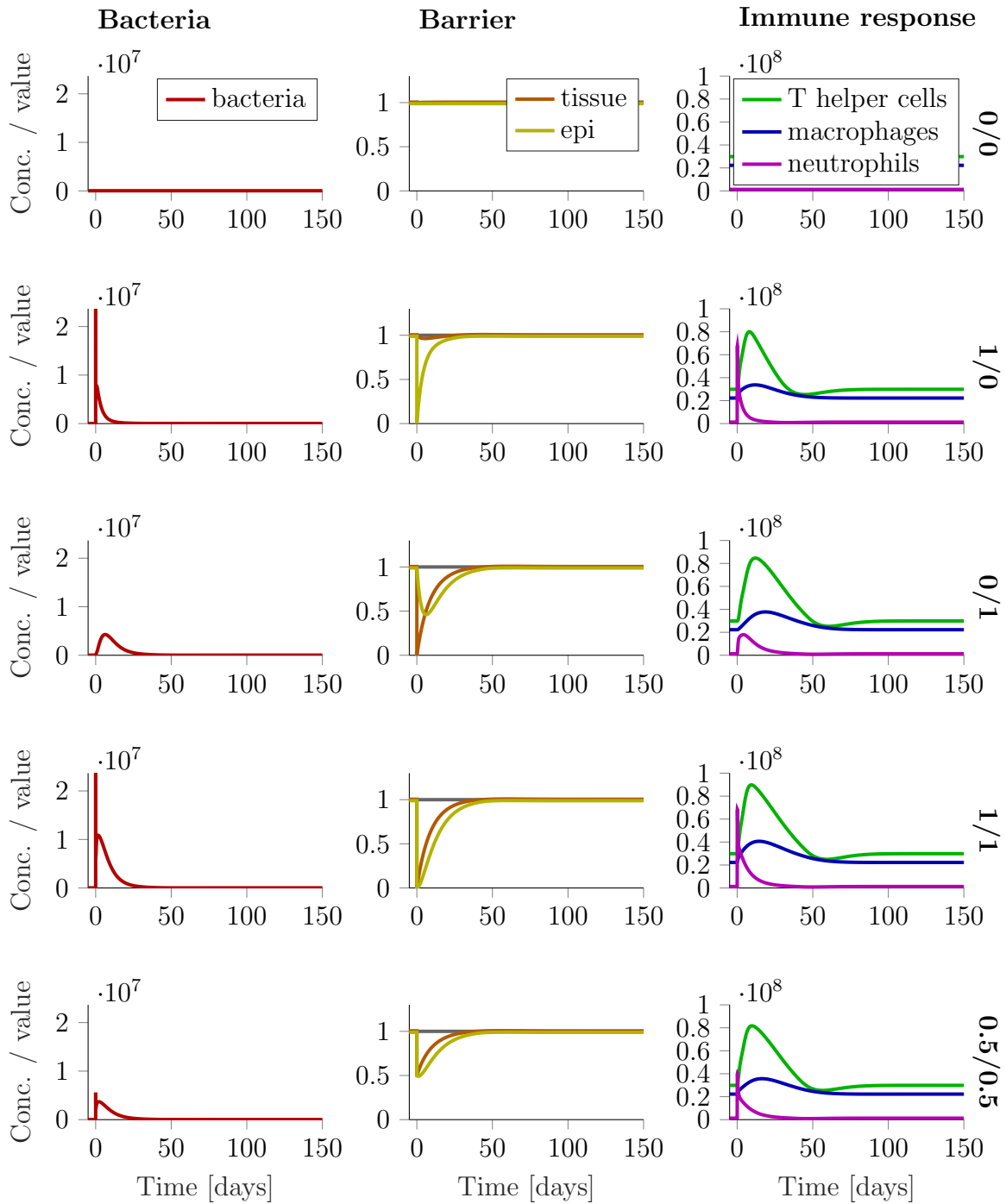


Figure 22: **Time course of mucosal injury.** Concentrations of bacteria and selected immune cells in LP and barrier state variables (unitless) over time in response to different extents of mucosal injury at time point  $t = 0$ . As described in Section 2.5, state variables describing tissue, epithelium and mucus layer are modelled as unitless values describing the relative functional intactness of the respective layer. The degree of mucosal injury is given as “relative epithelial destruction/relative tissue destruction”, where 0 means no destruction, and 1 means complete destruction, i.e. setting the state variable to 0 at  $t = 0$ . Bacteria:  $\sum_b \text{Bact}_{LP}$ , neutrophils:  $\text{Neut}$ , macrophages:  $M_{\text{tot}}$ , T helper cells:  $\text{Th} + \text{Tem1} + \text{Tem2} + \text{Tem17} + \sum_{i=1}^{N_{T,\text{prol}}} \text{Tn2Th}$ .

reported to depend on the concentration of DSS in drinking water [156]. The difference in DSS concentration probably results in different extents of epithelial destruction. We also observed this dependency in our simulations (compare Figure 22, row 4: 1/1 and row 5: 0.5/0.5): The increase in neutrophil, macrophage and T helper cell concentrations is higher for simulated complete than for half-maximal destruction of epithelium and tissue. The difference between these two simulations is, however, not as pronounced as the difference between the acute DSS colitis models resulting from 1 %, 2 % and 3 % DSS in drinking water (but we also don't know how the difference in DSS concentration translates to different extents of epithelial destruction). For a mucosal injury due to physical or drug effects in human, we expect the resulting inflammation to be self-limited after removing the trigger, which is described by our model as a timely return to healthy steady state for all extents of mucosal injury.

## 2.19 Conclusion

We aimed at developing a systems biology model describing the healthy mucosal immune response on a cellular level (for use in analysis of IBDs and their treatment, as described in the following chapters). The requirements for this model were to describe the mucosal immune system adequately both on the cellular level and on the level of the overall immune response, i.e. it had to adequately describe both the qualitative and quantitative characteristics known from literature about the separate cell types and processes of the mucosal immune response, and the overall time course of an immune response to different infectious and inflammatory stimuli. To achieve this aim, we performed an extensive literature research, based on which we determined the most important cell types and processes, also with respect to IBDs. See Figure 23 for a summary of our modelling approach. For each of the determined most important cell types and processes, we developed a sub-model based on the results of our literature research, to describe the available qualitative and quantitative data. Interactions between different cell types were implemented based on cell-cell contacts and cytokines. Simultaneously, we designed the model so that the integrated systems biology model was able to describe the key characteristics of the different inflammation scenarios, especially the successful fighting of pathogen or commensal bacteria, and the timely return to healthy steady state.

The resulting systems biology model is a systematic combination of available knowledge on the local gut immune effects, which sets isolated findings from various literature sources into context. It is relatively robust to variations in the parameter values, as will be further described in Chapter 4, where the large majority of a virtual population generated by introducing variability in the parameters react adequately to inflammatory triggers, comparable to the reference individual described in the current chapter. Our novel systems biology model provides a quantitative (cell concentration-based) and time-resolved, very detailed description of the mucosal immune response, based on an extensive literature research, where we separately investigated the dynamics of each implemented cell type and process. None of the previously published mathematical models of the mucosal immune response and IBDs known to us [24–27] fulfil all of these points.

*Limitations.* Due to the limited data situation and the simplification of complex physiological processes that is required to develop a systems biology model with acceptable

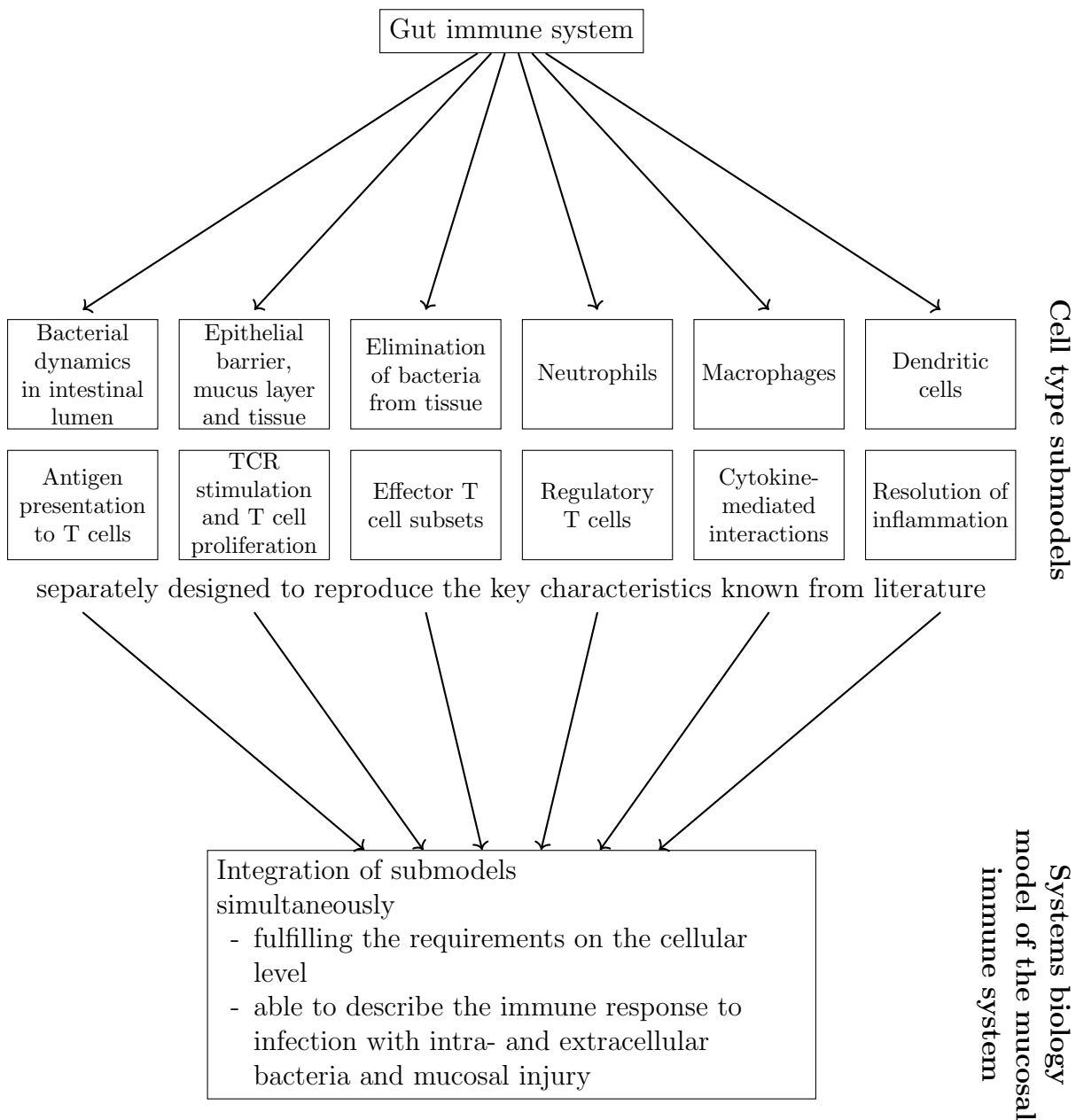


Figure 23: **Summary of the modelling approach.** Overview of the different steps of the modelling approach and the different levels of the resulting systems biology model: The model represents the gut immune system on the cellular level, which we separated into different submodels representing separate cell types or processes. Each submodel on its own was designed based on qualitative and quantitative data from literature, to adequately reproduce the key characteristics of this cell type or process. Combination of all submodels into the systems biology model of the mucosal immune system ensures that the requirements on the cellular level are fulfilled. In addition, the integrated model is able to describe the overall response of the gut immune system in different infection scenarios.

runtimes, our model has—as any (systems biology) model—limitations:

To validate the model using the overall time courses of our different inflammation scenarios, time course data of different immune cell concentrations in an inflammation setting representable by our model would have been ideal. Unfortunately, such data were not available to us. Therefore we had to use qualitative data (e.g. knowledge on the chronological succession of cell concentration increases and decreases) and isolated experimental findings (e.g. the relative increase of specific cell concentrations in inflammation) (see Sections 2.18.2 and 2.18.3). Note that these isolated findings come from different experiments with different experimental settings (regarding e.g. model species, extents of stimulus or measurement time points), and quantitative comparisons were therefore not expected to be very accurate.

For parameterisation of the submodels, we integrated many different experimental data from various sources, including data from *in vivo* experiments in different species (human, mouse, rat) and *in vitro* and *in silico* studies. For several parameters, no quantitative data could be obtained from the literature, so that we had to define the parameters based on rough estimates of their magnitude and the resulting model behaviour on the cellular and overall levels. Note that, however, more suitable data than those we built our model on are unfortunately currently not available, and therefore a more reliable parameterisation is currently hardly possible. Apart from that, this model can in the future be used to plan further, targeted experiments, to generate hypotheses, and to demonstrate where additional knowledge is required for a deeper and more quantitative understanding of the mucosal immune response.

Not only the parameter values, but also the model structure is based on different hypotheses obtained from the literature, which naturally only repeat the current state of knowledge. In the previous sections (Section 2.2-2.18.3) we stated the assumptions we made to derive the model structure of the different submodels. In addition, we focused on those cell types and processes we identified as being most important for the mucosal immune response, especially with regard to IBDs. Other cell types were neglected, although their roles in the mucosal immune response and IBDs have been stated in literature (e.g. NK cells, NKT cells, fibroblasts or B cells), in order to keep the model complexity manageable. This leads (as in every model) to a simplification. Additional processes and cell types, however, can easily be incorporated into the systems biology model by providing the respective ODEs and parameters.

The representation of the mucosal immune system using only two spatial compartments, the LP and the mesenteric LNs, is also a simplification: The different spatial distributions of cell types inside the tissue are neglected, i.e. we implicitly assumed that all cell types are equally distributed among the tissue. It is, however, known that some cells (e.g. macrophages [157]) typically reside closer to the epithelium. We modelled transport of cells via blood as an immediate reaction from one compartment to the other, without accounting for loss of cells on the way or for the duration of this transport. The effect of food antigens on the mucosal immune system was not accounted for by our model. In our model we focus on the mucosal immune system of the colon; other parts of the gastrointestinal tract—which are also important for IBDs—are, however, known to differ, e.g. regarding cell concentrations. Simulating the gut immune response in such an isolated way also implies that the influence of the rest of the body (e.g. infections in other parts of the body) is neglected. Nonetheless, we showed that our novel systems biology model is, despite all those simplifications, able to qualitatively and to a certain extent quantitatively describe the healthy mucosal immune response to various inflammatory

stimuli.

Using this novel systems biology model, in the next steps we analysed possible IBD dispositions and generated hypotheses about IBD pathogenesis using a virtual population of IBD patients. In addition, we implemented different treatment mechanisms into the systems biology model, proposed how to predict individual patients' responsiveness to different drugs, analysed differences between virtual responders and non-responders, and evaluated different combination treatments. These are of course only a few possible applications of the novel systems biology model; for a list of suggested additional applications, see the Discussion (Section 7.6).

---

## 3 Model evaluation

In the previous chapter, we developed a mathematical model of the healthy mucosal immune system, which we will use in the following chapter to generate a virtual population of individuals by including variability in the model parameters, with the aim to get insights into the development and potential treatment of IBD. Before, however, we would like to evaluate the model, by challenging it to see how accurate it can describe the mucosal immune response, and to find out its limitations. In addition, via basic model analyses, we want to get first insights into the role of the different parameters and cell types on the immune response.

### 3.1 Knockout scenarios

To confirm the functionality of the model and identify limitations, which is fundamental for the evaluation of the results on IBD development and treatment that we will generate in the following chapters based on this novel systems biology model, we simulated different knockout studies and compared the resulting mucosal immune response (salmonella infection and mucosal injury) to comparable literature studies. All knockout scenarios were based on the reference individual, where specific reactions were inhibited (full or partial) to obtain a “knockout individual” for each scenario. Using that “knockout individual”, first the steady state was simulated, which was, depending on the knockout scenario, different from the healthy steady state of the reference individual. Then, the time course of inflammation as response to salmonella infection or mucosal injury was simulated (in the same ways as for the reference individual in Figure 18). All figures below include the reference individual’s time course for comparison. Please note that the literature studies of knockout scenarios cited below mainly described observations in mice. In addition, as we only simulate and observe cell concentrations within the gut, neglecting interactions with and consequences on the rest of the body, those knockout simulation results have to be treated with care and have only limited interpretability.

#### 3.1.1 T cell knockout

We implemented full knockout of T cells by inhibiting the inflow of naive and memory T cells into the LN, which, in our model, is the source of also all effector T cells (T helper cells and regulatory T cells). In Figure 50 (appendix) we show the time course of salmonella infection and mucosal injury in a “knockout individual” with full T cell knockout (i.e. 100% inhibition of T cell inflow) or partial knockout.

For salmonella infection, we observed that without T cells, salmonellae could not be eliminated from the tissue, and a new steady state with persisting levels of bacterial cells in the LP and consequently higher levels of neutrophils was reached. This is in

accordance with many literature sources (e.g. [29, 36, 158]), describing that especially T helper cells of type 1 are crucial for successful elimination of salmonellae from the tissue. In addition, to show the dependence of salmonella elimination on T helper cells in more detail, we show the time course of salmonella infection for a partial knockout of T cells. For a partial knockout of T cells, we observed a recurrent salmonella infection, i.e. the bacterial cells could not be completely eliminated from the tissue, but could be kept at a lower concentration than for the full T cell knockout. In this case, the model did not reach a steady state, but the simulation showed a recurring pattern of increasing salmonella concentrations, resulting in increasing concentrations of immune cells that led to a decrease in bacterial concentrations and subsequently in immune cell concentrations. For the mucosal injury scenario, we observed that the overall time courses of neutrophils and macrophages did not differ significantly from the respective time courses in the healthy reference individual.

### 3.1.2 T helper cell knockout

To directly assess the influence of T helper cells on the time course, we implemented a knockout of T helper cell functionality, i.e. cytokine production by T helper cells was inhibited (which is the only means of impact of T helper cells on other model state variables). In comparison to the full T cell knockout described in the previous section, here the regulatory T cells remained functional. In Figure 51 (appendix) we compare the time course of salmonella infection and mucosal injury in a “knockout individual” with full T helper cell knockout (i.e. 100 % inhibition of cytokine production by T helper cells) or partial knockout. Note that, as only the effects of T helper cells are inhibited in this simulation, their concentrations will still add to the concentrations of T cells shown in Figure 51.

Simulation results are very comparable to the simulation of the full T cell knockout: Salmonella infection can not be resolved without T helper cells. The “knockout individual” with partial knockout of T helper cells can keep the salmonellae at a lower concentration than the “knockout individual” with full T helper cell inhibition, although only by keeping a high concentration of immune cells and not being able to completely eliminate the salmonellae. For the mucosal injury scenario we again observed no large impact of the knockout on the overall time course, although the diminished increase of macrophages in the “knockout individual” shows the close interaction of the different cell types.

### 3.1.3 Regulatory T cell knockout

Regulatory T cell knockout was implemented by inhibiting the functionality of regulatory T cells, i.e. its inhibiting effects on dendritic cells and macrophages and anti-inflammatory cytokine production. In Figure 52 (appendix) we compare the time course of salmonella infection and mucosal injury in a “knockout individual” with full regulatory T cell knockout (i.e. 100 % inhibition of cytokine production and effects) or partial knockout.

For the “knockout individual” with full regulatory T cell knockout, we already observed significant differences to the healthy reference individual in steady state (before salmonella infection or mucosal injury), where the “knockout individual” showed higher



concentrations of macrophages and much higher concentrations of T helper cells. This highlights the importance of regulatory T cells for keeping the constant low levels of inflammatory cells in the gut tissue. The “knockout individual” can resolve the salmonella infection, but the inflammation during the course of the infection, and the resulting tissue destruction (not shown), are worse and take longer to resolve, in accordance with above observation of higher levels inflammatory cells due to the missing control by regulatory T cells. The higher inflammation levels due to the regulatory T cell knockout have also been described widely in literature (e.g. [119–121]).

### 3.1.4 Commensal bacteria knockout

It is widely known that the frequent encounter of commensal bacteria is crucial for the mucosal immune response to develop its full functionality [29, 159, 160]. To examine if this behaviour can also be reproduced by our novel systems biology model, we simulated partial commensal bacteria knockout by reducing proliferation of commensal bacteria in the lumen, leading to lower commensal bacteria levels. In Figure 53 (appendix) we show the time course of salmonella infection and mucosal injury in a “knockout individual” with reduced level of commensal bacteria.

For 50 % reduction of commensal bacteria, we observed chronic inflammation already in steady state. For 30 % reduction of commensal bacteria, we observed that salmonellae could not be eliminated from the tissue (leading to chronic infection with high levels of immune cell concentrations), and the mucosal injury could not be resolved, resulting in chronic inflammation after the mucosal injury. This means that our systems biology model can, at least to some degree, reproduce the complex interplay of commensal bacteria with the healthy mucosal immune response. Interestingly, the mucosal injury time course is similar to responses in our virtual IBD patients in the following chapter, indicating already the complex role of commensal bacteria in the development of IBD.

### 3.1.5 Neutrophil knockout

We implemented neutrophil knockout by inhibiting neutrophil inflow into the LP. In Figure 54 (appendix) we show the time course of salmonella infection and mucosal injury in a “knockout individual” with full neutrophil knockout (i.e. 100 % inhibition of neutrophil inflow).

For both the salmonella infection and the mucosal injury, we observed that our virtual mucosal immune system is still able to eliminate the invading pathogens and commensal bacteria, and also to resolve the inflammation, but much higher concentrations of T cells and especially macrophages are needed, therefore the inflammation takes longer and is much more pronounced, with much higher tissue damage (not shown). This is in accordance with the clinical observations of neutropenia (abnormally low levels of neutrophils), where patients show much worse (up to life-threatening) reactions to infections than healthy subjects [29, 161].

### 3.2 Local sensitivity analysis

To analyse, which parameters of our novel systems biology model were most important for the mucosal immune response, we conducted a local sensitivity analysis. Sensitivity analyses are used to analyse the effects of parameter changes on model outputs, to determine how the response quantitatively depends on the parameter values, and which parameters determine the response most strongly. In contrast to a global sensitivity analysis, where the influence of large variations in the parameter set is examined, a local sensitivity analysis (LSA) quantifies effects of very small perturbations of single model parameters on the model output, via the so-called sensitivity coefficients, which are defined as the derivatives of the model output with respect to the model parameters [162]. We used finite difference approximation as a simple method to approximate those sensitivity coefficients [162]: For a system of ODEs  $\frac{d}{dt}\mathbf{x}(t) = f(\mathbf{x}(t))$ , with an output function  $y(t) = h(x(t))$ , for each parameter  $p_j$ , the derivative of the output  $y(t)$  with respect to the parameter  $p_j$  is approximated by introducing a small perturbation factor  $\Delta = 0.01$ ,

$$\frac{\partial y(t, p_j)}{\partial p_j} \approx \frac{y(t, p_j + \Delta p_j) - y(t, p_j)}{\Delta p_j}.$$

To facilitate comparison of sensitivity coefficients between parameters, which have different magnitudes, we further normalised to obtain the normalised sensitivity coefficient [162]

$$\begin{aligned} S(t) &= \frac{\partial y(t, p_j)}{\partial p_j} \cdot \frac{p_j}{y(t, p_j)} \\ &= \frac{y(t, p_j + \Delta p_j) - y(t, p_j)}{\Delta \cdot y(t, p_j)}. \end{aligned}$$

Our aim was to analyse the importance of our model parameters on the mucosal immune response. As the mucosal injury scenario will be our starting point for analysis of IBD in the following chapter, we chose this inflammation scenario as reference. As the extent of the mucosal immune response is not trivially quantifiable, we regarded three different model outputs, the concentrations of total T helper cells ( $\text{Th}_{\text{tot,LP}}$ ), total macrophages ( $M_{\text{tot}}$ ) and neutrophils (Neut) over time, to obtain a broad overview. In Figure 24 we show the sensitivity coefficients of the parameters with highest sensitivity coefficients (maximal value over the timespan) for the three different outputs.

Sensitivity coefficients can be negative or positive, dependent if an increase of the parameter leads to an increase or decrease of the output, respectively. In Figure 24, we show the sensitivity coefficients before mucosal injury ( $t < 0$ ), which describe the dependence of the steady state concentration of the output on the parameters, and over the time course of inflammation after mucosal injury, which show how the different parameters play different roles during different stages of the inflammation time course. Naturally, we see large differences in the sensitivity coefficients, and the ranking of the most important parameters, between the different outputs. However, three parameters appeared among the highest sensitivity coefficients for all three outputs: The T cell proliferation rate constant  $p_{\text{Tn},>1}$ , the macrophage death rate constant  $\mu_M$  and the neutrophil recruitment Hill factor  $h_{\text{rec,Neut}}$ . The fact that those three universally important parameters relate to three different cell types nicely shows the high complexity of our virtual immune system,

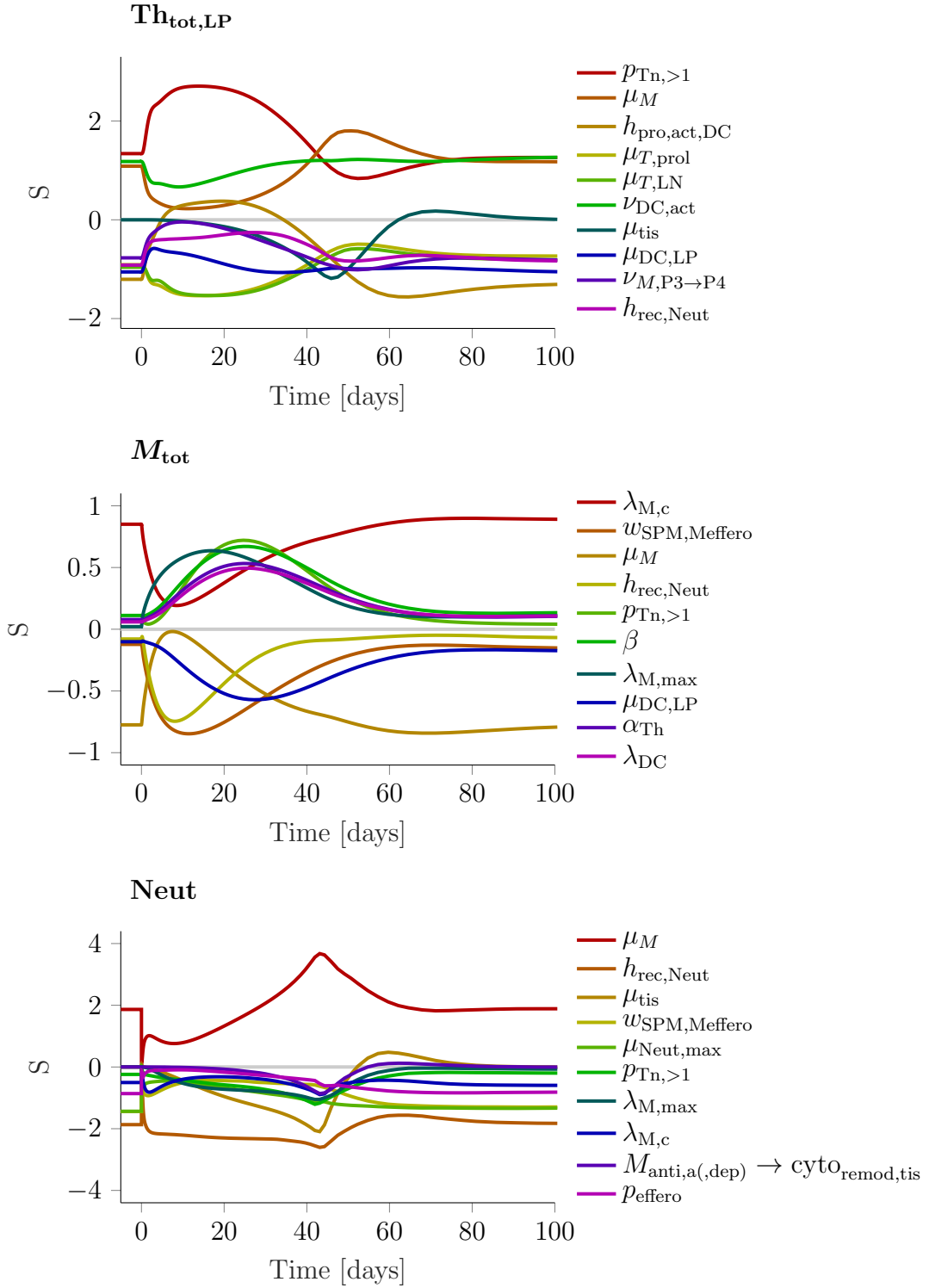


Figure 24: **Sensitivity coefficients over time for different outputs.** Sensitivity coefficients over a time span of 100 d after mucosal injury, using T helper cells ( $Th_{tot,LP}$ ), macrophages ( $M_{tot}$ ) or neutrophils (Neut) as output. Sensitivity coefficients for  $t < 0$  show the dependence of the steady state concentration on the parameter values. Here we show only the ten state variables with highest maximal value. The legend shows the sensitivity coefficients ordered by their maximal value. (Note that the colours are therefore not comparable among the subplots.) The grey line indicates  $S = 0$ .

and the importance of the interplay between the different cell types.

For T helper cells, we observed several parameters that are approximately equally important for the steady state concentration (all of the shown parameters except  $\mu_{\text{tis}}$ ). During acute inflammation, however, the T helper cell concentrations appears to be mainly determined by the three parameters  $p_{\text{Tn},>1}$ ,  $\mu_{T,\text{LN}}$  and  $\mu_{T,\text{prol}}$ , i.e. the parameters describing T cell proliferation and death. However, the other parameters among the top 10 sensitivity coefficients, determining mainly steady state and the resolution phase of the inflammation, again relate to various different parts of the model: macrophages ( $\mu_M$ ,  $\nu_{M,\text{P3}\rightarrow\text{P4}}$ ), neutrophils ( $h_{\text{rec,Neut}}$ ), dendritic cells ( $h_{\text{pro,act,DC}}$ ,  $\nu_{\text{DC,act}}$ ,  $\mu_{\text{DC,LP}}$ ) and epithelial barrier ( $\mu_{\text{tis}}$ ).

For macrophages, we could clearly determine the two parameters determining the steady state concentration: the constant macrophage recruitment rate  $\lambda_{M,c}$  and the macrophage death rate constant  $\mu_M$ . Those two parameters become much less important during acute inflammation, where other parameters become dominant, nicely mimicking the chronological order of the inflammation time course: In the earlier stage,  $\lambda_{M,\text{max}}$ ,  $h_{\text{rec,Neut}}$  and  $w_{\text{SPM,Meffero}}$  are most dominant, as neutrophils are the first immune cells recruited to the site of inflammation, and therefore the first cells that recruit macrophages via pro-inflammatory cytokines. In the later stage, the macrophage concentration becomes stronger dependent on T cells ( $p_{\text{Tn},>1}$ ,  $\beta$  and  $\alpha_{\text{Th}}$ ), which are in turn dependent on dendritic cells ( $\lambda_{\text{DC}}$  and  $\mu_{\text{DC,LP}}$ ).  $w_{\text{SPM,Meffero}}$  plays an important role also during the later stage, highlighting the important role of SPM for the resolution of the inflammation.

For neutrophils, we observed the macrophage death rate constant  $\mu_M$  as the most influential parameter, with positive influence on neutrophil concentration, probably because higher macrophage death rate leads to lower secretion of SPM and thereby diminished resolution. The importance of SPM production on neutrophil concentration also becomes apparent via the high negative sensitivity coefficient of  $w_{\text{SPM,Meffero}}$  and the rate constant for transition of macrophages to the SPM-producing efferocytosis type,  $p_{\text{effero}}$ . Other important parameters on the neutrophil concentration, all negatively influencing neutrophil concentration, are related to neutrophil recruitment and death ( $h_{\text{rec,Neut}}$ ,  $\mu_{\text{Neut,max}}$ ), tissue remodelling ( $\mu_{\text{tis}}$ ,  $M_{\text{anti,a(dep)}\rightarrow\text{cyto}_{\text{remod,tis}}}$ ), macrophage recruitment ( $\lambda_{M,c}$ ,  $\lambda_{M,\text{max}}$ ) and T cell proliferation ( $p_{\text{Tn},>1}$ ). Again, the identified important parameters relate to various cell types and processes of our model.

### 3.3 Input-response indices

In addition to the influence of the different parameters, we were also interested to see which state variables play major roles in the simulated mucosal immune response. For this, we used the concept of input-response (IR) indices, introduced by Knöchel et al. (2018) [163]. The IR indices quantify the effect of a specific input on a state variable at a specific time point, and the effect of this variation on a specific output over the remaining time interval.

In our case, we chose the mucosal injury scenario, i.e. the input was destruction of epi and tissue by factor 0.5 at time point  $t = 0$  (see Section 2.18.3), with the resulting time course of all state variables as reference time course  $x_{\text{ref}}$ . Then the input was perturbed by different factors  $\Delta_u = \{0.5, 0.8, 1.2, 1.5\}$ , resulting in the time course  $x_{\Delta_u}$ . For each time point  $t^* \in [0, t_{\text{end}} = 100 \text{ d}]$ , the effect of the perturbed input on all state variables  $x_i$  was calculated as the difference to the reference time course,  $\Delta x_i(t^*) = (x_{\Delta_u}(t^*) - x_{\text{ref}}(t^*))_i$ ;

this refers to the controllability of the state variables. In a next step, for each state variable  $x_i$ , at each time point  $t^*$ , the effect of this difference  $\Delta x_i(t^*)$  on the remaining time course  $[t^*, t_{\text{end}}]$  was calculated by solving the ODE system from  $t^*$  to  $t_{\text{end}}$ , using as initial values  $x_{\text{ref}}(t^*)$ , with  $\Delta x_i(t^*)$  added to the respective state variable concentration  $x_{\text{ref},i}(t^*)$ ; this refers to observability of the state variables. The time- and state variable-specific IR index  $ir_i(t^*)$  is calculated as the integrated difference of the resulting output from the reference output over the remaining time interval  $[t^*, t_{\text{end}}]$  and further normalised, averaged over the different perturbation factors. For details see Knöchel et al. (2018) [163]. As for the LSA, we chose the concentrations of T helper cells ( $\text{Th}_{\text{tot,LP}}$ ), macrophages ( $M_{\text{tot}}$ ) and neutrophils (Neut) as outputs. For each of the three outputs, we show the ten IR indices with the highest maximal values over the full time span in Figure 25.

Note that the IR index is high only if both the effect of the input on the state variable is high and the effect of this variation on the output over the remaining time course is high. As expected, *epi* and *tissue* were very important for all three outputs, as they were directly affected by the input, i.e. destruction of epithelium and *tissue*, and this destruction was the cause for the resulting immune reaction. Their importance, however, decreases over time, and at later time points other state variables are more important. In addition, antigen-experienced efferocytosis-type macrophages ( $M_{\text{effero,a}}$ ) were among the highest IR indices for all three outputs, and were the most important state variables in the later phase of the immune response, showing the highest IR indices from  $\approx 20$  d to  $\approx 50$  d. In the end phase, from  $\approx 50$  d, antigen-experienced macrophages of population P4 ( $M_{\text{P4,a}}$ ) were dominant on both T helper cells and macrophages as output. Naturally, the most important state variables include Th1 for the output of total T helper cells, various subpopulations of macrophages for the output of total macrophages, and neutrophils for the output of neutrophils. For T helper cells, the pro-inflammatory macrophage populations  $M_{\text{P1,a}}$  and  $M_{\text{P3,a}}$ , as well as several dendritic cell state variables in LP, have high IR indices. This is due to the dependence of T helper cells to be activated by antigen-experienced dendritic cells or macrophages in LP. For macrophages, we also observed stimulatory dendritic cells ( $\text{sDC}_{\text{LP}}$ ) among the highest IR indices. As those do not have a direct effect on macrophages in our model, this effect is probably due to their effect on T helper cell activation, which subsequently secrete pro-inflammatory cytokines acting on macrophage recruitment and activation. For neutrophils, we also observed *mucus* among the most important state variables, which is directly controlled by *epi*, highlighting the role of neutrophils as the first cells responding to bacterial inflow resulting from barrier destruction. In addition, several antigen-experienced macrophage subpopulations, both pro- and anti-inflammatory, have high IR indices, showing that the neutrophil concentration depends on the cytokine milieu, which is mainly secreted by pro- and anti-inflammatory macrophages. Interestingly, also the pMHCII-depleted anti-inflammatory macrophages ( $M_{\text{P4,a,dep}}$  and  $M_{\text{effero,a,dep}}$ ) have high IR indices, showing also the influence of regulatory T cells (which deplete macrophages) on the time course of inflammation.

We conclude that a wide variety of different state variables play important roles during the time course of inflammation resulting from mucosal injury. The importance of the different state variables, naturally, varies with the regarded output, but especially macrophages seem to be important for all three analysed outputs, confirming their important role in the mucosal immune response, which has also been widely reported in literature [52, 72, 164, 165].

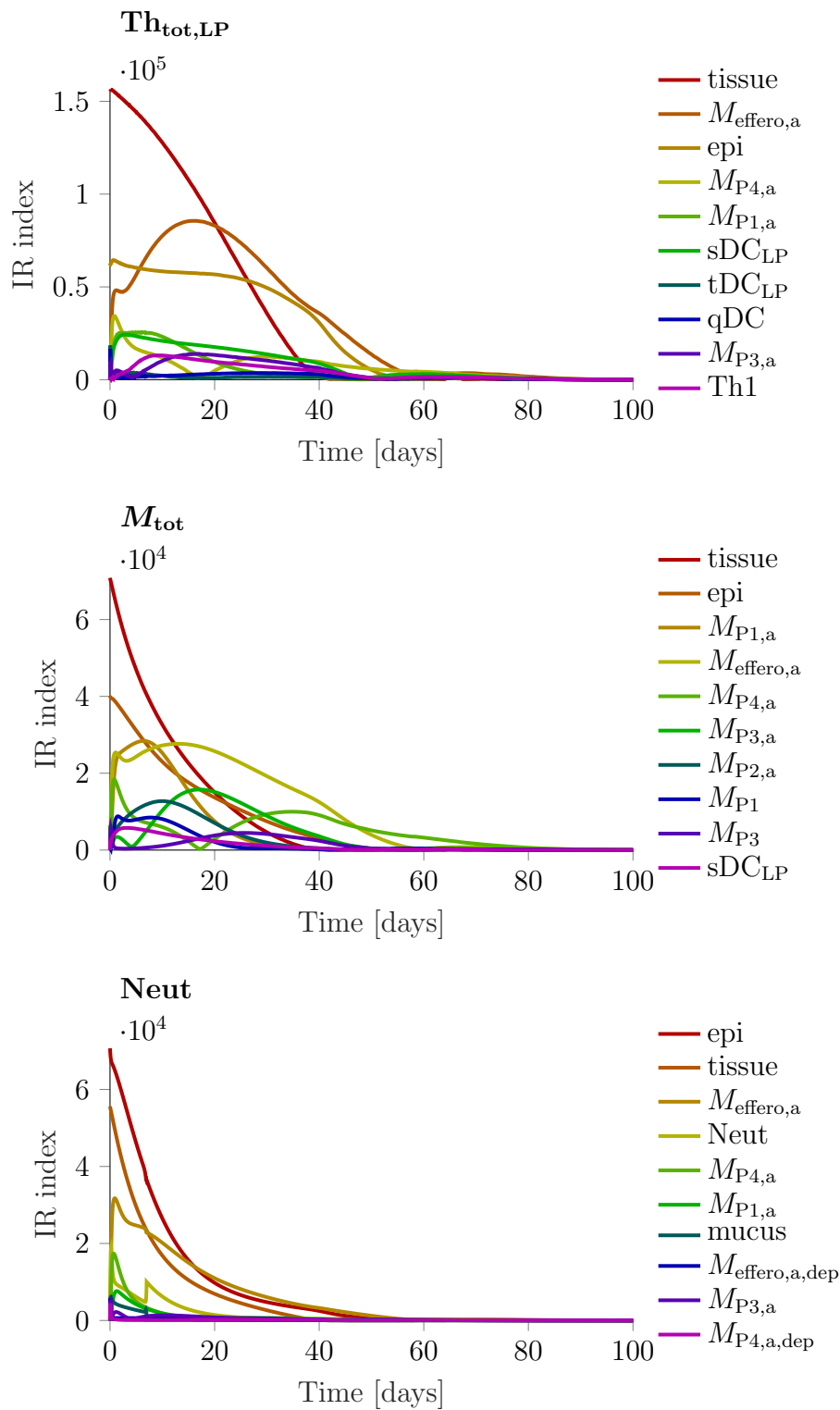


Figure 25: **IR indices for different outputs.** IR indices [163] over a time span of 100 d after mucosal injury, using T helper cells ( $Th_{tot,LP}$ ), macrophages ( $M_{tot}$ ) or neutrophils (Neut) as output. Here we show only the ten state variables with highest maximal value. The legend shows the IR indices ordered by their maximal value. (Note that the colours are therefore not comparable among the subplots.)

### 3.4 Conclusion

The presented knockout scenarios show that our novel systems biology model is able to reproduce a wide range of findings from experimental knockout experiments. The sensitivity analyses of influence of parameters (LSA) and state variables (IR) on the time course of main cell types (T cells, macrophages, neutrophils) for an exemplary inflammation scenario (mucosal injury) confirmed the complex interplay of different cell types and processes in the model, as different parameters related to different cell types/processes, and different state variables describing cell types could be identified as important for the extent of the mucosal immune response to mucosal injury.

In the next chapter, we will analyse in detail, which parameters and state variables are important for the development of IBD. As in the presented sensitivity analyses we used the mucosal injury scenario as input, which will also be the starting point for the analysis of IBD, we expect that the parameters and state variables we identified as important here, may also prove important on the development of IBD in the next chapter.





---

## 4 Simulation and analysis of IBD using a virtual population

The aim of this chapter is to use our novel systems biology model of the healthy mucosal immune response to get insights into the development of IBD, and to provide a population of virtual IBD patients to study their reaction to different treatment effects (see Chapter 5).

*Pathogenesis of IBD.* IBDs are chronic diseases defined by chronic inflammation of various parts of the gastrointestinal tract, due to overreaction of the mucosal immune system to commensal bacteria [1, 7]. The disease course is characterised by relapses (so-called “flares”) and remitting phases [166, 167]. The full pathogenesis is still unclear. With the exception of early-onset IBD, where patients develop IBD at a very young age and the disease can often be traced back to a single mutation, IBD is a multifactorial disease [168, 169]. A wide variety of genetic predispositions and environmental risk factors for IBD have been found to be linked to the disease [3, 170]. Every patient has accumulated several changes compared to healthy individuals, which together lead to the outbreak of disease. Some of those changes are genetic predispositions, some are environmental (i.e. accumulate over time). This means that before the outbreak of the disease, IBD patients must be in a pre-disease state, having accumulated several risk factors, where one additional trigger leads to the outbreak of the disease. The exact trigger, which is probably highly variable between patients, is not completely known. Many literature sources, however, discuss environmental factors such that perturb the mucosal barrier, alter the balance of gut microbiota and abnormally stimulate the immune system of the gut, as triggers for the onset of disease [4, 6, 7].

*Representation of IBD in the systems biology model.* We assume the accumulation of risk factors for IBD to be the result of the normal variability, i.e. in a population of many different individuals, some will develop IBD. Therefore, in a virtual population of individuals, based on the presented systems biology model of the healthy mucosal immune response, where each individual is characterised by a set of parameters that are sampled around the reference parameters, we expect to find some IBD patients.

To detect those IBD patients, we assumed the following characteristics: As described in the last paragraph, an IBD patient is an individual in a pre-disease state, that after some final trigger develops chronic inflammation. We defined this pre-disease state as the steady state of the individual. Regarding the trigger, we focused on perturbation of the mucosal barrier, as discussed in literature [4, 6, 7]. Therefore we used the mucosal injury scenario presented in Section 2.18.3 as trigger. After response to this trigger, a healthy individual is expected to be able to resolve the inflammation and return to healthy steady state, whereas a virtual IBD patient is expected not to be able to resolve the inflammation and to develop chronic inflammation.

Our virtual representation of IBD does of course have limitations: Naturally it can only describe the patients given the underlying model, i.e. only describe the disease in the represented space of the colon mucosa, and only in the level of detail of the model. This level of detail does, for example, not allow for discrimination between CD and UC. In addition, as we did not account for changing environmental factors, the model can only describe the development of a single flare in a previously asymptomatic individual. The return to the asymptomatic state after the flare without further intervention can therefore not be described by the model; only the effects of treatment, as described in Chapter 5.

#### 4.1 Generation of a virtual population

*Sampling of virtual individuals using variability.* We generated a virtual population by sampling 1,000,000 sets of parameters around the reference parameter set described in Chapter 2 (Table 10 in the appendix). We used a lognormal distribution with mean  $\mu = 0$  and standard deviation  $\sigma = 0.4$  of the underlying normal distribution for generation. We then multiplied the reference parameter set with the variation factors to obtain the individual parameter sets. We are aware that it is a rough simplification to assume the same distribution for all parameters. The literature, however, is very rare. In addition, one of our aims was to analyse the possible influence of the single parameters on the development of IBD; hence using the same distribution on all parameters might at the time prevent bias. Each of the resulting parameter sets represented one individual of our virtual population, with a specific time course of the mucosal immune response to the mucosal injury trigger.

*Classification of virtual individuals.* We then classified the individuals of the generated virtual population. For this we simulated for each individual the pre-trigger steady state (compare healthy steady state of the reference individual, Section 2.17) and the response to the mucosal injury trigger (Section 2.18.3) until the post-trigger steady state was reached.

We expected to observe different types of individual behaviour in our virtual population:

- (i) Healthy individuals: comparable, healthy, response to the mucosal injury trigger, i.e. invading commensal bacteria are eliminated from the tissue, the inflammation is resolved and the system returns to the pre-trigger healthy steady state (post-trigger steady state = pre-trigger steady state)
- (ii) Chronic inflammation: out-of-control immune response, i.e. chronic inflammation already in the pre-trigger steady state and never an asymptomatic steady state. These virtual individuals do not necessarily relate to any real-world patients.
- (iii) Chronic infection: individuals not able to deal with the amount of inflowing bacteria and developing a chronic infection, i.e. a high concentration of commensal bacteria in LP, probably resulting also in high concentrations of immune cells, in the post-trigger steady state
- (iv) IBD: pre-trigger steady state comparable to the healthy reference individual's steady state, but high concentrations of immune cells in the post-trigger steady state

Based on these considerations, we classified the virtual individuals into four classes (i)-(iv). For this, we used the concentrations of T helper cells ( $\text{Th}_{\text{tot,LP}}$ ), macrophages

( $M_{\text{tot}}$ ) and neutrophils (Neut) and considered the pre-trigger steady-state concentrations normalised by the reference individual's steady state and the ratio of post-trigger to pre-trigger steady-state concentration. In addition, we used the concentration of bacteria in LP ( $\text{Bact}_{\text{LP}}$ ) to identify chronic infection. See Section 9.5 in the appendix for details on the classification. We obtained a virtual population of 695.101 healthy individuals (69.5%), 22.252 IBD individuals (2.2%), 197.074 chronic inflammation individuals (19.7%), and 31.163 chronic infection individuals (31.1%). In addition, in some cases (54.410 individuals/5.4%), the pre-trigger steady state could not be simulated because of oscillations. We excluded those individuals, as such behaviour, although it may not be completely unphysiologic, was hindering further analyses. Note that we use the term ‘‘IBD individual’’ to denote both, IBD patients and individuals with IBD predispositions before the outbreak of disease.

Figure 26 shows the time course of the mucosal immune response (bacteria, barrier state variables, T cells, macrophages and neutrophils in IBD) to mucosal injury for the different classes. Figure 27 shows the distributions of pre-trigger and post-trigger steady-state concentrations of the same immune cells for healthy and IBD individuals. Healthy individuals show an immune response comparable to the reference individual's immune response (for the reference individual's immune response, compare Figure 22, third row). The chronic inflammation individuals show a high concentration of immune cells and reduced epithelial barrier integrity already before the trigger; the reaction to the mucosal injury trigger is relatively small, as there are already enough immune cells available. The distribution of pre-trigger steady-state concentrations in the chronic infection individuals is comparable to healthy individuals, but following the mucosal injury trigger, the bacterial concentration rises fast to its maximal concentration ( $C_{\text{max,Bact,ref}} = 10^{10} \frac{1}{\text{mL}}$ ), resulting in a post-trigger steady state with immune cell concentrations higher and epithelial barrier state variable lower than in healthy individuals.

The distribution of pre-trigger steady-state concentrations in IBD individuals is comparable to healthy individuals, but following the mucosal injury trigger, the average increase of immune cells is much higher, and concentrations do not return to the pre-trigger steady state. In the post-trigger steady state, immune cell concentrations are much higher than in healthy individuals (see bottom row in Figure 27). In addition, the epithelial barrier state variable is  $\text{epi} < 1$ , describing the reduced integrity of the epithelium that leads to constant bacterial inflow into the LP, resulting in bacteria levels in LP higher than in healthy individuals. Note that the concentration of bacteria in LP decreases after the first peak, but is higher in post-trigger steady state than in pre-trigger or healthy steady state. In some virtual patients, the tissue state variable is  $\text{tissue} > 1$ , representing fibrosis.

For the following analyses, we only considered healthy individuals and IBD individuals. The fraction of IBD individuals in the virtual population (3.1%) depends on  $\sigma$  and was on purpose designed to be higher than the reported prevalence of 0.3% [2]. The reason was that we intended to make sure not to miss out on extreme values for some parameters potentially leading to IBD.

## 4.2 Evaluation of the model representation of IBD by comparison with literature

Figure 28 shows a comparison of selected LP cell type concentrations with literature. As absolute concentration values of cells in human healthy and diseased LP are rarely

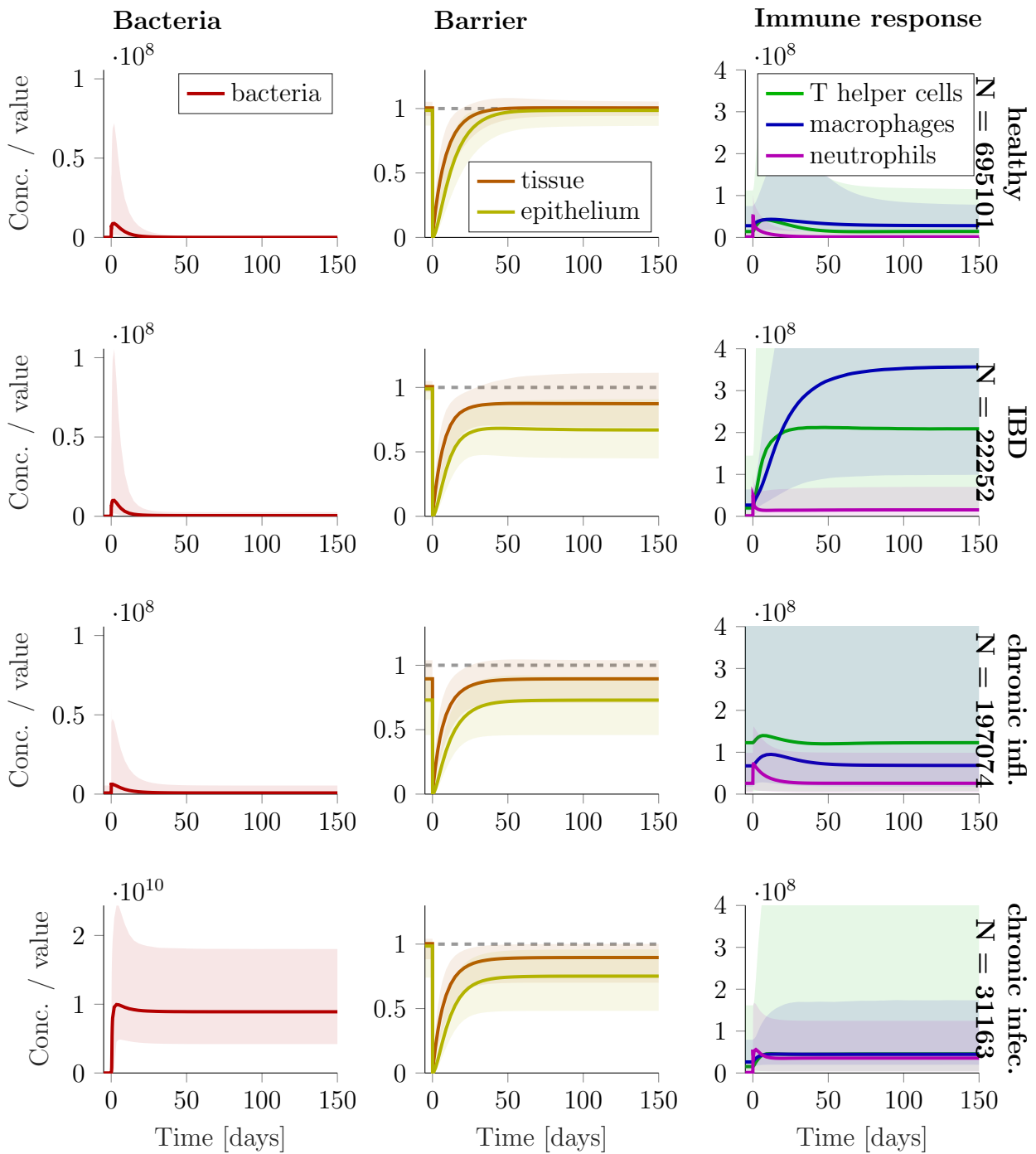


Figure 26: **Time course of mucosal injury in the different classes.** Concentrations of bacteria and selected immune cells in LP and barrier state variables (unitless) over time in response to mucosal injury at time point  $t = 0$ . Note the different y-axis scale for bacteria for chronic infection. Median (solid line) and 90% variability in virtual population (area). The distribution of pre-trigger and post-trigger steady-state concentrations of the shown immune cells and bacteria are also shown in Figure 27.

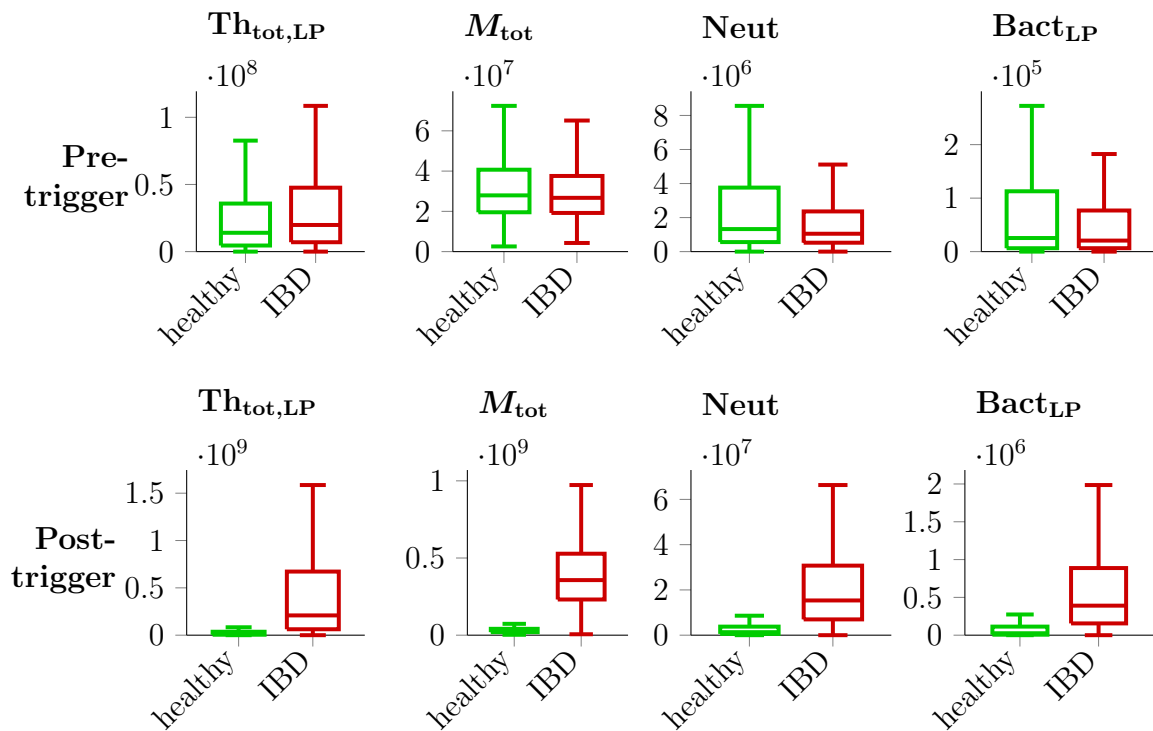


Figure 27: **Pre-trigger and post-trigger steady-state concentrations in healthy and IBD individuals.** Boxplots show the median (central line), 25th and 75th percentiles (box) and the most extreme data points not considered outliers, i.e. not more than 1.5 times the inter-quartile range from the box (whiskers), for the distributions of LP concentrations of T helper cells, macrophages, neutrophils and bacteria before (pre-) and after (post-) the trigger in the virtual populations of healthy and IBD individuals.

reported in literature, we compared to an analysis of fractions of the different cell types in UC patients and healthy controls [171]. For this, we calculated for the different cell types analysed by Xue et al. (2021) [171] (corresponding to sums of state variables simulated by our systems biology model) the fractions from the total simulated LP cell concentrations. As Xue et al. [171] reported also additional cell types that were not simulated by our systems biology model (e.g. B cells), we adapted their reported fractions of those cell types also simulated by our systems biology model to also sum up to 1. In Figure 28, we show the simulated and literature-reported [171] fractions for healthy and IBD individuals (post-trigger steady state). The shown literature data were not used for model development or generation of the virtual population. Comparing the fractions in healthy individuals (green) between simulation (left) and literature (right), we observed an over-prediction of T cell activation, i.e. fractions of activated memory T cells and regulatory T cells were simulated higher, and the fraction of resting memory T cells was simulated lower than the respective literature values. In addition, fractions of anti-inflammatory (M2) macrophages and activated dendritic cells are lower in simulations compared to literature. Despite those differences, the simulated *changes* of fractions from healthy to IBD largely agree with the changes in the literature values, as can be seen by comparing the grey trend lines between simulated (left) and literature-reported (right) healthy and IBD fractions. This confirms that the model representation of IBD is in high accordance with real-life IBD phenotype and therefore increases confidence in the presented systems biology model.

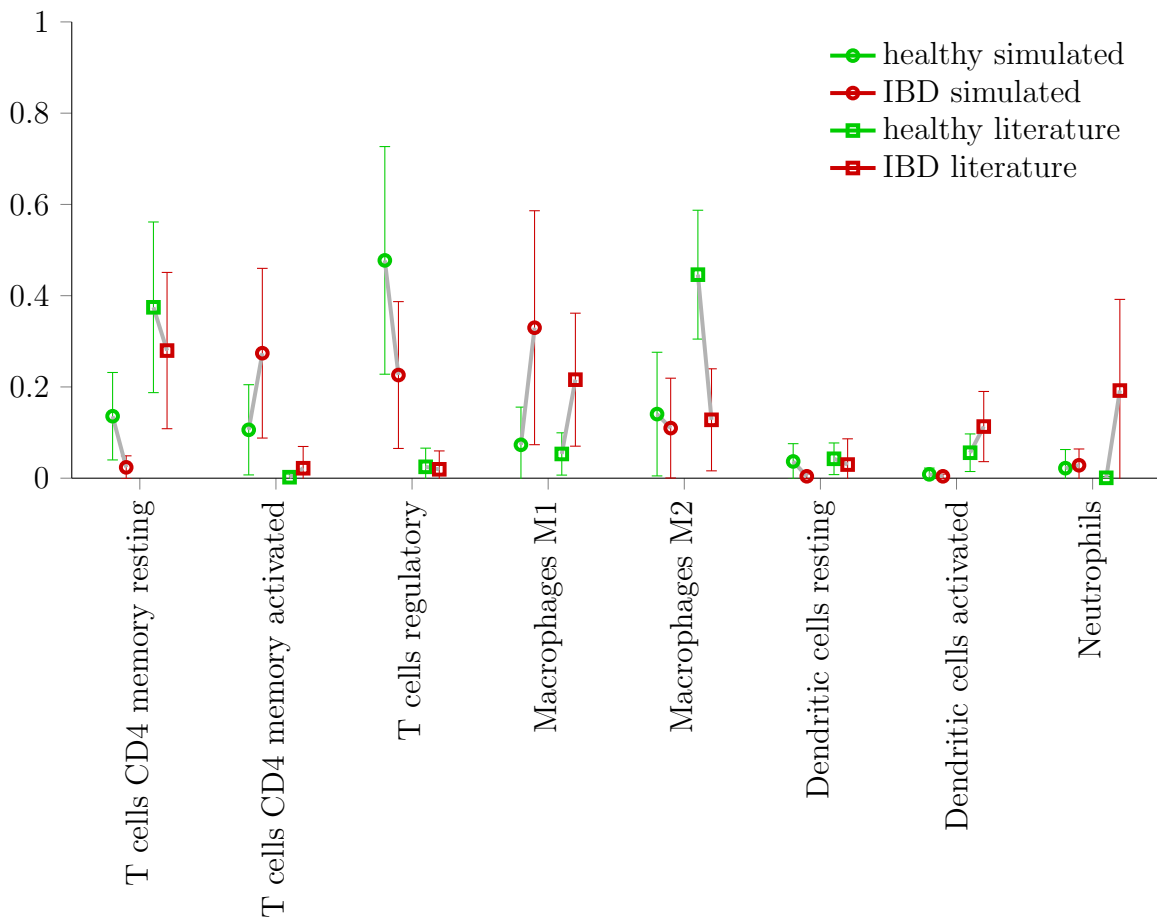


Figure 28: **Post-trigger steady state concentrations in healthy individuals and IBD patients, in comparison with literature data.** Means of simulated (circles) and literature-reported (squares) fractions of different LP cell types (corresponding to sums of state variables in the model simulations) for the populations of healthy (green) and IBD (red) individuals, with standard deviation. Grey trend lines highlight the changes of the fractions between healthy and IBD. Literature values taken from Xue et al. (2021), Supplementary table 10 [171], reporting the fractions in UC patients and healthy controls.

### 4.3 Comparison of parameters to detect IBD predispositions

In Section 4.1, we have generated a virtual population of individuals, where most individuals show a healthy immune response to the mucosal injury trigger, but some develop IBD. As we only defined healthy and IBD individuals based on their phenotype, we do not know the reason for these different reactions to the mucosal injury trigger yet. As our virtual individuals are defined by sets of parameters, the cause for the development of IBD must be due to parameter differences. To find these parameter differences, we compared parameters between healthy and IBD individuals. We expected that the cause of the disease could be either in a change of (i) a single parameter or (ii) a combination of parameters. Parameter differences identified for our novel systems biology model could then be translated to predispositions or risk factors for IBD and give valuable insight into IBD pathogenesis.

We compared the distributions of all parameters between healthy and IBD individ-

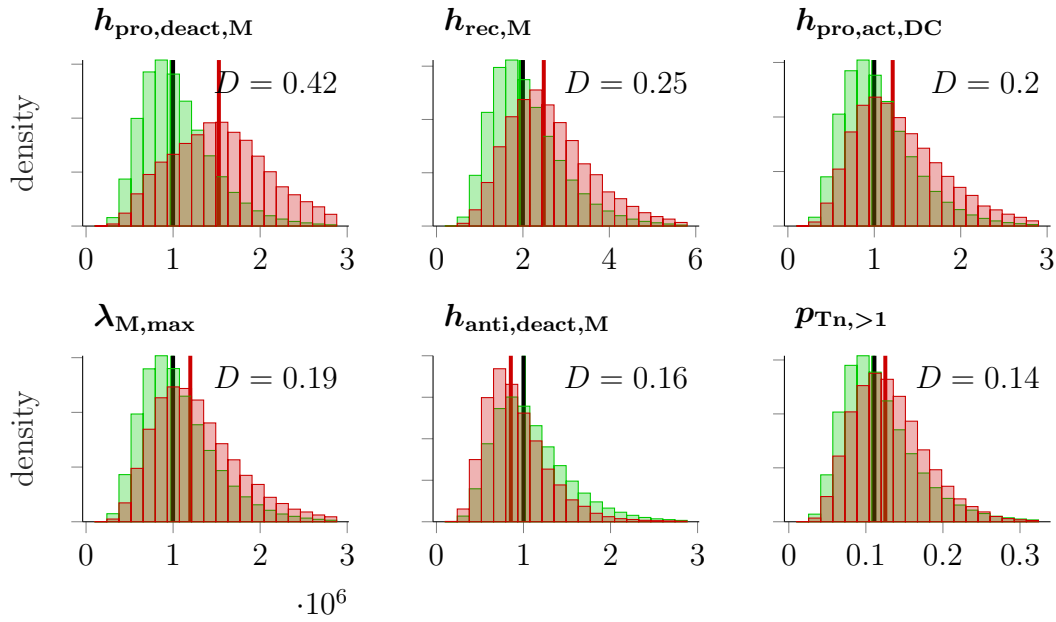


Figure 29: **Comparison of parameter distributions between healthy individuals and IBD patients.** Histograms show the parameter value distributions for the six parameters with highest Kolmogorov-Smirnov test statistic  $D$  (testing for difference between healthy and IBD), for healthy (green) and IBD (red) individuals. Green and red vertical lines indicate the corresponding population medians; the black line indicates the reference value (mostly overlying the healthy median). Outliers (values above 1.5 times the 95th quantile) were removed to improve readability of the plot. Kolmogorov-Smirnov test statistic  $D$ . Parameter “ $M_{\text{pro,a,(dep)}} \rightarrow \text{cyto}_{\text{pro,deact,M}}$ ” refers to the weight of pro-inflammatory macrophages in the production of cytokines inhibiting macrophage deactivation.

uals. To quantify the difference between the two distributions, we used the two-sample Kolmogorov-Smirnov test. The test statistic  $D$  of the two-sample Kolmogorov-Smirnov test is the maximum absolute difference between the cumulative density functions of the two sample distributions (Matlab function `kstest2`), i.e. a value between 0 and 1, where 0 means the two distributions are similar, and 1 means that there is a clear threshold between the two distributions where all parameter values of one distribution are below and all of the other distribution are above the threshold.

In Figure 29 we show the parameter distributions for the six parameters with highest Kolmogorov-Smirnov test statistic  $D$ , indicating largest difference, i.e. potentially strongest correlation to the outcome (healthy or IBD). The corresponding p-values for the Kolmogorov-Smirnov test are very low for a wide range of parameters ( $p < 0.01$  for 59% of parameters). This means that there seems to be a strong correlation of more than half of the parameter distributions with the outcome (healthy vs IBD), although the corresponding correlations may be very small and therefore may not be clinically significant.

Four of the six parameters with strongest correlation to the outcome are Hill factors ( $h$ ). Those Hill factors determine how sensitive the reaction rate is to a change in the cytokine concentration driving this reaction. They have a large potential to favour the switch between asymptomatic and chronically inflamed steady states that we see in IBD

individuals (the different pre-trigger and post-trigger steady states), as a larger Hill factor results in a larger difference in reaction rates for small changes in the cytokine concentration. Since Hill kinetics are often used as an empirical simplified model for a saturable, cooperative process (as in our case), the physiological interpretation of Hill factors beyond “sensitivity” is difficult. In our model, we used Hill kinetics for all reactions influenced by pro- and/or anti-inflammatory cytokines (i.e. recruitment, activation and deactivation). Due to lack of detailed knowledge on the cooperativity of those reactions, most Hill factors were set to 1, i.e. no cooperativity, in the reference individual. The Hill factors were, however, still included in the model to allow for cooperativity in individuals of the virtual population, as we could not exclude that they may be important. This analysis showed that Hill factors are indeed potentially very important for the development of IBD in our virtual population. Among the parameters that are strongly correlated with the disease, five out of six relate to macrophages. This suggests an important role of macrophages for the development of IBD, which again is in line with extensive reports in literature [52, 172].

#### 4.4 Disease-relevant parameter changes for IBD

Next we analysed which parameters led to the disease in single patients, i.e. if a single parameter change compared to the healthy reference individual was sufficient, or if a combination of parameter changes was needed, and if, which combinations could elicit the disease.

In every virtual IBD individual, all parameters differ more or less from the reference individual, as variability was included in all parameters. We aimed at finding those parameter changes that are crucial to elicit IBD in an individual, i.e. those parameter changes without which the individual would be healthy. That means, for each IBD individual, we determined the combination of parameter changes that led to the development of IBD (termed “disease-relevant parameter changes” in the following). See Section 9.6 for the derivation of disease-relevant changes.

Figure 30 shows the distribution of the number of disease-relevant parameter changes per IBD individual. This number ranged from 1 to 60 in our virtual IBD population (22,252 individuals), with a mean of 4.54 and median of 4 disease-relevant parameter changes.

*Parameter changes that are most frequently disease-relevant.* Figure 31 shows the ten parameters that are most frequently among the sets of disease-relevant parameter changes. Those are largely correlated with those parameters identified to be most different between healthy and IBD individuals in the previous section, and are related to very different cell types and processes of our systems biology model, which emphasises the complexity of the disease development due to changes in different parts of the mucosal immune system. Of note, each parameter of the model was at least once among the disease-relevant parameter changes of an IBD individual.

By far the most frequent parameter among the disease-relevant parameter changes was  $h_{\text{pro,deact,M}}$ .  $h_{\text{pro,deact,M}}$  is the Hill factor for the pro-inflammatory cytokine concentration  $\text{cyto}_{\text{pro,deact,M}}$  in the deactivation of macrophages, i.e. it describes how sensitive the macrophage deactivation rate is to a change in the pro-inflammatory cytokine con-



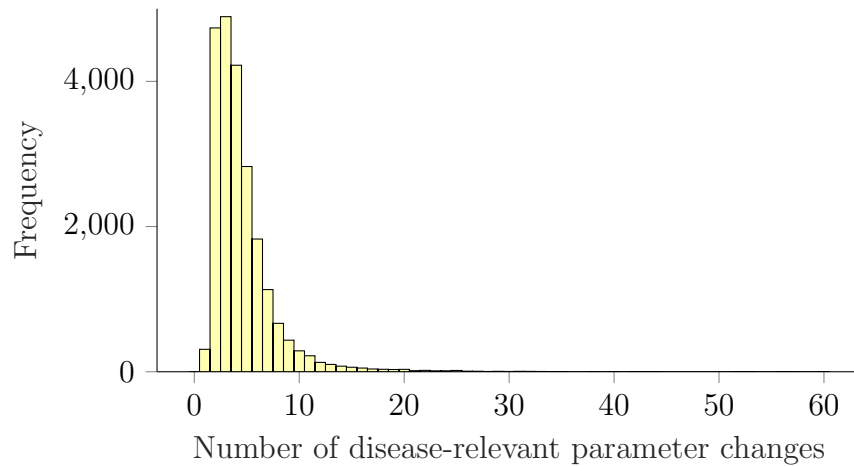


Figure 30: **Distribution of the number of disease-relevant parameter changes per IBD individual.** For details, see description in Section 4.4.

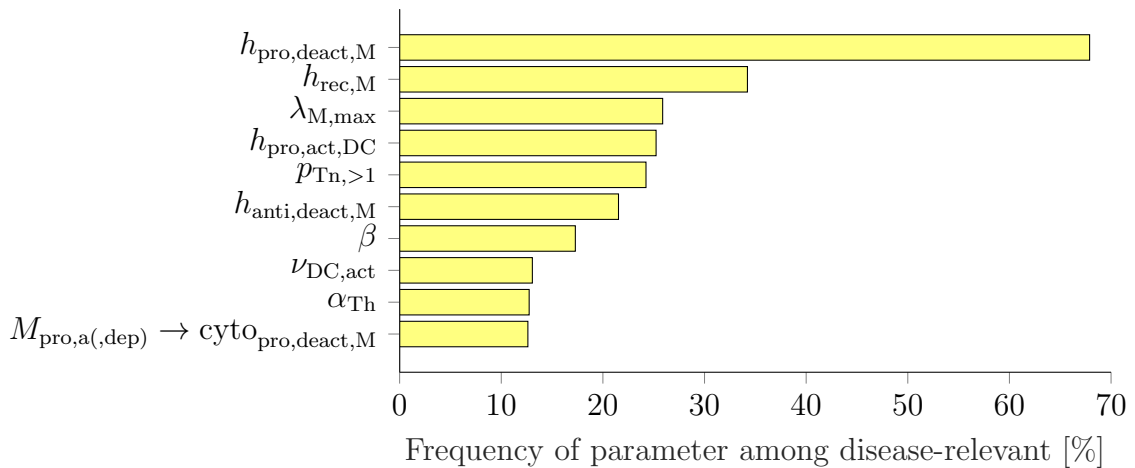


Figure 31: **Most frequent disease-relevant parameter changes.** Barplot of the frequency of parameters among the disease-relevant parameter sets. Shown are the ten most frequent parameters. Parameter “ $M_{\text{pro,a,(dep)}} \rightarrow \text{cyto}_{\text{pro,deact,M}}$ ” refers to the weight of pro-inflammatory macrophages in the production of cytokines inhibiting macrophage deactivation.

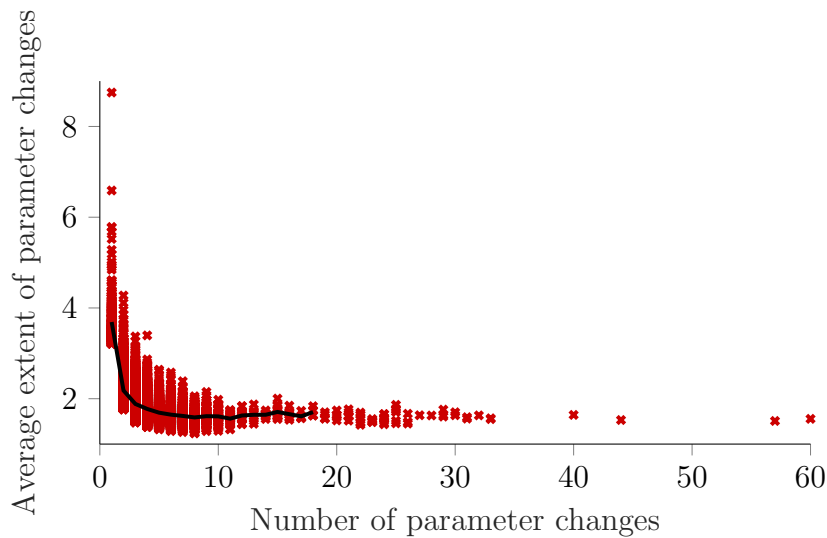


Figure 32: **Extent of disease-relevant parameter change versus number of disease-relevant parameter changes.** Each cross marks for one IBD individual the average extent of disease-relevant parameter changes vs the number of disease-relevant parameter changes.

centration. This seems to have a high influence on IBD development. However, although disease-relevant in 67.9% of the IBD individuals, this parameter is not absolutely required to develop the disease, as the other 32.1% developed IBD without this parameter change.  $h_{\text{pro,deact,M}}$  is also the only parameter that we identified to be able to cause IBD on its own. See Section 9.7 for a more detailed analysis of  $h_{\text{pro,deact,M}}$ .

*Extent of disease-relevant parameter changes for IBD.* Figure 32 shows for each IBD individual the average extent of its disease-relevant parameter changes and its number of disease-relevant parameter changes. We observed a negative correlation between the average extent and the number of disease-relevant parameter changes. This means that the development of IBD in our virtual population can result from both a small number of large parameter changes or a higher number of small parameter changes.

*Combinations of disease-relevant parameter changes for IBD.* In the previous section, we have seen that IBD in our virtual population, with very few exceptions, develops due to a change in several parameters. This leads to the question whether there are frequent combinations of parameter changes that can be observed in a large number of IBD individuals, and that we could use to stratify the IBD population into subgroups of individuals that are very similar to each other, as their disease is caused by the same combination of parameter changes (i.e. physiologically interpretable as a common combination of predispositions).

The most frequent combination of two disease-relevant parameter changes (on their own or together with other parameter changes) was  $h_{\text{rec,M}}$  and  $h_{\text{pro,deact,M}}$ , in 22.3% of the IBD individuals. The most frequent combination of three disease-relevant parameter changes (on their own or together with other parameter changes) was  $h_{\text{rec,M}}$ ,  $h_{\text{pro,deact,M}}$  and  $h_{\text{anti,deact,M}}$ , in 5.7% of the IBD individuals. The small percentages show that the IBD individuals can not be easily grouped into large subgroups with similar combinations

of parameter changes, and the population is rather very heterogeneous regarding their individual combinations of disease-relevant parameter changes.

*Processes affected by disease-relevant parameter changes for IBD.* To analyse the IBD development in more detail, we next determined, which processes were most frequently affected by disease-relevant parameter changes. The aim was to get a better understanding of which cell types and processes have the potential to influence disease development. To this end, we stratified the parameters based on the processes (or cell types) they affect: bacteria, neutrophils, macrophages, dendritic cells, T cells, phagocytosis, resolution, barrier and other. With 93.1 % of IBD individuals, parameters affecting macrophages are most often among the disease-relevant parameter changes. Parameters affecting T cells (54.5 %) and dendritic cells (46.1 %) each are also among the disease-relevant parameter changes in about half of the cases, whereas bacteria (17.5 %), neutrophils (9.2 %), barrier (6.0 %), phagocytosis (4.6 %) and resolution (4.3 %) are less often affected. Note that of course every parameter does not only affect a single process/cell type, but does also have indirect effects on the rest of the system.

As we were not successful in finding large subgroups of IBD individuals with the same combinations of disease-relevant parameter changes, we next tried to find subgroups of IBD individuals with the same combinations of affected processes. We could group 71.0 % of the IBD individuals into five groups of combinations of affected processes. The largest subgroup consisted of IBD individuals with only disease-relevant parameter changes directly affecting macrophages. Other large subgroups consisted of IBD individuals with disease-relevant parameter changes affecting macrophages in combination with T cells, or additionally in combination with dendritic cells, or additionally in combination with bacteria. The fifth-largest subgroup consisted of IBD individuals where only T cells and dendritic cells were affected, but not macrophages. This analysis again showed the very important, but not exclusive, role of macrophages on IBD development.

In summary, the analysis of necessary parameter changes revealed the large heterogeneity of our virtual population of IBD individuals. This aligns well with the heterogeneity in clinical studies of IBD predispositions.

#### **4.5 Comparison of the pre-trigger steady state to detect early biomarkers for IBD**

To draw conclusions on potential biomarkers for very early detection of IBD, we aimed at identifying differences in steady-state concentrations between healthy and IBD individuals before the outbreak of the disease (i.e. before the mucosal injury trigger). To this end, we compared the distribution of all pre-trigger steady-state levels between healthy and IBD individuals and quantified the difference between the two distributions using the two-sample Kolmogorov-Smirnov test.

In Figure 33 we show the distribution of the six pre-trigger steady state variables with highest Kolmogorov-Smirnov test statistic  $D$ , indicating strongest correlation to the outcome (healthy or IBD). Although the correlations of the distributions with the outcome (healthy vs IBD) were statistically significant for almost all pre-trigger steady state variables, the differences between the distributions of healthy and IBD individuals

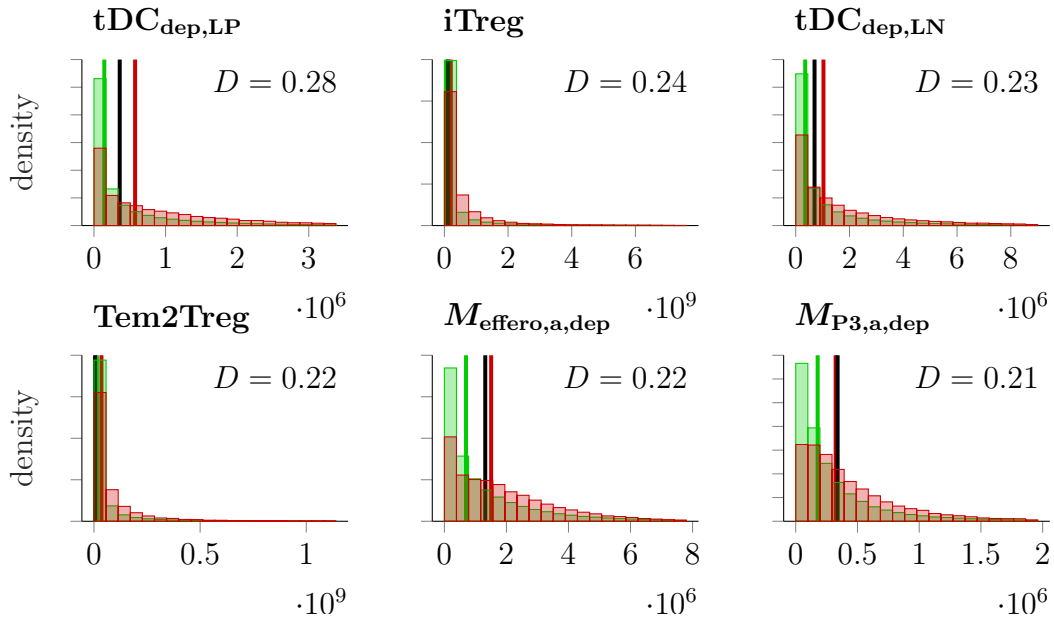


Figure 33: **Comparison of pre-trigger steady state distributions between healthy and IBD individuals.** Histograms show the pre-trigger steady state distributions for the pre-trigger steady state variables with highest Kolmogorov-Smirnov test statistic  $D$  (testing for difference between healthy and IBD), for healthy (green) and IBD (red) individuals. Green and red vertical lines indicate the corresponding population medians; the black line indicates the reference value. Outliers (values above 1.5 times the 95th quantile) were removed to improve readability of the plot. Kolmogorov-Smirnov test statistic  $D$ .

were very small, as can be seen in the plot, where only the distributions with largest correlation to the outcome are shown, and even then only small differences between the distributions can be observed. Unfortunately, those comparisons do not allow to draw any conclusion on potential biomarkers for detection of IBD before the outbreak of the disease.

The differences in pre-trigger steady state could, however, give some more insight into the disease: The largest differences were observed in regulatory T cells (both fully differentiated and proliferating) and pMHCII-depleted tolerogenic dendritic cells and macrophages (i.e. inhibited by regulatory T cells). This emphasises the role of regulatory T cells and the anti-inflammatory role of macrophages for IBD in our virtual population, which is in line with many studies in literature describing the importance of those cell types for IBD [118, 172–174].

#### 4.6 Prediction of IBD based on selected parameters and pre-trigger state variables

As we saw in the previous sections, we could not determine a priori if an individual develops IBD based on single parameters or pre-trigger steady-state levels. In this section, therefore, we aim at predicting the development of IBD based on combinations of parameter values or pre-trigger steady-state levels (without solving the ODEs). In addition, we want to reduce the number of parameters/state variables (i.e. features) used

for this prediction to find the best predictors of disease. This is called feature selection. See Section 9.8 for a short introduction to classification and feature selection, and for a comparison of different classification methods tested on our datasets of parameters or pre-trigger steady-state values. We determined linear discriminant analysis (LDA), which has an embedded method for feature selection, to be the best suited classification method for our analysis.

In Figure 34, the performance (i.e. fraction of correctly classified individuals) dependent on the number of features is shown for the different datasets of parameters or pre-trigger steady-state variables. For each of those datasets, we used two different versions: including all virtual IBD individuals (blue line); or, using a virtual analog of the disease score CDEIS (described in Section 9.10 in the appendix), excluding patients with low disease activity, defined by  $CDEIS < 6$ , to increase the difference between IBD and healthy individuals (violet line). In addition, for pre-trigger steady-state variables, we reduced and summarised the state variables to include only measurable state variables (red and green lines). Each dataset contained the same number of IBD and healthy individuals. Table 5 gives for each of those datasets the linear models including one, two and three features. For more details and interpretation, see the following paragraphs.

*Feature selection based on parameters.* Comparing distributions of single parameters (see Section 4.3) did not yield a means to directly identify healthy and IBD individuals based on parameter values. Therefore we used LDA to find a combination of parameters that can be used for classification of individuals into healthy and IBD individuals. Using all parameters in a linear model resulted in a performance of 87% of correctly classified individuals. The best predictors identified by the LDA were  $h_{\text{pro,deact,M}}$ ,  $h_{\text{rec,M}}$  and  $h_{\text{pro,act,DC}}$ , resulting in 71, 73 or 76% correctly classified if used alone, two together or all three together, respectively. When excluding IBD individuals with low disease activity, i.e. only including those with  $CDEIS > 6$ , the performance was even higher, resulting in 91% correctly classified using all features or 79, 80 or 82% correctly classified using only one, two or three features, respectively, and the best predictors were  $h_{\text{pro,deact,M}}$ ,  $\lambda_{\text{M,max}}$  and  $h_{\text{rec,M}}$ . Those four parameters ( $h_{\text{pro,deact,M}}$ ,  $h_{\text{rec,M}}$ ,  $\lambda_{\text{M,max}}$ ,  $h_{\text{pro,act,DC}}$ ) were already identified as most important parameters for development of IBD based on differences between parameter distributions of healthy and IBD individuals (see Section 4.3) and based on disease-relevant parameter changes (see Section 4.4). In summary, the linear models allowed for a good classification based on parameters values. However, as (most) parameter values can not be measured in humans, this result is only interesting with regards to the theoretical analysis of differences between IBD and healthy individuals, but can not be used to classify real-life individuals.

*Feature selection based on pre-trigger state variables.* As pre-trigger steady state variables, in contrast to parameter values, are at least to some degree measurable in real-life individuals, we also performed a LDA using the pre-trigger steady-state values as features. Compared to using parameters as features, the performance was substantially lower; only 67% of individuals could be correctly classified using all features. Surprisingly, excluding IBD individuals with low disease activity did not improve the performance. When only using measurable state variables (i.e. excluding state variables that are not expected to be measurable in real-life patients or pooling state variables describing different subsets of a cell type), the performance was only 60% correctly classified individuals, i.e.

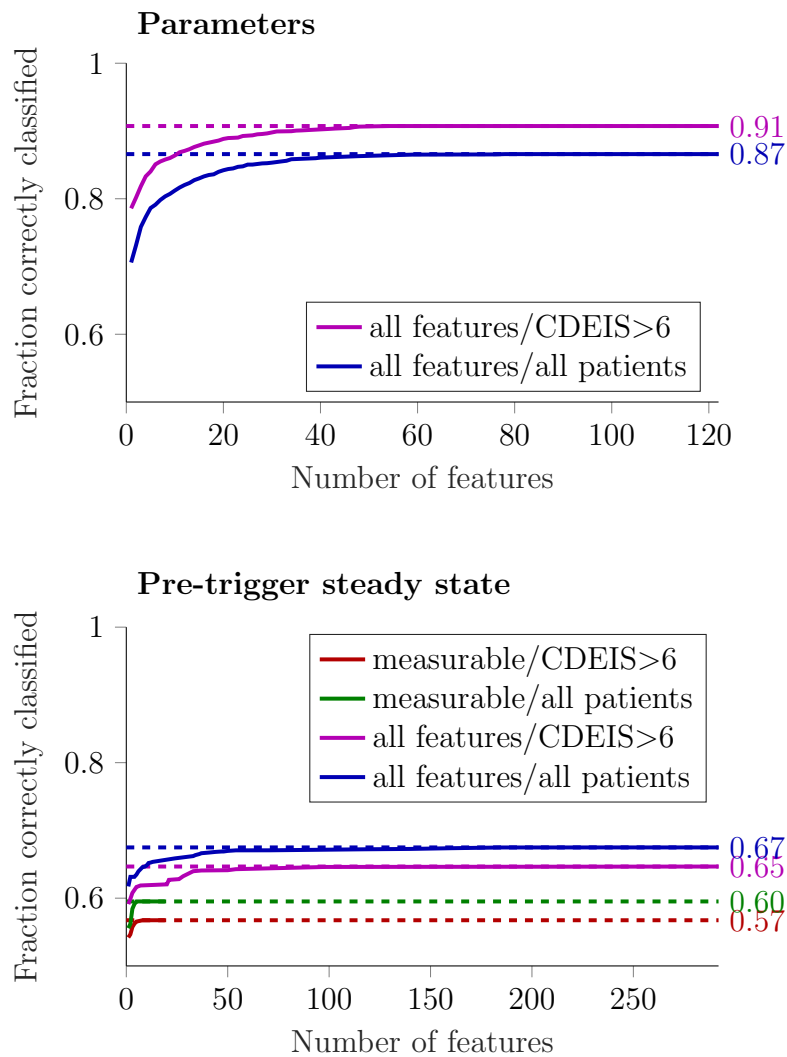


Figure 34: **Performance of linear models dependent on number of included features.** Performance, given as fraction of correctly classified individuals, over number of features included in the linear model, for datasets containing parameters or pre-trigger steady state variables, including all IBD individuals or only IBD individuals with CDEIS  $> 6$ , using all features or only measurable features. All datasets contain in addition the same number of healthy individuals as IBD individuals. Dashed lines indicate the highest performance per dataset, i.e. including all features.

Table 5: **Linear models.** For each dataset from Figure 34, top and middle row, we give three linear models including one, two or three features and the resulting performance (Perf., fraction correctly classified). The linear model is applied to an individual by substituting the values for the features; if the result is  $> 0$ , the individual is classified as IBD individual, otherwise it is classified as healthy individual. In some cases, adding a feature did not improve the performance, only in combination with a second added feature. In this case, we show the next higher number of features. Features (state variables and parameters) are coloured blue to improve readability.

Dataset	Linear model	Perf.
Parameters		
all features/ all patients	$-3.01 + 2.28 \cdot h_{\text{pro,deact,M}}$	0.71
	$-4.36 + 0.678 \cdot h_{\text{rec,M}} + 2.08 \cdot h_{\text{pro,deact,M}}$	0.73
	$-6.11 + 1.28 \cdot h_{\text{pro,act,DC}} + 0.713 \cdot h_{\text{rec,M}} + 2.18 \cdot h_{\text{pro,deact,M}}$	0.76
all features/ CDEIS $> 6$	$-4.54 + 3.21 \cdot h_{\text{pro,deact,M}}$	0.79
	$-6.51 + 1.53 \cdot 10^{-6} \cdot \lambda_{\text{M,max}} + 3.29 \cdot h_{\text{pro,deact,M}}$	0.80
	$-6.94 + 1.19 \cdot 10^{-6} \cdot \lambda_{\text{M,max}} + 0.619 \cdot h_{\text{rec,M}} + 2.84 \cdot h_{\text{pro,deact,M}}$	0.82
Pre-trigger steady state		
all features/ all patients	$-0.219 + 2.93 \cdot 10^{-7} \cdot \text{tDC}_{\text{dep,LP}}$	0.62
	$0.0351 + 2.56 \cdot 10^{-7} \cdot \text{tDC}_{\text{dep,LP}} - 0.0766 \cdot \text{SPM}$	0.63
	$0.261 + 2.28 \cdot 10^{-7} \cdot \text{tDC}_{\text{dep,LP}} - 1.18 \cdot 10^{-8} \cdot M_{\text{P4,a}}$ $- 9.78 \cdot 10^{-7} \cdot M_{\text{effero}} - 0.0699 \cdot \text{SPM}$	0.63
all features/ CDEIS $> 6$	$-0.178 + 2.52 \cdot 10^{-7} \cdot \text{tDC}_{\text{dep,LP}}$	0.59
	$0.0384 + 2.7 \cdot 10^{-7} \cdot \text{tDC}_{\text{dep,LP}} - 0.076 \cdot \text{SPM}$	0.60
	$0.176 + 2.31 \cdot 10^{-7} \cdot \text{tDC}_{\text{dep,LP}} - 1.31 \cdot 10^{-6} \cdot M_{\text{effero}} - 0.0629 \cdot \text{SPM}$	0.61
measurable/ all patients	$-0.0993 + 4.39 \cdot 10^{-9} \cdot \text{Th1}_{\text{tot}}$	0.56
	$-0.389 + 4 \cdot 10^{-8} \cdot \text{DC}_{\text{tot,LP}} + 4.4 \cdot 10^{-9} \cdot \text{Th1}_{\text{tot}}$	0.56
	$-0.32 - 4.3 \cdot 10^{-8} \cdot \text{Neut} + 4.06 \cdot 10^{-8} \cdot \text{DC}_{\text{tot,LP}} + 6.11 \cdot 10^{-9} \cdot \text{Th1}_{\text{tot}}$	0.58
measurable/ CDEIS $> 6$	$-0.108 + 4.98 \cdot 10^{-9} \cdot \text{Th1}_{\text{tot}}$	0.54
	$0.136 - 2.92 \cdot 10^{-8} \cdot M_{\text{pro}} + 6.15 \cdot 10^{-9} \cdot \text{Th1}_{\text{tot}}$	0.55
	$-0.135 + 3.37 \cdot 10^{-8} \cdot \text{DC}_{\text{tot,LP}} - 2.36 \cdot 10^{-8} \cdot M_{\text{pro}} + 5.14 \cdot 10^{-9} \cdot \text{Th1}_{\text{tot}}$	0.56

only slightly higher than the 50% correctly classified individuals that are expected by chance. Nevertheless, the identified best predictors can still give valuable information on the development of the disease: As already identified based on differences between pre-trigger steady state distributions of healthy and IBD individuals (see Section 4.5), the best predictors using all pre-trigger steady state variables ( $tDC_{dep,LP}$ ,  $SPM$ ,  $M_{effero}$  and  $M_{P4,a}$ ) emphasise the importance of anti-inflammatory and pro-resolving mechanisms on the disease development. The best predictors using only measurable pre-trigger steady state variables ( $Th1_{tot}$ ,  $DC_{tot,LP}$ ,  $M_{pro}$ ,  $Neut$ ) show again the interplay of different cell types and processes in this complex disease.

We conclude that (i) classification into healthy and IBD individuals using LDA based on parameter values is feasible with reasonably good performance (87% correctly classified), but classification based on pre-trigger steady-state variables is much less reliable (67% correctly classified); and (ii) parameters and state variables identified as important by the LDA are in the main the same as identified by the comparison of parameter and pre-trigger steady-state distributions between healthy and IBD individuals.

#### 4.7 Subclasses of IBD individuals based on required trigger extent

In our virtual population, we triggered IBD by a complete mucosal injury, i.e. setting the values for  $epi$  and  $tissue$  to 0. However, it is also of interest, which amount of mucosal injury is needed to trigger the disease, if this required mucosal injury differs between different virtual IBD individuals, and how the amount of required mucosal injury might correlate with predispositions and severity. For this, we simulated the response of each IBD individual (defined by elicitation of disease after the highest mucosal injury trigger, i.e.  $epi = tissue = 0$ , see Section 4.1) to different extents of mucosal injury. We used identical levels of destruction of  $epi$  and  $tissue$  and a step-size of 0.1. We observed that some individuals only developed the disease after a strong trigger (i.e.  $epi$  and  $tissue$  set to very low values), whereas other individuals developed the disease also in response to a very small trigger (i.e.  $epi$  and  $tissue$  set to values close to 1). Interestingly, in almost all IBD individuals (> 99.9%), the post-trigger steady state is independent of the extent of mucosal injury, i.e. there is only one inflamed steady state per patient; after any mucosal injury trigger, the IBD individual either reaches its inflamed steady state or its asymptomatic (pre-trigger) steady state. We then classified the IBD individuals based on their minimally required extent of mucosal injury to elicit the disease: Type 1 for a minimal required trigger of  $epi = tissue = 0.9$ , type 2 for a minimal required trigger of  $epi = tissue = 0.8$ , ... , type 10 for a minimal required trigger of  $epi = tissue = 0$ . (Naturally, the minimal required trigger is a continuous variable, which we discretised here to obtain groups of IBD individuals for comparison.) To illustrate the different IBD types, Figure 35 shows the time courses of two exemplary virtual IBD individuals (named patient A and patient B) after a high mucosal injury trigger ( $epi = tissue = 0$ ) and a lower mucosal injury trigger ( $epi = tissue = 0.5$ ). Patient A, which has IBD type 8, only develops the disease after a relatively high trigger ( $epi = tissue \leq 0.2$ ) so that in Figure 35 the disease is only elicited after the high trigger, but not after the lower trigger. Patient B, which has IBD type 3, only requires a lower trigger to elicit the disease ( $epi = tissue \leq 0.7$ ) so that in Figure 35 the disease is elicited after both tested trigger extents. Note that patient B's post-trigger steady state is the same after the two different trigger extents



eliciting the disease. As shown in Figure 36, lower types (lower extent of trigger required) are more frequent in the population than higher types (higher extent of trigger needed).

Figure 37 shows the median time course of bacteria, epithelium, tissue, T helper cells, macrophages and neutrophils for the different IBD types. Note that, of course, there is variability between individuals of the same IBD type, which is not shown here. By comparing the median, however, we can observe that there is a clear correlation between IBD type and time course of epithelium, tissue, T helper cells, macrophages and neutrophils. Epithelium and tissue tend to be repaired more slowly, but reaching a higher level (i.e. less destruction) at steady state for lower types. T helper cell levels are on average higher in lower IBD types. Macrophage levels tend to increase faster in lower IBD types, but reach lower levels in steady state (note that the time frame shown in Figure 37 does not show the steady state in all individuals, i.e. median macrophage levels of high IBD types still increase at 150 days post trigger). Post-trigger neutrophil steady-state levels are lower in lower IBD types. For the higher IBD types we observed that the average individuals tend to take longer to reach the post-trigger steady state than for lower IBD types, that the epithelium and tissue values first rise and then decrease again and the neutrophil levels first decrease and then increase again, i.e. the inflammation first seems to resolve, but then worsens again.

To have a closer look at the difference in the inflamed steady states (i.e. the post-trigger steady state when the disease is elicited) between different IBD types, we calculated the Pearson correlation coefficient  $\rho$  between the inflamed steady-state levels and IBD type for all state variables. See Figure 56 in the appendix for the distribution of the six state variables with largest correlation of IBD type to inflamed steady state value. Highest correlation was observed for epithelium, tissue, and different macrophage subpopulations. For those state variables, the inflamed steady-state levels were closer to the reference (healthy) steady-state levels for lower IBD types. This was well in line with our previous observation that lower IBD types seemed to correlate with less tissue destruction and inflammation.

Correlation of parameter value with IBD type was highest for  $h_{\text{pro,deact,M}}$  ( $\rho = 0.16$ ),  $\mu_M$  ( $\rho = -0.11$ ) and  $h_{\text{rec,M}}$  ( $\rho = 0.10$ ); see Figure 57 in the appendix for the distributions. These parameters were among the parameters previously identified to be most correlated with the development of disease (see Section 4.3).

Finally, we analysed whether the disease is less severe for IBD type 1, in terms of the CDEIS, a score for the severity of CD (described in Section 9.10 in the appendix). Indeed, the distribution of CDEIS values was lower for lower IBD types, especially for type 1, as can be seen in Figure 38. In clinical studies, a CDEIS value of 4 is a frequently used threshold for mucosal healing [175]. In Figure 38 we see that approximately half of our virtual patients of IBD type 1 have CDEIS values below 4, whereas only about one quarter of the virtual patients of IBD types 5 to 10 have CDEIS values below 4.

We conclude that in our virtual population, IBD individuals differ in the extent of trigger required to elicit the disease. The extent of required trigger correlates with parameter values, inflamed steady-state levels and severity of the disease. IBD individuals with higher required trigger tend to develop more severe disease. In a physiological interpretation, we expect the extent of required trigger to be inversely related to the number of flares, i.e. when a lower trigger is needed, a flare can be more easily elicited and flares will occur more frequently. Then, the number of flares and the severity of disease would also be inversely related, i.e. patients with more flares tend to develop less severe disease,

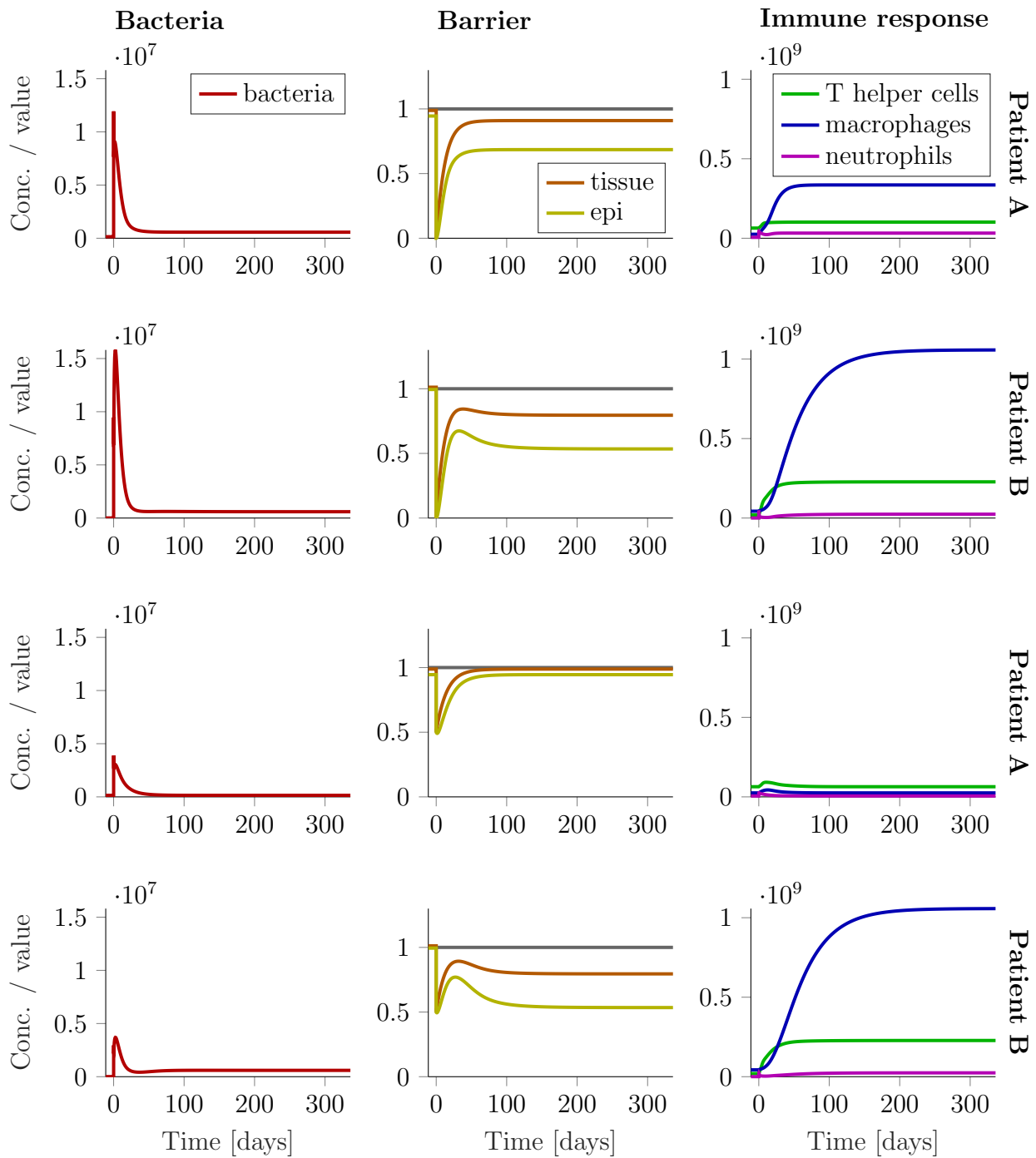


Figure 35: **Exemplary time courses in response to different mucosal injury extents.** Concentrations of bacteria and selected immune cells in LP and barrier state variables (unitless) over time in response to two different mucosal injury extents at time point  $t = 0$ . Top rows: high trigger, i.e. epi = tissue = 0. Bottom rows: lower trigger, i.e. epi = tissue = 0.5.

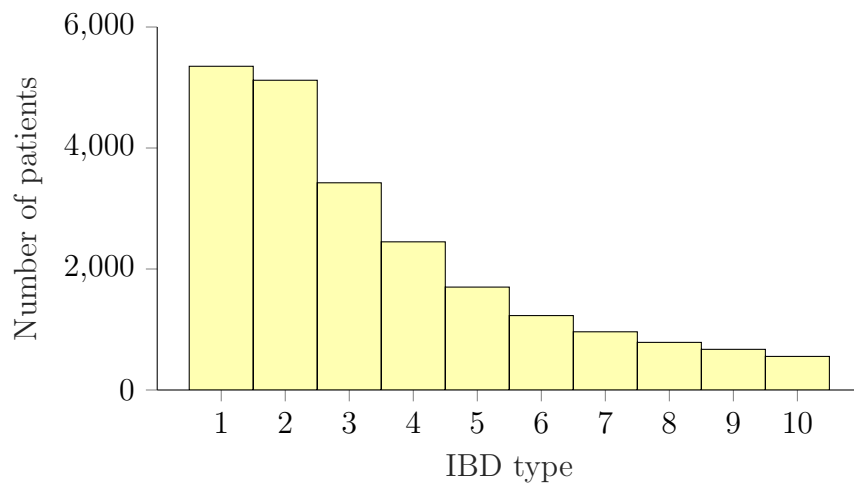


Figure 36: **Distribution of IBD types.** Histogram of IBD types in the virtual IBD population. The IBD type is defined by the minimally required extent of mucosal injury to elicit the disease, where a lower IBD type (e.g. type 1) requires less mucosal injury (e.g.  $\text{epi} = \text{tissue} = 0.9$ ).

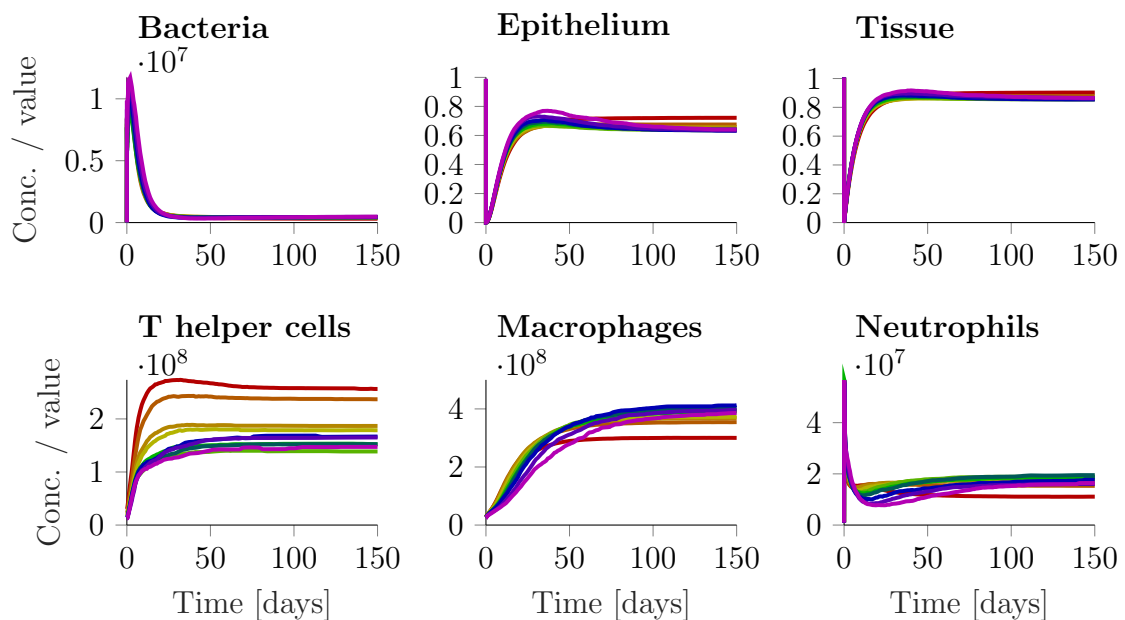


Figure 37: **Time course of mucosal injury for different IBD types.** Concentrations of bacteria and selected immune cells in LP and barrier state variables (unitless) over time in response to mucosal injury at time point  $t = 0$ . To compare the different types, we show the reaction to the highest trigger ( $\text{epi} = \text{tissue} = 0$ ). Compare Figure 26 (2nd row) for the time course of the total IBD population. The lines show the median time course of the different IBD types: Type 1, 2, 3, 4, 5, 6, 7, 8, 9, 10.

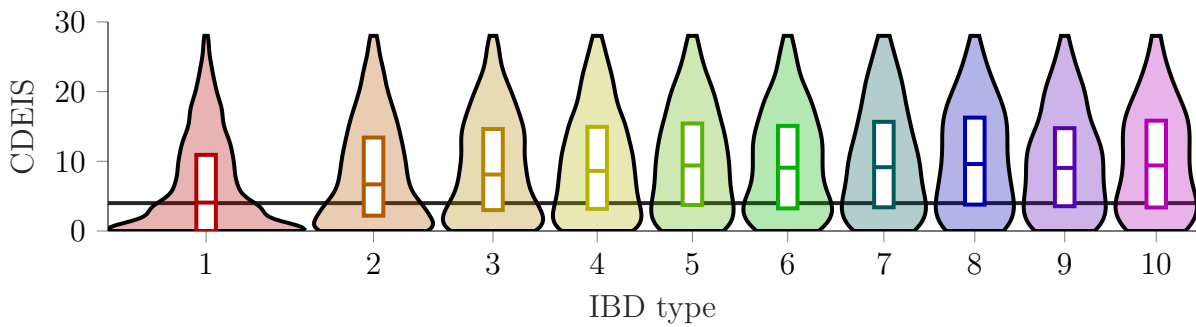


Figure 38: **CDEIS distribution among IBD types.** Violin plots (showing median, quartiles, and the density function) for CDEIS per IBD type. Type 1, 2, 3, 4, 5, 6, 7, 8, 9, 10. Black line indicates CDEIS = 4, which is a frequently used threshold for mucosal healing.

whereas patients with less flares tend to develop more severe disease. This is, however, only a general trend, and does not hold for all patients, as the IBD population is very heterogeneous and also includes patients with high amount of required trigger (i.e. fewer flares) and mild disease and patients with low amount of required trigger (i.e. more flares) and severe disease.

Interestingly, this finding in our virtual population is in contrast to the finding of a large internet-based survey [176] that asked patients about their flare frequency and severity and found a positive correlation between frequency and severity. However, as the CDEIS distribution in Figure 38 shows, a lot of the virtual patients of IBD type 1 have very low CDEIS values (note that CDEIS refers to the inflamed steady state, i.e. during a flare), which means that those would probably not be diagnosed as IBD patients in clinics, as they would probably have no or very few/low symptoms. When we consider only virtual IBD individuals with  $CDEIS > 4$ , the difference in CDEIS distribution between the IBD types is much smaller. While the model includes important processes of the mucosal immune system, it does not, however, include individual difference in perception or intensification of the disease. In addition, the model does not include disease progression so far. This has to be taken into account when comparing survey data with model predictions.

From a model perspective, we observed that all our virtual IBD patients have (at least) two steady states: the asymptomatic pre-trigger steady state and the inflamed steady state (post-trigger steady state for at least the highest trigger  $\text{epi} = \text{tissue} = 0$ ). The patients, however, differ in the amount of disturbance required to switch from the asymptomatic steady state to the inflamed steady state (different IBD types). The switch from the inflamed steady state back to the asymptomatic pre-trigger steady state will be the subject of the next chapter (Chapter 5 about treatment of IBD).

## 4.8 Conclusion

In this chapter, we described the successful generation of a virtual population of healthy and IBD individuals. We want to especially emphasise that we defined IBD only phenotypically, without any a-priori assumptions on parameter differences between healthy and IBD individuals. This is in contrast to the approach taken by many other computational disease models (e.g. [24, 28]), where single parameters are changed to describe the disease

or where differences between healthy and diseased subjects are limited to a pre-specified set of parameters. For a complex, heterogenous disease such as IBD, our approach is preferable as (i) a high level of unknowns in the disease development make it impossible to correctly foresee the disease-eliciting parameters, and (ii) it simultaneously allows to draw valuable conclusions and hypotheses on causes and development of the disease. Our novel systems biology model, which was only based on literature from the healthy mucosal immune response, not including IBD-specific information, in itself contains the ability to also describe IBD as result of variability, where the resulting IBD individuals show convincing similarities to real-life IBD patients.

Analysis of the parameter distributions of healthy and IBD individuals revealed significant differences, which were most pronounced in Hill factors and in parameters relating to macrophages. We could not detect a single parameter or simple parameter combination that allows for definite discrimination between healthy and IBD individuals—this is in line with the known heterogeneity in the development of the disease. Prediction of disease based on parameter values was possible with 91 % precision using a high number of different parameters, and with > 70 % precision using only 1-3 parameters. The analysis of disease-relevant parameter changes revealed that also only one parameter change is able to elicit the disease on its own, and that in general either a small number of large parameter changes or a higher number of small parameter changes are needed to elicit the disease. The identified most frequently changed parameters in IBD individuals were related to many different processes, which emphasises how different processes of the mucosal immune response can be involved in the development of this highly complex disease. Although this parameter comparison is useful to get insights on the pathogenesis of the disease, it can, however, not be used for identification of IBD patients, as parameter values can in general not be clinically measured.

Analysis of the pre-trigger steady-state distributions in healthy and IBD individuals showed only small differences. In addition, a LDA confirmed that prediction of IBD based on pre-trigger cell concentrations is limited.

IBD individuals of our virtual population differed in the extent of the mucosal injury trigger required to elicit the disease. This required extent also correlated with parameter values, inflamed steady-state levels and severity of the disease (measured by a virtual analog of the CDEIS disease score), where a higher needed extent correlated with more severe disease.

In summary, we obtained and characterised a very heterogenous virtual population of IBD individuals, with many convincing similarities to available literature reports on development and phenotype of IBD in real life. This virtual population is a good basis for evaluation of existing and potential new treatment options for IBD, as described in the next chapter.



---

## 5 Implementation and analysis of different treatment effects

The aims of this chapter are to describe virtual IBD patients' time courses in response to different treatment effects based on our novel systems biology model and the virtual IBD population generated in the previous chapter. From the virtual treatment of virtual IBD patients, we aim at drawing conclusions and to generate hypotheses on possible reasons for non-response or relapse of some patients by comparing responders, non-responders and relapsing patients in terms of the different implemented treatment effects and pre-treatment (i.e. inflamed steady-state) cell levels.

We will first give a general introduction to our approach for virtual study simulations and translation of model results to clinical study outcomes, followed by the general description of implementation of treatment, and detailed descriptions of the specific implemented treatment effects. Then we will describe the resulting response in our virtual population, and the analysis of non-response and relapse.

### 5.1 Virtual study simulation

For the simulation of the response of a specific virtual IBD individual to a treatment effect, the initial values were set to the pre-treatment steady state, i.e. the post-trigger steady state of the specific IBD individual. Then the parameters were adapted to account for the treatment as described below and the time course was simulated for the treatment duration. Using the predicted states at the end of the treatment duration as initial values, the further time course without treatment effect was simulated until a steady state was reached, i.e. the post-treatment steady state.

To calculate response rates from individual time courses, a means of translation of the individual immune cell concentrations and state variables to an outcome parameter defining response is required. In clinical studies, different disease scores are in use to define response to treatment. One of the most commonly used disease scores is the Crohn's disease endoscopic index of severity (CDEIS), which evaluates the disease state based on an endoscopic examination of different segments of the colon [177]. To retain comparability of our virtual studies to clinical studies, we designed a virtual CDEIS analog based on model variables. For more details, see Section 9.10 in the appendix. Using this method, the virtual CDEIS analog (called CDEIS in the following) can be calculated for every time point (before, during or after treatment). Then, using the CDEIS, we defined a (binary) response using a threshold for the CDEIS.

We used the CALM study design (Colombel et al., 2017 [175]) as a guiding example of a clinical study in IBD patients, and defined our virtual IBD study population and the response threshold accordingly: According to the inclusion criteria, only IBD individuals with  $\text{CDEIS} > 6$  were included, which resulted in a virtual IBD study population of 13.421

subjects (i.e. 60.1 % of the 22.252 subjects in the full virtual IBD population as defined in the previous chapter). Response was defined as CDEIS  $< 4$  at end-of-treatment (EOT). For a specific treatment effect, the response rate is thus defined as:

$$\text{response rate} = \% \text{ IBD individuals with CDEIS} < 4 \text{ at EOT}$$

In addition, we calculated response at the post-treatment steady state; the relapse rate is then given by the percentage of IBD individuals with CDEIS  $\geq 4$  at post-treatment steady state among the responders. This relapse of virtual patients has to be treated with caution, as it is not directly comparable to relapse of real patients after stop of treatment. Relapse of real patients can occur in response to various reasons, non-sufficient treatment effects, but also events or environmental stimuli triggering a new disease flare. Additional events and environmental stimuli, however, are not accounted for in our virtual study so that the relapse analysed here only describes relapse due to non-sufficient treatment effects. Note that also relapse under treatment (i.e. initial response to treatment but loss of response over time) can not yet be described by our model.

## 5.2 Implementation of treatment effects

In principal, drug effects can be implemented on all targets (e.g. parameters or concentrations) that are part of the model, using an additional parameter  $\eta$  on a specific parameter or reaction rate. This parameter  $\eta$  is dependent on the drug concentration (i.e. time-dependent), in many cases by

$$\eta(t) = \frac{C_{\text{effect}}(t)}{K_I + C_{\text{effect}}(t)}.$$

To simulate response to a specific drug, therefore, we would need to know the drug concentration in the effective compartment over time  $C_{\text{effect}}(t)$  and the drug concentration resulting in half-maximal inhibition  $K_I$ . As those data are rarely accessible, we simplified by implementing the effects of groups of drugs with a shared target, called “treatment effects” in the following, with a variable treatment effect extent parameter  $\eta$ . As those groups of drugs would naturally not have the same pharmacokinetics (PK), we also simplified with respect to PK, assuming a constant drug effect for a treatment duration of 24 weeks for all implemented treatment effects. This approach also allowed to analyse the dependence of the response rate on the treatment effect extent parameter  $\eta$ . We would like to emphasise, however, that with the knowledge of drug-specific PK and binding behaviour, a specific drug effect can easily be implemented in the presented systems biology model.

Each constant treatment effect was implemented by a treatment effect extent parameter  $\eta$ , which specified the extent of the change of the affected parameters and/or rates over the treatment duration. As the affected parameter(s)/rate(s) were multiplied by  $(1 - \eta)$  to incorporate the treatment effect,  $\eta = 0$  means no treatment effect,  $\eta = 1$  means complete inhibition of the affected parameter(s) and  $\eta < 0$  means stimulation or increase of the affected parameter(s). Note that in one case (FMT), the treatment effect extent parameter  $\eta$  was defined not as a relative change of the parameter, but as the respective parameter itself.



Implementation of the effects of specific treatments will be explained in the following sections (Sections 5.3-5.9), including a short introduction to the mechanism of action described in literature, our implementation in the model, and an interpretation of the virtual study outcome in the context of clinical study outcomes. As the treatment effect extent parameters cannot be directly derived from literature, we tested for each treatment effect different treatment effect extent parameters  $\eta$ . To reasonably compare different treatment mechanisms (see Section 5.10-6.2), we determined for each treatment effect the treatment effect extent parameters  $\eta$  that resulted in 30 % and 50 % response rates in the virtual IBD study population.

Figure 39 shows the simplified model scheme (Figure 1), including the targets of all implemented treatment effects described in this chapter. Figure 40 shows the time courses of the mucosal immune response for two exemplary virtual IBD individuals to two different treatment mechanisms (cytokine inhibitor and anti-cell adhesion treatment; see Sections 5.3 and 5.4). Figures 41 and 42 show the response rates over the treatment effect extent parameter  $\eta$  for the different implemented treatment effects. Note that, naturally, not the full range of displayed treatment effect extent parameters is physiologically relevant, and that the response rates per tested treatment effect extent parameter do not allow to draw conclusions on comparison of achievable response rates of the different drugs, as we do not know how easily the different treatment effect extents  $\eta$  can be achieved with the available drugs. Figure 43 shows the relapse rates for the different treatment effects for the treatment effect extent parameters resulting in 30 % and 50 % response in the virtual IBD population.

### 5.3 Monoclonal antibodies targeting cytokines/cytokine production

Several different drug classes aim at decreasing pro-inflammatory cytokine levels, e.g. monoclonal antibodies targeting tumour necrosis factor (TNF)- $\alpha$  (e.g. adalimumab, infliximab), the IL-23 pathway (e.g. Ustekinumab inhibiting a subunit of IL-12/IL-23) or IL-6 [14]. In addition, JAK inhibitors, small molecules inhibiting the Janus kinase (JAK), part of the JAK-STAT pathway involved in the production of many different cytokines, also result in a decrease in the production of several pro-inflammatory cytokines [14]. We comprised all those different modes of action into one treatment effect, which is decrease of pro-inflammatory cytokine concentrations (collectively called “cytokine inhibitors” in the following). Note that potential other direct effects of the above mentioned drug classes (e.g. anti-TNF- $\alpha$  monoclonal antibodies inducing T cell apoptosis via inhibition of membrane-bound TNF- $\alpha$ ) were neglected here. In the model, pro-inflammatory cytokines are not further differentiated into different cytokines and are represented by a linear combination of the cytokine-producing cell concentrations (see Section 2.14). The treatment effect of cytokine inhibitors was implemented by reducing all cytokine production weights for pro-inflammatory cytokines (i.e. cytokines acting in the processes of neutrophil recruitment, macrophage recruitment, macrophage deactivation, dendritic cell activation, damage to epithelium and damage to tissue; see Table 2) by the treatment effect extent parameter  $\eta$ .

As shown in Figure 41 (top left), the response rate of the virtual IBD study population to cytokine inhibitors increases with higher treatment effect extent parameters  $\eta$ , with 100 % response for  $\eta$  close to 1. Note that, however,  $\eta$  values close to 1 are neither physiologically plausible (as this would include complete inhibition of all pro-inflammatory

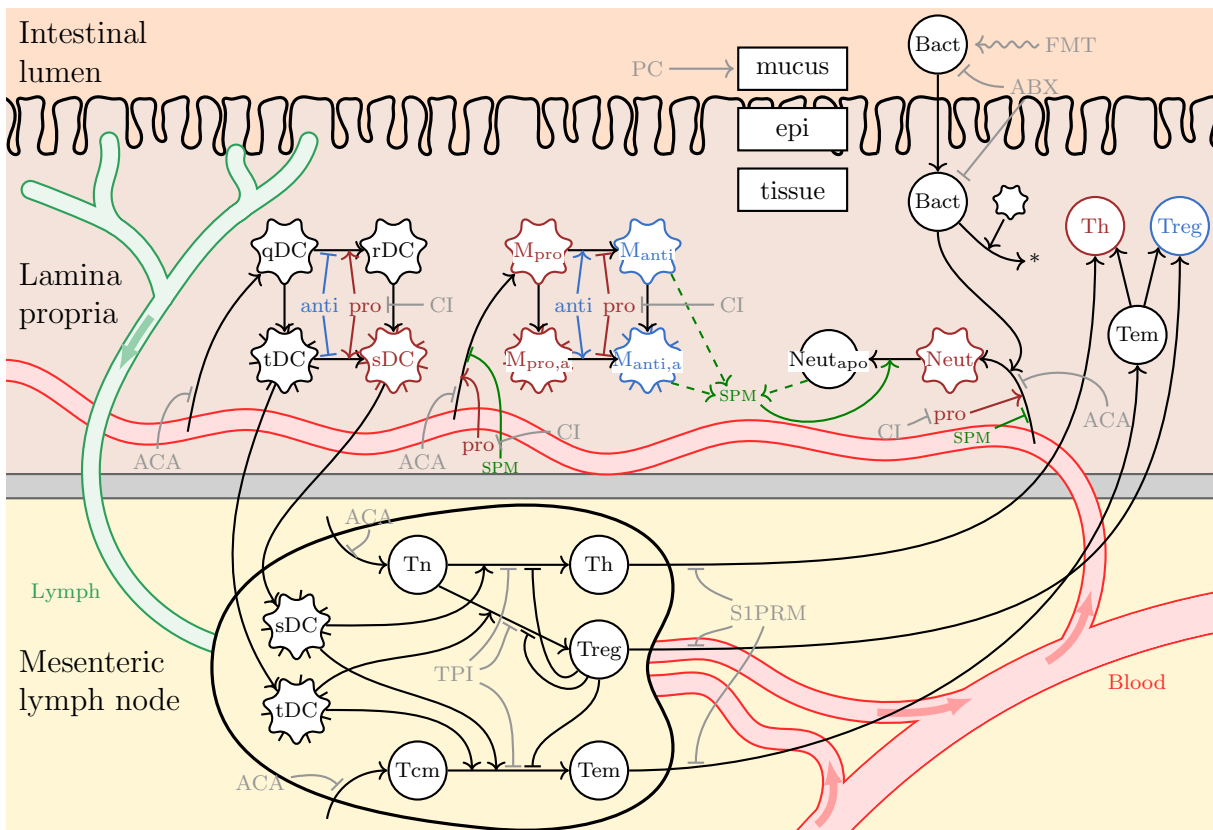


Figure 39: **Simplified model scheme including targets of treatment effects.** Overview of the cell types that we included into the model, and their interactions. See Figure 1 for the legend. Grey arrows (stimulating or inhibiting) show the implementation of different treatment effects (CI cytokine inhibitor, ACA anti-cell adhesion, S1PRM S1PR modulator, PC orally administered phosphatidylcholine, FMT faecal microbial transplant, TPI T cell proliferation inhibitor, ABX antibiotics).

cytokines of the mucosal immune response) nor clinically desirable (as a certain level of pro-inflammatory cytokines is required to maintain normal activities of the mucosal immune response). Treatment effect extent parameters  $\eta = 0.1456$  and  $\eta = 0.2258$  result in response rates of 30 % and 50 % in the virtual IBD study population. The relapse rate, see Figure 43, was moderate, e.g. 30 % for a response rate of 50 % and 39 % for a response rate of 30 %. Note that, although the numbers are comparable, those simulated rates of relapse after EOT can not be compared to the literature-reported clinical loss-of-response rates of anti-TNF- $\alpha$  monoclonal antibodies under treatment ( $\approx 40$  % [14]).

Obviously, the collective implementation of the effects of all drug classes described above in the same way is a crude approximation, not accounting for the different modes of action, different affected pro-inflammatory cytokines or additional effects beyond cytokine inhibition. Nevertheless, our simulations show the potential of cytokine-inhibiting drugs for the treatment of IBD. The implementation of the effect of a specific cytokine-inhibiting drug into our systems biology model is feasible, but requires knowledge on the specific targeted cytokines and on their respective contribution to the different cytokine-mediated processes.

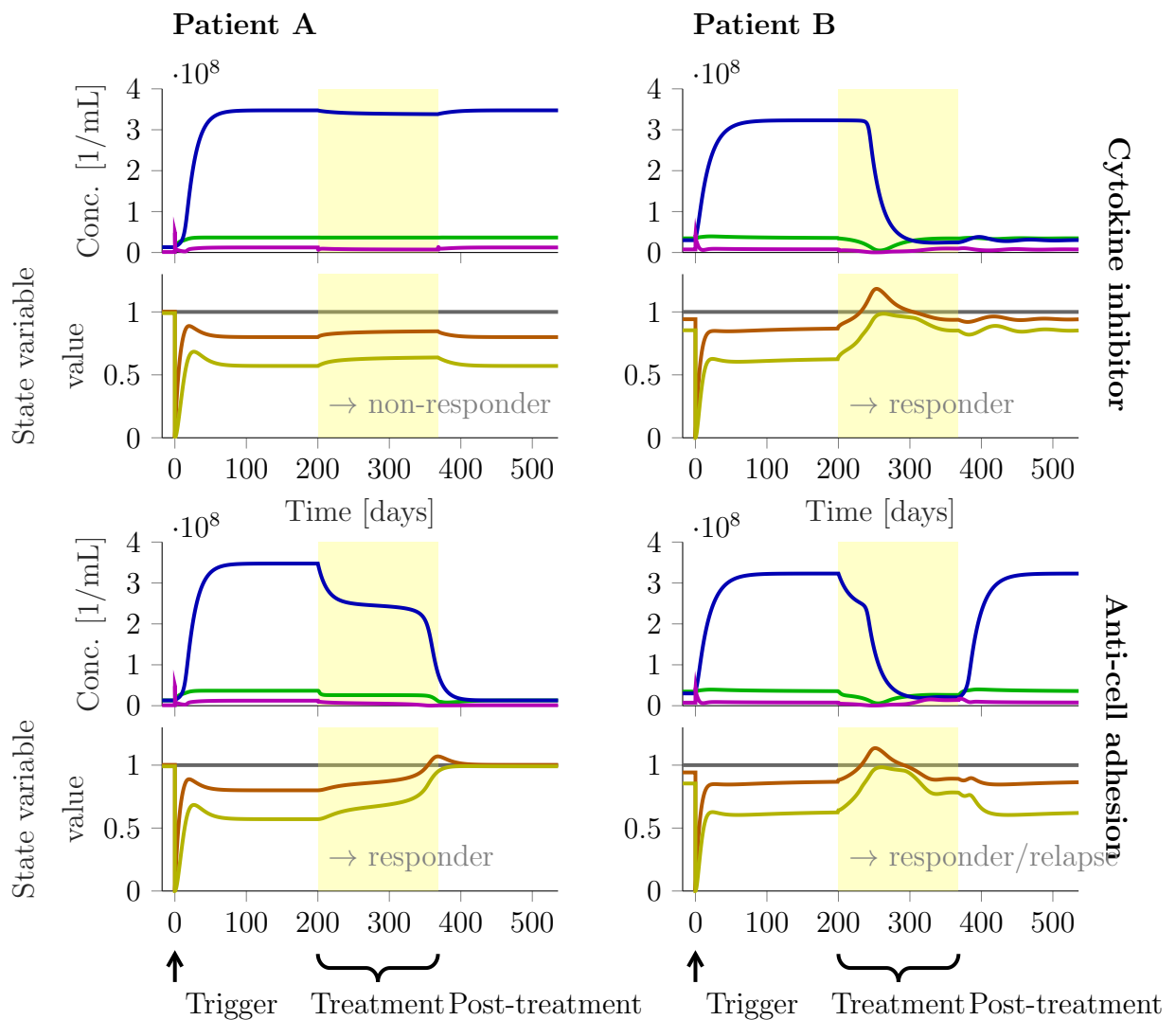


Figure 40: **Exemplary virtual patient time courses of treatment with cytokine inhibitor or anti-cell adhesion treatment.** Concentrations of bacteria and selected immune cells in LP and barrier state variables (unitless) over time in two selected virtual IBD patients (defined by their specific sets of parameters). The first 200 days show the response to the mucosal injury trigger, resulting in an inflamed steady state. The following 24 weeks (yellow) show the response to the two different treatment mechanisms (cytokine inhibitor or anti-cell adhesion treatment), i.e. initial values equal the post-trigger steady state and parameters are modified according to treatment mechanism ( $\eta = 0.1456$  for cytokine inhibitor and  $\eta = 0.2610$  for anti-cell adhesion treatment, corresponding to response rates of 30% in the virtual IBD study population). The last part of the time course shows the post-treatment time course, i.e. initial values equal the EOT state with no treatment effect on the parameter values.

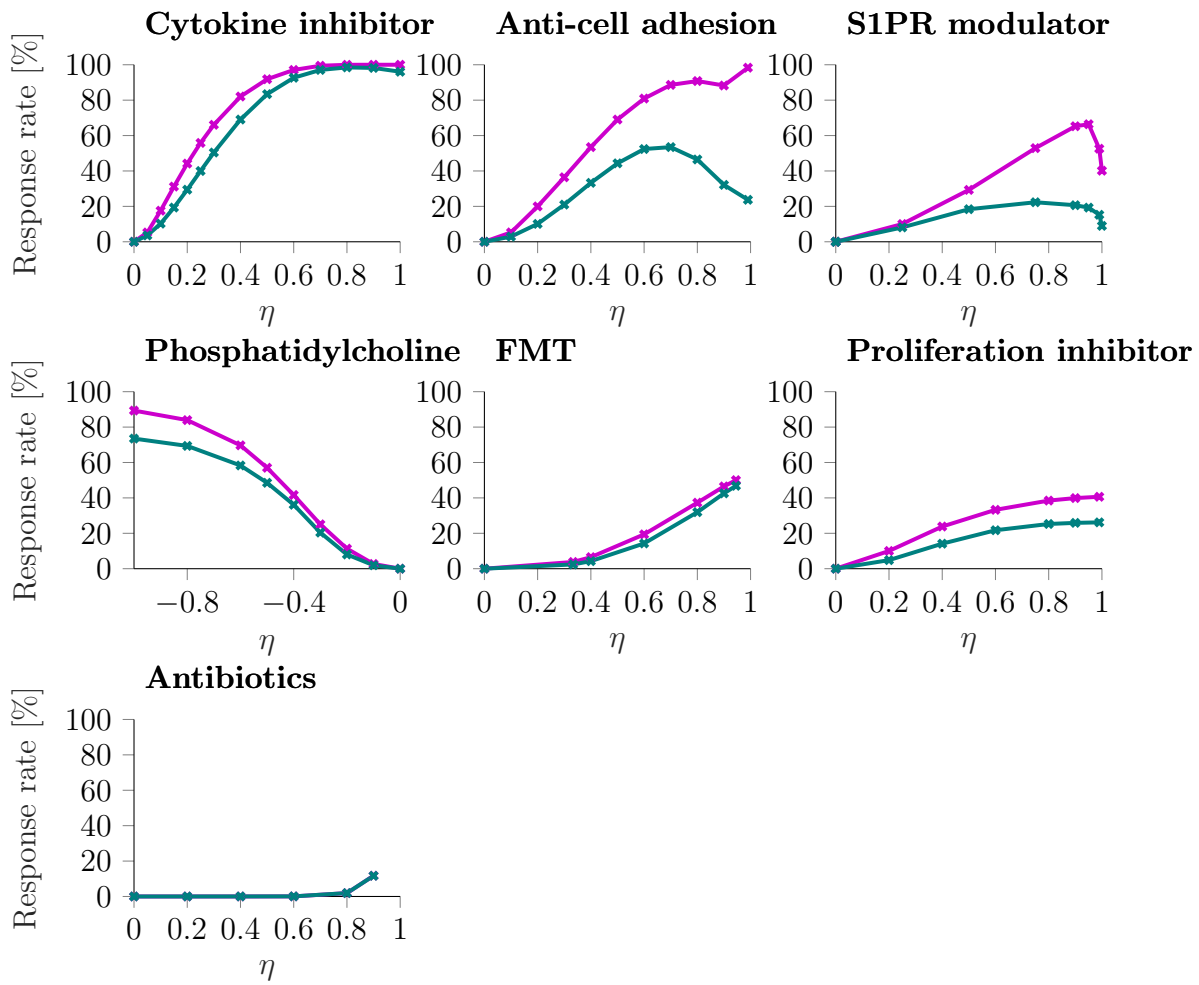


Figure 41: **Response rate over treatment effect extent parameter  $\eta$  for different treatment effects.** Response rate at **end-of-treatment (EOT) (violet)** and in **post-treatment steady state (turquoise)**. (Note that for antibiotics the two curves overlap.) The difference of the two response rates equals the percentage of patients that relapse. For the S1PR1 modulator, only the response rate over the treatment effect extent parameter  $\eta_{\text{egress}}$  is shown; see Figure 42 for the response rate over both treatment effect extent parameters  $\eta_{\text{egress}}$  and  $\eta_{\text{Treg}}$ .

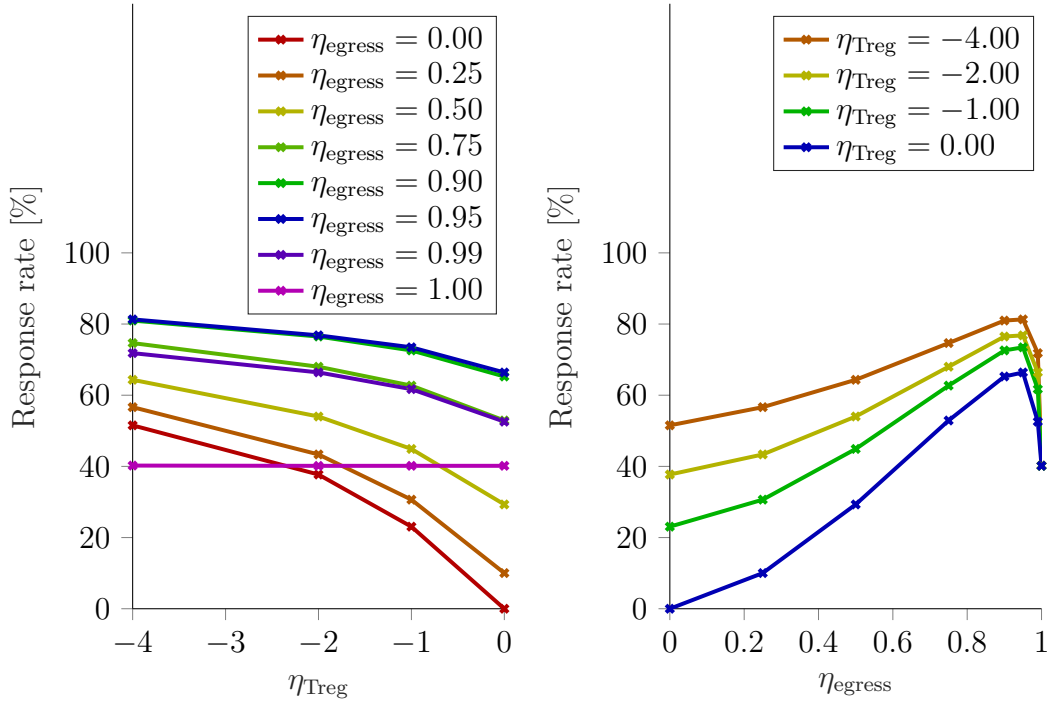


Figure 42: **Response rate over treatment effect extent parameters  $\eta$  for S1PR modulators.** The left plot shows the response rate over treatment effect extent parameter  $\eta_{Treg}$  for different treatment effect extent parameters  $\eta_{egress}$  (by colour). The right plot shows the response rate over treatment effect extent parameter  $\eta_{egress}$  for different treatment effect extent parameters  $\eta_{Treg}$  (by colour). Note that both plots show exactly the same data points. In Figure 41, only the response rate over  $\eta_{egress}$  is shown, assuming  $\eta_{Treg} = 0$ , i.e. the blue curve of the right plot shown here. For implementation and interpretation of the two treatment effect extent parameters, see Section 5.5.

## 5.4 Anti-cell adhesion molecules

A further means to limit mucosal inflammation is the inhibition of the migration of immune cells into the LP. This concept is used by anti-cell adhesion molecules (e.g. the monoclonal antibodies vedolizumab, natalizumab or etrolizumab) that block specific integrins on the surface of immune cells. As those integrins are required for the adhesion of immune cells to endothelial cells, integrin inhibition prevents adhesion to and subsequent migration through the endothelium into the LP [14]. The treatment effect of anti-cell adhesion molecules was implemented by reducing the inflow rate constants of macrophages (constant  $\lambda_{M,c}$  and cytokine-dependent  $\lambda_{M,max}$ ; see Section 2.8, paragraph *Recruitment*), dendritic cells ( $\lambda_{DC}$ ; see Section 2.9, paragraph *Migration to LN*), and neutrophils ( $\lambda_{Neut,max}$ ; see Section 2.7, paragraph *Recruitment*) into the LP and the inflow rate constant of T cells (naive  $\lambda_{Tn}$  and central memory  $\lambda_{Tcm}$ ; see Section 2.11, paragraphs *Naive T cells (LN)* and *Central memory T cells (LN)*) into the LN. The extent of reduction was approximated to be the same for all described inflow rate constants, given by the treatment effect extent parameter  $\eta$ .

As shown in Figure 41 (top middle), the response rate increases with higher  $\eta$  values, up to  $\approx \eta = 0.8$ , but for  $\eta > 0.7$ , long-term effects of the treatment decrease, i.e. higher  $\eta$  values result in a lower percentage of responders that do not relapse after EOT. This is

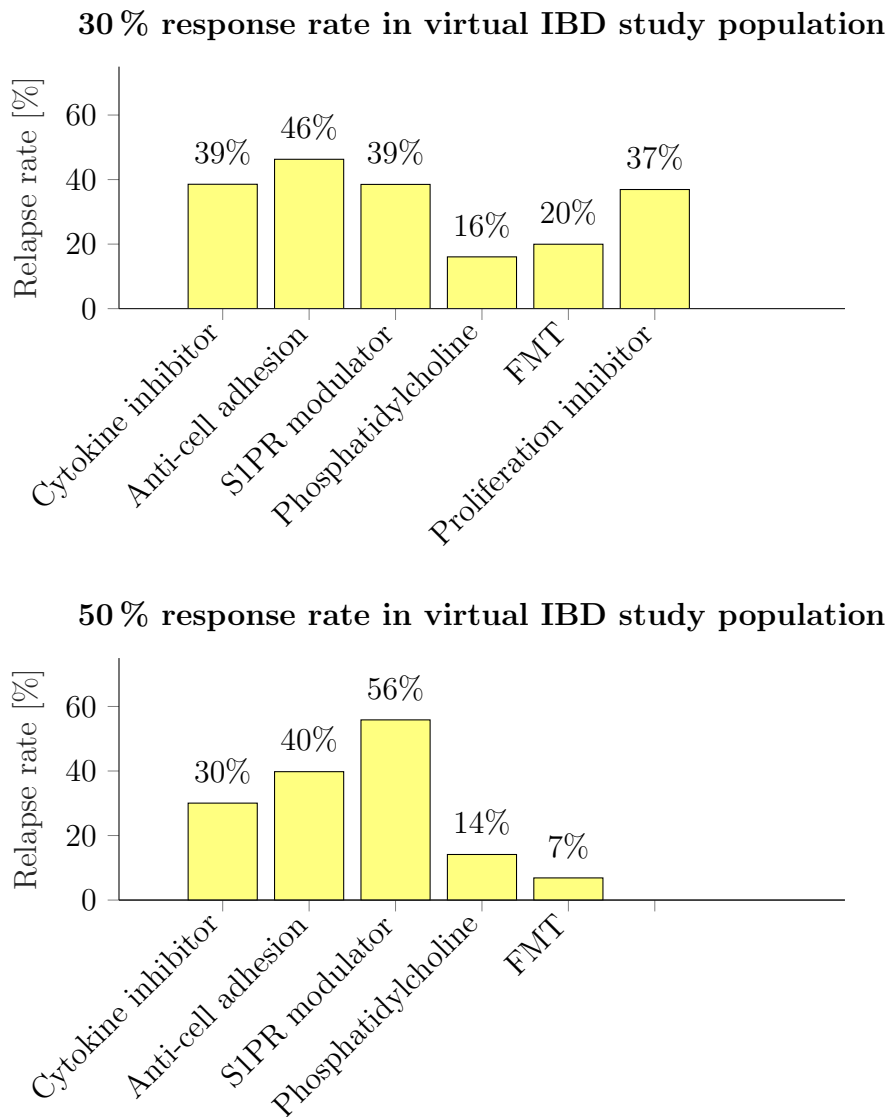


Figure 43: **Relapse rates for different treatment effects.** Percentage of responders that relapse, per treatment effect, for the treatment effect extent parameters  $\eta$  that result in 30 % (top) or 50 % (bottom) response rates in the virtual IBD population for each of the treatment effects. Note that for the proliferation inhibitor 50 % response rate, and for antibiotics 30 % and 50 % response rates could not be reached in the simulation, so that no relapse rate could be given in this case.

probably due to the fact that inhibiting T cell inflow also inhibits the beneficial regulatory T cells. Treatment effect extent parameters  $\eta = 0.261$  and  $\eta = 0.3785$  result in response rates of 30 % and 50 % in the virtual IBD study population.

## 5.5 Sphingosine-1-phosphate receptor modulators

Egress of T cells from the LN is mediated by sphingosine-1-phosphate receptor type 1 (S1PR1) on the T cells' surface, see Section 2.11. S1PR modulators (e.g. fingolimod, ozanimod, etrasimod) are small molecules down-regulating S1PR1, thereby inhibiting the outflow of T cells out of the LN [14]. Another described effect of S1PR1 is suppression of regulatory T cell development, so that S1PR modulators down-regulating S1PR1 lead to higher regulatory T cell concentrations [178]. We separately implemented those two different mechanisms: The treatment effect of inhibition of T cell egress from LN was implemented by reducing the egress rate constant of naive and central memory T cells  $\mu_{T, LN}$  (see Section 2.11, paragraphs *Naive T cells (LN)* and *Central memory T cells (LN)*), and of differentiated T cells (see Section 2.11, paragraphs *Naive T cells (LN)*) from the LN by treatment effect extent parameter  $\eta_{\text{egress}}$ . The treatment effect of regulatory T cell activation was implemented by increasing the effects of regulatory T cells (without directly increasing regulatory T cell concentrations), i.e. by increasing the anti-inflammatory cytokine production weights by regulatory T cells (relevant for the processes of macrophage deactivation and dendritic cell activation; see Table 2) and the Treg-mediated pMHCII-depletion of APCs (macrophages and dendritic cells in LP and LN). The extent of increase was described by treatment effect extent parameter  $\eta_{\text{Treg}}$ , with  $\eta_{\text{Treg}} < 1$ .

Figure 42 shows the response rate in the virtual IBD study population over the treatment effect extent parameters  $\eta_{\text{Treg}}$  and  $\eta_{\text{egress}}$ . The response rate increases for lower values of  $\eta_{\text{Treg}}$  (i.e. for higher regulatory T cells increase). The response rate also increases for higher values of  $\eta_{\text{egress}}$ , up to  $\eta_{\text{egress}} \approx 0.95$ , but decreases for higher values of  $\eta_{\text{egress}}$ . This is probably due to the fact that inhibition of T cell egress also includes inhibition of regulatory T cell egress.

As the quantitative relation of the two treatment effects (inhibition of T cell egress and activation of regulatory T cells) is unclear, and the main described effect in literature is inhibition of T cell egress [14], we focused on the treatment effect of inhibition of T cell egress in the following analyses, i.e. activation of regulatory T cells was neglected ( $\eta_{\text{Treg}} = 0$  and  $\eta = \eta_{\text{egress}}$ ). For this scenario, the treatment effect extent parameters  $\eta = 0.51$  and  $\eta = 0.723$  result in response rates of 30 % and 50 % in the virtual IBD study population.

## 5.6 Orally administered phosphatidylcholine

Although the respective Phase III trial has been stopped, another interesting approach to counteract mucosal inflammation in IBD is orally administered phosphatidylcholine [14]. Phosphatidylcholine is a main part of the mucus layer, which is increasingly destroyed in IBD. We implemented this treatment effect as an increase in mucus production rate (see Section 2.5) by treatment effect extent parameter  $\eta$ , with  $\eta < 0$ .

As shown in Figure 41 (middle left), where we evaluated an increased mucus production rate of up to 2-fold (corresponding to  $\eta = -1$ ), the response rate increases with lower

$\eta$  values, while the relapse rates after EOT are relatively low. Treatment effect extent parameters  $\eta = -0.3292$  and  $\eta = -0.4507$  result in response rates of 30 % and 50 % in the virtual IBD study population.

## 5.7 Faecal microbial transplant

The local milieu of commensal bacteria (microbiota) is known to highly influence the mucosal immune response; among others the differentiation of T cells into different T helper cell types (Th1, Th2 and Th17) are dependent on the bacteria providing the bacterial antigen (see Section 2.12). Modification of the microbiota, e.g. via faecal microbial transplant (FMT) (infusion of faecal solution from a healthy donor to the IBD patient), has shown positive results in several studies [14].

See Section 2.12 for the implementation of the differential effects of the microbiota composition on phagocytic cells and subsequent differentiation of T helper cells in our systems biology model. In summary, the fractions of T helper cell types 1, 2 and 7 are determined by host-specific and bacteria-specific parameters, where both the host-specific parameters and the bacteria-specific parameter define a distribution between the three cell types, which are then combined into the resulting fractions. We implemented the treatment effect of FMT by increasing the bacteria-specific fraction of Th2 induction, where the treatment effect extent parameter  $\eta$  was defined as the fraction of Th2 (fractions for Th1 and Th17 were set to  $\frac{1-\eta}{2}$ , each). As shown in Figure 41 (middle middle), the response rate of the virtual IBD study population to FMT increases with higher treatment effect extent parameters  $\eta$ , but is limited at 50 %. Treatment effect extent parameters  $\eta = 0.721$  and  $\eta = 0.945$  result in response rates of 30 % and 50 % in the virtual IBD study population.

## 5.8 T cell proliferation inhibitors

Some drugs used in treatment of IBD, e.g. the small molecule drugs azathioprine or (among other discussed effects) methotrexate, use inhibition of T cells proliferation to limit the mucosal inflammation [179–181].

We implemented the effect of T cell proliferation inhibitors by decreasing the T cell proliferation rate constants  $p_{Tn,1}$  and  $p_{Tn,>1}$  (see Section 2.11) by the treatment effect extent parameter  $\eta$ . As shown in Figure 41 (middle right), the response rate increases for higher  $\eta$  values, but is limited at 41 %, i.e. in 59 % of the virtual IBD study population, even complete inhibition of T cell proliferation does not result in response. Treatment effect extent parameter  $\eta = 0.518$  results in a response rate of 30 % in the virtual IBD study population.

## 5.9 Antibiotics

Another approach in the treatment of IBD is the use of antibiotics, although data are limited and controversial [14].

We implemented the treatment effect of antibiotics by decreasing the bacterial proliferation rate constants in the intestinal lumen ( $p_{Bact,Lu}$ ) and LP ( $p_{Bact,LP}$ ) by the treatment



effect extent parameter  $\eta$ .

As shown in Figure 41 (bottom left), the response rates in the virtual IBD study population were very low ( $< 2\%$  for  $\eta \leq 0.8$ ,  $12\%$  for  $\eta = 0.9$ , and numerical problems for  $\eta > 0.9$ ). This is, however, in accordance with the controversial data about success of antibiotics treatment in IBD in clinical studies [14]. In addition, it has to be noted that our simulations show the (low) effectiveness of giving antibiotics if the flare is already present; it may be more effective at preventing flares, i.e. when given before the mucosal injury eliciting the flare. Interestingly, we did not observe any relapse after EOT with antibiotics.

## 5.10 Comparison of parameters between responders and non-responders

The high rates of non-responders observed in the treatment of real-life IBD patients pose a large burden, both financially and for the individual patient, as in many cases several treatments have to be tried before finding a successful treatment option. It would be highly desirable to be able to a priori choose the treatment option with best chance of success for a specific patient. To that end, we would need to know what determines success of a treatment effect, i.e. what are the differences between responders and non-responders to a treatment effect.

For each treatment effect, we compared the distributions of all parameters between responders and non-responders, as described previously in Section 4.3. Table 6 shows for each treatment effect the two-sample Kolmogorov-Smirnov test statistic  $D$ , testing for the difference between responders and non-responders, for the 5 most different parameters. For the simulation, for each treatment effect the treatment effect extent parameter  $\eta$  resulting in 30% response rate in the virtual IBD study population was assumed. (Note that, therefore, antibiotics were not included in this analysis.) Assuming treatment effect extent parameters  $\eta$  resulting in 50% response rates in the virtual IBD study populations (data not shown) yields, with few small exceptions, the same lists of most different parameters between responders and non-responders.

The shown parameters are those that best distinguish responders from non-responders, i.e. that are most probably responsible for the success of a therapy. Overall, we observed that macrophages seem to be important in describing the differences between responders and non-responders, as parameters related to macrophages appear among the most different for all treatment effects. Especially for cytokine inhibitors and anti-cell adhesion treatment, only parameters relating to macrophages appear among the most different. For S1PR modulators, we observed T cell proliferation and death rate constants to be highly influential, which is in accordance with their treatment mechanism of inhibition of T cell egress from the LN. For orally administered phosphatidylcholine, also in accordance with its treatment mechanism, in addition to parameters relating to macrophages, parameters relating to the mucosal barrier destruction and bacterial death in the lumen appeared among the most different. For FMT, we observed both parameters relating to macrophages and to T cells among the most different. Of special interest was the identified parameter  $H_1$ , which describes the host's tendency to differentiate T cells into T helper cells of type 1, as it is directly related to the treatment effect of changing the fractions of T helper cell types. For proliferation inhibitors, in addition to macrophage-related parameters, we identified the T cell proliferation rate constant to be most important, which also directly relates to the treatment mechanism. In summary, the connection between

Table 6: **Comparison of parameter distributions between responders and non-responders.** Kolmogorov-Smirnov test statistic  $D$ , testing for the difference in parameter distributions between responders and non-responders, for the 5 most different parameters, for each treatment effect. Treatment effect extent parameters  $\eta$  resulting in 30% response rate in the virtual IBD study population were assumed. Parameter “ $M_{\text{pro,a,(dep)}} \rightarrow \text{cytO}_{\text{pro,deact,M}}$ ” refers to the weight of pro-inflammatory macrophages in the production of cytokines inhibiting macrophage deactivation.  $D = 0$  indicates no difference, i.e. perfectly overlapping distributions;  $D = 1$  indicates maximal difference, i.e. completely separated distributions. The corresponding p-values are  $p < 0.001$  for all shown parameters.

Cytokine inhibitor		Anti-cell adhesion		S1PR modulator	
$h_{\text{pro,deact,M}}$	0.18	$\lambda_{\text{M,max}}$	0.14	$p_{\text{Tn,>1}}$	0.45
$\mu_M$	0.15	$\mu_M$	0.14	$h_{\text{pro,deact,M}}$	0.23
$\lambda_{\text{M,max}}$	0.11	$h_{\text{pro,deact,M}}$	0.12	$\mu_{T,\text{prol}}$	0.22
$h_{\text{rec,M}}$	0.09	$h_{\text{rec,M}}$	0.1	$\mu_{T,\text{LN}}$	0.18
$M_{\text{pro,a,(dep)}} \rightarrow$ $\text{cytO}_{\text{pro,deact,M}}$	0.07	$M_{\text{pro,a,(dep)}} \rightarrow$ $\text{cytO}_{\text{pro,deact,M}}$	0.09	$\lambda_{\text{M,max}}$	0.12
Phosphatidylcholine		FMT		Proliferation inhibitor	
$\mu_M$	0.20	$h_{\text{pro,deact,M}}$	0.25	$h_{\text{pro,deact,M}}$	0.34
$F_{\text{max,epi}}$	0.18	$p_{\text{Tn,>1}}$	0.24	$p_{\text{Tn,>1}}$	0.28
$h_{\text{pro,deact,M}}$	0.11	$M_{\text{pro,a,(dep)}} \rightarrow$ $\text{cytO}_{\text{pro,deact,M}}$	0.21	$M_{\text{pro,a,(dep)}} \rightarrow$ $\text{cytO}_{\text{pro,deact,M}}$	0.26
$\mu_{\text{Bact,Lu}}$	0.10	$\lambda_{\text{M,max}}$	0.18	$h_{\text{pro,act,DC}}$	0.25
$\lambda_{\text{M,max}}$	0.09	$h_{\text{rec,M}}$	0.17	$\lambda_{\text{M,max}}$	0.19

the treatment targets and the identified most influential parameters for treatment success was very prominent. As a result, the different treatment effects showed large differences with regard to the most influential parameters, which could be a promising evidence that different IBD individuals, characterised by different sets of parameters, might benefit from different treatments.

### 5.11 Influence of disease-relevant parameter changes on response to treatment

In addition to comparing the parameter distributions between responders and non-responders to the different treatment effects, we compared the disease-relevant parameter changes (see Section 4.4) between responders and non-responders, with the aim to gain additional insights into the differences between responders and non-responders with regard to their individual disease-causing factors. For this analysis, we used for each IBD individual of the virtual IBD study population its specific set of disease-relevant parameters, as determined in Section 4.4. Figure 44 shows, for the 10 most frequent disease-relevant parameter changes in the virtual IBD study population, the response rates in the subpopulations where the respected parameters are or are not disease-relevant.

From this comparison we could draw conclusions on the influence of the disease-causing

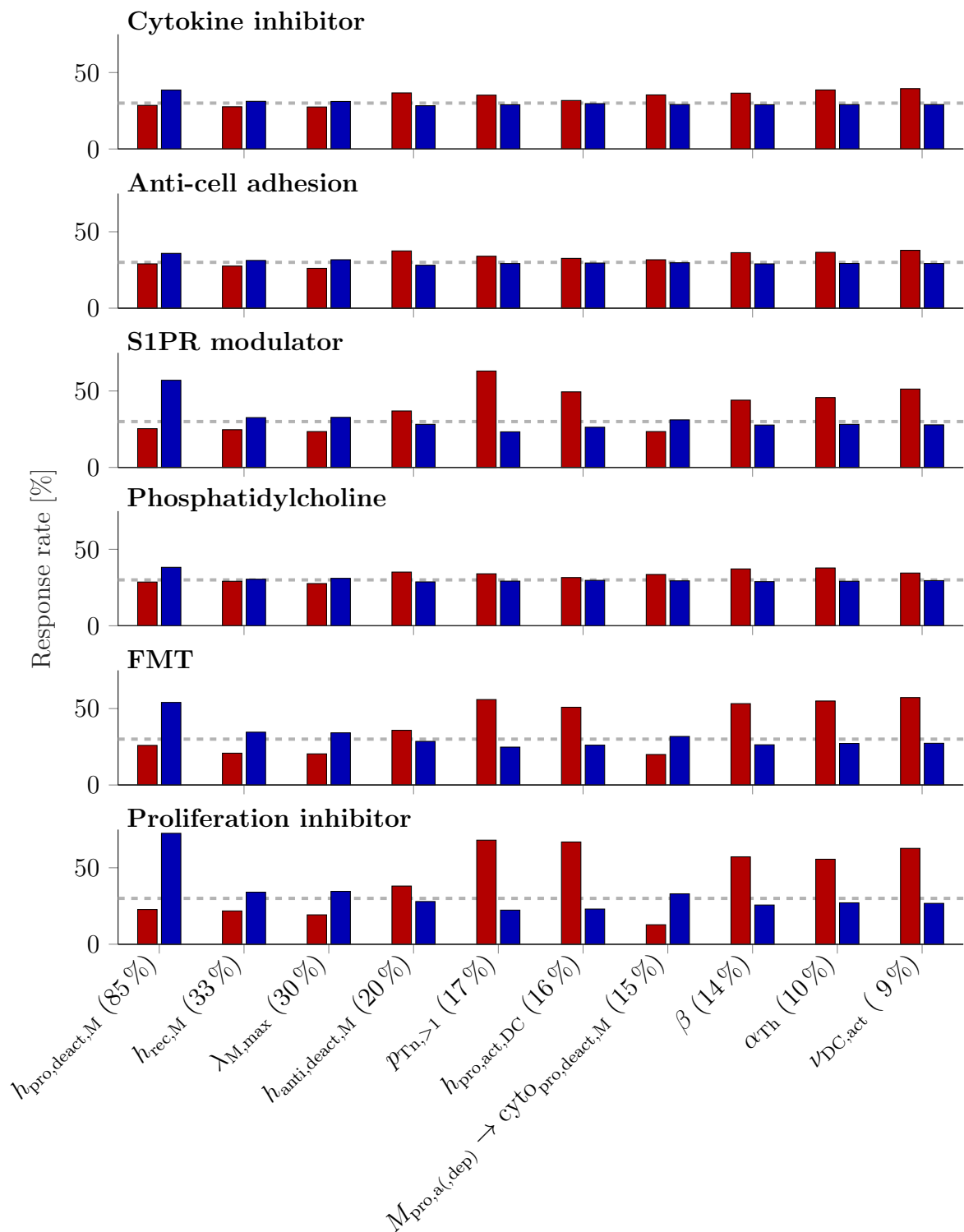


Figure 44: **Response rates by disease-relevant parameter changes.** Response rates to the different treatment effects, for subpopulations of the virtual IBD study population where specific parameters (on x-axis) are **disease-relevant** (red) or are **not disease-relevant** (blue). The grey dashed line indicates the response rate of 30% in the full virtual IBD study population. Shown are the ten parameters that were most frequently disease-relevant in the virtual IBD study population. The percentages in brackets of the x-axis labels give the frequencies of the respective parameters to be disease-relevant in the full virtual IBD study population.

factors, i.e. the disease-relevant parameter changes, on the response to the different treatment effects. If the red bar is higher than the blue bar, then the respective disease-relevant parameter change is correlated with better response, i.e. patients for which this parameter change is disease-relevant have better prospects of success to the respective treatment effect. If the blue bar is higher than the red bar, then the respective disease-relevant parameter change is correlated with worse response, i.e. patients for which this parameter change is disease-relevant have worse prospects of success to the respective treatment effect.

For most of the shown parameters (all except  $M_{\text{pro,a,(dep)}} \rightarrow \text{cyto}_{\text{pro,deact,M}}$ ), the influence of parameter change on response was the same for all implemented treatment effects. I.e. when disease was caused by  $h_{\text{anti,deact,M}}$ ,  $p_{\text{Tn,>1}}$ ,  $h_{\text{pro,act,DC}}$ ,  $\beta$ ,  $\alpha_{\text{Th}}$  or  $\nu_{\text{DC,act}}$ , the IBD patients generally had better prospects to be successfully treated than when the disease was caused by  $h_{\text{pro,deact,M}}$ ,  $h_{\text{rec,M}}$  or  $\lambda_{\text{M,max}}$ , independent of the chosen treatment effect. Based on the profiles of response rates we could distinguish two groups of treatment effects with similar profiles: For the first group, consisting of cytokine inhibitors, anti-cell adhesion treatment and orally administered phosphatidylcholine, the influence of all shown disease-relevant parameter changes on response rate was relatively small. For the second group, consisting of S1PR modulators, FMT and T cell proliferation inhibitions, the observed influence was considerably larger. These three treatment effects are those that directly concern T (helper) cells, and the observed influences of disease-relevant parameter changes on response rate are related to this treatment target: For IBD patients where parameter changes related to T cell activation or proliferation ( $\alpha_{\text{Th}}$ ,  $\beta$ ,  $p_{\text{Tn,>1}}$ ), or to activation of dendritic cells (which in turn activate T helper cells) ( $h_{\text{pro,act,DC}}$ ,  $\nu_{\text{DC,act}}$ ), were disease-relevant, the prospects of success to these treatment effects were much higher than for other IBD patients. In addition, the prospects of success were much higher if parameter changes highly related to macrophages ( $h_{\text{pro,deact,M}}$ ,  $M_{\text{pro,a,(dep)}} \rightarrow \text{cyto}_{\text{pro,deact,M}}$ ) were *not* among the disease-relevant parameter changes.

## 5.12 Comparison of the pre-treatment steady state between responders and non-responders

As the interpretation of state variables (i.e. mostly cellular concentrations) in the context of real-life IBD patients is much easier than for parameter values, we also compared the pre-treatment steady-state variable distributions between responders and non-responders, with the aim to find promising means to differentiate responders from non-responders to the different treatment effects before start of treatment.

For each treatment effect, we compared the distributions of all pre-treatment steady-state variables between responders and non-responders, as described previously in Section 4.5. Table 7 shows for each treatment effect the two-sample Kolmogorov-Smirnov test statistic  $D$ , testing for the difference between responders and non-responders, for the 5 most different state variables. For the simulation, for each treatment effect the treatment effect extent parameter  $\eta$  resulting in 30% response rate in the virtual IBD study population was assumed.

The shown steady-state variables are those that best distinguish responders from non-responders, i.e. that are the best predictors for treatment success (when only looking at single state variables as predictors). For cytokine inhibitors, anti-cell adhesion treatment and orally administered phosphatidylcholine, the state variables describing functional in-

Table 7: **Comparison of pre-treatment steady-state distributions between responders and non-responders.** Kolmogorov-Smirnov test statistic  $D$ , testing for the difference in pre-treatment steady-state distributions between responders and non-responders, for the 5 most different state variables, for each treatment effect. Treatment effect extent parameters  $\eta$  resulting in 30% response rate in the virtual IBD study population were assumed.  $D = 0$  indicates no difference, i.e. perfectly overlapping distributions;  $D = 1$  indicates maximal difference, i.e. completely separated distributions. The corresponding p-values are  $p < 0.001$  for all shown state variables.

Cytokine inhibitor		Anti-cell adhesion		S1PR modulator	
epi	0.46	epi	0.49	iTreg <sub>LP</sub>	0.65
mucus	0.46	mucus	0.49	Tem2Treg	0.61
$M_{P4}$	0.43	tissue	0.38	Th1	0.58
$M_{P3}$	0.40	$M_{P1,a}$	0.37	Th2	0.57
$M_{P1,a}$	0.39	$M_{P4}$	0.35	Th17	0.56
Phosphatidylcholine		FMT		Proliferation inhibitor	
epi	0.62	$M_{P1,a}$	0.54	$M_{P1,a}$	0.57
mucus	0.62	$M_{P4,a,dep}$	0.50	$M_{P4,a,dep}$	0.53
$M_{P4}$	0.40	$M_{P3,a,dep}$	0.47	$M_{P3,a,dep}$	0.49
$M_{P1,a}$	0.38	$M_{P4}$	0.43	$M_{P4}$	0.47
$M_{P3}$	0.38	sDC <sub>dep,LP</sub>	0.42	sDC <sub>dep,LP</sub>	0.47

tegrity of the epithelial barrier (epi, mucus and tissue) are most strongly correlated to response. In this case, higher integrity of the epithelial barrier before start of treatment correlates with better response. In addition to epithelial barrier state variables, only macrophages state variables were observed among the most different for those treatment effects, which is in accordance to the results of the previous comparison of parameter distributions between responders and non-responders, where parameters relating to macrophages were identified to be most different. For S1PR modulators, we observed regulatory T cells (fully differentiated and maturing), and T helper cells to be most correlated to the response, which is in accordance with its T-cell-related mechanism. For FMT and T cell proliferation inhibitors, we observed mainly macrophages (also pMHCII-depleted) and stimulatory dendritic cells to be most correlated to the response.

### 5.13 Prediction of individual patients' responsiveness based on the pre-treatment steady state

Although correlations of response to the different treatment effects with single pre-treatment steady-state variables could be detected, for better prediction of treatment success before start of treatment, a combination of pre-treatment steady-state variables has to be considered. We used, as described in Section 4.6, linear discriminant analysis (LDA) to find linear models to predict if an IBD individual will respond to a specific treatment effect.

Each dataset used in the LDA contained the same number of responders and non-responders to a specific treatment. Therefore, where possible, the treatment effect extent

Table 8: **Linear models to predict response based on pre-treatment steady state.** For each treatment effect, we give the best linear model including two features, for the full dataset (all features) and the measurable dataset (defined as in Section 4.6). Performance (Perf.) given as fraction correctly classified, as described in the text. The linear model is applied to an individual by substituting the values for the features (pre-treatment steady state variables); if the result is  $> 0$ , the individual is predicted to be a responder, otherwise it is predicted to be a non-responder. In some cases, adding the second feature did not improve the performance, only in combination with a third added feature. In this case, we show the best linear model including three features. For cytokine inhibitors, anti-cell adhesion treatment, S1PR modulators and orally administered phosphatidylcholine, treatment effect extent parameters  $\eta$  resulting in 50 % response rate in the virtual IBD study population were assumed. For FMT and T cell proliferation inhibitors, treatment effect extent parameters  $\eta$  resulting in 30 % response rate in the virtual IBD study population were assumed. For antibiotics, treatment effect extent parameter  $\eta = 0.9$ , resulting in 12 % response rate in the virtual IBD study population, was assumed. Features (pre-treatment steady-state variables) are coloured blue to improve readability.

Drug	Linear model	Perf.
All features		
Cytokine inhibitor	$-7.18 + 14.5 \cdot \text{epi} - 4.39 \cdot 10^{-9} \cdot M_{P1,tot}$	0.76
Anti-cell adhesion	$-8.28 + 16.5 \cdot \text{epi} - 4.63 \cdot 10^{-9} \cdot M_{P1,tot}$	0.77
S1PR modulator	$0.359 + 8.34 \cdot 10^{-8} \cdot T_{cm2Temreg_7} - 6.95 \cdot 10^{-9} \cdot M_{P1,a}$	0.79
Phosphatidylcholine	$-16.4 + 6.53 \cdot 10^{-9} \cdot M_{P1} + 27.2 \cdot \text{epi}$	0.84
FMT	$0.387 - 4.54 \cdot 10^{-9} \cdot M_{P1,a} + 3.37 \cdot 10^{-8} \cdot M_{P2,a,dep}$	0.82
Prol. inhibitor	$1.73 - 4.75 \cdot 10^{-9} \cdot M_{P1,a} - 1.48 \cdot 10^{-8} \cdot \text{Neut} - 2.70 \cdot 10^{-9} \cdot M_{P1,tot}$	0.77
Antibiotics	$-0.280 - 2.35 \cdot \text{Bact}_{Lu} + 1.51 \cdot \text{nutrients}$	0.81
Measurable features		
Cytokine inhibitor	$-6.42 + 12.0 \cdot \text{epi} - 1.64 \cdot 10^{-9} \cdot M_{pro}$	0.74
Anti-cell adhesion	$-6.85 + 13.1 \cdot \text{epi} - 2.08 \cdot 10^{-9} \cdot M_{pro}$	0.76
S1PR modulator	$-0.117 - 1.16 \cdot 10^{-9} \cdot M_{pro} + 1.62 \cdot 10^{-9} \cdot T_{cm_{pro}}$	0.69
Phosphatidylcholine	$-15.4 + 26.8 \cdot \text{epi} - 3.06 \cdot 10^{-7} \cdot \text{Bact}_{LP}$	0.84
FMT	$0.118 - 2.04 \cdot 10^{-9} \cdot M_{pro} + 1.90 \cdot 10^{-9} \cdot T_{cm_{pro}}$	0.73
Prol. inhibitor	$-0.944 + 4.69 \cdot 10^{-9} \cdot M_{anti} + 1.12 \cdot 10^{-9} \cdot T_{cm_{pro}}$	0.65
Antibiotics	$1.02 - 4.92 \cdot 10^{-7} \cdot \text{Bact}_{LP} - 1.90 \cdot 10^{-9} \cdot M_{pro}$	0.68

parameter  $\eta$  was chosen such that the response rate in the virtual IBD study population was 50 % (and consequently all virtual patients were included in the dataset); otherwise (for FMT and T cell proliferation inhibitors)  $\eta$  was chosen such that the response rate was 30 % (and some non-responders were randomly excluded from the dataset to obtain the same number of responders and non-responders); or (for antibiotics) the highest possible  $\eta$  value was chosen. Table 8 gives the best linear models including two features (either all pre-treatment steady-state variables or only measurable pre-treatment steady-state variables; see Section 4.6 for definition) to predict response for each of the treatment effects.

For cytokine inhibitors, anti-cell adhesion treatment and orally administered phosphatidylcholine, the best predictors were epithelial barrier functionality and pro-inflammatory macrophages, for phosphatidylcholine also bacteria in LP. For antibiotics, bacterial load in lumen and LP were the best predictors, as expected by the treatment mechanism. For S1PR modulators, FMT and T cell proliferation inhibitors, proliferating T cell concentrations were identified as good predictors, in addition pro- and anti-inflammatory macrophages.

We achieved performances of the linear models for the different treatment effects of 76-84 % for all features or 65-84 % using only measurable features. Compared to the random chance of correct identification of responders and non-responders (50 %), using the linear models provides a considerably better prediction of response. Note, however, that still 16-35 % of patients are wrongly predicted using the shown linear models.

#### 5.14 Correlation of treatment response with IBD type

To analyse if the IBD type, referring to the extent of the mucosal injury trigger required to elicit the disease (see Section 4.7), has an influence on the prospect of success for the different treatment effects, we looked at the correlation of the response rate with the IBD type. Remember that IBD type 1 meant that less mucosal injury ( $\text{epi} = \text{tissue} = 0.9$ ) was required to elicit the disease, whereas IBD type 10 meant that more mucosal injury ( $\text{epi} = \text{tissue} = 0$ ) was required.

Figure 45 shows the response rate over the IBD type for the different implemented treatment effects. We observed moderate correlations between IBD type and response rate for all treatment effects except phosphatidylcholine, with p-values (of Pearson correlations coefficients) of  $p < 0.05$  and response rate differences of 3 to 17 % between IBD types 1 and 10. Interestingly, for cytokine inhibitors, anti-cell adhesion treatment and S1PR modulators, the response rate is positively correlated with IBD type, whereas for FMT and proliferation inhibitors, it is negatively correlated.

#### 5.15 Prediction of (immediate) relapse post-treatment

As described above (Section 5.1) and shown in Figures 41 and 43, we calculated the rate of relapse after EOT, defined as response at EOT but not at post-treatment steady state. This relapse rate only describes relapse due to non-sufficient treatment effects, but not relapse due to additional stimuli (triggering new disease flares) and that it should not be mistaken for relapse under treatment (i.e. initial response to treatment but loss of response over time), which can not be described by our model.

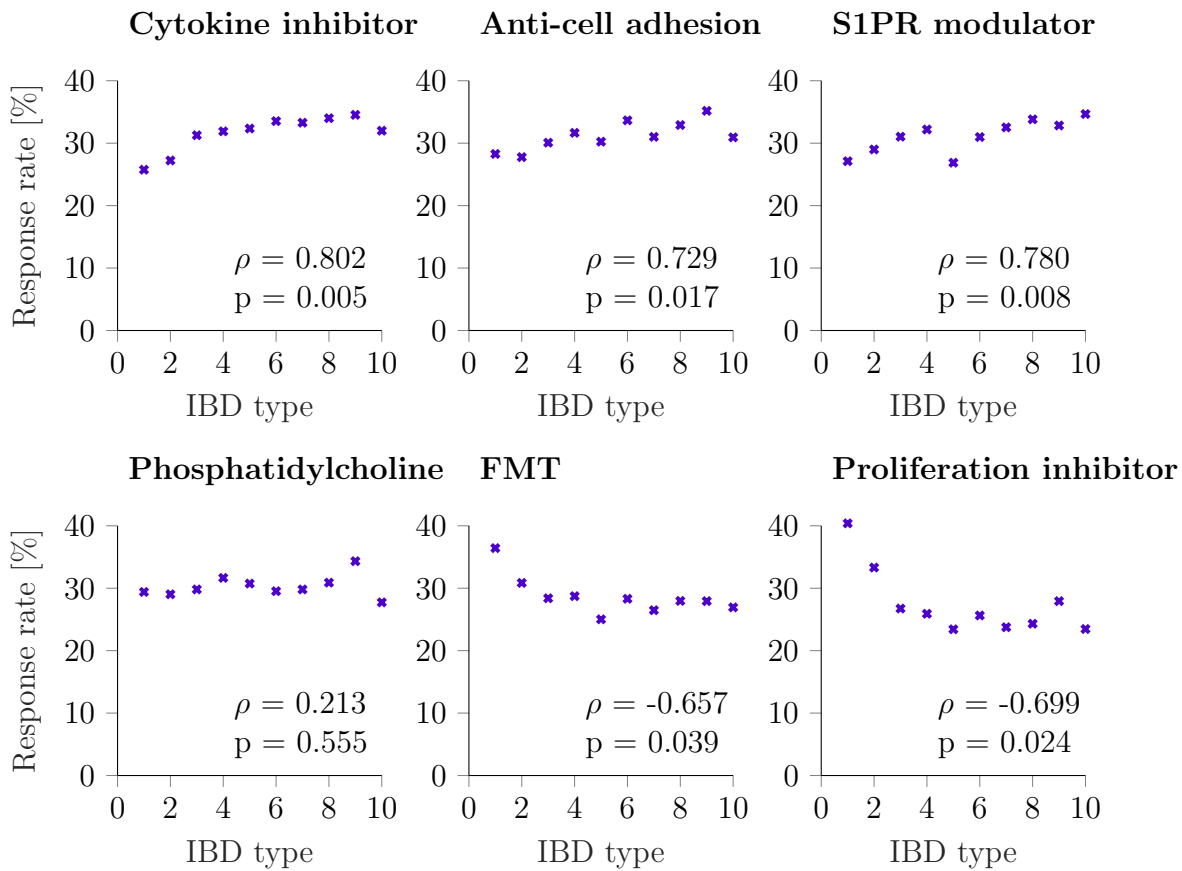


Figure 45: **Response rates per IBD type.** Response rates to the different treatment effects, for subpopulations of the virtual IBD study population with different IBD types. IBD type 1 means mucosal injury of extent  $\text{epi} = \text{tissue} = 0.9$  is required to elicit the disease; IBD type 10 means mucosal injury of extent  $\text{epi} = \text{tissue} = 0$  is required to elicit the disease; with uniform steps in between. Treatment effect extent parameters  $\eta$  resulting in 30 % response rate in the virtual IBD study population were assumed.  $\rho$  denotes the Pearson correlation coefficient between the IBD type (1-10) and the response rate.  $\rho = -1$  indicates perfect negative correlation;  $\rho = 1$  indicates perfect positive correlation,  $\rho = 0$  indicates no correlation. p denotes the corresponding p-value.



To support the decision if it is safe to stop treatment, a means to predict the probability of relapse after EOT would be very helpful. Therefore we applied LDA to find the best linear models to predict relapse after EOT for the different treatment effects. Analogous to the derivation of datasets for the prediction of response described in Section 5.13, each dataset contained the same number of responders that relapse and responders that do not relapse, with the same treatment effect extent parameters  $\eta$  as in Section 5.13 to obtain the largest possible datasets. Antibiotics were excluded from the analysis due to the very small dataset (among the virtual IBD study population only 8 individuals responded to antibiotics and showed relapse after EOT). In addition to separate models to predict relapse after EOT for the different treatment effects, we also applied LDA to a combination of all those datasets, to find the best overall linear model to predict relapse based on the EOT state, independent of the treatment effect.

Table 9 gives the best linear models including two features (either all EOT state variables or only measurable EOT state variables; see Section 4.6 for definition) to predict relapse for each of the treatment effects and independent of the treatment effect. For the overall model, adding the performance of the best linear model including two features was only very slightly better than for the best linear model including one feature; therefore we reported the best linear model including one feature.

We observed that the epithelial barrier functionality (epi) was the best single predictor of relapse after EOT for all treatment effects except S1PR modulators. Therefore it is not surprising that for the overall model, epi was the best predictor, achieving very high performance (82-96 %) for all treatment effects except S1PR modulators, with performance only slightly lower than using the best treatment effect-specific linear models. The differences in performance of linear models based on the full and measurable datasets were negligible, as epi (the best predictor) was available in both datasets. Interestingly, prediction of relapse after EOT with S1PR modulators was much worse than for the other treatment effects, with only moderate performance of 65 % correctly classified using the treatment effect-specific linear model. For this treatment effect, the epithelial barrier functionality had no predictive benefit at all, as the overall model based on epi only resulted in a performance of 50 % (i.e. not better than random classification).

In summary, we conclude that (except for S1PR modulators) the epithelial barrier integrity is a very good predictor of relapse after EOT, and therefore the disease scores assessing epithelial barrier integrity (such as CDEIS) are a useful means to support the decision of stop of treatment.

## 5.16 Conclusion

In this chapter, we described the implementation of different treatment effects into the systems biology model and showed how to use it to draw conclusions on the prediction of treatment success and relapse. We broke down different treatment effects currently used in treatment of IBD to a level that could easily be implemented in the model and simulated virtual clinical studies by simulating the virtual IBD study population's response to the different treatment effects. By providing a virtual analog of the frequently used disease score CDEIS, we could quantify the response rates of the virtual IBD study population to the different treatment effects. Analysing parameters and pre-treatment steady states of the responders and non-responders to the different treatment effects, we found which disease-causing factors and which phenotypes were influencing the prospects of success of

Table 9: **Linear models to predict (immediate) relapse based on EOT state.** For each treatment effect, we give the best linear model including two features, for the full dataset (all features) and the measurable dataset (defined as in Section 4.6). Performance (Perf.) given as fraction correctly classified, as described in the text. The last column gives the performance of the overall model applied to the different treatment effect datasets. The linear model is applied to an individual by substituting the values for the features (EOT state variables); if the result is  $> 0$ , the individual is predicted to relapse, otherwise it is predicted not to relapse. For cytokine inhibitors, anti-cell adhesion treatment, S1PR modulators and orally administered phosphatidylcholine, treatment effect extent parameters  $\eta$  resulting in 50 % response rate in the virtual IBD study population were assumed. For FMT and T cell proliferation inhibitors, treatment effect extent parameters  $\eta$  resulting in 30 % response rate in the virtual IBD study population were assumed. Antibiotics were excluded from the analysis due to the very small size of the dataset. Features (EOT state variables) are coloured blue to improve readability.

Drug	Linear model	Perf.	
All features			
Overall model	$15.5 - 16.9 \cdot \text{epi}$		0.80
Cytokine inhibitor	$74.5 - 86.4 \cdot \text{epi} + 9.64 \cdot 10^{-9} \cdot M_{\text{tot}}$	0.96	0.96
Anti-cell adhesion	$38.0 - 2.78 \cdot 10^{-6} \cdot \text{Neut}_{\text{apo}} - 42.7 \cdot \text{epi}$	0.91	0.89
S1PR modulator	$-0.591 + 2.43 \cdot 10^{-7} \cdot \text{tDC}_{\text{dep,LP}} + 7.72 \cdot 10^{-11} \cdot \text{Tem1}$	0.65	0.50
Phosphatidylcholine	$23.1 - 5.56 \cdot 10^{-7} \cdot \text{tDC}_{\text{LP}} - 23.9 \cdot \text{epi}$	0.90	0.85
FMT	$73.6 - 86.2 \cdot \text{epi} + 1.07 \cdot 10^{-8} \cdot M_{\text{tot}}$	0.96	0.95
Prol. inhibitor	$18.1 + 5.56 \cdot 10^{-7} \cdot \text{sDC}_{\text{LP}} - 20.9 \cdot \text{epi}$	0.85	0.82
Measurable features			
Overall model	$23.0 - 25.1 \cdot \text{epi}$		0.80
Cytokine inhibitor	$81.2 - 94.0 \cdot \text{epi} + 1.60 \cdot 10^{-8} \cdot M_{\text{pro}}$	0.96	0.96
Anti-cell adhesion	$36.8 - 43.3 \cdot \text{epi} + 1.95 \cdot 10^{-8} \cdot M_{\text{pro}}$	0.91	0.89
S1PR modulator	$-0.372 + 1.07 \cdot 10^{-11} \cdot \text{Tem} + 1.84 \cdot 10^{-12} \cdot \text{iTreg}_{\text{tot,LP}}$	0.65	0.50
Phosphatidylcholine	$34.6 - 38.7 \cdot \text{epi} + 7.91 \cdot 10^{-9} \cdot M_{\text{tot}}$	0.89	0.85
FMT	$76.0 - 88.8 \cdot \text{epi} + 1.78 \cdot 10^{-8} \cdot M_{\text{pro}}$	0.96	0.95
Prol. inhibitor	$18.1 - 20.1 \cdot \text{epi} + 1.93 \cdot 10^{-8} \cdot \text{Th1}_{\text{tot}}$	0.84	0.82

the different treatment effects in individual virtual IBD patients. In addition, we found that the relative intactness of the epithelial barrier was a good predictor to predict the virtual patients' relapse after EOT (except for the treatment effect of S1PR modulators).

Naturally, all assumptions and simplifications made in the development of the model also limit the predictive capability of the response to treatment. In addition, we made further simplifications in the implementation of the treatments themselves on different levels: (i) We implemented single treatment effects, although often treatments/drugs cause and work via a combination of several different treatment effects. (ii) Each treatment effect was quantified using a single treatment effect extent parameter that described the inhibition of several model reactions or parameters (e.g. for anti-cell adhesion treatment, inflow rates of different cell types), thereby assuming the same extent of inhibition. (iii) The mechanisms of action of the different drugs were translated to the cellular level that our systems biology model focuses on, i.e. implementation of drugs targeting sub-cellular processes such as specific signalling cascades or receptors was done on the cellular level, by implementing the effect of the sub-cellular change on the cellular level. Especially in the case of cytokine inhibitors, the simultaneous and equal reduction of all pro-inflammatory cytokines is a relatively crude simplification. This can already be seen by the fact that several different drug classes (e.g. monoclonal antibodies targeting TNF- $\alpha$ , IL-23 inhibitors and JAK inhibitors) were pooled into the same implementation. This simplification is due to the—in our opinion—insufficient quantitative knowledge on specific cytokine effects on the cellular level, which caused us to implement cytokine effects on the less detailed level described in Section 2.14, using weighted sums of cytokine-producing cell types specific for different cytokine-influenced processes. In order to implement more detailed treatment mechanisms of specific cytokine inhibitors, more specific quantitative knowledge on the respective inhibited cytokine(s) would be needed, regarding the cytokine's production from different cell types and its influence on the cytokine-influenced processes, especially with respect to the proportionate effects with regard to other cytokines influencing this process. (iv) Lastly, we implemented the treatment effects as constant effects over the treatment duration, neglecting the influence of the drugs' PK. In addition, our model does not account for side effects, which are, of course, important limitations of every drug treatment.

The structure of our model, however, allows for easy extension, implementation of more detail, and integration of drug PK. A user aiming to predict or simulate the effects of a specific drug in the virtual population of IBD patients would have to make sure enough detail with respect to the targeted process is included in the model, implement all treatment effects caused by the drugs, and link a PK model, where the treatment effect extent parameter has to be written as a function of the drug concentration. Then the user can easily follow the steps described in this chapter to simulate the response of the virtual IBD study population to the drug, to compare responders and non-responders with regard to underlying disease-causing factors or pre-treatment phenotype, and to derive predictors for response and relapse.



## 6 Model-guided choice of second-line treatments and combination therapies

In Section 5.13 we gave linear models to predict the success of different treatment mechanisms in individual virtual patients. Our prediction accuracy was, however, only 65-84 %, i.e. a considerable percentage of our virtual IBD patients does not respond to their initial treatment. In addition, it remains questionable if the required predictors for our linear models would be available for all patients in a clinical setting. Therefore, another main task in treatment of IBD patients is the selection of a second-line treatment in non-responders to the first-line treatment (termed “first-line non-responders” in the following). In addition, combination therapies may increase response rates to treatment.

### 6.1 Correlations between responsiveness to different treatments

Using our virtual IBD study population and their response to the implemented treatment effects, we calculated the response rates to second-line treatments in first-line non-responders for all combinations of first- and second-line treatments. As, of course, the response rate mainly depends on the treatment effect extent parameter  $\eta$ , we chose  $\eta$  for each treatment effect to result in the same response rate of 30 % or 50 % in the full virtual IBD study population (as antibiotics and T cell proliferation inhibitors resulted in response rates  $< 30\%$  or  $< 50\%$ , respectively, those treatment effects were not included in the respective analyses). Note that our simulations do not account for PK-related non-response such as too low dosing or anti-drug antibodies, but only refer to the molecular treatment mechanisms.

The resulting response rates to second-line treatments in first-line non-responders are shown in Figures 46 and 47 for  $\eta$  values resulting in response rates of 30 % and 50 % in the virtual IBD study population, respectively. For the analysis using  $\eta$  resulting in 30 % (or 50 %) response rate, the response rate to the second-line treatment would be 30 % (or 50 %, respectively) if the response rates were completely independent, and 0 % if the response rates were completely dependent (i.e. if the individual does not respond to the first-line treatment, it also doesn't respond to the second-line treatment). Note that the response rates in the virtual IBD study population are not exactly 30/50 %, but only correct to one decimal place, so that the resulting matrices (Figures 46 and 47) are not completely symmetrical.

Figures 47 and 46 show that the response rates to the second-line treatments differ substantially between the treatment effects. Hence the knowledge about the non-response of a patient to a first-line treatment is informative for choosing the best second-line treatment. If first-line treatment is cytokine inhibitors, anti-cell adhesion treatment or orally administered phosphatidylcholine, the best second-line treatment is an S1PR modulator, resulting in response rates in the population of first-line non-responders close to the re-

30 % response rate  
in the virtual IBD  
study population

**Second-line treatment**

		Second-line treatment					
		cytokine inhibitor	anti-cell adhesion	phosphatidylcholine	S1PR modulator	FMT	proliferation inhibitor
First-line treatment	cytokine inhibitor	0	6.7	9	25.1	16	20.5
	anti-cell adhesion	6.7	0	11.2	28.3	17.1	19.1
	phosphatidylcholine	9	11.2	0	26.1	18.4	21.9
	S1PR modulator	25.1	28.3	26.2	0	18.8	21.6
	FMT	16	17.1	18.4	18.8	0	11.9
	proliferation inhibitor	20.5	19.2	21.9	21.5	11.9	0

Figure 46: **Response rates to second-line treatments in first-line non-responders, assuming  $\eta$  resulting in 30 % response rate in the virtual IBD study population.** Note that the matrix is not completely symmetrical, as the response rates in the virtual IBD study population are not exactly 30 %, but only correct to one decimal place.

response rate of 30 % or 50 % in the virtual IBD population, indicating that the response rates are almost independent. If first-line treatment is FMT or proliferation inhibitors, the best second-line treatments are cytokine inhibitors, anti-cell adhesion treatment, orally administered phosphatidylcholine or S1PR modulators; however, the resulting response rates in the population of first-line non-responders are lower. The response to cytokine inhibitors and anti-cell adhesion treatment was observed to be highly correlated, resulting in very poor response rates when one of them was used as second-line treatment in first-line non-responders to the other.

Comparing those results to our observations from the comparison of parameter and pre-treatment steady-state distributions between responders and non-responders to the different treatment effects (Sections 5.10 and 5.12), we infer: Those treatment effects that showed the same parameters or pre-treatment steady state variables to be important in distinguishing responders from non-responders, also show high correlation here, emphasizing that those treatment effects work well in the same subpopulations of our virtual IBD study population (and therefore using one of them as second-line treatment in first-line non-responders to the other is not a good choice).

50 % response rate  
in the virtual IBD  
study population

Second-line treatment

First-line treatment	Second-line treatment				
	cytokine inhibition	anti-cell adhesion	phosphatidylcholine	S1PR modulator	FMT
cytokine inhibition	0	12.3	16.8	42.6	31.9
anti-cell adhesion	12.4	0	19.1	46.2	32.7
phosphatidylcholine	16.8	19.1	0	44.6	36
S1PR modulator	42.6	46.2	44.7	0	26.9
FMT	31.9	32.6	36	26.8	0

Figure 47: **Response rates to second-line treatments in first-line non-responders, assuming  $\eta$  resulting in 50 % response rate in the virtual IBD study population.** Note that the matrix is not completely symmetrical, as the response rates in the virtual IBD study population are not exactly 50%, but only correct to one decimal place.

## 6.2 Combination treatments

When single treatments are not successful (e.g. as the dose can not be increased due to side effects, or the mechanism of effect is limited in itself; as can be seen in Figure 41, for some treatment effects the treatment effect extent parameter  $\eta$  can not be increased such that all patients respond), then a combination treatment of two different treatment effects could be an option. Of course, using a combination of two treatments naturally also comes with higher risks for side effects and higher costs. Therefore it is important to carefully ponder the benefits of a combination treatment versus a single treatment, or sequential trying of different single treatments, e.g. as first- and second-line treatments (see previous Section 6.1). For sake of illustration, we simulated combinations of cytokine inhibitors with other treatment effects, assuming that all treatment effects were similarly effective on their own, i.e. assuming treatment effect extent parameters  $\eta$  resulting in 30 % response rates in the virtual IBD study population for each treatment effect on its own (so that all treatment effects except antibiotics could be included in the analysis).

Figure 48 shows the response rates to the different combination treatments (cytokine inhibitors with other treatment effects; red bars) in comparison to the (total) response rates when using the same treatment effects as second-line treatments for non-responders to the cytokine inhibitor (blue bars). The benefit of the combination treatment compared to both treatments sequentially (as first- and second-line treatment) is quantified by the difference of the red bar to the blue bar. This difference is composed of two fractions of patients: (i) those that respond to the combination treatment, but neither to the first- nor second-line treatment alone (yellow bar); those are the patients that benefit

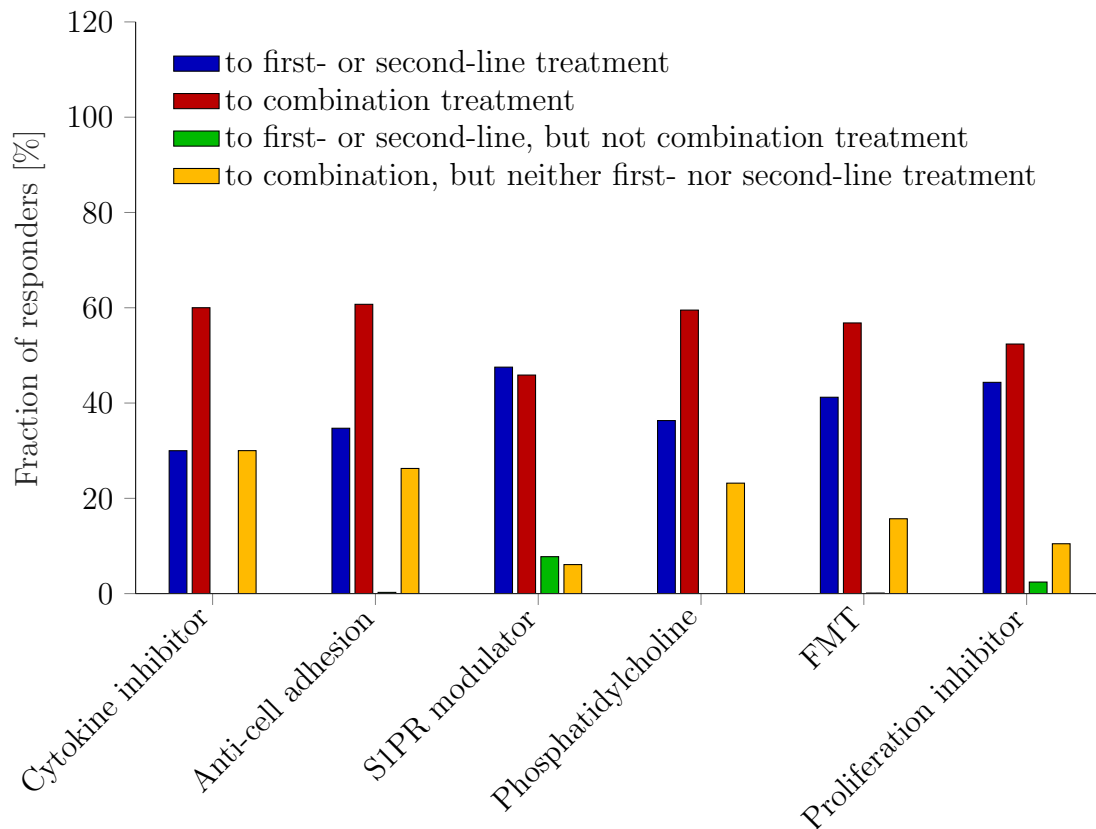


Figure 48: **Response rates to combinations of cytokine inhibitors with other treatment effects.** The blue bars show the fractions of patients (i.e. response rates) responding to first-line treatment (cytokine inhibitor) or second-line treatment (indicated on x-axis) or both. The red bars show the fractions of patients (i.e. response rates) responding to the simultaneous combination treatment of both treatment effects (cytokine inhibitor and treatment effect indicated on x-axis). The green bars show the fractions of patients responding to the first- or second-line treatment, but not to the combination treatment. The yellow bars show the fractions of patients responding to the combination treatment, but neither to the first- nor second-line treatment alone. All fractions are given in % of the virtual IBD study population. Treatment effect extent parameters  $\eta$  resulting in 30 % response rate in the virtual IBD study population were assumed.



from the combination treatment in comparison to sequential trying of first- and second-line treatment. (ii) However, for some combinations of treatments, there are patients that respond to the first- or second-line treatment alone, but do not respond to the combination treatment (green bar). Hence, the benefit of the combination treatment is highest if the yellow bar is high and the green bar is low.

Especially for the combination of the cytokine inhibitor with another cytokine inhibitor, but also with anti-cell adhesion treatment, orally administered phosphatidylcholine or FMT, our model simulations predict a high benefit of the combination treatment, as large proportions of the non-responders to the sequential treatments (i.e. neither to first- nor second-line treatment) respond to the combination treatment (see yellow bar). In contrast, the model predicted the combination treatment of the cytokine inhibitor with an S1PR modulator to be less successful than using the S1PR modulator as second-line treatment for non-responders to the cytokine inhibitor. The main reason is that a large proportion of patients that respond to the cytokine inhibitor (25.9%) do not respond to the combination of cytokine inhibitor plus S1PR modulator (see green bar), while S1PR modulators are quite effective as second-line treatment (see blue bar). This effect was also observed to a lower extent for the combination treatment of the cytokine inhibitor with a T cell proliferation inhibitor.

Overall, we observed that if two treatments are successful in the same subpopulation of patients (e.g. cytokine inhibitor and anti-cell adhesion treatment), our analysis suggests to use them in a combination therapy, whereas if two treatments are successful in different subpopulations of patients (e.g. cytokine inhibitor and S1PR modulator), our analysis suggests to rather start with one of them and switch to the other as second-line treatment.



---

## 7 Discussion

### 7.1 Summary

We presented in this thesis a novel systems biology model in the context of IBD that can be viewed a comprehensive summary of available knowledge on the mucosal immune response. We used this model to generate a virtual population representing healthy individuals and IBD patients. Importantly, we defined IBD via its phenotype, i.e. the response of the patient's immune system to a potential trigger, rather than in terms of hypothesised changes of a number of parameter values. This approach allowed us to study potential IBD predispositions in an unbiased way. We implemented different treatment effects into the model, allowing for analysis of characteristics of individual drug therapy. Lastly, we illustrated how the model can be used to decide for alternative treatments with best prospects in the case of non-response, and to identify promising combination therapies.

### 7.2 Setting our work in context

A few systems biology models for IBD have been previously published (e.g. [24–28, 34]), as critically discussed in Section 2.1, including the reasons why we decided to develop a novel systems biology model that we assess more appropriate as underlying model for the presented analyses. The unique feature of our model, setting it apart from all previously published systems biology models in the context of IBD known to us ([24–28, 34]), is that it was developed to describe the *healthy* mucosal immune response, without including any data from IBD patients. Also in the generation of the virtual population from the model, by including inter-individual variability in all model parameters, we did not need to rely on any prior knowledge on IBD development (such as knowledge on parameters likely to differ between healthy and IBD). Only in the step to identify IBD patients in the virtual population, we obviously used information on IBD. Through this, we ensured to have included the most important processes of the mucosal immune response, as the healthy immune response can be adequately simulated, and obtained an “unbiased” IBD population covering the space of possible parameter combinations that (based on the underlying model) could lead to IBD.

*Comparison to the model by Rogers et al. (2020).* After research for this thesis was completed (February 2020), Rogers et al. (2020) [28, 34] published a systems biology model of IBD that also aimed at analysing treatment effects using a virtual IBD population, but with differences both in the underlying model structure describing the mucosal immune response and the generation of the virtual population of healthy and IBD individuals. In contrast to the previously published models discussed in Section 2.1, the model by Rogers et al. [28, 34] was, in our opinion, well suitable for the analyses they present (which highly overlap with the analyses presented in this thesis).

Their approach was in many regards similar to our approach, developing a structural model including different cell types and processes of the mucosal immune response, which was then used to generate a virtual population of healthy and IBD individuals that were each defined by a set of parameters. In summary, Rogers et al. developed a systems biology model comprising 334 parameters and 116 reactions (compared to 79 parameters and 133 reactions in our model). Based on steady-state protein concentrations of healthy and diseased subjects, an ensemble of plausible parameter sets was generated. Only 24 pre-defined parameters were allowed to differ between healthy, CD and UC patients. To compare simulations to clinical study results, the ensemble of parameter sets was further stratified based on matching of C-reactive protein (CRP) and fecal calprotectin (FCP) concentrations. Using the generated virtual populations, they simulated the response to IL-17 inhibition, identified important parameters by performing a sensitivity analysis of CRP and FCP, simulated treatments of CD patients with anti-TNF- $\alpha$ , anti-IL-12p40, anti-IL-23 and anti-IL-6 treatment and a combination of anti-TNF- $\alpha$  and anti-IL-12p40, and identified differences in baseline species (i.e. pre-treatment steady states) and parameters between responders and non-responders.

We would like, however, to point out some significant differences between the two approaches: In contrast to our decision to focus on the cellular level, with many different states of each cell type, Rogers et al. focused more on specific cytokines, which they modelled as explicit state variables. As pointed out previously, we did not restrict the differences between healthy and IBD individuals by including prior knowledge on parameter differences, whereas Rogers et al. only allowed 24 parameters to be different between healthy and IBD. The derivation of parameters differed, as we derived the model parameters from literature, carefully evaluating the resulting model behaviour on the level of single cell types and processes to ensure that each process or cell type itself was appropriately described by the model, and then sampled the parameter sets of the virtual population based on those reference parameters. In contrast, Rogers et al. generated the parameter sets of the virtual population by setting wide limits for each parameter and selecting plausible parameter sets by random sampling of parameters within the limits and comparison of the simulation output with experimental steady-state protein data. For simulation of treatment, Rogers et al. implemented specific drug PK models and binding reactions to the target cytokines, whereas we focused on generalised treatment mechanisms implemented by constant treatment effects. In our opinion, their approach includes two critical limitations, (i) the usage of only steady-state concentrations to estimate model parameters, but subsequent interpretation of the model simulations in a time-resolved manner, and (ii) the very high number of 334 model parameters compared to the very small virtual CD population size of 357 individuals, which, in our opinion, can not be sufficient to appropriately cover the possible parameter space. Interestingly, and in contrast to our findings, Rogers et al. did not observe different steady states of the model, i.e. after stop of treatment, all subjects returned to the pre-treatment steady state (according to Figures 3, 4, 5 and 7 in [34]).

### 7.3 Limitations

As every (mathematical) model describing a complex biological process, our systems biology model is based on simplifications and thus has limitations, which naturally also affect its predictive capabilities. Although the complexity of the presented model is already

considerably high (133 reactions, 47 state variables), it is of course far from representing the full complexity of the human mucosal immune system. In Section 2.19 a detailed description of the limitations of the model is given. Including additional processes, cell types or reactions in the model would aim to increase its predictive capacity, but at the same time would require additional data needed for parameterisation (which are often not available in literature).

Naturally, the generated virtual IBD population is highly dependent on the underlying systems biology model of the mucosal immune response and all included assumptions and simplifications. Therefore, all conclusions drawn from the analysis of the virtual IBD population are conditional on the accuracy of the systems biology model (see also Section 4.8).

Those limitations consequently also apply to the simulations of the virtual IBD population's response to the different treatment effects (see also Section 5.16).

In summary, results from our model simulations are intended rather qualitative, e.g. finding parameters with high potential for IBD predispositions, identifying cell concentrations that could be used as predictors for responsiveness, or testing hypotheses on novel drug targets.

## 7.4 Main findings

The analysis of the virtual IBD population resulted in a number of important findings with regard to IBD predispositions and treatment of IBD.

We were able to qualitatively describe the mucosal immune response to the different inflammatory stimuli of pathogenic infection and mucosal injury. In addition, we were able to generate a virtual population that contained both healthy and IBD patients, by simply adding inter-individual variability to all parameters, without need for inclusion of any prior knowledge on parameter differences between healthy and IBD. Therefore, we conclude that the implemented processes suffice to qualitatively describe the mucosal immune response to different inflammatory stimuli and the occurrence of IBD as result of inter-individual variability.

The population of virtual IBD individuals showed a high heterogeneity (regarding both the time course of cell concentrations and the predispositions), which reflects the heterogeneity known from clinical studies of IBD. Throughout the enormous diversity of predispositions, we found that IBD can result from both a small number of large parameter changes or a higher number of small parameter changes.

When analysing the IBD predispositions, which are reflected by parameters in the model, one type of parameters seemed to play a dominant role: Hill factors (for recruitment or activation of macrophages, dendritic cells or neutrophils) were most often among the identified disease-relevant parameters. Although a direct biological interpretation of those Hill factors is difficult, they describe the sensitivity of the respective activation or recruitment rates on changes of cytokine concentrations and thereby highly influence the switch of the model system between the asymptomatic and the inflamed steady state.

Using the virtual IBD population generated with the systems biology model and different implemented treatment effects, we were able to identify predictors for responsiveness (e.g. pro-inflammatory macrophages and epithelial destruction for cytokine inhibitors). In addition, we could provide possible explanations for the high inter-individual differences in treatment responsiveness via identification of parameter differences between responders

and non-responders. This does, however, not imply that they all relate to differences in real IBD patients, but they can give a good overview of possible reasons, and be a good starting point for further analyses in clinical studies via biomarkers.

The model allowed for an analysis of sequential (first- and second-line) treatments and combination treatments. We showed which second-line treatments are most promising in non-responders to the different treatments, and which treatment mechanisms are most promising for combination therapies with cytokine inhibitors. Interestingly, we found that good choices of treatments in a sequential therapy are less promising when used as combination treatments.

## 7.5 Further research questions

Although the presented systems biology model is already quite complex, it still includes many simplifications and assumptions, focusing only on specific parts of the mucosal immune response (regarding processes, spatial location and detail, e.g. cell-level as compared to molecular level), naturally limiting the conclusions drawn from model simulations. To also quantitatively improve the accuracy of model predictions and to expand the predictions to a broader context, the level of detail in the systems biology model could be improved. Of note, including more complexity, especially when additional assumptions have to be taken, also increases the risk for inaccuracies.

It would be very interesting to use the model to identify differences in predispositions for CD and UC to see if the differences in risk factors between CD and UC described in literature can be reproduced by the systems biology model. For this, more detail regarding different cytokines and spatial location of the disease would be required in the model, so that the virtual IBD population could be divided into a CD population and a UC population.

With regard to predictions in the context of clinical drug development, the specific effects of specific drugs can be implemented. Then, the systems biology model can be combined with a drug-specific PK model, using the time-dependent drug concentration predicted by the PK model to calculate the treatment effect extent, e.g. via a binding reaction to the target. This will allow for the simulation of time-resolved treatment effects (as opposed to the constant treatment effects assumed in our simulations), enabling also analyses of the influence of PK parameters on the treatment response (e.g. increased clearance dependent on the level of inflammation or anti-drug antibodies emerging over time), and quantitative comparison of PK-related and mechanism-related reasons for the missing treatment success in non-responders to the respective treatment. It requires, however, additional data on the dependency of the treatment effect on the drug concentration, e.g. parameter values of the binding reaction, and reliable prediction of the drug concentrations in the respective tissue (not only in blood, i.e. the central compartment of most classical PK models).

Another improvement of the model with regard to predictions for clinical drug development would be the inclusion of relevant biomarkers used in clinical studies of IBD, e.g. fecal calprotectin (FCP). FCP is a highly abundant protein in neutrophils, which is probably released from the neutrophils due to cell disruption and death, i.e. it is assumed to be correlated with the amount of neutrophils migrating from the LP into the intestinal lumen via the disrupted epithelial barrier [182]. For the implementation of FCP into the systems biology model we therefore suggest to simulate the FCP concentrations based on

the neutrophil concentration in LP and the barrier integrity.

## 7.6 Potential applications of the novel systems biology model

In addition to the results described in this thesis, we are confident that the presented systems biology model, and the virtual IBD population generated with it, can be applied in multiple more occasions to gain additional insights into the disease and to support development and optimisation of treatment of IBD.

The presented systems biology model is easily applicable to test new hypotheses on disease development: To analyse the effect of changes (e.g. inhibition or increase) of single parameters or small combinations of parameters on the healthy mucosal immune response, those can easily be changed based on the reference parameters and the resulting time course, also with regard to specific cell types of interest, can be compared to the reference individual's time course. To test a hypothesised risk factor, we suggest to generate an additional virtual population by applying inter-individual variability to all parameters (as described in Section 4.1), and adding the risk factor (e.g. inhibition of a specific parameter) to all individuals. In a subsequent comparison of the fraction of IBD individuals with the original virtual population, it can easily be evaluated if the population with the hypothesised risk factor tends to more development of IBD.

We recommend to use our systems biology model for an easy and very cheap pre-evaluation of potential new treatment targets: For that, the proposed drug effect can be implemented into the model so that the response of the virtual IBD study population can be simulated. Through this, the user can get valuable information on the potential efficacy of the proposed treatment mechanism, e.g. how strong the inhibition of the targeted parameter or process has to be for a reasonable response rate.

In summary, we believe that the presented systems biology model of the mucosal immune response and analyses of the generated virtual IBD population are an important step towards better understanding IBD and the different treatment options.





## Abbreviations

<i>S. epidermidis</i>	<i>Staphylococcus epidermidis</i>
<i>S. Typhimurium</i>	<i>Salmonella</i> Typhimurium
AMP	antimicrobial peptide
APC	antigen-presenting cell
BCR	B cell receptor
bl	blood
BM	bone marrow
BrdU	bromodeoxyuridine
CD	Crohn's disease
CDEIS	Crohn's disease endoscopic index of severity
CRP	C-reactive protein
DSS	dextran sodium sulfate
ECM	extracellular matrix
EOT	end-of-treatment
FCP	fecal calprotectin
FMT	faecal microbial transplant
GALT	gut-associated lymphoid tissue
GM-CSF	granulocyte-macrophage colony-stimulating factor
IBD	inflammatory bowel disease
IFN	interferon
IL	interleukin
IR	input-response
iTreg	induced regulatory T cell
JAK	Janus kinase
LDA	linear discriminant analysis
LN	lymph node
LP	lamina propria
LSA	local sensitivity analysis
LT	lymphotoxin
MMP	matrix metalloproteinase
MOI	multiplicity of infection
NEC	neutrophil equivalent concentration

<b>NSAID</b>	non-steroidal anti-inflammatory drug
<b>nTreg</b>	natural regulatory T cell
<b>ODE</b>	ordinary differential equation
<b>PK</b>	pharmacokinetics
<b>QSS</b>	quasi-steady state
<b>ROS</b>	reactive oxygen species
<b>S1P</b>	sphingosine-1-phosphate
<b>S1PR1</b>	sphingosine-1-phosphate receptor type 1
<b>SIgA</b>	secretory immunoglobulin A
<b>SPM</b>	specialised pro-resolving mediators
<b>TCR</b>	T cell receptor
<b>TGF</b>	transforming growth factor
<b>Th</b>	T helper cell
<b>TNF</b>	tumour necrosis factor
<b>Treg</b>	regulatory T cell
<b>UC</b>	Ulcerative colitis

## List of Figures

1	Simplified model scheme . . . . .	11
2	Barrier dynamics . . . . .	17
3	Critical neutrophil equivalent concentration . . . . .	20
4	Neutrophil submodel . . . . .	21
5	Neutrophil dynamics . . . . .	24
6	Macrophage submodel . . . . .	26
7	Macrophage submodel fit . . . . .	29
8	Macrophage populations in inflammation . . . . .	31
9	Macrophage dynamics . . . . .	32
10	Dendritic cell submodel . . . . .	35
11	Dendritic cell dynamics . . . . .	36
12	Submodel of naive T cell stimulation, proliferation and differentiation . . .	44
13	Dynamics of proliferating T cells . . . . .	47
14	Submodel of T cell proliferation and differentiation . . . . .	49
15	Regulatory T cell dynamics . . . . .	53
16	Dynamics of pMHCII-depleted APCs . . . . .	57
17	Cytokine production dynamics . . . . .	60
18	Time course of inflammation . . . . .	67
19	Time course of infection with generic extracellular pathogen for different initial loads . . . . .	69
20	Time course of <i>S. Typhimurium</i> infection for different initial loads . . . . .	72
21	Infected macrophages by <i>S. Typhimurium</i> and their control by Th1 over time . . . . .	73
22	Time course of mucosal injury . . . . .	76
23	Summary of the modelling approach . . . . .	78
24	Sensitivity coefficients over time for different outputs . . . . .	85
25	IR indices for different outputs . . . . .	88
26	Time course of mucosal injury in the different classes . . . . .	94
27	Pre-trigger and post-trigger steady-state concentrations in healthy and IBD individuals . . . . .	95
28	Post-trigger steady state concentrations in healthy individuals and IBD patients, in comparison with literature data . . . . .	96
29	Comparison of parameter distributions between healthy individuals and IBD patients . . . . .	97
30	Distribution of the number of disease-relevant parameter changes per IBD individual . . . . .	99
31	Most frequent disease-relevant parameter changes . . . . .	99
32	Extent of disease-relevant parameter change versus number of disease- relevant parameter changes . . . . .	100

33	Comparison of pre-trigger steady state distributions between healthy and IBD individuals . . . . .	102
34	Performance of linear models dependent on number of included features . .	104
35	Exemplary time courses in response to different mucosal injury extents . .	108
36	Distribution of IBD types . . . . .	109
37	Time course of mucosal injury for different IBD types . . . . .	109
38	CDEIS distribution among IBD types . . . . .	110
39	Simplified model scheme including targets of treatment effects . . . . .	116
40	Exemplary virtual patient time courses of treatment with cytokine inhibitor or anti-cell adhesion treatment . . . . .	117
41	Response rate over treatment effect extent parameter $\eta$ for different treatment effects . . . . .	118
42	Response rate over treatment effect extent parameters $\eta$ for S1PR modulators	119
43	Relapse rates for different treatment effects . . . . .	120
44	Response rates by disease-relevant parameter changes . . . . .	125
45	Response rates per IBD type . . . . .	130
46	Response rates to second-line treatments in first-line non-responders, assuming $\eta$ resulting in 30 % response rate in the virtual IBD study population	136
47	Response rates to second-line treatments in first-line non-responders, assuming $\eta$ resulting in 50 % response rate in the virtual IBD study population	137
48	Response rates to combinations of cytokine inhibitors with other treatment effects . . . . .	138
49	Full model scheme . . . . .	179
50	Time course of T cell knockout . . . . .	182
51	Time course of T helper cell knockout . . . . .	183
52	Time course of regulatory T cell cell knockout . . . . .	184
53	Time course of commensal bacteria knockout . . . . .	185
54	Time course of neutrophil knockout . . . . .	186
55	Influence of Hill factor $h_{\text{pro,deact,M}}$ on macrophage deactivation rate dependent on pro-inflammatory cytokine concentration $\text{cyto}_{\text{pro,deact,M}}$ . . . . .	189
56	Comparison of inflamed state distributions between IBD types . . . . .	192
57	Comparison of parameter distributions between IBD types . . . . .	193

---

## List of Tables

1	Macrophage parameter estimates . . . . .	28
2	Cytokine production weights . . . . .	59
3	SPM production weights . . . . .	63
4	Healthy steady state: comparison of simulated and literature values . . . .	66
5	Linear models . . . . .	105
6	Comparison of parameter distributions between responders and non-responders	124
7	Comparison of pre-treatment steady-state distributions between responders and non-responders . . . . .	127
8	Linear models to predict response based on pre-treatment steady state . .	128
9	Linear models to predict (immediate) relapse based on EOT state . . . . .	132
10	Parameter values . . . . .	177
11	Centroids for classification of virtual individuals . . . . .	187
12	Performance of classification methods . . . . .	191
13	CDEIS calculation . . . . .	194



---

## References

- [1] Daniel C Baumgart and Simon R Carding. Inflammatory bowel disease: cause and immunobiology. *The Lancet*, 369:1627–1640, 2007.
- [2] Siew C. Ng, Hai Yun Shi, Nima Hamidi, Fox E. Underwood, Whitney Tang, Eric I. Benchimol, Remo Panaccione, Subrata Ghosh, Justin C.Y. Wu, Francis K.L. Chan, Joseph J.Y. Sung, and Gilaad G. Kaplan. Worldwide incidence and prevalence of inflammatory bowel disease in the 21st century: a systematic review of population-based studies. *The Lancet*, 390(10114):2769–2778, 2017.
- [3] Teodora-Ecaterina M Manuc, Mircea M Manuc, and Mircea M Diculescu. Recent insights into the molecular pathogenesis of Crohn’s disease: a review of emerging therapeutic targets. *Clinical and experimental gastroenterology*, 9:59–70, 2016.
- [4] Ray Boyapati, Jack Satsangi, and Gwo Tzer Ho. Pathogenesis of Crohn’s disease. *F1000Prime Reports*, 7(April), 2015.
- [5] Julien Matricon. Immunopathogenesis of inflammatory bowel disease. *World Journal of Gastroenterology*, 21(14(3)):390–400, 2008.
- [6] Lena Antoni, Sabine Nuding, Jan Wehkamp, and Eduard F. Stange. Intestinal barrier in inflammatory bowel disease. *World Journal of Gastroenterology*, 20(5):1165–1179, 2014.
- [7] Warren Strober, Ivan Fuss, and Peter Mannon. The fundamental basis of inflammatory bowel disease. *Journal of Clinical Investigation*, 117(3):514–21, 2007.
- [8] Mauro D’Amato and John D. Rioux. *Molecular Genetics of Inflammatory Bowel Disease*. Springer Science+Business Media, New York, 2013.
- [9] Jonathan S. Levine and Robert Burakoff. Extraintestinal Manifestations of Inflammatory Bowel Disease. *Gastroenterology & hepatology*, 7(4):235–241, 2011.
- [10] Marietta Iacucci, Shanika De Silva, and Subrata Ghosh. Mesalazine in inflammatory bowel disease: A trendy topic once again? *Canadian Journal of Gastroenterology*, 24(2):127–133, 2010.
- [11] Warren Strober, Bjorn R Ludviksson, and Ivan J Fuss. The Pathogenesis of Mucosal Inflammation in Murine Models of Inflammatory Bowel Disease and Crohn Disease. *Annals of Internal Medicine*, 128(10):848–856, 1998.
- [12] Imke Atreya and Markus F Neurath. Azathioprine in inflammatory bowel disease: improved molecular insights and resulting clinical implications. *Expert review of gastroenterology & hepatology*, 2(1):23–34, 2008.

- [13] B. Cronstein. How does methotrexate suppress inflammation? *Clinical and Experimental Rheumatology*, 28(5 SUPPL. 61):8–10, 2010.
- [14] Philipp Schreiner, Markus F. Neurath, Siew C. Ng, Emad M. El-Omar, Ala I. Sharara, Taku Kobayashi, Tadakazu Hisamatsu, Toshifumi Hibi, and Gerhard Rogler. Mechanism-Based Treatment Strategies for IBD: Cytokines, Cell Adhesion Molecules, JAK Inhibitors, Gut Flora, and More. *Inflammatory Intestinal Diseases*, 4(3):79–96, 2019.
- [15] Pieter Hindryckx, Filip Baert, Ailsa Hart, Fernando Magro, Alessandro Armuzzi, and Laurent Peyrin-Biroulet. Clinical trials in ulcerative colitis: A Historical Perspective. *Journal of Crohn's and Colitis*, 9(7):580–588, 2015.
- [16] Tal Engel, Bella Ungar, Diana E. Yung, Shomron Ben-Horin, Rami Eliakim, and Uri Kopylov. Vedolizumab in IBD-Lessons from real-world experience; A systematic review and pooled analysis. *Journal of Crohn's and Colitis*, 12(2):245–257, 2017.
- [17] William J. Sandborn, Brian G. Feagan, Stephen Hanauer, Severine Vermeire, Subrata Ghosh, Wenzhong J. Liu, Ann Katrin Petersen, Lorna Charles, Vivian Huang, Keith Usiskin, Douglas C. Wolf, and Geert D'Haens. Long-Term Efficacy and Safety of Ozanimod in Moderately to Severely Active Ulcerative Colitis: Results from the Open-Label Extension of the Randomized, Phase 2 TOUCHSTONE Study. *Journal of Crohn's and Colitis*, 15(7):1120–1129, 2021.
- [18] W. Stremmel, U. Merle, A. Zahn, F. Autschbach, U. Hinz, and R. Ehehalt. Retarded release phosphatidylcholine benefits patients with chronic active ulcerative colitis. *Gut*, 54(7):966–971, 2005.
- [19] Nathalie Van den Berghe, Ann Gils, and Debby Thomas. Achieving Mucosal Healing in Inflammatory Bowel Diseases: Which Drug Concentrations Need to Be Targeted? *Clinical Pharmacology and Therapeutics*, 106(5):945–954, 2019.
- [20] Andres J. Yarur, Anjali Jain, Daniel A. Sussman, Jamie S. Barkin, Maria A. Quintero, Fred Princen, Richard Kirkland, Amar R. Deshpande, Sharat Singh, and Maria T. Abreu. The association of tissue anti-TNF drug levels with serological and endoscopic disease activity in inflammatory bowel disease: The ATLAS study. *Gut*, 65(2):249–255, 2016.
- [21] Raja Atreya, Helmut Neumann, Clemens Neufert, Maximilian J Waldner, Ulrike Billmeier, Yurdagül Zopf, Marcus Willma, Christine App, Tino Münster, Hermann Kessler, Stefanie Maas, Bernd Gebhardt, Ralph Heimke-Brinck, Eva Reuter, Frank Dörje, Tilman T Rau, Wolfgang Uter, Thomas D Wang, Ralf Kiesslich, Michael Vieth, Ewald Hannappel, and Markus F Neurath. In vivo imaging using fluorescent antibodies to tumor necrosis factor predicts therapeutic response in Crohn's disease. *Nat Med.*, 20(3):313–318, 2014.
- [22] Edda Klipp, Wolfram Liebermeister, Christoph Wierling, Axel Kowald, Hans Lehrach, and Ralf Herwig. *Systems Biology: A Textbook*. John Wiley & sons, 2009.



- [23] Sara Sadat Aghamiri, Rada Amin, and Tomáš Helikar. Recent applications of quantitative systems pharmacology and machine learning models across diseases. *Journal of Pharmacokinetics and Pharmacodynamics*, 49(1):19–37, 2022.
- [24] Katherine Wendelsdorf, Josep Bassaganya-Riera, Raquel Hontecillas, and Stephen Eubank. Model of colonic inflammation: Immune modulatory mechanisms in inflammatory bowel disease. *Journal of Theoretical Biology*, 264(4):1225–1239, 2010.
- [25] Wing-Cheong Lo, Razvan I. Arsenescu, and Avner Friedman. Mathematical Model of the Roles of T Cells in Inflammatory Bowel Disease. *Bulletin of Mathematical Biology*, 75(9):1417–1433, 2013.
- [26] G Dwivedi, L Fitz, M Hegen, S W Martin, J Harrold, A Heatherington, and C Li. A multiscale model of interleukin-6-mediated immune regulation in Crohn’s disease and its application in drug discovery and development. *CPT: pharmacometrics & systems pharmacology*, 3(1):e89, 2014.
- [27] Violeta Balbas-Martinez, Leire Ruiz-Cerdá, Itziar Irurzun-Arana, Ignacio González-García, An Vermeulen, José David Gómez-Mantilla, and Iñaki F. Trocóniz. A systems pharmacology model for inflammatory bowel disease. *PLoS ONE*, 13(3):1–19, 2018.
- [28] Katharine V. Rogers, Steven W. Martin, Indranil Bhattacharya, Ravi Shankar Prasad Singh, and Satyaprakash Nayak. A Dynamic Quantitative Systems Pharmacology Model of Inflammatory Bowel Disease: Part 1 – Model Framework. *Clinical and Translational Science*, 2020.
- [29] Kenneth Murphy. *Janeway’s immunobiology*. Garland Science, Taylor & Francis Group, LLC, 8 edition, 2012.
- [30] Alan S. Perelson, Avidan U. Neumann, Martin Markowitz, John M. Leonard, and David D. Ho. HIV-1 dynamics in vivo: Virion clearance rate, infected cell life-span, and viral generation time. *Science*, 271(5255):1582–1586, 1996.
- [31] Max von Kleist, Stephan Menz, and Wilhelm Huisinga. Drug-class specific impact of antivirals on the reproductive capacity of HIV. *PLoS Computational Biology*, 6(3), 2010.
- [32] Herbert W Hethcote. The Mathematics of Infectious Diseases. *SIAM review*, 42(4):599–653, 2000.
- [33] Diego I. Cattoni, Osvaldo Chara, Sergio B. Kaufman, and F. Luis González Flecha. Cooperativity in binding processes: New insights from phenomenological modeling. *PLoS ONE*, 10(12):1–14, 2015.
- [34] Katharine V. Rogers, Steven W. Martin, Indranil Bhattacharya, Ravi Shankar Prasad Singh, and Satyaprakash Nayak. A Dynamic Quantitative Systems Pharmacology Model of Inflammatory Bowel Disease: Part 2 – Application to Current Therapies in Crohn’s Disease. *Clinical and Translational Science*, 2020.
- [35] Detlev Drenckhahn and Jens Waschke. *Taschenbuch Anatomie*. Elsevier GmbH, München, 1 edition, 2008.

- [36] Stephen J. Mcsorley. Immunity to intestinal pathogens: Lessons learned from Salmonella. *Immunological Reviews*, 260(1):168–182, 2014.
- [37] Nico. Schlömer. matlab2tikz. <https://de.mathworks.com/matlabcentral/fileexchange/22022-matlab2tikz-matlab2tikz>, 2018.
- [38] W S Snyder, M J Cook, E S Nasset, L R Karhausen, G Parry Howells, and I H Tipton. Report of the Task Group on Reference Man. *International Commission on Radiological Protection*, 23:1–365, 1975.
- [39] Herbert F Helander and Lars Fändriks. Surface area of the digestive tract - revisited. *Scandinavian journal of gastroenterology*, 49(6):681–9, 2014.
- [40] I Dhesi, M N Marsh, C Kelly, and P Crowe. Morphometric analysis of small intestinal mucosa. *Virchows Arch [Pathol Anat]*, 403:173–180, 1984.
- [41] Martin Faderl, Mario Noti, Nadia Corazza, and Christoph Mueller. Keeping bugs in check: The mucus layer as a critical component in maintaining intestinal homeostasis. *IUBMB Life*, 67(4):275–285, 2015.
- [42] Richard L Guerrant, Ted S Steiner, Aldo A M Lima, and David A Bobak. How Intestinal Bacteria Cause Disease. *Journal of Infectious Diseases*, 179(Suppl 2):331–337, 1999.
- [43] Renate Luellmann-Rauch. *Taschenlehrbuch Histologie*. Georg Thieme Verlag, Stuttgart, 5 edition, 2015.
- [44] Lance W. Peterson and David Artis. Intestinal epithelial cells: Regulators of barrier function and immune homeostasis. *Nature Reviews Immunology*, 14(3):141–153, 2014.
- [45] F. E. Johansen and C. S. Kaetzel. Regulation of the polymeric immunoglobulin receptor and IgA transport: New advances in environmental factors that stimulate pIgR expression and its role in mucosal immunity. *Mucosal Immunology*, 4(6):598–602, 2011.
- [46] N. J. Mantis, N. Rol, and B. Corthésy. Secretory IgA’s complex roles in immunity and mucosal homeostasis in the gut. *Mucosal Immunology*, 4(6):603–611, 2011.
- [47] Valérie Gouyer, Frédéric Gottrand, and Jean Luc Desseyn. The extraordinarily complex but highly structured organization of intestinal mucus-gel unveiled in multicolor images. *PLoS ONE*, 6(4):13–16, 2011.
- [48] D.W. Powell, I.V. Pinchuk, J.I. Saada, Xin Chen, and R.C. Mifflin. Mesenchymal Cells of the Intestinal Lamina Propria. *Annual Review of Physiology*, 73(1):213–237, 2011.
- [49] Beatrice Yue. Biology of the extracellular matrix: An overview. *Journal of Glaucoma*, S20, 2014.
- [50] C. V. Srikanth and Beth A. McCormick. Interactions of the Intestinal Epithelium with the Pathogen and the Indigenous Microbiota: A Three-Way Crosstalk. *Interdisciplinary Perspectives on Infectious Diseases*, 2008:1–14, 2008.

- [51] Caroline Bonnans, Jonathan Chou, and Zena Werb. Remodelling the extracellular matrix in development and disease. *Nature Reviews Molecular Cell Biology*, 15(12):786–801, 2014.
- [52] Calum C. Bain and Allan McI Mowat. Macrophages in intestinal homeostasis and inflammation. *Immunological Reviews*, 260:102–117, 2014.
- [53] Anupama Sahoo, Shradha Wali, and Roza Nurieva. T helper 2 and T follicular helper cells: Regulation and Function of Interleukin-4. *Cytokine Growth Factor Rev*, 30:29–37, 2016.
- [54] F. Rieder, J. Brenmoehl, S. Leeb, J. Schölmerich, and G. Rogler. Wound healing and fibrosis in intestinal disease. *Gut*, 56(1):130–139, 2007.
- [55] Alexander Swidsinski, Axel Ladhoff, Annelie Pernthaler, Sonja Swidsinski, Vera Loenig-Baucke, Marianne Ortner, Jutta Weber, Uwe Hoffmann, Stefan Schreiber, Manfred Dietel, and Herbert Lochs. Bacterial flora in inflammatory bowel disease. *Gastroenterology*, 122(1):44–54, 2002.
- [56] B M Fournier and C a Parkos. The role of neutrophils during intestinal inflammation. *Mucosal Immunology*, 5(4):354–366, 2012.
- [57] David C. Dale, Laurence Boxer, and W. Conrad Liles. The phagocytes : neutrophils and monocytes. *Blood*, 112(4):935–946, 2008.
- [58] Yongmei Li, Arthur Karlin, John D Loike, and Samuel C Silverstein. Determination of the critical concentration of neutrophils required to block bacterial growth in tissues. *The Journal of experimental medicine*, 200(5):613–622, 2004.
- [59] C C Bain, C L Scott, H Uronen-Hansson, S Gudjonsson, O Jansson, O Grip, M Guilleliams, B Malissen, W W Agace, and a McI Mowat. Resident and pro-inflammatory macrophages in the colon represent alternative context-dependent fates of the same Ly6Chi monocyte precursors. *Mucosal immunology*, 6(3):498–510, 2013.
- [60] Adam D. Kennedy and Frank R. Deleo. Neutrophil apoptosis and the resolution of infection. *Immunologic Research*, 43(1-3):25–61, 2009.
- [61] Sofia de Oliveira, Emily E. Rosowski, and Anna Huttenlocher. Neutrophil migration in infection and wound repair: going forward in reverse. *Nat Rev Immunol.*, 16(6):378–391, 2016.
- [62] Kathryn Prame Kumar, Alyce J. Nicholls, and Connie H.Y. Wong. Partners in crime: neutrophils and monocytes/macrophages in inflammation and disease. *Cell and Tissue Research*, 371(3):551–565, 2018.
- [63] Brian E. Sansbury and Matthew Spite. Resolution of acute inflammation and the role of resolvins in immunity, thrombosis, and vascular biology. *Circulation Research*, 119(1):113–130, 2016.
- [64] Almudena Ortega-Gómez, Mauro Perretti, and Oliver Soehnlein. Resolution of inflammation: An integrated view. *EMBO Molecular Medicine*, 5(5):661–674, 2013.

- [65] Mallery C. Greenlee-Wacker. Clearance of apoptotic neutrophils and resolution of inflammation. *Immunological Reviews*, 273(1):357–370, 2016.
- [66] Jesmond Dalli and Charles N. Serhan. Specific lipid mediator signatures of human phagocytes: Microparticles stimulate macrophage efferocytosis and pro-resolving mediators. *Blood*, 120(15):60–73, 2012.
- [67] T. Tak, K. Tesselaar, J. Pillay, J. A. M. Borghans, and L. Koenderman. What’s your age again? Determination of human neutrophil half-lives revisited. *Journal of Leukocyte Biology*, 94(4):595–601, 2013.
- [68] Kok P.M. van Kessel, Jovanka Bestebroer, and Jos A.G. van Strijp. Neutrophil-mediated phagocytosis of *Staphylococcus aureus*. *Frontiers in Immunology*, 5(SEP):1–12, 2014.
- [69] Elizabeth R. Mann and Xuhang Li. Intestinal antigen-presenting cells in mucosal immune homeostasis: Crosstalk between dendritic cells, macrophages and B-cells. *World Journal of Gastroenterology*, 20(29):9653–9664, 2014.
- [70] Sarah E. Headland and Lucy V. Norling. The resolution of inflammation: Principles and challenges. *Seminars in Immunology*, 27(3):149–160, 2015.
- [71] P D Smith, L E Smythies, R Shen, T Greenwell-Wild, M Gliozzi, and S M Wahl. Intestinal macrophages and response to microbial encroachment. *Mucosal immunology*, 4(1):31–42, 2011.
- [72] Calum C. Bain and Allan Mci Mowat. Intestinal macrophages - specialised adaptation to a unique environment. *European Journal of Immunology*, 41(9):2494–2498, 2011.
- [73] Oliver Pabst and Günter Bernhardt. The puzzle of intestinal lamina propria dendritic cells and macrophages. *European Journal of Immunology*, 40(8):2107–2111, 2010.
- [74] Olga Schulz, Elin Jaensson, Emma K Persson, Xiaosun Liu, Tim Worbs, William W Agace, and Oliver Pabst. Intestinal CD103+, but not CX3CR1+, antigen sampling cells migrate in lymph and serve classical dendritic cell functions. *The Journal of experimental medicine*, 206(13):3101–14, 2009.
- [75] Derrick D. Eichele and Kusum K. Kharbanda. Dextran sodium sulfate colitis murine model: An indispensable tool for advancing our understanding of inflammatory bowel diseases pathogenesis. *World Journal of Gastroenterology*, 23(33):6016–6029, 2017.
- [76] Honorio Torres-Aguilar, Sergio R Aguilar-Ruiz, Gabriela González-Pérez, Rosario Munguía, Sandra Bajaña, Marco a Meraz-Ríos, and Carmen Sánchez-Torres. Tolerogenic dendritic cells generated with different immunosuppressive cytokines induce antigen-specific anergy and regulatory properties in memory CD4+ T cells. *Journal of immunology (Baltimore, Md. : 1950)*, 184(4):1765–1775, 2010.

- [77] Jacques Banchereau, Francine Briere, Christophe Caux, Jean Davoust, Serge Lebecque, Yong-Jun Liu, Bali Pulendran, and Karolina Palucka. Immunobiology of Dendritic Cells. *Annual Review of Immunology*, 18:767–811, 2000.
- [78] Darren Thomas Ruane and Ed C. Lavelle. The role of CD103+ dendritic cells in the intestinal mucosal immune system. *Frontiers in Immunology*, 2(JUL):1–6, 2011.
- [79] Miriam Merad, Priyanka Sathe, Julie Helft, Jennifer Miller, and Arthur Mortha. The dendritic cell lineage: ontogeny and function of dendritic cells and their subsets in the steady state and the inflamed setting. *Annual review of immunology*, 31:563–604, 2013.
- [80] Gloria Cuevas Preza, Otto O Yang, Julie Elliott, Peter A Anton, and Maria T Ochoa. T lymphocyte density and distribution in human colorectal mucosa, and inefficiency of current cell isolation protocols. *PloS one*, 10(4):e0122723, 2015.
- [81] Y. Junker, H. Bode, U. Wahnschaffe, A. Kroesen, C. Loddenkemper, R. Duchmann, M. Zeitz, and R. Ullrich. Comparative analysis of mononuclear cells isolated from mucosal lymphoid follicles of the human ileum and colon. *Clinical and Experimental Immunology*, 156(2):232–237, 2009.
- [82] David Bernardo, Lydia Durant, Elizabeth R. Mann, Elizabeth Bassity, Enrique Montalvillo, Ripple Man, Rakesh Vora, Durga Reddi, Fahri Bayiroglu, Luis Fernández-Salazar, Nick R. English, Simon T C Peake, Jon Landy, Gui H. Lee, George Malietzis, Yi Harn Siaw, Aravinth U. Muruganathan, Phil Hendy, Eva Sánchez-Recio, Robin K S Phillips, Jose A. Garrote, Paul Scott, Julian Parkhill, Malte Paulsen, Ailsa L. Hart, Hafid O. Al-Hassi, Eduardo Arranz, Alan W. Walker, Simon R. Carding, and Stella C. Knight. Chemokine (C-C Motif) Receptor 2 Mediates Dendritic Cell Recruitment to the Human Colon but Is Not Responsible for Differences Observed in Dendritic Cell Subsets, Phenotype, and Function Between the Proximal and Distal Colon. *CMGH Cellular and Molecular Gastroenterology and Hepatology*, 2(1):22–39.e5, 2016.
- [83] Miriam Merad and Markus G Manz. Dendritic cell homeostasis. *Cell*, 113(15):3418–3427, 2009.
- [84] A Lanzavecchia and F Sallusto. Regulation of T cell immunity by dendritic cells. *Cell*, 106:263–266, 2001.
- [85] Kang Liu, Claudia Waskow, Xiangtao Liu, Kaihui Yao, Josephine Hoh, and Michel Nussenzweig. Origin of dendritic cells in peripheral lymphoid organs of mice. *Nature Immunology*, 8(6):578–583, 2007.
- [86] Sarah L. Keasey, Kara E. Schmid, Michael S. Lee, James Meegan, Patricio Tomas, Michael Minto, Alexander P. Tikhonov, Barry Schweitzer, and Robert G. Ulrich. Extensive Antibody Cross-reactivity among Infectious Gram-negative Bacteria Revealed by Proteome Microarray Analysis. *Molecular & Cellular Proteomics*, 8(5):924–935, 2009.
- [87] Mark J Miller, Arsalan S Hejazi, Sindy H Wei, Michael D Cahalan, and Ian Parker. T cell repertoire scanning is promoted by dynamic dendritic cell behavior and random T cell motility in the lymph node. *PNAS*, 101(4):998–1003, 2004.

- [88] Joost B Beltman, Athanasius F M Marée, Jennifer N Lynch, Mark J Miller, and Rob J de Boer. Lymph node topology dictates T cell migration behavior. *The Journal of experimental medicine*, 204(4):771–80, 2007.
- [89] J. N. Mandl, R. Liou, F. Klauschen, N. Vrisekoop, J. P. Monteiro, a. J. Yates, a. Y. Huang, and R. N. Germain. Quantification of lymph node transit times reveals differences in antigen surveillance strategies of naive CD4+ and CD8+ T cells. *Proceedings of the National Academy of Sciences*, 109(44):18036–18041, 2012.
- [90] Mark J. Miller, Olga Safrina, Ian Parker, and Michael D. Cahalan. Imaging the Single Cell Dynamics of CD4<sup>+</sup> T Cell Activation by Dendritic Cells in Lymph Nodes. *The Journal of Experimental Medicine*, 200(7):847–856, 2004.
- [91] Melanie P. Matheu, Shivashankar Othy, Milton L. Greenberg, Tobias X. Dong, Martijn Schuijs, Kim Deswarte, Hamida Hammad, Bart N. Lambrecht, Ian Parker, and Michael D. Cahalan. Imaging regulatory T cell dynamics and CTLA4-mediated suppression of T cell priming. *Nature Communications*, 6:1–11, 2015.
- [92] En Cai, Kyle Marchuk, Peter Beemiller, Casey Beppler, Matthew G. Rubashkin, Valerie M. Weaver, Audrey Gérard, Tsung-Li Liu, Bi-Chang Chen, Eric Betzig, Frederic Bartumeus, and Matthew F. Krummel. Visualizing dynamic microvillar search and stabilization during ligand detection by T cells. *Science*, 356(6338):eaal3118, 2017.
- [93] Ramon Roozendaal, Reina E. Mebius, and Georg Kraal. The conduit system of the lymph node. *International Immunology*, 20(12):1483–1487, 2008.
- [94] Jason G. Cyster and Susan R. Schwab. Sphingosine-1-Phosphate and Lymphocyte Egress from Lymphoid Organs. *Annual Review of Immunology*, 30(1):69–94, 2012.
- [95] Alexandre P. Benechet, Manisha Menon, Daqi Xu, Tasleem Samji, Leigh Maher, Thomas T. Murooka, Thorsten R. Mempel, Brian S. Sheridan, Francois M. Lemoine, and Kamal M. Khanna. T cell-intrinsic S1PR1 regulates endogenous effector T-cell egress dynamics from lymph nodes during infection. *Proceedings of the National Academy of Sciences*, 113(8):2182–2187, 2016.
- [96] Sebastian Zundler and Markus F. Neurath. Novel Insights into the Mechanisms of Gut Homing and Antiadhesion Therapies in Inflammatory Bowel Diseases. *Inflammatory Bowel Diseases*, 23(4):617–627, 2017.
- [97] Z Q Zhang, D W Notermans, G Sedgewick, W Cavert, S Wietgreffe, M Zupancic, K Gebhard, K Henry, L Boies, Z Chen, M Jenkins, R Mills, H McDade, C Goodwin, C M Schuwirth, S A Danner, and A T Haase. Kinetics of CD4+ T cell repopulation of lymphoid tissues after treatment of HIV-1 infection. *Proceedings of the National Academy of Sciences of the United States of America*, 95(3):1154–9, 1998.
- [98] Taheri Sathaliyawala, Masaru Kubota, Naomi Yudanin, Damian Turner, Philip Camp, Joseph J C Thome, Kara L. Bickham, Harvey Lerner, Michael Goldstein, Megan Sykes, Tomoaki Kato, and Donna L. Farber. Distribution and Compartmentalization of Human Circulating and Tissue-Resident Memory T Cell Subsets. *Immunity*, 38(1):187–197, 2013.

- [99] Xiaohong Zhang, Lizzie Giangreco, H Elizabeth Broome, Catherine M Dargan, and Susan L Swain. Control of CD4 Effector Fate: Transforming Growth Factor beta1 and Interleukin 2 Synergize to Prevent Apoptosis and Promote Effector Expansion. *J. Exp. Med.*, 182(September):699–709, 1995.
- [100] Rebekka Geiger, Thomas Duhon, Antonio Lanzavecchia, and Federica Sallusto. Human naive and memory CD4+ T cell repertoires specific for naturally processed antigens analyzed using libraries of amplified T cells. *The Journal of experimental medicine*, 206(7):1525–1534, 2009.
- [101] E. D. Hawkins, M. L. Turner, M. R. Dowling, C. van Gend, and P. D. Hodgkin. A model of immune regulation as a consequence of randomized lymphocyte division and death times. *Proceedings of the National Academy of Sciences*, 104(12):5032–5037, 2007.
- [102] Julia M. Marchingo, Andrey Kan, Robyn M. Sutherland, Ken R. Duffy, Cameron J. Wellard, Gabrielle T. Belz, Andrew M. Lew, Mark R. Dowling, Susanne Heinzl, and Philip D. Hodgkin. Antigen affinity, costimulation, and cytokine inputs sum linearly to amplify T cell expansion. *Science*, 346(6213):1123–1127, 2014.
- [103] J. M. Marchingo, G. Prevedello, A. Kan, S. Heinzl, P. D. Hodgkin, and K. R. Duffy. T-cell stimuli independently sum to regulate an inherited clonal division fate. *Nature Communications*, 7:1–12, 2016.
- [104] Mark R. Dowling, Andrey Kan, Susanne Heinzl, Julia M. Marchingo, Philip D. Hodgkin, and Edwin D. Hawkins. Regulatory T Cells Suppress Effector T Cell Proliferation by Limiting Division Destiny. *Frontiers in immunology*, 9(October):2461, 2018.
- [105] Clemente F. Arias, Miguel A. Herrero, Francisco J. Acosta, and Cristina Fernandez-Arias. A mathematical model for a T cell fate decision algorithm during immune response. *Journal of Theoretical Biology*, 349(February 2014):109–120, 2014.
- [106] Amanda V. Gett and Philip D. Hodgkin. A cellular calculus for signal integration by T cells. *Nature Immunology*, 1(3):239–244, 2000.
- [107] Trung H.M. Pham, Takaharu Okada, Mehrdad Matloubian, Charles G. Lo, and Jason G. Cyster. S1P1 Receptor Signaling Overrides Retention Mediated by Gai-Coupled Receptors to Promote T Cell Egress. *Immunity*, 28(1):122–133, 2008.
- [108] T. P. Arstila. A Direct Estimate of the Human T Cell Receptor Diversity. *Science*, 286(5441):958–961, 1999.
- [109] Liset Westera, Julia Drylewicz, Ineke den Braber, Tendai Mugwagwa, Iris van der Maas, Lydia Kwast, Thomas Volman, Elise H R van de Weg-Schrijver, István Bartha, Gerrit Spierenburg, Koos Gaiser, Mariëtte T. Ackermans, Becca Asquith, Rob J. de Boer, Kiki Tesselaar, and José A M Borghans. Closing the gap between T-cell life span estimates from stable isotope-labeling studies in mice and humans. *Blood*, 122(13):2205–2212, 2013.

- [110] Kathryn E Foulds, Lauren a Zenewicz, Devon J Shedlock, Jiu Jiang, Amy E Troy, and Hao Shen. Cutting edge: CD4 and CD8 T cells are intrinsically different in their proliferative responses. *Journal of Immunology*, 168(4):1528–32, 2002.
- [111] Dagmar Breitfeld, Lars Ohl, Elisabeth Kremmer, Joachim Ellwart, Federica Sallusto, Martin Lipp, and Reinhold Förster. Follicular B helper T cells express CXC chemokine receptor 5, localize to B cell follicles, and support immunoglobulin production. *Journal of Experimental Medicine*, 192(11):1545–1551, 2000.
- [112] Patrick Schaerli, Katharina Willimann, Alois B. Lang, Martin Lipp, Pius Loetscher, and Bernhard Moser. CXC chemokine receptor 5 expression defines follicular homing T cells with B cell helper function. *Journal of Experimental Medicine*, 192(11):1553–1562, 2000.
- [113] Valérie Dardalhon, Amit Awasthi, Hyoung Kwon, George Galileos, Wenda Gao, Raymond A. Sobel, Meike Mitsdoerffer, Terry B. Strom, Wassim Elyaman, I. Cheng Ho, Samia Khoury, Mohamed Oukka, and Vijay K. Kuchroo. IL-4 inhibits TGF- $\beta$ -induced Foxp3+ T cells and, together with TGF- $\beta$ , generates IL-9+ IL-10+ Foxp3-effector T cells. *Nature Immunology*, 9(12):1347–1355, 2008.
- [114] Marc Veldhoen, Catherine Uyttenhove, Jacques van Snick, Helena Helmby, Astrid Westendorf, Jan Buer, Bruno Martin, Christoph Wilhelm, and Brigitta Stockinger. Transforming growth factor- $\beta$  'reprograms' the differentiation of T helper 2 cells and promotes an interleukin 9-producing subset. *Nature Immunology*, 9(12):1341–1346, 2008.
- [115] Esmat S Yolcu, Shifra Ash, Ayelet Kaminitz, Yuval Sagiv, Nadir Askenasy, and Shai Yarkoni. Apoptosis as a mechanism of T-regulatory cell homeostasis and suppression. *Immunology and cell biology*, 86(8):650–658, 2008.
- [116] Rob J De Boer, Mihaela Oprea, Rustom Antia, Rafi Ahmed, Alan S Perelson, and Kaja Murali-krishna. Recruitment Times, Proliferation, and Apoptosis Rates during the CD8+ T-Cell Response to Lymphocytic Choriomeningitis Virus. *Journal of virology*, 75(22):10663–10669, 2001.
- [117] Sara Omenetti and Theresa T. Pizarro. The Treg/Th17 axis: A dynamic balance regulated by the gut microbiome. *Frontiers in Immunology*, 6(DEC):1–8, 2015.
- [118] Christopher G Mayne and Calvin B Williams. Induced and natural regulatory T cells in the development of inflammatory bowel disease. *Inflammatory bowel diseases*, 19(8):1772–88, 2013.
- [119] Dario A A Vignali, Lauren W Collison, and Creg J Workman. How regulatory T cells work. *Nat Rev Immunol.*, 8(7):523–532, 2008.
- [120] Angelika Schmidt, Nina Oberle, and Peter H Krammer. Molecular mechanisms of treg-mediated T cell suppression. *Frontiers in immunology*, 3(March), 2012.
- [121] James D. Lord. Promises and paradoxes of regulatory T cells in inflammatory bowel disease. *World Journal of Gastroenterology*, 21(40):11236–11245, 2015.



- [122] Angela M. Thornton and Ethan M. Shevach. Suppressor Effector Function of CD4 + CD25 + Immunoregulatory T Cells Is Antigen Nonspecific . *The Journal of Immunology*, 164(1):183–190, 2000.
- [123] Mahzuz Karim, Gang Feng, Kathryn J. Wood, and Andrew R. Bushell. CD25+CD4+ regulatory T cells generated by exposure to a model protein antigen prevent allograft rejection: Antigen-specific reactivation in vivo is critical for bystander regulation. *Blood*, 105(12):4871–4877, 2005.
- [124] Billur Akkaya, Yoshihiro Oya, Munir Akkaya, Jafar Al Souz, Amanda H. Holstein, Olena Kamenyeva, Juraj Kabat, Ryutaro Matsumura, David W. Dorward, Deborah D. Glass, and Ethan M. Shevach. Regulatory T cells mediate specific suppression by depleting peptide-MHC class II from dendritic cells. *Nature Immunology*, 20(2):218–231, 2019.
- [125] Theresa L Whiteside. Cytokines and Cytokine Measurements in a Clinical Laboratory. *Clin. Diagn. Lab. Immunol.*, 1(3):257–260, 1994.
- [126] Christian M. Hedrich and Jay H. Bream. Cell type-specific regulation of IL-10 expression in inflammation and disease. *Immunologic Research*, 47(1-3):185–206, 2010.
- [127] Giang T. Nguyen, Erin R. Green, and Joan Meccas. Neutrophils to the ROScue: Mechanisms of NADPH oxidase activation and bacterial resistance. *Frontiers in Cellular and Infection Microbiology*, 7(AUG), 2017.
- [128] Charles N. Serhan. Pro-resolving lipid mediators are leads for resolution physiology. *Nature*, 510(7503):92–101, 2014.
- [129] Andrea Cerutti and Maria Rescigno. The Biology of Intestinal Immunoglobulin A Responses. *Immunity*, 28(6):740–750, 2008.
- [130] Julia Benckert, Nina Schmolka, Cornelia Kreschel, Markus Josef Zoller, Andreas Sturm, Bertram Wiedenmann, and Hedda Wardemann. The majority of intestinal IgA+ and IgG+ plasmablasts in the human gut are antigen-specific. *Journal of Clinical Investigation*, 121(5):1946–1955, 2011.
- [131] Manuela Buettner and Matthias Lochner. Development and function of secondary and tertiary lymphoid organs in the small intestine and the colon. *Frontiers in Immunology*, 7(SEP):1–11, 2016.
- [132] Masayuki Saruta, Qi T. Yu, Phillip R. Fleshner, Pierre Yves Mantel, Carsten B. Schmidt-Weber, Alison H. Banham, and Konstantinos A. Papadakis. Characterization of FOXP3+CD4+ regulatory T cells in Crohn’s disease. *Clinical Immunology*, 125(3):281–290, 2007.
- [133] James D. Lord, Donna M. Shows, Janice Chen, and Richard C. Thirlby. Human blood and mucosal regulatory T cells express activation markers and inhibitory receptors in inflammatory bowel disease. *PLoS ONE*, 10(8):1–14, 2015.

- [134] Hualin Fu, Yue Ma, Meng Yang, Chunlei Zhang, Hai Huang, Ying Xia, Lungen Lu, Weilin Jin, and Daxiang Cui. Persisting and increasing neutrophil infiltration associates with gastric carcinogenesis and e-cadherin downregulation. *Scientific Reports*, 6(June):1–14, 2016.
- [135] Vania Camilo, Toshiro Sugiyama, and Eliette Touati. Pathogenesis of *Helicobacter pylori* infection. *Helicobacter*, 22:1–6, 2017.
- [136] I. Hansson, M. Sandberg, I. Habib, R. Lowman, and E. O. Engvall. Knowledge gaps in control of *Campylobacter* for prevention of campylobacteriosis. *Transboundary and Emerging Diseases*, 65:30–48, 2018.
- [137] Jacek Czepiel, Mirosław Drózdź, Hanna Pituch, Ed J. Kuijper, William Perucki, Aleksandra Mielimonka, Sarah Goldman, Dorota Wultańska, Aleksander Garlicki, and Grażyna Biesiada. *Clostridium difficile* infection: A review. *European Journal of Clinical Microbiology & Infectious Diseases*, 38:1211–1221, 2019.
- [138] Jason B. Harris, Regina C. LaRocque, Firdausi Qadri, Edward T. Ryan, and Stephen B. Calderwood. Cholera. *The Lancet*, 379(9835):2466–2476, 2012.
- [139] Tânia A.T. Gomes, Waldir P. Elias, Isabel C.A. Scaletsky, Beatriz E.C. Guth, Juliana F. Rodrigues, Roxane M.F. Piazza, Luís C.S. Ferreira, and Marina B. Martinez. Diarrheagenic *Escherichia coli*. *Brazilian Journal of Microbiology*, 47:3–30, 2016.
- [140] Samir Patel and Beth A. McCormick. Mucosal inflammatory response to *Salmonella typhimurium* infection. *Frontiers in Immunology*, 5(JUL):1–10, 2014.
- [141] Elena V. Gart, Jan S. Suchodolski, Thomas H. Welsh, Robert C. Alaniz, Ronald D. Randel, and Sara D. Lawhon. *Salmonella typhimurium* and multidirectional communication in the gut. *Frontiers in Microbiology*, 7(NOV):1–18, 2016.
- [142] Anamaria M.P. dos Santos, Rafaela G. Ferrari, and Carlos A. Conte-Junior. Virulence Factors in *Salmonella Typhimurium*: The Sagacity of a Bacterium. *Current Microbiology*, 76(6):762–773, 2019.
- [143] Manja Barthel, Siegfried Hapfelmeier, Leticia Quintanilla-Martínez, Marcus Kremer, Manfred Rohde, Michael Hogardt, Klaus Pfeffer, Holger Rüssmann, and Wolf-Dietrich Hardt. Pretreatment of mice with streptomycin provides a *Salmonella enterica* serovar *Typhimurium colitis* model that allows analysis of both pathogen and host. *Infection and Immunity*, 71(5):2839–2858, 2003.
- [144] Sam P. Brown, Stephen J. Cornell, Mark Sheppard, Andrew J. Grant, Duncan J. Maskell, Bryan T. Grenfell, and Pietro Mastroeni. Intracellular demography and the dynamics of *Salmonella enterica* infections. *PLoS Biology*, 4(11):2091–2098, 2006.
- [145] J. R. Gog, A. Murcia, N. Osterman, O. Restif, T. J. McKinley, M. Sheppard, S. Achouri, B. Wei, P. Mastroeni, J. L. N. Wood, D. J. Maskell, P. Cicuta, and C. E. Bryant. Dynamics of *Salmonella* infection of macrophages at the single cell level. *Journal of The Royal Society Interface*, 9(75):2696–2707, 2012.

- [146] Daniel T Gillespie. A general method for numerically simulating coupled chemical reactions, 1976.
- [147] Aurelien Alfonsi, Eric Cances, Gabriel Turinici, Barbara Di Ventura, and Wilhelm Huisinga. Adaptive simulation of hybrid stochastic and deterministic models for biochemical systems. *ESAIM: proceedings*, 14(September):1–13, 2005.
- [148] Andreas J. Müller, Patrick Kaiser, Kurt E.J. Dittmar, Thomas C. Weber, Sabine Haueter, Kathrin Endt, Pascal Songhet, Christa Zellweger, Marcus Kremer, Hans Jörg Fehling, and Wolf Dietrich Hardt. Salmonella gut invasion involves TTSS-2-dependent epithelial traversal, basolateral exit, and uptake by epithelium-sampling lamina propria phagocytes. *Cell Host and Microbe*, 11(1):19–32, 2012.
- [149] Filip Van Immerseel, Jeroen De Buck, Isabel De Smet, Jan Mast, Freddy Haesebrouck, and Richard Ducatelle. Dynamics of immune cell infiltration in the caecal lamina propria of chickens after neonatal infection with a Salmonella Enteritidis strain. *Developmental and Comparative Immunology*, 26(4):355–364, 2002.
- [150] Sung Jae Shin, Choong-Kyun Noh, Sun Gyo Lim, Kee Myung Lee, and Kwang Jae Lee. Non-steroidal anti-inflammatory drug-induced enteropathy. *Intestinal research*, 15(4):446–455, 2017.
- [151] T. Ohkusa, T. Terai, S. Abe, O. Kobayashi, K. Beppu, N. Sakamoto, A. Kurosawa, T. Osada, M. Hojo, A. Nagahara, T. Ogihara, and N. Sato. Colonic mucosal lesions associated with long-term administration of non-steroidal anti-inflammatory drugs. *Alimentary Pharmacology and Therapeutics*, 2(1):88–95, 2006.
- [152] Anil B. Nagar. Isolated colonic ulcers: Diagnosis and management. *Current Gastroenterology Reports*, 9(5):422–428, 2007.
- [153] Jayshil J. Patel, Martin D. Rosenthal, Keith R. Miller, and Robert G. Martindale. The gut in trauma. *Current Opinion in Critical Care*, 22(4):339–346, 2016.
- [154] Mike M. Bismar and Frank A. Sinicrope. Radiation enteritis. *Current Gastroenterology Reports*, 4:361–365, 2002.
- [155] Shiran Gerassy-Vainberg, Alexandra Blatt, Yael Danin-Poleg, Katya Gershovich, Edmond Sabo, Alex Nevelsky, Shahar Daniel, Aviva Dahan, Oren Ziv, Rishu Dheer, Maria T. Abreu, Omry Koren, Yechezkel Kashi, and Yehuda Chowers. Radiation induces proinflammatory dysbiosis: transmission of inflammatory susceptibility by host cytokine induction. *Gut*, 67(1):97–107, 2017.
- [156] Natalia Schneider Nunes, Saejeong Kim, Maggie Sundby, Parwathy Chandran, Scott Robert Burks, Ana Helena Paz, and Joseph Alan Frank. Temporal clinical, proteomic, histological and cellular immune responses of dextran sulfate sodium-induced acute colitis. *World J Gastroenterol*, 24(38):4341–4355, 2018.
- [157] Anja A. Kühn, Ulrike Erben, Lea I. Kredel, and Britta Siegmund. Diversity of intestinal macrophages in inflammatory bowel diseases. *Frontiers in Immunology*, 6(DEC):1–7, 2015.

- [158] P. Mastroeni, B. Villarreal-Ramos, and C. E. Hormaeche. Adoptive transfer of immunity to oral challenge with virulent salmonellae in innately susceptible BALB/c mice requires both immune serum and T cells. *Infection and Immunity*, 61(9):3981–3984, 1993.
- [159] Danping Zheng, Timur Liwinski, and Eran Elinav. Interaction between microbiota and immunity in health and disease. *Cell Research*, 30(6):492–506, 2020.
- [160] Na Shi, Na Li, Xinwang Duan, and Haitao Niu. Interaction between the gut microbiome and mucosal immune system. *Military Medical Research*, 4(1):1–7, 2017.
- [161] Laurence A. Boxer. How to approach neutropenia. *Hematology / the Education Program of the American Society of Hematology. American Society of Hematology. Education Program*, 2012:174–182, 2012.
- [162] Z. Zi. Sensitivity analysis approaches applied to systems biology models. *IET Systems Biology*, 5(6):336, 2011.
- [163] Jane Knöchel, Charlotte Kloft, and Wilhelm Huisinga. Understanding and reducing complex systems pharmacology models based on a novel input-response index. *Journal of Pharmacokinetics and Pharmacodynamics*, 45(1):139–157, 2018.
- [164] Shehzad Z Sheikh and Scott E Plevy. The role of the macrophage in sentinel responses in intestinal immunity. *Current opinion in gastroenterology*, 26(6):578–82, 2010.
- [165] Raymond A Isidro and Caroline B Appleyard. Colonic macrophage polarization in homeostasis, inflammation, and cancer. *American Journal of Physiology - Gastrointestinal and Liver Physiology*, 311(1):G59–G73, 2016.
- [166] Yue Sun, Lu Li, Runxiang Xie, Bangmao Wang, Kui Jiang, and Hailong Cao. Stress Triggers Flare of Inflammatory Bowel Disease in Children and Adults. *Frontiers in Pediatrics*, 7(October), 2019.
- [167] Elisa Liverani, Eleonora Scaioli, Richard John Digby, Matteo Bellanova, and Andrea Belluzzi. How to predict clinical relapse in inflammatory bowel disease patients. *World Journal of Gastroenterology*, 22(3):1017–1033, 2016.
- [168] Judith R. Kelsen, Pierre Russo, and Kathleen E. Sullivan. Early-Onset Inflammatory Bowel Disease. *Immunol Allergy Clin North Am.*, 39(1):63–79, 2019.
- [169] Anna Monica Bianco, Martina Girardelli, and Alberto Tommasini. Genetics of inflammatory bowel disease from multifactorial to monogenic forms. *World Journal of Gastroenterology*, 21(43):12296–12310, 2015.
- [170] Amit Kumar Dutta and Ashok Chacko. Influence of environmental factors on the onset and course of inflammatory bowel disease. *World Journal of Gastroenterology*, 22(3):1088–1100, 2016.
- [171] Guohui Xue, Lin Hua, Nanjin Zhou, and Junming Li. Characteristics of immune cell infiltration and associated diagnostic biomarkers in ulcerative colitis: results from bioinformatics analysis. *Bioengineered*, 12(1):252–265, 2021.

- [172] Ji Wang, Wei Dong Chen, and Yan Dong Wang. The Relationship Between Gut Microbiota and Inflammatory Diseases: The Role of Macrophages. *Frontiers in Microbiology*, 11(June):1–9, 2020.
- [173] Akiko Yamada, Rieko Arakaki, Masako Saito, Takaaki Tsunematsu, Yasusei Kudo, and Naozumi Ishimaru. Role of regulatory T cell in the pathogenesis of inflammatory bowel disease. *World Journal of Gastroenterology*, 22(7):2195–2205, 2016.
- [174] Charles N. Serhan. Novel lipid mediators and resolution mechanisms in acute inflammation: To resolve or not? *American Journal of Pathology*, 177(4):1576–1591, 2010.
- [175] Jean Frederic Colombel, Remo Panaccione, Peter Bossuyt, Milan Lukas, Filip Baert, Tomas Vanasek, Ahmet Danalioglu, Gottfried Novacek, Alessandro Armuzzi, Xavier Hébuterne, Simon Travis, Silvio Danese, Walter Reinisch, William J. Sandborn, Paul Rutgeerts, Daniel Hommes, Stefan Schreiber, Ezequiel Neimark, Bidan Huang, Qian Zhou, Paloma Mendez, Joel Petersson, Kori Wallace, Anne M. Robinson, Roopal B. Thakkar, and Geert D’Haens. Effect of tight control management on Crohn’s disease (CALM): a multicentre, randomised, controlled phase 3 trial. *The Lancet*, 390(10114):2779–2789, 2017.
- [176] Susan C Bolge, Heidi Waters, and Catherine Tak Piech. Self-reported frequency and severity of disease flares, disease perception, and flare treatments in patients with ulcerative colitis: results of a national internet-based survey. *Clinical therapeutics*, 32(2):238–245, 2010.
- [177] Jean-Yves Mary and Robert Modigliani. Development and validation of an endoscopic index of the severity for Crohn’s disease: A prospective multicentre study. *Gut*, 30:983–989, 1989.
- [178] Victoria A. Blaho and Timothy Hla. An update on the biology of sphingosine 1-phosphate receptors. *Journal of Lipid Research*, 55(8):1596–1608, 2014.
- [179] Jonathan S. Maltzman and Gary A. Koretzky. Azathioprine: Old drug, new actions. *Journal of Clinical Investigation*, 111(8):1122–1124, 2003.
- [180] Jolanda M. Van Dieren, Ernst J. Kuipers, Janneke N. Samsom, Edward E. Nieuwenhuis, and C. Janneke Van Der Woude. Revisiting the immunomodulators tacrolimus, methotrexate, and mycophenolate mofetil: Their mechanisms of action and role in the treatment of IBD. *Inflammatory Bowel Diseases*, 12(4):311–327, 2006.
- [181] Laurence J. Egan and William J. Sandborn. Methotrexate for inflammatory bowel disease: Pharmacology and preliminary results. *Mayo Clinic Proceedings*, 71(1):69–80, 1996.
- [182] Stacy B. Menees, Corey Powell, Jacob Kurlander, Akash Goel, and William D. Chey. A meta-analysis of the utility of C-reactive protein, erythrocyte sedimentation rate, fecal calprotectin, and fecal lactoferrin to exclude inflammatory bowel disease in adults with IBS. *American Journal of Gastroenterology*, 110(3):444–454, 2015.
- [183] Isabelle Guyon and Andre Elisseeff. An Introduction to Variable and Feature Selection. *Journal of Machine Learning Research*, 3:1157–1182, 2003.

- [184] Yaqian Guo, Trevor Hastie, and Robert Tibshirani. Regularized linear discriminant analysis and its application in microarrays. *Biostatistics*, 8(1):86–100, 2007.

## 9 Appendix

### 9.1 ODEs of the model

Only ODEs for infection with commensal bacteria or generic extracellular pathogen are shown here. To simulate infection with salmonellae, additional terms and ODEs have to be added as described in Section 2.18.2 to account for infection of macrophages by salmonellae. The ODEs shown here suffice to generate the virtual population of IBD patients.

$$\begin{aligned}
\frac{d}{dt}\text{nutrients} &= \lambda_{\text{nutrients}} - \sum_b p_{\text{Bact,Lu},b} \cdot \text{Bact}_{\text{Lu},b} \cdot \text{nutrients} \\
\frac{d}{dt}\text{Bact}_{\text{Lu},b} &= p_{\text{Bact,Lu},b} \cdot \text{Bact}_{\text{Lu},b} \cdot \text{nutrients} - \mu_{\text{Bact,Lu}} \cdot \text{Bact}_{\text{Lu},b} \\
\frac{d}{dt}\text{tissue} &= \lambda_{\text{tis}} \cdot \left(1 + \frac{F_{\text{max,tis}} \cdot \text{cyto}_{\text{remod,tis}}}{1 + \text{cyto}_{\text{remod,tis}}}\right) \\
&\quad - \mu_{\text{tis}} \cdot \text{tissue} \cdot \left(1 + \frac{F_{\text{max,tis}} \cdot \text{cyto}_{\text{destr,tis}}}{1 + \text{cyto}_{\text{destr,tis}}}\right) \\
\frac{d}{dt}\text{epi} &= \lambda_{\text{epi}} \cdot \min(\text{tissue}, 1) - \mu_{\text{epi}} \cdot \text{epi} \cdot \left(1 + \frac{F_{\text{max,epi}} \cdot \text{cyto}_{\text{destr,epi}}}{1 + \text{cyto}_{\text{destr,epi}}}\right) \\
&\quad - \mu_{\text{epi,Bact}} \cdot \sum_b \epsilon_{\text{Bact},2,b} \cdot (1 - \text{mucus}) \cdot \text{epi} \cdot \text{Bact}_{\text{Lu}} \\
\frac{d}{dt}\text{mucus} &= \lambda_{\text{mucus}} \cdot \text{epi} - \mu_{\text{mucus}} \cdot \text{mucus} \\
\frac{d}{dt}\text{Bact}_{\text{LP},b} &= \text{bacterial inflow}_b + p_{\text{Bact,LP},b} \cdot \left(1 - \frac{\sum_b \text{Bact}_{\text{LP},b}}{C_{\text{max,Bact}}}\right) \cdot \text{Bact}_{\text{LP},b} \\
&\quad - \frac{V_{\text{max,Phago}} \cdot \text{Bact}_{\text{LP},b}}{\frac{K_{\text{mPhago}}}{R_{\text{phago},b}} + \sum_b \text{Bact}_{\text{LP},b}} \cdot \text{NEC}_{\text{LP}} \\
\frac{d}{dt}\text{Neut} &= \frac{\lambda_{\text{Neut,max}} \cdot ((\text{cyto}_{\text{rec,Neut}})^{h_{\text{rec,Neut}}} + w_{\text{pro,Bact}} \cdot \sum_b \text{Bact}_{\text{LP}})}{1 + \text{SPM}^{h_{\text{rec,Neut}}} + (\text{cyto}_{\text{rec,Neut}})^{h_{\text{rec,Neut}}} + w_{\text{pro,Bact}} \cdot \sum_b \text{Bact}_{\text{LP}}} \\
&\quad - \mu_{\text{Neut,c}} \cdot \text{Neut} \\
&\quad - \mu_{\text{Neut,Phago}} \cdot \sum_b \left( \frac{V_{\text{max,Phago}} \cdot \text{Bact}_{\text{LP},b}}{\frac{K_{\text{mPhago}}}{R_{\text{phago},b}} + \sum_b \text{Bact}_{\text{LP},b}} \right) \cdot \text{Neut} \\
&\quad - \frac{\mu_{\text{Neut,max}} \cdot \text{Neut} \cdot \text{SPM}}{1 + \text{cyto}_{\text{rec,Neut}} + \text{SPM}} \\
\frac{d}{dt}\text{Neut}_{\text{apo}} &= \mu_{\text{Neut,c}} \cdot \text{Neut}
\end{aligned}$$

$$\begin{aligned}
& + \mu_{\text{Neut,Phago}} \cdot \sum_b \left( \frac{V_{\text{max,Phago}} \cdot \text{Bact}_{\text{LP},b}}{\frac{\text{Km}_{\text{Phago}}}{R_{\text{phago},b}} + \sum_b \text{Bact}_{\text{LP},b}} \right) \cdot \text{Neut} \\
& + \frac{\mu_{\text{Neut,max}} \cdot \text{Neut} \cdot \text{SPM}}{1 + \text{cyto}_{\text{rec,Neut}} + \text{SPM}} \\
& - \frac{V_{\text{max,Phago}} \cdot \text{Neut}_{\text{apo}}}{\text{Km}_{\text{Phago}} + \text{Neut}_{\text{apo}}} \cdot \text{NEC}_{\text{M,LP}} \\
& - \mu_{\text{Neut,apo}} \cdot \text{Neut}_{\text{apo}} \\
\frac{d}{dt} M_{\text{P1}} & = \text{M recruitment rate} - \text{transition rate } M_{\text{P1}} \rightarrow M_{\text{P2}} \\
& - M_{\text{P1}} \text{ efferocytosis rate} - M_{\text{P1}} \text{ antigen uptake rate} - \mu_M \cdot M_{\text{P1}} \\
\frac{d}{dt} M_{\text{P1,a}} & = - \text{transition rate } M_{\text{P1,a}} \rightarrow M_{\text{P2,a}} \\
& - M_{\text{P1,a}} \text{ efferocytosis rate} + M_{\text{P1}} \text{ antigen uptake rate} - \mu_M \cdot M_{\text{P1,a}} \\
& - \frac{i\text{Treg}_{\text{tot,LP}}}{T_{\text{tot,LP}}} \cdot \frac{M_{\text{P1,a}} \cdot \text{bs}_{\text{perM}} \cdot \left( 1 - \frac{\text{Tem2Th1}}{\text{sDC}_{\text{LP}} \cdot \text{bs}_{\text{perDC}} + M_{\text{pro,a}} \cdot \text{bs}_{\text{perM}}} \right)}{\text{BS}_{\text{APC,av,LP}}} \\
& \quad \cdot \frac{\alpha_{\text{Th},b} \cdot \beta}{T_{\text{contact}}} \cdot \text{contacts}_{\text{LP}} \cdot \text{bs}_{\text{perM}}^{-1} \\
& + M_{\text{P1,a,dep}} \text{ antigen uptake rate} \\
\frac{d}{dt} M_{\text{P2}} & = \text{transition rate } M_{\text{P1}} \rightarrow M_{\text{P2}} - \text{transition rate } M_{\text{P2}} \rightarrow M_{\text{P3}} \\
& - M_{\text{P2}} \text{ efferocytosis rate} - M_{\text{P2}} \text{ antigen uptake rate} - \mu_M \cdot M_{\text{P2}} \\
\frac{d}{dt} M_{\text{P2,a}} & = \text{transition rate } M_{\text{P1,a}} \rightarrow M_{\text{P2,a}} - \text{transition rate } M_{\text{P2,a}} \rightarrow M_{\text{P3,a}} \\
& - M_{\text{P2,a}} \text{ efferocytosis rate} + M_{\text{P2}} \text{ antigen uptake rate} - \mu_M \cdot M_{\text{P2,a}} \\
& - \frac{i\text{Treg}_{\text{tot,LP}}}{T_{\text{tot,LP}}} \cdot \frac{M_{\text{P2,a}} \cdot \text{bs}_{\text{perM}} \cdot \left( 1 - \frac{\text{Tem2Th1}}{\text{sDC}_{\text{LP}} \cdot \text{bs}_{\text{perDC}} + M_{\text{pro,a}} \cdot \text{bs}_{\text{perM}}} \right)}{\text{BS}_{\text{APC,av,LP}}} \\
& \quad \cdot \frac{\alpha_{\text{Th},b} \cdot \beta}{T_{\text{contact}}} \cdot \text{contacts}_{\text{LP}} \cdot \text{bs}_{\text{perM}}^{-1} \\
& + M_{\text{P2,a,dep}} \text{ antigen uptake rate} \\
\frac{d}{dt} M_{\text{P3}} & = \text{transition rate } M_{\text{P2}} \rightarrow M_{\text{P3}} - \text{transition rate } M_{\text{P3}} \rightarrow M_{\text{P4}} \\
& - M_{\text{P3}} \text{ efferocytosis rate} - M_{\text{P3}} \text{ antigen uptake rate} - \mu_M \cdot M_{\text{P3}} \\
\frac{d}{dt} M_{\text{P3,a}} & = \text{transition rate } M_{\text{P2,a}} \rightarrow M_{\text{P3,a}} - \text{transition rate } M_{\text{P3,a}} \rightarrow M_{\text{P4,a}} \\
& - M_{\text{P3,a}} \text{ efferocytosis rate} + M_{\text{P3}} \text{ antigen uptake rate} - \mu_M \cdot M_{\text{P3,a}} \\
& - \frac{i\text{Treg}_{\text{tot,LP}}}{T_{\text{tot,LP}}} \cdot \frac{M_{\text{P3,a}} \cdot \text{bs}_{\text{perM}} \cdot \left( 1 - \frac{\text{Tem2Th1}}{\text{sDC}_{\text{LP}} \cdot \text{bs}_{\text{perDC}} + M_{\text{pro,a}} \cdot \text{bs}_{\text{perM}}} \right)}{\text{BS}_{\text{APC,av,LP}}} \\
& \quad \cdot \frac{\alpha_{\text{Th},b} \cdot \beta}{T_{\text{contact}}} \cdot \text{contacts}_{\text{LP}} \cdot \text{bs}_{\text{perM}}^{-1} \\
& + M_{\text{P3,a,dep}} \text{ antigen uptake rate}
\end{aligned}$$



$$\begin{aligned}
\frac{d}{dt}M_{P_4} &= \text{transition rate } M_{P_3} \rightarrow M_{P_4} \\
&\quad - M_{P_4} \text{ efferocytosis rate} - M_{P_4} \text{ antigen uptake rate} - \mu_M \cdot M_{P_4} \\
\frac{d}{dt}M_{P_{4,a}} &= \text{transition rate } M_{P_{3,a}} \rightarrow M_{P_{4,a}} \\
&\quad - M_{P_{4,a}} \text{ efferocytosis rate} + M_{P_4} \text{ antigen uptake rate} - \mu_M \cdot M_{P_{4,a}} \\
&\quad - \frac{iTreg_{\text{tot,LP}}}{T_{\text{tot,LP}}} \cdot \frac{M_{P_{4,a}} \cdot bs_{\text{perM}} \cdot \left(1 - \frac{\text{Tem2Treg}_1}{tDC_{\text{LP}} \cdot bs_{\text{perDC}} + M_{\text{anti,a}} \cdot bs_{\text{perM}}}\right)}{BS_{\text{APC,av,LP}}} \\
&\quad \cdot \frac{\alpha_{\text{Th},b} \cdot \beta}{T_{\text{contact}}} \cdot \text{contacts}_{\text{LP}} \cdot bs_{\text{perM}}^{-1} \\
&\quad + M_{P_{4,a,dep}} \text{ antigen uptake rate} \\
\frac{d}{dt}M_{\text{effero}} &= M_{P_1} \text{ efferocytosis rate} + M_{P_2} \text{ efferocytosis rate} \\
&\quad + M_{P_3} \text{ efferocytosis rate} + M_{P_4} \text{ efferocytosis rate} \\
&\quad - M_{\text{effero}} \text{ antigen uptake rate} - \mu_M \cdot M_{\text{effero}} \\
\frac{d}{dt}M_{\text{effero,a}} &= M_{P_{1,a}} \text{ efferocytosis rate} + M_{P_{2,a}} \text{ efferocytosis rate} \\
&\quad + M_{P_{3,a}} \text{ efferocytosis rate} + M_{P_{4,a}} \text{ efferocytosis rate} \\
&\quad + M_{\text{effero}} \text{ antigen uptake rate} - \mu_M \cdot M_{\text{effero,a}} \\
&\quad - \frac{iTreg_{\text{tot,LP}}}{T_{\text{tot,LP}}} \cdot \frac{M_{\text{effero,a}} \cdot bs_{\text{perM}} \cdot \left(1 - \frac{\text{Tem2Treg}_1}{tDC_{\text{LP}} \cdot bs_{\text{perDC}} + M_{\text{anti,a}} \cdot bs_{\text{perM}}}\right)}{BS_{\text{APC,av,LP}}} \\
&\quad \cdot \frac{\alpha_{\text{Th},b} \cdot \beta}{T_{\text{contact}}} \cdot \text{contacts}_{\text{LP}} \cdot bs_{\text{perM}}^{-1} \\
&\quad + M_{\text{effero,a,dep}} \text{ antigen uptake rate} \\
\frac{d}{dt}M_{P_{1,a,dep}} &= \sum_b \frac{iTreg_{\text{tot,LP}}}{T_{\text{tot,LP}}} \cdot \frac{M_{P_{1,a}} \cdot bs_{\text{perM}} \cdot \left(1 - \frac{\text{Tem2Th}_1}{sDC_{\text{LP}} \cdot bs_{\text{perDC}} + M_{\text{pro,a}} \cdot bs_{\text{perM}}}\right)}{BS_{\text{APC,av,LP}}} \\
&\quad \cdot \frac{\alpha_{\text{Th},b} \cdot \beta}{T_{\text{contact}}} \cdot \text{contacts}_{\text{LP}} \cdot bs_{\text{perM}}^{-1} \\
&\quad - \mu_M \cdot M_{P_{1,a,dep}} - \text{transition rate } P_1 \rightarrow P_2 \\
&\quad - M_{P_{1,a,dep}} \text{ antigen uptake rate} - M_{P_{1,a}} \text{ efferocytosis rate} \\
\frac{d}{dt}M_{P_{2,a,dep}} &= \sum_b \frac{iTreg_{\text{tot,LP}}}{T_{\text{tot,LP}}} \cdot \frac{M_{P_{2,a}} \cdot bs_{\text{perM}} \cdot \left(1 - \frac{\text{Tem2Th}_1}{sDC_{\text{LP}} \cdot bs_{\text{perDC}} + M_{\text{pro,a}} \cdot bs_{\text{perM}}}\right)}{BS_{\text{APC,av,LP}}} \\
&\quad \cdot \frac{\alpha_{\text{Th},b} \cdot \beta}{T_{\text{contact}}} \cdot \text{contacts}_{\text{LP}} \cdot bs_{\text{perM}}^{-1} \\
&\quad - \mu_M \cdot M_{P_{2,a,dep}} + \text{transition rate } P_1 \rightarrow P_2 - \text{transition rate } P_2 \rightarrow P_3 \\
&\quad - M_{P_{2,a,dep}} \text{ antigen uptake rate} - M_{P_{2,a}} \text{ efferocytosis rate} \\
\frac{d}{dt}M_{P_{3,a,dep}} &= \sum_b \frac{iTreg_{\text{tot,LP}}}{T_{\text{tot,LP}}} \cdot \frac{M_{P_{3,a}} \cdot bs_{\text{perM}} \cdot \left(1 - \frac{\text{Tem2Th}_1}{sDC_{\text{LP}} \cdot bs_{\text{perDC}} + M_{\text{pro,a}} \cdot bs_{\text{perM}}}\right)}{BS_{\text{APC,av,LP}}}
\end{aligned}$$

$$\begin{aligned}
& \cdot \frac{\alpha_{Th,b} \cdot \beta}{T_{\text{contact}}} \cdot \text{contacts}_{LP} \cdot \text{bs}_{\text{perM}}^{-1} \\
& - \mu_M \cdot M_{P3,a,\text{dep}} + \text{transition rate } P2 \rightarrow P3 - \text{transition rate } P3 \rightarrow P4 \\
& - M_{P3,a,\text{dep}} \text{ antigen uptake rate} - M_{P3,a} \text{ efferocytosis rate} \\
\frac{d}{dt} M_{P4,a,\text{dep}} &= \sum_b \frac{iTreg_{\text{tot},LP}}{T_{\text{tot},LP}} \cdot \frac{M_{P4,a} \cdot \text{bs}_{\text{perM}} \cdot \left(1 - \frac{\text{Tem2Treg}_1}{tDC_{LP} \cdot \text{bs}_{\text{perDC}} + M_{\text{anti},a} \cdot \text{bs}_{\text{perM}}}\right)}{BS_{APC,av,LP}} \\
& \cdot \frac{\alpha_{Th,b} \cdot \beta}{T_{\text{contact}}} \cdot \text{contacts}_{LP} \cdot \text{bs}_{\text{perM}}^{-1} \\
& - \mu_M \cdot M_{P4,a,\text{dep}} + \text{transition rate } P3 \rightarrow P4 \\
& - M_{P4,a,\text{dep}} \text{ antigen uptake rate} - M_{P4,a} \text{ efferocytosis rate} \\
\frac{d}{dt} M_{\text{effero},a,\text{dep}} &= \sum_b \frac{iTreg_{\text{tot},LP}}{T_{\text{tot},LP}} \cdot \frac{M_{\text{effero},a} \cdot \text{bs}_{\text{perM}} \cdot \left(1 - \frac{\text{Tem2Treg}_1}{tDC_{LP} \cdot \text{bs}_{\text{perDC}} + M_{\text{anti},a} \cdot \text{bs}_{\text{perM}}}\right)}{BS_{APC,av,LP}} \\
& \cdot \frac{\alpha_{Th,b} \cdot \beta}{T_{\text{contact}}} \cdot \text{contacts}_{LP} \cdot \text{bs}_{\text{perM}}^{-1} \\
& - \mu_M \cdot M_{\text{effero},a,\text{dep}} - M_{\text{effero},a,\text{dep}} \text{ antigen uptake rate} \\
& + M_{P1,a} \text{ efferocytosis rate} + M_{P2,a} \text{ efferocytosis rate} \\
& + M_{P3,a} \text{ efferocytosis rate} + M_{P4,a} \text{ efferocytosis rate} \\
\frac{d}{dt} qDC &= \lambda_{DC} - \mu_{DC,LP} \cdot qDC - qDC \text{ antigen uptake rate} - qDC \text{ activation rate} \\
\frac{d}{dt} rDC &= - \mu_{DC,LP} \cdot rDC - rDC \text{ antigen uptake rate} + qDC \text{ activation rate} \\
\frac{d}{dt} tDC_{LP} &= qDC \text{ antigen uptake rate} - tDC \text{ activation rate} - (\mu_{DC,LP} + \epsilon_{DC}) \cdot tDC_{LP} \\
& - \frac{iTreg_{\text{tot},LP}}{T_{\text{tot},LP}} \cdot \frac{tDC_{LP} \cdot \text{bs}_{\text{perDC}} \cdot \left(1 - \frac{\text{Tem2Treg}_1}{tDC_{LP} \cdot \text{bs}_{\text{perDC}} + M_{\text{anti},a} \cdot \text{bs}_{\text{perM}}}\right)}{BS_{APC,av,LP}} \\
& \cdot \frac{\alpha_{Th,b} \cdot \beta}{T_{\text{contact}}} \cdot \text{contacts}_{LP} \cdot \text{bs}_{\text{perDC}}^{-1} \\
& + tDCi \text{ antigen uptake rate} \\
\frac{d}{dt} sDC_{LP} &= rDC \text{ antigen uptake rate} + tDC \text{ activation rate} - (\mu_{DC,LP} + \epsilon_{DC}) \cdot sDC_{LP} \\
& - \frac{iTreg_{\text{tot},LP}}{T_{\text{tot},LP}} \cdot \frac{sDC_{LP} \cdot \text{bs}_{\text{perDC}} \cdot \left(1 - \frac{\text{Tem2Th}_1}{sDC_{LP} \cdot \text{bs}_{\text{perDC}} + M_{\text{pro},a} \cdot \text{bs}_{\text{perM}}}\right)}{BS_{APC,av,LP}} \\
& \cdot \frac{\alpha_{Th,b} \cdot \beta}{T_{\text{contact}}} \cdot \text{contacts}_{LP} \cdot \text{bs}_{\text{perDC}}^{-1} \\
& + sDCi \text{ antigen uptake rate} \\
\frac{d}{dt} tDC_{LN} &= \epsilon_{DC} \cdot tDC_{LP} \cdot \frac{V_{LP}}{V_{LN}} - \mu_{DC,LP} \cdot tDC_{LN} \\
& - \frac{iTreg_{\text{tot},LN}}{T_{\text{tot},LN}} \cdot \frac{tDC_{LN} \cdot \text{bs}_{\text{perDC}} - (\text{Tn2Treg}_1 + \text{Tcm2Temreg}_1)}{BS_{APC,av,LN}}
\end{aligned}$$

$$\begin{aligned}
& \cdot \frac{\alpha_{Th,b} \cdot \beta}{T_{contact}} \cdot contacts_{LN} \cdot bs_{perDC}^{-1} \\
\frac{d}{dt} sDC_{LN} &= \epsilon_{DC} \cdot sDC_{LP} \cdot \frac{V_{LP}}{V_{LN}} - \mu_{DC,LP} \cdot sDC_{LN} \\
& - \frac{iTreg_{tot,LN}}{T_{tot,LN}} \cdot \frac{sDC_{LN} \cdot bs_{perDC} - (Tn2Th_1 + Tcm2Temh_1)}{BS_{APC,av,LN}} \\
& \cdot \frac{\alpha_{Th,b} \cdot \beta}{T_{contact}} \cdot contacts_{LN} \cdot bs_{perDC}^{-1} \\
\frac{d}{dt} tDC_{dep,LP} &= \sum_b \frac{iTreg_{tot,LP}}{T_{tot,LP}} \cdot \frac{tDC_{LP} \cdot bs_{perDC} \cdot \left(1 - \frac{Tem2Treg_1}{tDC_{LP} \cdot bs_{perDC} + M_{anti,a} \cdot bs_{perM}}\right)}{BS_{APC,av,LP}} \\
& \cdot \frac{\alpha_{Th,b} \cdot \beta}{T_{contact}} \cdot contacts_{LP} \cdot bs_{perDC}^{-1} \\
& - \mu_{DC,LP} \cdot tDC_{dep,LP} - \epsilon_{DC} \cdot tDC_{dep,LP} \\
& - tDCi \text{ activation rate} - tDCi \text{ antigen uptake rate} \\
\frac{d}{dt} sDC_{dep,LP} &= \sum_b \frac{iTreg_{tot,LP}}{T_{tot,LP}} \cdot \frac{sDC_{LP} \cdot bs_{perDC} \cdot \left(1 - \frac{Tem2Th_1}{sDC_{LP} \cdot bs_{perDC} + M_{pro,a} \cdot bs_{perM}}\right)}{BS_{APC,av,LP}} \\
& \cdot \frac{\alpha_{Th,b} \cdot \beta}{T_{contact}} \cdot contacts_{LP} \cdot bs_{perDC}^{-1} \\
& - \mu_{DC,LP} \cdot sDC_{dep,LP} - \epsilon_{DC} \cdot sDC_{dep,LP} \\
& + tDCi \text{ activation rate} - sDCi \text{ antigen uptake rate} \\
\frac{d}{dt} tDC_{dep,LN} &= \epsilon_{DC} \cdot tDC_{dep,LP} \cdot \frac{V_{LP}}{V_{LN}} - \mu_{DC,LN} \cdot tDC_{dep,LN} \\
& + \sum_b \frac{iTreg_{tot,LN}}{T_{tot,LN}} \cdot \frac{tDC_{LN} \cdot bs_{perDC} - (Tn2Treg_1 + Tcm2Temreg_1)}{BS_{APC,av,LN}} \\
& \cdot \frac{\alpha_{Th,b} \cdot \beta}{T_{contact}} \cdot contacts_{LN} \cdot bs_{perDC}^{-1} \\
\frac{d}{dt} sDC_{dep,LN} &= \epsilon_{DC} \cdot sDC_{dep,LP} \cdot \frac{V_{LP}}{V_{LN}} - \mu_{DC,LN} \cdot sDC_{dep,LN} \\
& + \sum_b \frac{iTreg_{tot,LN}}{T_{tot,LN}} \cdot \frac{sDC_{LN} \cdot bs_{perDC} - (Tn2Th_1 + Tcm2Temh_1)}{BS_{APC,av,LN}} \\
& \cdot \frac{\alpha_{Th,b} \cdot \beta}{T_{contact}} \cdot contacts_{LN} \cdot bs_{perDC}^{-1} \\
\frac{d}{dt} Tn &= \lambda_{Tn} - \mu_{T,LN} \cdot Tn - Tn \text{ activation rate} \\
\frac{d}{dt} Tn2Teff_1 &= Tn \text{ activation rate} - p_{Tn,1} \cdot Tn2Teff_1 - \mu_{T,prol} \cdot Tn2Teff_1 \\
\frac{d}{dt} Tn2Teff_2 &= p_{Tn,1} \cdot Tn2Teff_1 - p_{Tn,>1} \cdot Tn2Teff_2 - \mu_{T,prol} \cdot Tn2Teff_2 \\
\frac{d}{dt} Tn2Teff_i &= p_{Tn,>1} \cdot Tn2Teff_{i-1} - p_{Tn,>1} \cdot Tn2Teff_i - \mu_{T,prol} \cdot Tn2Teff_i \\
& - (1 + 0.1 \cdot (i - 5)) \cdot \mu_{T,LN} \cdot Tn2Teff_i \cdot \mathbf{1}_{\{i \geq 5\}}
\end{aligned}$$

for  $i = 3, \dots, N_{T,\text{prol}}$

$$\text{where } \mathbf{1}_{\{i \geq 5\}} = \begin{cases} 1, & \text{if } i \geq 5 \\ 0, & \text{if } i < 5 \end{cases}$$

$$\frac{d}{dt} \text{Tcm} = \lambda_{\text{Tcm}} - \mu_{T,\text{LN}} \cdot \text{Tcm} - \text{Tcm activation rate}$$

$$\frac{d}{dt} \text{Tcm2Tem}_1 = \text{Tcm activation rate} - p_{\text{Tn},>1} \cdot \text{Tcm2Tem}_1 - \mu_{T,\text{prol}} \cdot \text{Tcm2Tem}_1$$

$$\frac{d}{dt} \text{Tcm2Tem}_i = p_{\text{Tn},>1} \cdot \text{Tcm2Tem}_{i-1} - p_{\text{Tn},>1} \cdot \text{Tcm2Tem}_i - \mu_{T,\text{prol}} \cdot \text{Tcm2Tem}_i \\ - (1 + 0.1 \cdot (i - 1)) \cdot \mu_{T,\text{LN}} \cdot \text{Tcm2Tem}_i$$

for  $i = 2, \dots, N_{T,\text{prol}}$

$$\frac{d}{dt} \text{Tem} = \sum_{i=1}^{N_{T,\text{prol}}} (1 + 0.1 \cdot (i - 1)) \cdot \mu_{T,\text{LN}} \cdot \text{Tcm2Tem}_i \cdot \frac{V_{\text{LN}}}{V_{\text{LP}}} \\ - \mu_{\text{Tem}} \cdot \text{Tem} - \text{Tem activation rate}$$

$$\frac{d}{dt} \text{Tem2Teff}_1 = \text{Tem activation rate} - p_{\text{Tn},>1} \cdot \text{Tem2Teff}_1 - \mu_{T,\text{prol}} \cdot \text{Tem2Teff}_1$$

$$\frac{d}{dt} \text{Tem2Teff}_i = p_{\text{Tn},>1} \cdot \text{Tem2Teff}_{i-1} - p_{\text{Tn},>1} \cdot \text{Tem2Teff}_i - \mu_{T,\text{prol}} \cdot \text{Tem2Teff}_i \\ - (1 + 0.1 \cdot (i - 1)) \cdot \mu_{T,\text{LN}} \cdot \text{Tem2Teff}_i$$

for  $i = 2, \dots, N_{T,\text{prol}}$

$$\frac{d}{dt} \text{iTreg} = \sum_{i=5}^{N_{T,\text{prol}}} (1 + 0.1 \cdot (i - 5)) \cdot \mu_{T,\text{LN}} \cdot \text{Tn2Treg}_i \cdot \frac{V_{\text{LN}}}{V_{\text{LP}}} \\ + \sum_{i=1}^{N_{T,\text{prol}}} (1 + 0.1 \cdot (i - 1)) \cdot \mu_{T,\text{LN}} \cdot \text{Tem2Teff}_i - \mu_{T,\text{eff}} \cdot \text{iTreg}$$

$$\frac{d}{dt} \text{Th1} = \sum_{i=5}^{N_{T,\text{prol}}} (1 + 0.1 \cdot (i - 5)) \cdot \mu_{T,\text{LN}} \cdot \text{Tn2Th1}_i \cdot \frac{V_{\text{LN}}}{V_{\text{LP}}} \\ + \sum_{i=1}^{N_{T,\text{prol}}} (1 + 0.1 \cdot (i - 1)) \cdot \mu_{T,\text{LN}} \cdot \text{Tem2Th1}_i - \mu_{T,\text{eff}} \cdot \text{Th1}$$

$$\frac{d}{dt} \text{Th2} = \sum_{i=5}^{N_{T,\text{prol}}} (1 + 0.1 \cdot (i - 5)) \cdot \mu_{T,\text{LN}} \cdot \text{Tn2Th2}_i \cdot \frac{V_{\text{LN}}}{V_{\text{LP}}} \\ + \sum_{i=1}^{N_{T,\text{prol}}} (1 + 0.1 \cdot (i - 1)) \cdot \mu_{T,\text{LN}} \cdot \text{Tem2Th2}_i - \mu_{T,\text{eff}} \cdot \text{Th2}$$

$$\frac{d}{dt} \text{Th17} = \sum_{i=5}^{N_{T,\text{prol}}} (1 + 0.1 \cdot (i - 5)) \cdot \mu_{T,\text{LN}} \cdot \text{Tn2Th17}_i \cdot \frac{V_{\text{LN}}}{V_{\text{LP}}} \\ + \sum_{i=1}^{N_{T,\text{prol}}} (1 + 0.1 \cdot (i - 1)) \cdot \mu_{T,\text{LN}} \cdot \text{Tem2Th17}_i - \mu_{T,\text{eff}} \cdot \text{Th17}$$

with

$$\begin{aligned}
\text{bacterial inflow}_b &= \epsilon_{\text{Bact},1} \cdot (1 - \text{mucus}) \cdot (1 - \text{epi}) \cdot \text{Bact}_{\text{Lu},b} \\
&\quad + \epsilon_{\text{Bact},2,b} \cdot (1 - \text{mucus}) \cdot \text{epi} \cdot \text{Bact}_{\text{Lu},b} \\
\text{cNEC}_b &= p_{\text{Bact},\text{LP},b} \cdot \left(1 - \frac{\sum_b \text{Bact}_{\text{LP},b}}{C_{\text{max},\text{Bact}}}\right) \cdot \frac{\frac{\text{Km}_{\text{Phago}}}{R_{\text{phago},b}} + \sum_b \text{Bact}_{\text{LP},b}}{V_{\text{max},\text{Phago}}} \\
\text{M recruitment rate} &= \lambda_{\text{M},c} + \frac{\lambda_{\text{M},\text{max}} \cdot (\text{cyto}_{\text{rec},\text{M}})^{h_{\text{rec},\text{M}}}}{1 + \text{SPM} + (\text{cyto}_{\text{rec},\text{M}})^{h_{\text{rec},\text{M}}}} \\
\text{transition rate } M_{\text{Pi}(,a)} \rightarrow M_{\text{Pj}(,a)} &= \frac{\nu_{\text{M},\text{Pi} \rightarrow \text{Pj}} \cdot \text{cyto}_{\text{anti},\text{deact},\text{M}}^{h_{\text{anti},\text{deact},\text{M}}}}{1 + \text{cyto}_{\text{anti},\text{deact},\text{M}}^{h_{\text{anti},\text{deact},\text{M}}} + \text{cyto}_{\text{pro},\text{deact},\text{M}}^{h_{\text{pro},\text{deact},\text{M}}}} \cdot M_{\text{Pi}(,a)} \\
M_{\text{Pi}(,a)} \text{ efferocytosis rate} &= p_{\text{effero}} \cdot \frac{V_{\text{max},\text{Phago}} \cdot \text{Neut}_{\text{apo}}}{\text{Km}_{\text{Phago}} + \text{Neut}_{\text{apo}}} \cdot M_{\text{Pi}(,a)} \cdot w_{\text{phago},\text{Pi}} \\
M_{\text{Pi}} \text{ antigen uptake rate}_b &= \nu_{\text{ant.upt}} \cdot \text{Bact}_{\text{Lu},b} \cdot M_{\text{Pi}} \cdot w_{\text{phago},\text{Pi}} \\
&\quad + \frac{V_{\text{max},\text{Phago}} \cdot \text{Bact}_{\text{LP},b}}{\frac{\text{Km}_{\text{Phago}}}{R_{\text{phago},b}} + \sum_b \text{Bact}_{\text{LP},b}} \cdot M_{\text{Pi}} \cdot w_{\text{phago},\text{Pi}} \\
\text{q/tDC activation rate} &= \frac{\nu_{\text{DC,act}} \cdot \text{cyto}_{\text{pro,act,DC}}^{h_{\text{pro,act,DC}}}}{1 + \text{cyto}_{\text{pro,act,DC}}^{h_{\text{pro,act,DC}}} + \text{cyto}_{\text{anti,act,DC}}^{h_{\text{anti,act,DC}}}} \cdot \text{q/tDC} \\
\text{q/rDC antigen uptake rate} &= \nu_{\text{ant.upt}} \cdot \text{Bact}_{\text{Lu},b} \cdot \text{q/rDC} \\
&\quad + \frac{V_{\text{max},\text{Phago}} \cdot \text{Bact}_{\text{LP},b}}{\frac{\text{Km}_{\text{Phago}}}{R_{\text{phago},b}} + \sum_b \text{Bact}_{\text{LP},b}} \cdot \text{q/rDC}
\end{aligned}$$

contacts<sub>LN</sub>

$$= \frac{\text{BS}_{\text{T},\text{LN}} + \text{BS}_{\text{APC},\text{av},\text{LN}} + \frac{k_{\text{off}}}{k_{\text{on}}} - \sqrt{(\text{BS}_{\text{T},\text{LN}} + \text{BS}_{\text{APC},\text{av},\text{LN}} + \frac{k_{\text{off}}}{k_{\text{on}}})^2 - 4 \cdot \text{BS}_{\text{T},\text{LN}} \cdot \text{BS}_{\text{APC},\text{av},\text{LN}}}}{2}$$

$$\text{with } k_{\text{on}} = \frac{k_{\text{T:DC},\text{LN}}}{\text{bs}_{\text{perT}} \cdot \text{bs}_{\text{perDC}}}$$

contacts<sub>LP</sub>

$$= \frac{\text{BS}_{\text{T},\text{LP}} + \text{BS}_{\text{APC},\text{av},\text{LP}} + \frac{k_{\text{off}}}{k_{\text{on}}} - \sqrt{(\text{BS}_{\text{T},\text{LP}} + \text{BS}_{\text{APC},\text{av},\text{LP}} + \frac{k_{\text{off}}}{k_{\text{on}}})^2 - 4 \cdot \text{BS}_{\text{T},\text{LP}} \cdot \text{BS}_{\text{APC},\text{av},\text{LP}}}}{2}$$

$$\text{with } k_{\text{on}} = \frac{k_{\text{T:DC},\text{LP}}}{\text{bs}_{\text{perT}} \cdot \text{bs}_{\text{perDC}}}$$

$$\text{BS}_{\text{T},\text{LN}} = \left( \text{Tn} + \text{Tcm} + \sum_b \sum_{i=2}^{N_{\text{T},\text{prol}}} \text{Tn2Teff}_i + \sum_b \sum_{i=2}^{N_{\text{T},\text{prol}}} \text{Tcm2Tem}_i \right) \cdot \text{bs}_{\text{perT}}$$

$$\text{BS}_{\text{T},\text{LP}} = \left( \sum_b \text{T}_{\text{eff}} + \sum_b \text{Tem} + \sum_b \sum_{i=2}^{N_{\text{T},\text{prol}}} \text{Tem2Teff}_i \right) \cdot \text{bs}_{\text{perT}}$$

$$\text{BS}_{\text{APC},\text{av},\text{LN}} = (\text{tDC}_{\text{LN}} + \text{sDC}_{\text{LN}} + \text{tDC}_{\text{dep},\text{LN}} + \text{sDC}_{\text{dep},\text{LN}}) \cdot \text{bs}_{\text{perDC}}$$

$$\begin{aligned}
& - (\text{Tn2Teff}_1 + \text{Tcm2Tem}_1) \\
\text{BS}_{\text{APC,av,LP}} &= (\text{tDC}_{\text{LP}} + \text{sDC}_{\text{LP}} + \text{tDC}_{\text{dep,LP}} + \text{sDC}_{\text{dep,LP}}) \cdot \text{bS}_{\text{perDC}} + (M_{\text{P1,a}} + M_{\text{P2,a}} \\
& + M_{\text{P3,a}} + M_{\text{P4,a}} + M_{\text{effero,a}} + M_{\text{P1,a,dep}} + M_{\text{P2,a,dep}} + M_{\text{P3,a,dep}} + M_{\text{P4,a,dep}} \\
& + M_{\text{effero,a,dep}}) \cdot \text{bS}_{\text{perM}} - \text{Tem2Teff}_1
\end{aligned}$$

$$\text{Tn activation rate} = \frac{\text{Tn}}{T_{\text{tot,LN}}} \cdot \frac{\alpha_{\text{Tn}} \cdot \beta}{T_{\text{contact}}} \cdot \text{contacts}_{\text{LN}}$$

$$\text{Tcm activation rate} = \frac{\text{Tcm}}{T_{\text{tot,LN}}} \cdot \frac{\alpha_{\text{Tm,b}} \cdot \beta}{T_{\text{contact}}} \cdot \text{contacts}_{\text{LN}}$$

$$\text{Tem}_{\text{APCtype}} \text{ activation rate} = \frac{\text{Tem}_{\text{APCtype}}}{T_{\text{tot,LP}}} \cdot \frac{\text{BS}_{\text{APCtype,av,LP}}}{\text{BS}_{\text{APC,av,LP}}} \cdot \frac{\alpha_{\text{Tm,b}} \cdot \beta}{T_{\text{contact}}} \cdot \text{contacts}_{\text{LP}}$$

$$\begin{aligned}
\text{Tn activation rate by sDC} &= \frac{\text{Tn}}{T_{\text{tot,LN}}} \cdot \frac{\text{sDC}_{\text{LN}} \cdot \text{bS}_{\text{perDC}} - (\text{Tn2Th}_1 + \text{Tcm2Temh}_1)}{\text{BS}_{\text{APC,av,LN}}} \\
&\cdot \frac{\alpha_{\text{Tn}} \cdot \beta}{T_{\text{contact}}} \cdot \text{contacts}_{\text{LN}}
\end{aligned}$$

$$\text{Tn2Teff} = \text{Tn2Treg} + \text{Tn2Th1} + \text{Tn2Th2} + \text{Tn2Th17}$$

$$\text{Tn2Th} = \text{Tn2Th1} + \text{Tn2Th2} + \text{Tn2Th17}$$

$$\text{Tcm2Temh} = \text{Tcm2Tem1} + \text{Tcm2Tem2} + \text{Tcm2Tem17}$$

$$\text{Tem2Th} = \text{Tem2Th1} + \text{Tem2Th2} + \text{Tem2Th17}$$

$$M_{\text{pro,a}} = M_{\text{P1,a}} + M_{\text{P2,a}} + M_{\text{P3,a}}$$

$$M_{\text{anti,a}} = M_{\text{P4,a}} + M_{\text{effero,a}}$$

$$M_{\text{pro,a,dep}} = M_{\text{P1,a}} + M_{\text{P2,a}} + M_{\text{P3,a}} + M_{\text{P1,a,dep}} + M_{\text{P2,a,dep}} + M_{\text{P3,a,dep}}$$

$$M_{\text{anti,a,dep}} = M_{\text{P4,a}} + M_{\text{effero,a}} + M_{\text{P4,a,dep}} + M_{\text{effero,a,dep}}$$

$$\text{iTreg}_{\text{tot,LP}} = \text{iTreg} + \text{Temreg} + \sum_{i=2}^{N_{\text{T,prol}}} \text{Tem2Treg}_i$$

$$\text{iTreg}_{\text{tot,LN}} = \sum_{i=2}^{N_{\text{T,prol}}} \text{Tn2Treg}_i$$

$$\text{Th1}_{\text{tot}} = \text{Th1} + \text{Tem1} + \sum_{i=2}^{N_{\text{T,prol}}} \text{Tem2Th1}_i$$

$$\text{Th2}_{\text{tot}} = \text{Th2} + \text{Tem2} + \sum_{i=2}^{N_{\text{T,prol}}} \text{Tem2Th2}_i$$

$$\text{Th17}_{\text{tot}} = \text{Th17} + \text{Tem17} + \sum_{i=2}^{N_{\text{T,prol}}} \text{Tem2Th17}_i$$

Subscripts  $b$  of the state variables are omitted for readability in several state variables.

## 9.2 Parameters of the model

Table 10: **Parameter values.** Parameters used in the novel systems biology model, including the literature references used for derivation and a reference to the section where the detailed derivation of the parameter is described.

Parameter	Value	Unit	Reference	Section
$\alpha_{Th,b}$	$\frac{1}{N_{antigen,b}}$	—	-	2.13
$\alpha_{Tn}$	$10^{-6}$	—	[99, 100]	2.11
$\alpha_{Tm,b}$	$1.66 \cdot 10^{-4} \cdot R_{Tm,b}$	—	-	2.11
$b_{SperDC}$	300	—	[87]	2.10
$b_{SperM}$	15	—	-	2.10
$b_{SperT}$	17.5	—	[87]	2.10
$C_{max,Bact}$	$10^{10}$	$\frac{1}{mL}$	-	2.6
$\epsilon_{Bact,2,commensal}$	0	$\frac{1}{mL \cdot h}$	-	2.5
$\epsilon_{Bact,2,salmonellae}$	$1 \cdot 10^{10}$	$\frac{1}{mL \cdot h}$	-	2.5
$\epsilon_{Bact,2,extracellular}$	$1 \cdot 10^{11}$	$\frac{1}{mL \cdot h}$	-	2.5
$\epsilon_{Bact,1}$	$3 \cdot 10^8$	$\frac{1}{mL \cdot h}$	-	2.5
$\epsilon_{DC}$	0.009	$\frac{1}{h}$	[55, 80–85]	2.9
$F_{max,epi}$	1	—	-	2.5
$h_{anti,deact,M}$	1	—	-	2.8
$h_{anti,act,DC}$	1	—	-	2.9
$h_{pro,deact,M}$	1	—	-	2.8
$h_{pro,act,DC}$	1	—	-	2.9
$h_{rec,Neut}$	2	—	-	2.7
$h_{rec,M}$	2	—	-	2.8
$K_{MPhago}$	$3.7 \cdot 10^7$	$\frac{1}{mL}$	[58]	2.6
$k_{T:DC,LN}$	$2 \cdot 10^{-5}$	$\frac{mL}{h}$	-	2.10
$k_{T:DC,LP}$	$2 \cdot 10^{-6}$	$\frac{mL}{h}$	-	2.10
$\lambda_{DC}$	$1.26 \cdot 10^5$	$\frac{1}{mL \cdot h}$	[55]	2.9
$\lambda_{epi}$	0.0096	$\frac{1}{h}$	[38]	2.5
$\lambda_{M,c}$	$6.2 \cdot 10^4$	$\frac{1}{mL}$	[59, 74, 80–82]	2.8
$\lambda_{M,max}$	$1 \cdot 10^6$	$\frac{1}{mL \cdot h}$	-	2.8
$\lambda_{mucus}$	$0.9 \cdot \mu_{mucus}$	$\frac{1}{h}$	-	2.5
$\lambda_{Neut,max}$	$1 \cdot 10^8$	$\frac{1}{mL \cdot h}$	-	2.7

$\lambda_{\text{nutrients}}$	$\frac{1}{24}$	$\frac{1}{\text{h}}$	-	2.4
$\lambda_{\text{Tcm}}$	$1.8 \cdot 10^7$	$\frac{1}{\text{mL}\cdot\text{h}}$	[98]	2.11
$\lambda_{\text{tis}}$	0.0048	$\frac{1}{\text{h}}$	[38]	2.5
$\lambda_{\text{Tn}}$	$1.9 \cdot 10^7$	$\frac{1}{\text{mL}\cdot\text{h}}$	[97, 98]	2.11
$\mu_{\text{Bact,Lu}}$	$\frac{1}{24}$	$\frac{1}{\text{h}}$	-	2.4
$\mu_{\text{DC,LP}}$	0.014	$\frac{1}{\text{h}}$	[83–85]	2.9
$\mu_{\text{DC,LN}}$	1.9	$\frac{1}{\text{d}}$	Vuk Cerovic, RWTH Aachen, unpublished observations	2.9
$\mu_{\text{epi}}$	0.0096	$\frac{1}{\text{h}}$	[38]	2.5
$\mu_{\text{epi,Bact}}$	$1 \cdot 10^{-10}$	mL	-	2.5
$\mu_M$	0.0031	$\frac{1}{\text{h}}$	[59]	2.8
$\mu_{\text{mucus}}$	0.46	$\frac{1}{\text{h}}$	[41]	2.5
$\mu_{\text{Neut,apo}}$	$\frac{1}{48}$	$\frac{1}{\text{h}}$	-	2.7
$\mu_{\text{Neut,c}}$	$\frac{1}{7}$	$\frac{1}{\text{d}}$	[67]	2.7
$\mu_{\text{Neut,max}}$	0.35	$\frac{1}{\text{h}}$	-	2.7
$\mu_{\text{Neut,Phago}}$	1/50	—	[68]	2.7
$\mu_{T,\text{eff}}$	0.5	$\frac{1}{\text{d}}$	[116]	2.12
$\mu_{\text{tis}}$	0.0048	$\frac{1}{\text{h}}$	[38]	2.5
$\mu_{T,\text{LN}}$	0.10	$\frac{1}{\text{h}}$	[97, 98]	2.11
$\mu_{\text{Tem}}$	$2.5 \cdot 10^{-4}$	$\frac{1}{\text{h}}$	[109]	2.11
$\mu_{T,\text{prol}}$	0.047	$\frac{1}{\text{h}}$	[106]	2.11
$N_{\text{Bact}}$	3	—	-	2.2
$N_{T,\text{prol}}$	18	—	-	2.11
$\nu_{\text{ant.upt}}$	0.0144	$\frac{1}{\text{h}}$	-	2.8
$\nu_{\text{DC,act}}$	0.03	$\frac{1}{\text{h}}$	-	2.9
$\nu_{M,P1 \rightarrow P2}$	$6.10 \cdot 10^{-2}$	$\frac{1}{\text{h}}$	[59]	2.8
$\nu_{M,P2 \rightarrow P3}$	$9.85 \cdot 10^{-2}$	$\frac{1}{\text{h}}$	[59]	2.8
$\nu_{M,P3 \rightarrow P4}$	$2.76 \cdot 10^{-2}$	$\frac{1}{\text{h}}$	[59]	2.8
$p_{\text{Bact,LP,commensal}}$	0.72	$\frac{1}{\text{h}}$	[58]	2.6
$p_{\text{Bact,LP,extracellular}}$	0.72	$\frac{1}{\text{h}}$	[58]	2.6
$p_{\text{Bact,LP,salmonellae}}$	0	$\frac{1}{\text{h}}$	-	2.6
$p_{\text{Bact,Lu,commensal}}$	$\frac{1}{24}$	$\frac{1}{\text{h}}$	-	2.4
$p_{\text{Bact,Lu,extracellular}}$	$0.8 \cdot p_{\text{Bact,Lu,commensal}}$	$\frac{1}{\text{h}}$	-	2.4

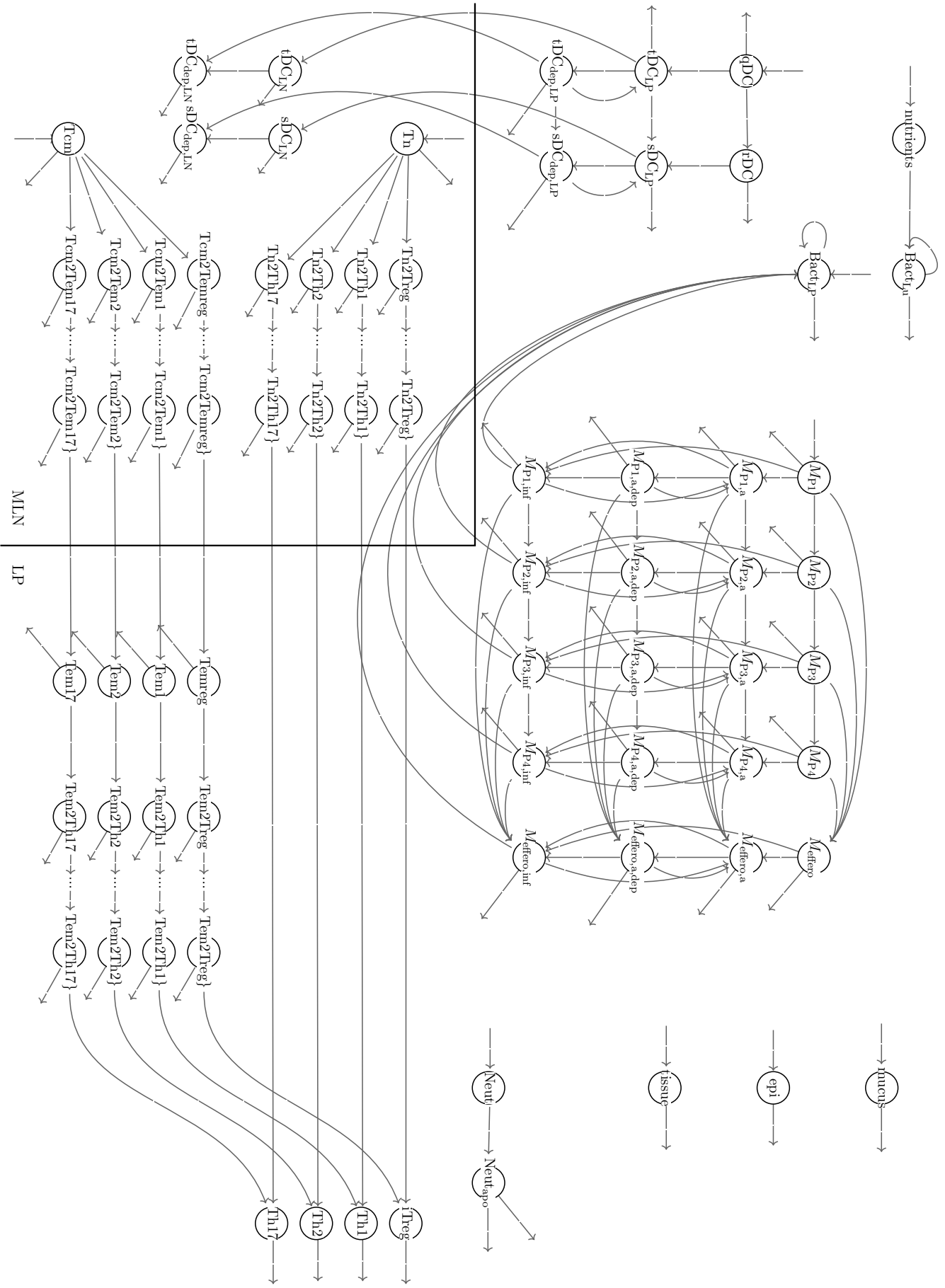


$p_{\text{Bact,Lu,salmonellae}}$	$0.8 \cdot p_{\text{Bact,Lu,commensal}}$	$\frac{1}{h}$	-	2.4
$p_{\text{effero}}$	0.1	—	-	2.8
$p_{\text{Tn},1}$	0.025	$\frac{1}{h}$	[101, 106]	2.11
$p_{\text{Tn},>1}$	0.11	$\frac{1}{h}$	[101, 106]	2.11
$R_{\text{phago,commensal}}$	1	—	-	2.9
$R_{\text{phago,extracellular}}$	0.1	—	-	2.9
$R_{\text{phago,salmonellae}}$	1	—	-	2.9
$R_{\text{Tm,commensal}}$	1	—	-	2.11
$R_{\text{Tm,commensal}}$	0.7	—	-	2.11
$R_{\text{Tm,commensal}}$	0.7	—	-	2.11
$T_{\text{contact}}$	2.3	min	[87–89, 91, 92]	2.10
$V_{\text{LN}}$	5.5	mL	[38]	2.3
$V_{\text{LP}}$	87	mL	[39, 40]	2.3
$V_{\text{max,Phago}}$	22.2	$\frac{1}{h}$	[58]	2.6
$w_{\text{phago,P1}}$	0.034	—	[59]	2.8
$w_{\text{phago,P2}}$	0.12	—	[59]	2.8
$w_{\text{phago,P3}}$	0.31	—	[59]	2.8
$w_{\text{phago,P4}}$	1	—	[59]	2.8
$w_{\text{pro,Bact}}$	$1 \cdot 10^{-6}$	—	-	2.7

For cytokine production weights and SPM production weights, see Tables 2 and 3, respectively.

### 9.3 Full model scheme

Figure 49: **Full model scheme.** Complete model scheme showing all state variables and reactions of the novel systems biology model, corresponding to the ODEs given in Section 9.1, including state variables and reactions describing infection by salmonellae. Bacteria-specific state variables are not shown separately, all entries of that state variable (each corresponding to one bacterial strain or combination of bacterial strains) are affected by the same reactions.



## 9.4 Knockout simulations

Simulations of mucosal immune response to salmonella infection and mucosal injury under different knockout conditions. See Section 3.1.

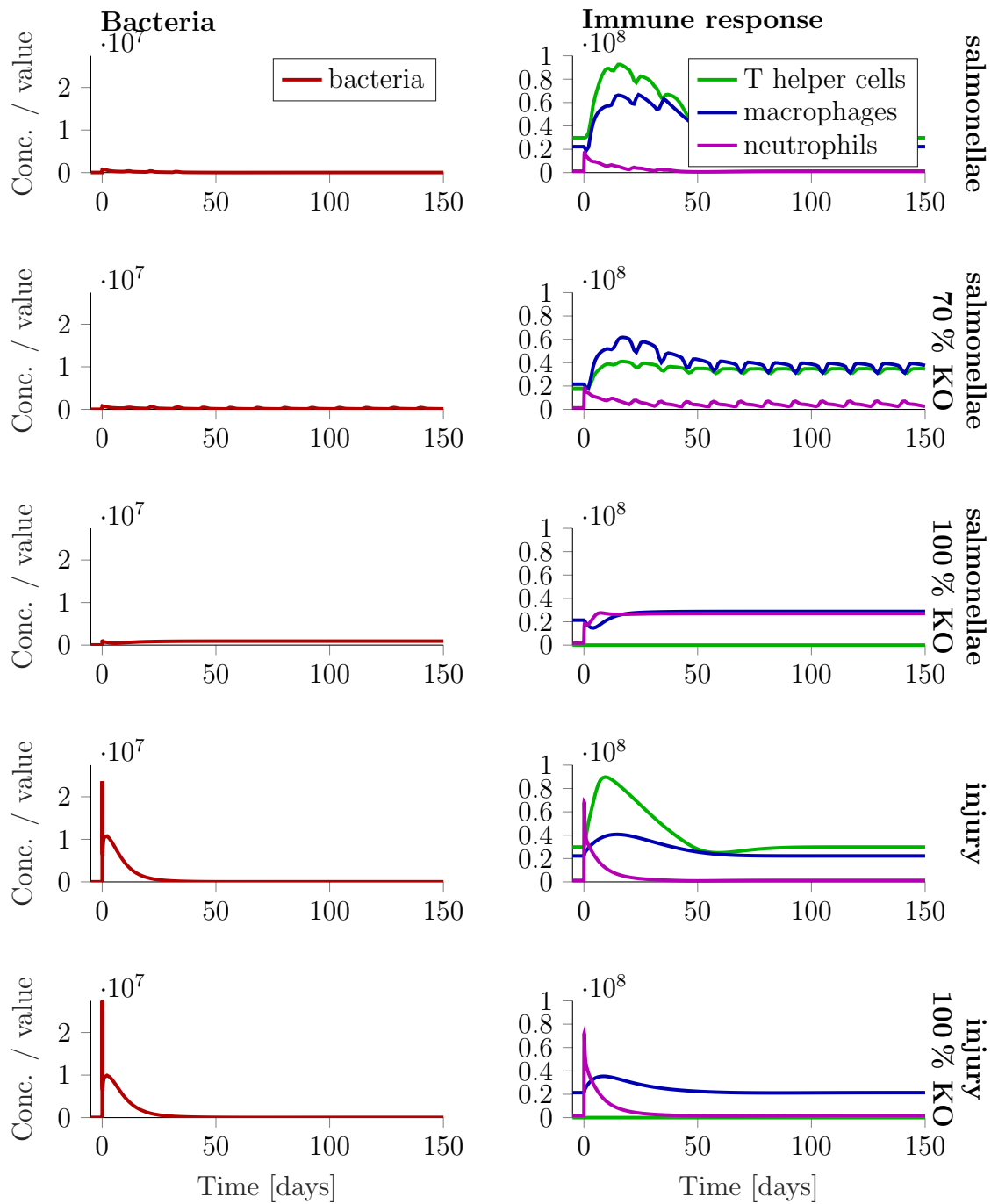


Figure 50: **Time course of T cell knockout.** Concentrations of bacteria and selected immune cells in LP over time in response to different initial amounts of *S. Typhimurium* at time point  $t = 0$  in lumen. As described in Section 2.4, pathogenic bacteria in the lumen are modelled by a unitless value describing the fraction of pathogenic bacteria from steady state commensal bacteria. i.e. initial = 0.01 corresponds to a pathogen load of 1% of the commensal bacteria in lumen at  $t = 0$ . Bacteria:  $\sum_b \text{Bact}_{\text{LP}}$ , neutrophils:  $\text{Neut}$ , macrophages:  $M_{\text{tot}}$ , T helper cells:  $\text{Th} + \text{Tem1} + \text{Tem2} + \text{Tem17} + \sum_{i=1}^{N_{\text{T,prol}}} \text{Tn2Th}$ .

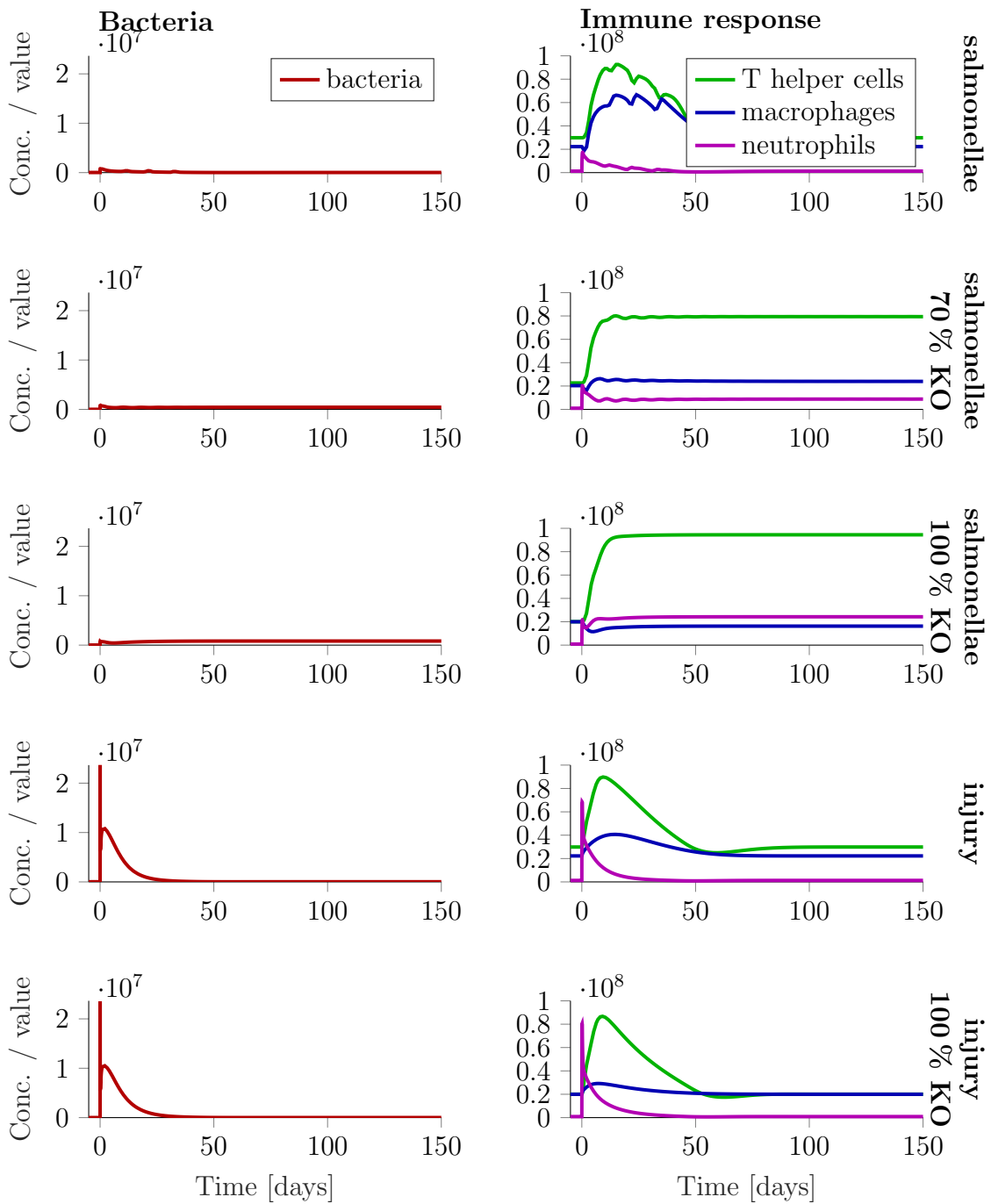


Figure 51: **Time course of T helper cell knockout.** Concentrations of bacteria and selected immune cells in LP over time in response to different initial amounts of *S. Typhimurium* at time point  $t = 0$  in lumen. As described in Section 2.4, pathogenic bacteria in the lumen are modelled by a unitless value describing the fraction of pathogenic bacteria from steady state commensal bacteria. i.e. initial = 0.01 corresponds to a pathogen load of 1% of the commensal bacteria in lumen at  $t = 0$ . Bacteria:  $\sum_b \text{Bact}_{\text{LP}}$ , neutrophils: Neut, macrophages:  $M_{\text{tot}}$ , T helper cells:  $\text{Th} + \text{Tem1} + \text{Tem2} + \text{Tem17} + \sum_{i=1}^{N_{\text{T,prol}}} \text{Tn2Th}$ .

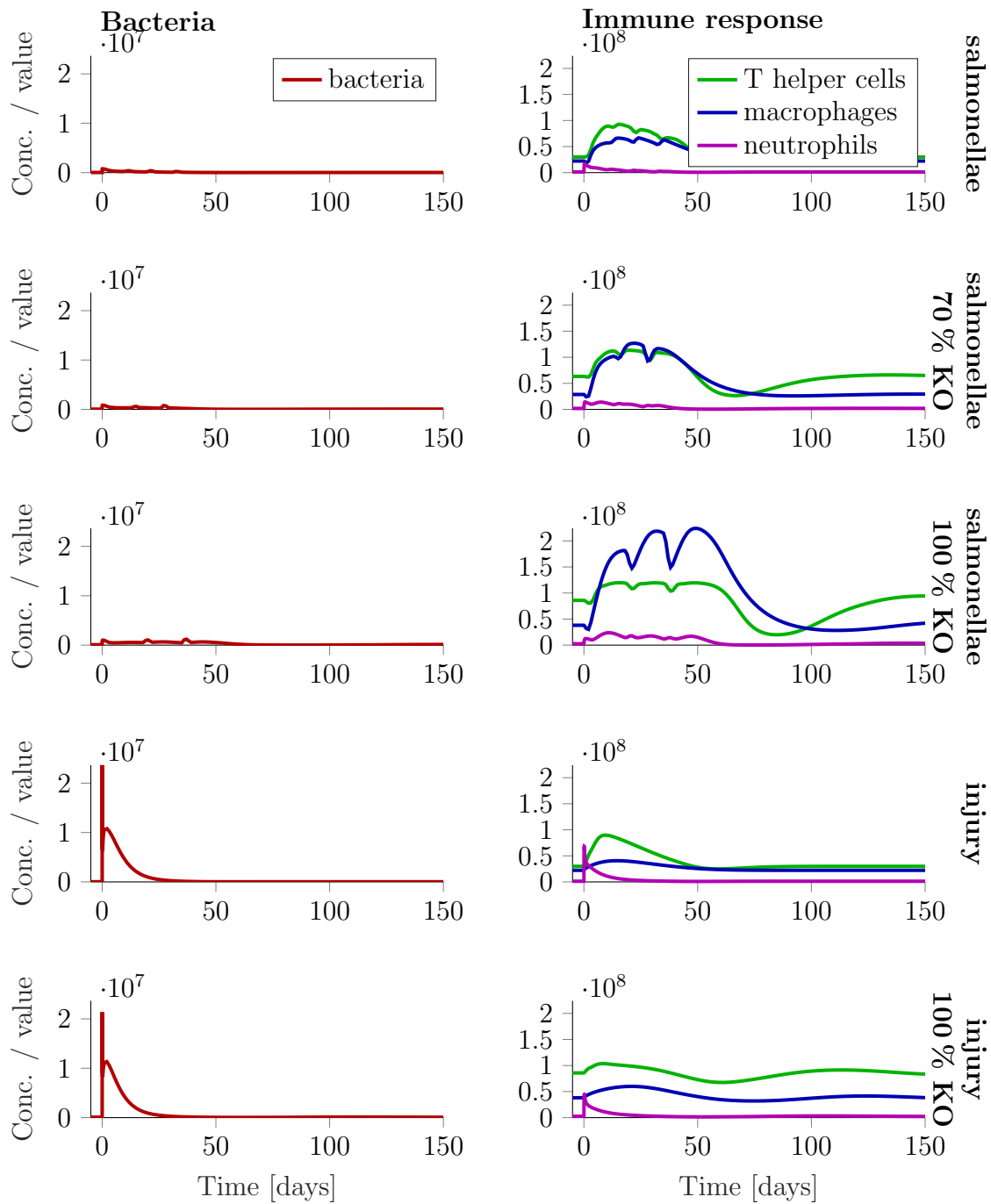


Figure 52: **Time course of regulatory T cell knockout.** Concentrations of bacteria and selected immune cells in LP over time in response to different initial amounts of *S. Typhimurium* at time point  $t = 0$  in lumen. As described in Section 2.4, pathogenic bacteria in the lumen are modelled by a unitless value describing the fraction of pathogenic bacteria from steady state commensal bacteria. i.e. initial = 0.01 corresponds to a pathogen load of 1% of the commensal bacteria in lumen at  $t = 0$ . Bacteria:  $\sum_b \text{Bact}_{\text{LP}}$ , neutrophils: Neut, macrophages:  $M_{\text{tot}}$ , T helper cells:  $\text{Th} + \text{Tem1} + \text{Tem2} + \text{Tem17} + \sum_{i=1}^{N_{\text{T,prol}}} \text{Tn2Th}$ .

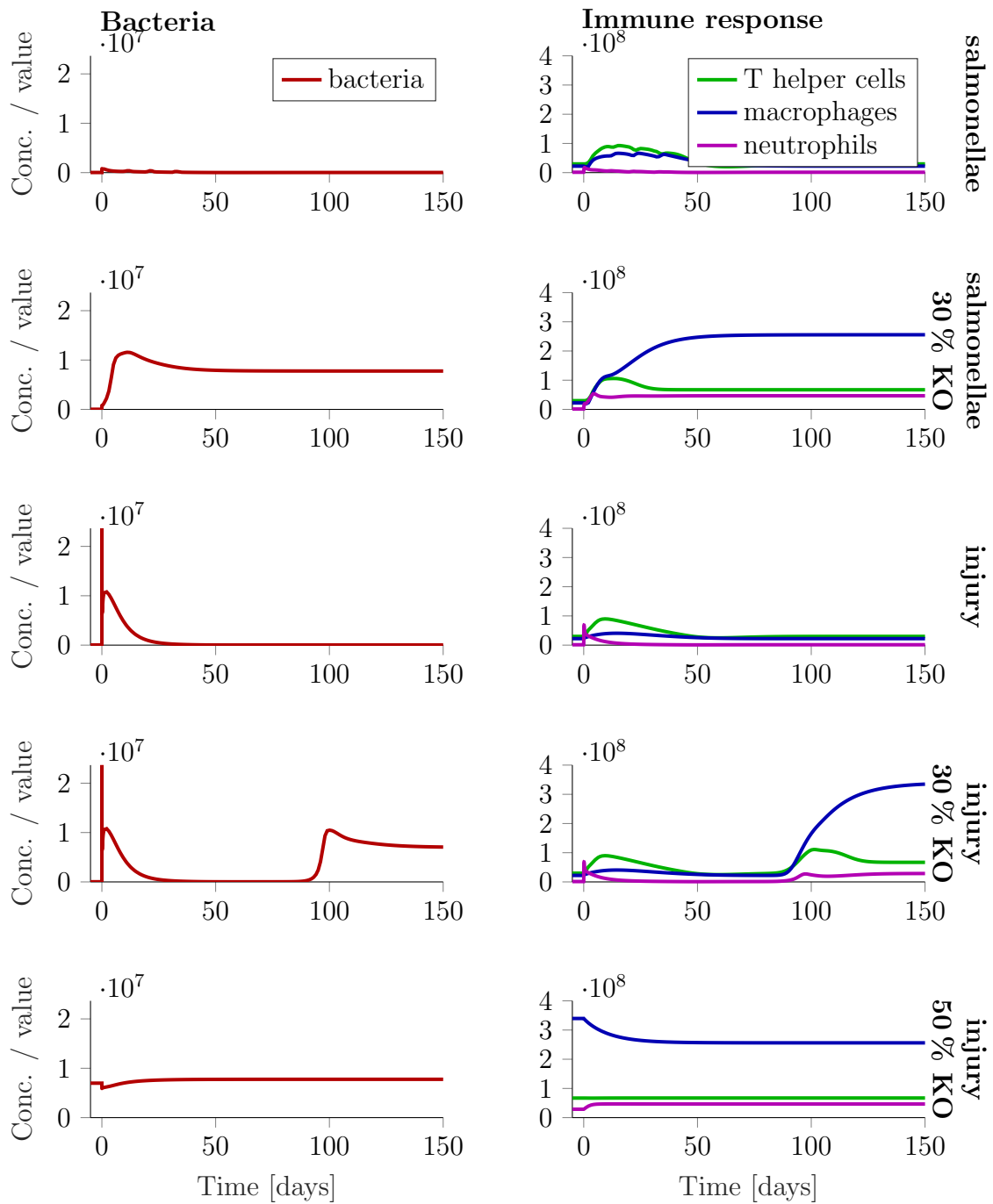


Figure 53: **Time course of commensal bacteria knockout.** Concentrations of bacteria and selected immune cells in LP over time in response to different initial amounts of *S. Typhimurium* at time point  $t = 0$  in lumen. As described in Section 2.4, pathogenic bacteria in the lumen are modelled by a unitless value describing the fraction of pathogenic bacteria from steady state commensal bacteria. i.e. initial = 0.01 corresponds to a pathogen load of 1% of the commensal bacteria in lumen at  $t = 0$ . Bacteria:  $\sum_b \text{Bact}_{\text{LP}}$ , neutrophils:  $\text{Neut}$ , macrophages:  $M_{\text{tot}}$ , T helper cells:  $\text{Th} + \text{Tem1} + \text{Tem2} + \text{Tem17} + \sum_{i=1}^{N_{\text{T,prol}}} \text{Tn2Th}$ .

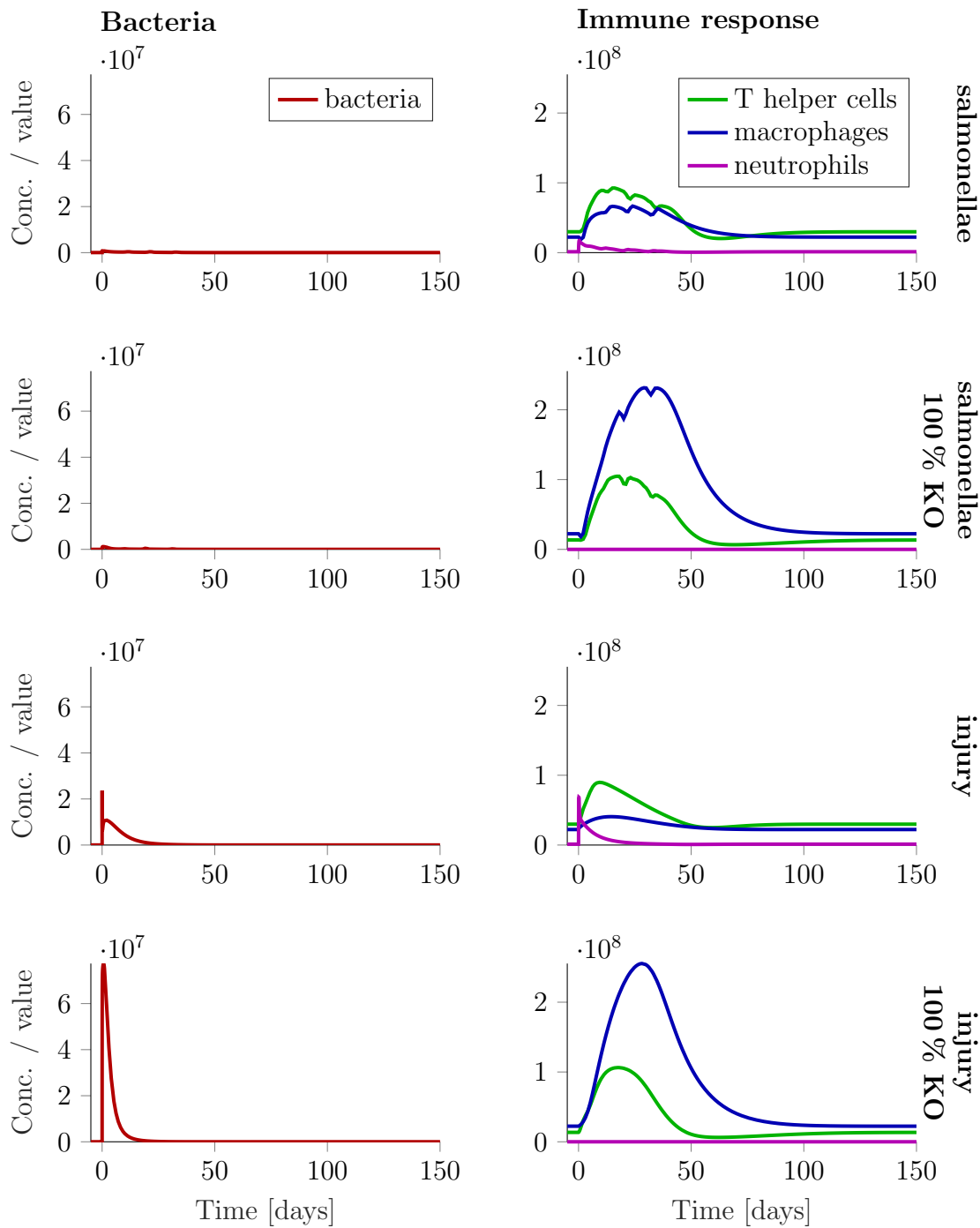


Figure 54: **Time course of neutrophil knockout.** Concentrations of bacteria and selected immune cells in LP over time in response to different initial amounts of *S. Typhimurium* at time point  $t = 0$  in lumen. As described in Section 2.4, pathogenic bacteria in the lumen are modelled by a unitless value describing the fraction of pathogenic bacteria from steady state commensal bacteria. i.e. initial = 0.01 corresponds to a pathogen load of 1% of the commensal bacteria in lumen at  $t = 0$ . Bacteria:  $\sum_b \text{Bact}_{\text{LP}}$ , neutrophils: Neut, macrophages:  $M_{\text{tot}}$ , T helper cells:  $\text{Th} + \text{Tem1} + \text{Tem2} + \text{Tem17} + \sum_{i=1}^{N_{\text{T,prol}}} \text{Tn2Th}$ .



## 9.5 Classification of the virtual population

We classified the virtual individuals into four classes (i)-(iv). For this, we used the concentrations of T helper cells ( $Th_{tot,LP}$ ), macrophages ( $M_{tot}$ ) and neutrophils (Neut) and considered the pre-trigger steady-state concentrations normalised by the reference individual's steady state and the ratio of post-trigger to pre-trigger steady-state concentration. In addition, we used the concentration of bacteria in LP ( $Bact_{LP}$ ) to identify chronic infection. We then defined class centroids for those concentration ratios describing our expectation of a typical individual of the respective class, i.e. the typical healthy individual is similar to the reference individual; the typical IBD patient is similar to the healthy individual before the trigger, but the post-trigger steady state immune cell concentrations are higher than before the trigger; the typical chronic inflammation individual has much higher immune cell concentrations already before the trigger; and the typical chronic infection individual has very high bacterial concentrations in LP (set to  $\frac{C_{max,Bact,ref}}{10}$ ). The class centroids are given in Table 11. Each individual was assigned to the class to which its Euclidian distance was smallest.

Table 11: Centroids for classification of virtual individuals.

	$\frac{\text{Pre-trigger steady state}}{\text{Reference steady state}}$			$\frac{\text{Post-trigger steady state}}{\text{Pre-trigger steady state}}$			$\frac{\text{Post-trigger steady state}}{\text{Reference steady state}}$
	$Th_{tot,LP}$	Neut	$M_{tot}$	$Th_{tot,LP}$	Neut	$M_{tot}$	$Bact_{LP}$
healthy	1	1	1	1	1	1	1
IBD	1	1	1	2	2	2	1
chronic inflammation	10	10	10	1	1	1	1
chronic infection	1	1	1	1	1	1	$\frac{N_{Bact,ref}}{10 \cdot C_{max,Bact,ref}}$

## 9.6 Derivation of disease-relevant parameter changes for IBD

We determined the set of disease-relevant parameter changes separately for each virtual IBD individual using the following workflow: Using the order of parameter correlation with the outcome determined in the last section, we started with the least correlated parameter and set it back to the reference parameter value. If this modified set of parameter values still resulted in an IBD individual (determined by simulating the mucosal injury scenario and classification as described above in Section 4.1), the parameter change was assumed not disease-relevant and the parameter was kept at the reference value. Otherwise, it was kept at its original value. This procedure was repeated for all parameters, in increasing order of correlation with the outcome. As it is possible that a parameter change results in IBD only in a certain combination with other parameter changes, we repeated the procedure until no further parameter could be changed to the reference value without losing IBD status. I.e. when any of the parameters of this resulting set of disease-relevant parameter changes is set back to the reference value, the resulting individual is not an IBD individual anymore.

Through the described procedure, we obtained for each IBD individual the set of disease-relevant parameter changes. This does also include parameters that lead to chronic

infection, chronic inflammation, or problems in steady state calculation (oscillations), when changed back to the reference value. Out of 22,252 disease-relevant parameter sets (one per original IBD individual), 995 (4.5%) contain at least one parameter that, if changed back to the reference value, results in problems (oscillations, no steady state, in the following called “problematic parameters”) and 4347 (19.54%) contain at least one parameter that, if changed back to the reference value, results in chronic inflammation (before trigger) or chronic infection (in the following called “chronic parameters”). In the parameter sets including “problematic parameters”, between 1 and 59 parameters cause those problems (mean 1.49, median 1). In the parameter sets including “chronic parameters”, between 1 and 28 parameters cause chronic inflammation/infection (mean 2.45, median 1). For most of the detected disease-relevant parameters, however, a change to the reference value results in a healthy individual, i.e. those parameters make the difference between health and disease for this individual. In the analysis of disease-relevant parameter changes, we only considered the parameter changes leading to a healthy individual if changed back to reference.

### 9.7 $h_{\text{pro,deact,M}}$ , the most frequent parameter among the disease-relevant parameter changes

By far the most frequent parameter among the disease-relevant parameter changes, and the only parameter that we identified to be able to cause IBD on its own, was  $h_{\text{pro,deact,M}}$ .  $h_{\text{pro,deact,M}}$  is the Hill factor for the pro-inflammatory cytokine concentration  $\text{cyto}_{\text{pro,deact,M}}$  in the deactivation of macrophages, i.e. it describes how sensitive the macrophage deactivation rate is to a change in the pro-inflammatory cytokine concentration. The reference value for this parameter is 1; the lowest value for  $h_{\text{pro,deact,M}}$  observed to cause IBD without any other parameter change is 3.21. Figure 55 shows the macrophage deactivation rate over the pro-inflammatory cytokine concentration  $\text{cyto}_{\text{pro,deact,M}}$  for different values of the Hill factor  $h_{\text{pro,deact,M}}$ . For the range of pro-inflammatory cytokine values influencing the deactivation of macrophages, compare Figure 17 ( $\text{cyto}_{\text{pro,deact,M}}$ , left column, middle row): in steady state  $\text{cyto}_{\text{pro,deact,M}} \approx 0.3$ , with a maximal value of  $\text{cyto}_{\text{pro,deact,M}} \approx 2$  over the time course of the mucosal injury scenario in the reference individual. In Figure 55 we can observe that the switch between very low and very high macrophage deactivation rates is more pronounced for higher Hill factors. A direct biological interpretation of the parameter  $h_{\text{pro,deact,M}}$  is difficult. It describes, how sensitive the macrophage deactivation rate is to a change in the pro-inflammatory cytokine concentration, and is therefore a summary of complex intracellular signalling cascades that take place inside the macrophage after the encounter of a pro-inflammatory cytokine eventually leading to deactivation.

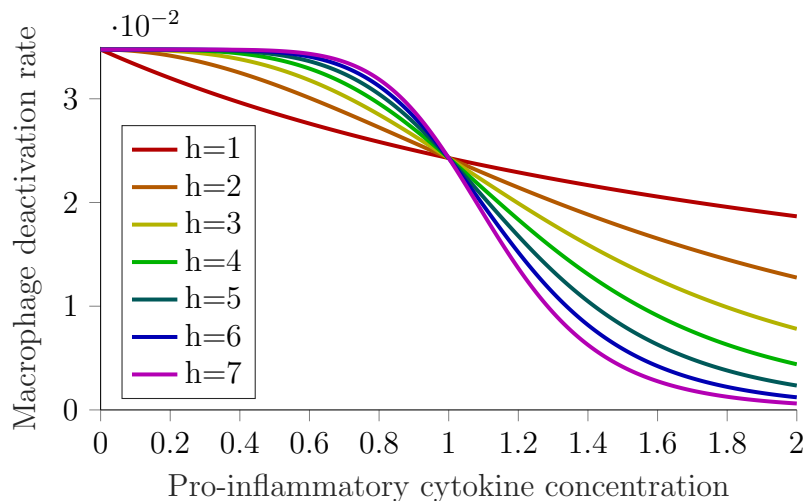


Figure 55: **Influence of Hill factor  $h_{\text{pro,deact,M}}$  on macrophage deactivation rate dependent on pro-inflammatory cytokine concentration  $\text{cyto}_{\text{pro,deact,M}}$ .** Relative macrophage deactivation rate (i.e. rate constant for the transition from macrophage population M1 to M2; transitions between other macrophage populations are only different by a constant factor) for a range of pro-inflammatory cytokine concentrations, assuming different Hill factors  $h = h_{\text{pro,deact,M}}$ . All other parameters were set to the reference values. For the calculation of the anti-inflammatory cytokines influencing the macrophage deactivation rate, the steady-state concentrations from the reference individual were used. For derivation of the macrophage deactivation rate, refer to Section 2.8, paragraph *Influence of inflammation on deactivation*. For the reference individual, the Hill factor was set to  $h = 1$ .

## 9.8 Classification and feature selection

*Short introduction to classification methods.* Classification methods aim at classifying  $n$  observations (here: individuals; subscript  $i$ ) based on  $p$  specific features (here: parameter values or pre-trigger steady-state levels) into their correct classes (here: IBD and healthy; subscript  $g$ ). The corresponding dataset is  $X \in \mathbb{R}^{p \times n}$ ,  $X_{g,i} \sim N(\mu_g, \Sigma)$ , i.e. we assume each individual to be described by features that are distributed with a multivariate normal distribution, where the mean  $\mu_g$  is specific for the class, and the standard deviation (matrix)  $\Sigma$  is equal for all classes (i.e.,  $\Sigma_{\text{healthy}} = \Sigma_{\text{IBD}}$ ). The classification method determines a classification model that maximises the number of correctly classified individuals. (Of course, in our case the best classification model is to solve the ODE system using the individual parameter values and to classify the individual based on the resulting mucosal injury time course as described in Section 4.1 (paragraph *Classification of virtual individuals*). This is, however, not our intention, as we want to learn about the importance of different parameters and cell types and to potentially draw conclusions for clinical settings.)

We tested the following classification methods on four different datasets: (i) parameter values and (ii) pre-trigger steady state values. (iii)-(iv) In addition, we used reduced datasets where patients with low disease activity were excluded. This was determined using the CDEIS score, see Section 9.10. Each dataset contained either all IBD patients (i)-(ii) or all IBD individuals with CDEIS  $> 6$  in the post-trigger steady state (iii)-(iv)

and the same number of randomly chosen healthy individuals. All values were normalised by the according value of the reference individual.

- **LDA** optimises a linear model to best discriminate between two (or more) classes (see next paragraph for more details). (Matlab function `fitcdiscr`)
- A **support vector machine** optimises a hyperplane to best discriminate between two classes. (Matlab function `fitcsvm`)
- A **Decision tree** or classification tree consists of ordered decisions based on tests on single features of the data. (Matlab function `fitctree`)
- A **Random forest** consists of a large number of decision trees, each trained on a bootstrap sample of the original dataset using a random subset of features. The results of the single decision trees are averaged to give the overall result. (Matlab function `TreeBagger` with 100 trees)
- In **k-nearest neighbours** classification, a test datapoint is classified to the class that the majority of its  $k$  nearest neighbours in the training dataset belong to. (Matlab function `fitcknn` with  $k = 20$ )
- An **artificial neural network** consists of different layers that process their inputs using nonlinear functions, returning the output to the next layer, where the weights of the different inputs are optimised. (Matlab functions `patternnet` and `train` with 10 hidden layers)
- **Gaussian process regression** models are nonparametric kernel-based probabilistic models. (Matlab function `fitrgp`, initial values for kernel parameters:  $\text{Sigma} = 0.7, \text{KernelParameters} = (5, 1)$ )

Except for the mentioned cases (where parameter values are given in the list above), the classifiers were used with default options of the respective Matlab functions.

To compare the performance of the different classification methods on our datasets ( $N = 44,504$  for full dataset,  $N = 26,842$  for  $\text{CDEIS} > 6$ ), we split each dataset into a test dataset of 1000 individuals and a training dataset containing the remaining individuals, trained each classifier on the training dataset and used the test dataset to determine the fraction of correctly classified individuals using the trained classification models. This was repeated 10 times with different random splitting into training and test datasets; the average performance (fraction of correctly identified individuals into healthy and IBD) per classification method and dataset is shown in Table 12.

As can be inferred from Table 12, Gaussian process regression shows the best performance for the parameter datasets, but not for the pre-trigger steady state datasets. LDA, random forests and artificial neural networks show comparably good performance for all datasets. Support vector machines show similar good performance on the parameter datasets, but fail for the pre-trigger steady state datasets (very high sensitivity, but very low specificity, i.e. almost all individuals classified as diseased). Decision trees and the k-nearest-neighbour algorithm show inferior performance to LDA, random forests and artificial neural networks for all datasets. In summary, we concluded that LDA, random forest and artificial neural network are the best of the tested classification methods when applied to our datasets.

Table 12: **Performance of classification methods.** Fraction of correctly classified individuals (to classes IBD or healthy) using different classification methods applied to the datasets of parameters (par) or pre-trigger steady state values (pre). In addition to the full datasets, reduced datasets excluding IBD patients with low disease activity (CDEIS < 6) are used. In all datasets, the number of healthy individuals equals the number of IBD patients. We used the following classification methods: linear discriminant analysis (LDA), support vector machine (SVM), decision tree (tree), random forest (forest), k-nearest neighbour (knn), artificial neural network (ANN), and Gaussian process regression (GPR) as described in the text.

		<b>LDA</b>	<b>SVM</b>	<b>tree</b>	<b>forest</b>	<b>knn</b>	<b>ANN</b>	<b>GPR</b>
<b>par</b>	full	0.86	0.86	0.74	0.84	0.77	0.85	0.90
	CDEIS > 6	0.90	0.90	0.80	0.87	0.83	0.90	0.93
<b>pre</b>	full	0.67	0.49	0.60	0.69	0.64	0.66	0.63
	CDEIS > 6	0.65	0.49	0.60	0.67	0.61	0.61	0.61

*Short introduction to feature selection.* Feature selection denotes the process of finding the best (combination of) predictors (also called features) among a set of possible predictors/features for a classification problem, in order to improve the prediction performance and better understand the underlying biological mechanisms. For our case, that means we aimed to find a combination of few selected features (parameters or steady-state levels) that best predict if the virtual individual is healthy or diseased. For a detailed overview of feature selection methods, see e.g. Guyon & Elisseeff (2003) [183]. For LDA, an embedded method is available, as described below. Therefore, the preferred classification algorithm for our datasets was LDA.

*Linear discriminant analysis (LDA).* In the following, we give a short introduction to LDA; for a more detailed derivation please see Guo et al. (2007) [184]. For a given dataset  $X \in \mathbb{R}^{p \times n}$ ,  $x_{g,i} \sim \text{MVN}(\mu_g, \Sigma)$  with  $n$  observations (individuals  $i$ ) and  $p$  features (parameters/pre-trigger steady state variables), covariance matrix  $\Sigma \in \mathbb{R}^{p \times p}$  estimated from data as  $\hat{\Sigma} = \frac{1}{n}(X - \bar{X})(X - \bar{X})^T$  (assuming the same covariance matrix for all classes) and feature means  $\mu_g$  for each class  $g$  (IBD or healthy) estimated from data as  $\hat{\mu}_g = \bar{x}_g = \frac{1}{n_g} \sum_{i=1}^{n_g} x_{g,i}$ ,  $x_{g,i}$  is classified to class  $\tilde{g}$  so that the likelihood of the observation is maximal. Including the prior knowledge of the proportion of the class  $\pi_g$ , this leads to the discriminant function  $\hat{d}_g(x) = x^T \hat{\Sigma}^{-1} \bar{x}_g - \frac{1}{2} \bar{x}_g^T \hat{\Sigma}^{-1} \bar{x}_g + \log \pi_g$ . In our case of two classes, an observation  $x$  is classified to class  $\tilde{g} = \text{IBD}$  if  $\hat{d}_{\text{IBD}}(x) > \hat{d}_{\text{healthy}}(x)$ , i.e.  $\hat{d}_{\text{IBD}}(x) - \hat{d}_{\text{healthy}}(x) > 0$ . This yields the (linear) discriminant function

$$d(x) = x^T \underbrace{\hat{\Sigma}^{-1}(\bar{x}_{\text{IBD}} - \bar{x}_{\text{healthy}})}_{\text{linear coefficients}} + \underbrace{\frac{1}{2}(\bar{x}_{\text{healthy}}^T \hat{\Sigma}^{-1} \bar{x}_{\text{healthy}} - \bar{x}_{\text{IBD}}^T \hat{\Sigma}^{-1} \bar{x}_{\text{IBD}})}_{\text{constant coefficient}}$$

[184].

Regularisation of this linear discriminant function using two additional parameters  $\gamma$  and  $\delta$  can be used for feature selection:

- To avoid singularity of the covariance matrix, and improve predictive performance, it is regularised using parameter  $\gamma$ :  $\tilde{\Sigma} = (1 - \gamma) \cdot \hat{\Sigma} + \gamma \cdot \text{diag}(\hat{X}^T \cdot \hat{X})$ . For this step, it is important to use centered data, i.e.  $\hat{X} = X - \mu_g$ .
- To reduce the number of features, all linear coefficients with absolute value smaller than parameter  $\delta$  are set to zero. The respective features do thus not influence the discriminant function anymore. This step also assumes normalised data, so that the same parameter  $\delta$  can be applied as threshold to all linear coefficients.

To find the optimal classification model(s), the linear discriminant function was determined for a large range of  $\gamma$  and  $\delta$  values (using Matlab function `cvshrink`), resulting for each combination of  $\gamma$  and  $\delta$  in a linear discriminant function with a specific number of features. Then, for each number of features (from 1 to  $p$ ), the combination of  $\gamma$  and  $\delta$  yielding best performance, i.e. highest fraction of correctly classified individuals in the test dataset, was selected. As all parameter and pre-trigger steady-state values in the datasets were normalised by the according value of the reference individual, for the resulting linear model, the coefficients were back-transformed to the original scale.

### 9.9 Subclasses of IBD individuals based on required trigger extent

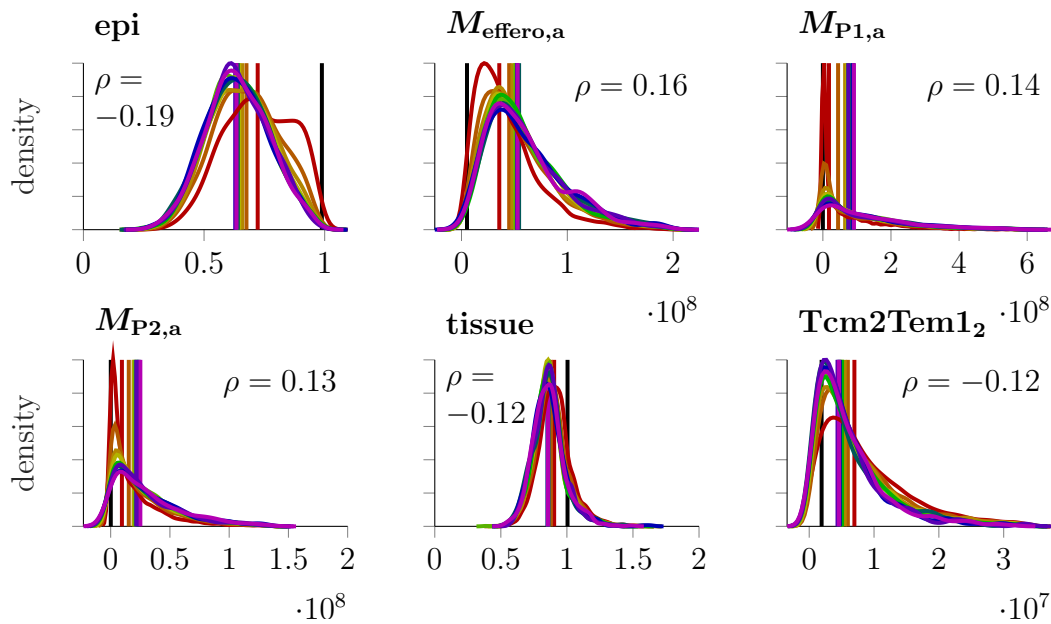


Figure 56: **Comparison of inflamed steady state distributions between IBD types.** Density function of inflamed steady-state levels per IBD type for the inflamed steady state variables with highest absolute Pearson correlation coefficient  $\rho$  to the IBD type. Type 1, 2, 3, 4, 5, 6, 7, 8, 9, 10. Vertical lines (in the respective colours) indicate medians of the distributions and the reference value, i.e. value in the healthy reference individual (black vertical line).

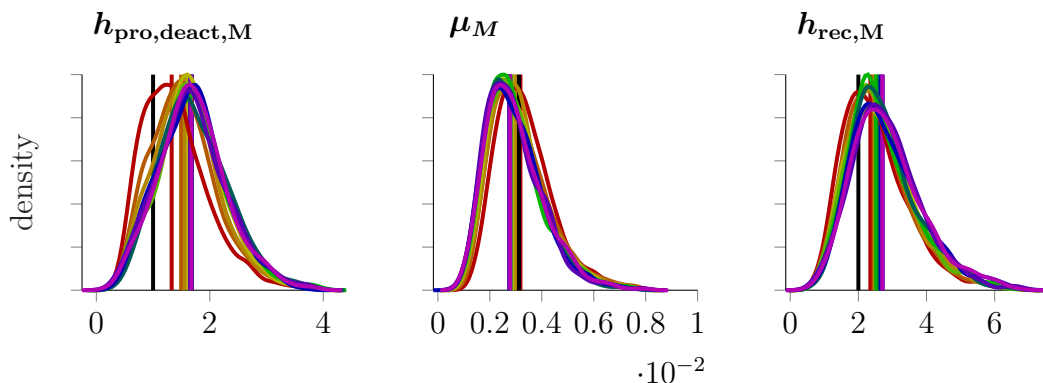


Figure 57: **Comparison of parameter distributions between IBD types.** Density function of parameter values per IBD type, for the parameters with highest absolute Pearson correlation coefficient  $\rho$  to the IBD type. Type 1, 2, 3, 4, 5, 6, 7, 8, 9, 10. Vertical lines (in the respective colours) indicate medians of the distributions and the reference value, i.e. value in the healthy reference individual (black vertical line).

## 9.10 Virtual CDEIS analog

The Crohn’s disease endoscopic index of severity (CDEIS) was described by Mary and Modigliani (1989) [177] and has been used in numerous clinical studies (e.g. [175]). It evaluates the disease state based on an endoscopic examination of different segments of the colon, giving scores to the amount and degree of ulcerations and diseased tissue. A simple one-to-one correspondence of the CDEIS is not available in the model, as the model does not simulate the appearance of tissue. In addition, the model simulates the dynamics of a generic position of the colon gut wall, and does currently not account for differences between segments. Nevertheless, we were able to determine a plausible CDEIS analog based on a combination of model outcomes; see Table 13 for details.

For the calculation of the virtual CDEIS analog, we determined close representations of the CDEIS subscores among our model outcome (i.e. post-trigger steady-state variables). Ulcerations are damages of the gut wall; the CDEIS differentiates between deep and superficial ulcerations. In our systems biology model, the gut wall is represented by the three state variables mucus, epi and tissue, where epi describes the layer of epithelial cells, tissue describes the underlying tissue of the LP, and mucus is secreted by the cells of the epithelial layer. Superficial ulcerations are translated to the model level as damage of the epithelial barrier of the gut wall; as the state variable epi describes the functional integrity of the epithelial barrier, this translates to a low value of epi. Deep ulcerations are translated to the model level as damage of the gut wall that also affects the underlying tissue; as the state variable tissue describes the functional integrity of the tissue, this translates to a low value of tissue. The cut-off values were chosen such that the majority of IBD individuals have CDEIS  $> 4$ , which is a frequently used threshold for mucosal healing, but all healthy individuals have CDEIS values close to zero and no healthy individual has CDEIS  $> 4$ . State variable values below the cut-off were linearly projected to the allowed subscore values (0-12 for deep ulcerations/ 0-6 for superficial ulcerations), with the highest subscore value for tissue = 0 or epi = 0, respectively. The CDEIS also evaluates the ulcerated surface, i.e. the fraction of the gut surface that is affected by ulcerations. For that, we combined the subscores of deep and superficial ulcerations to represent the relative occurrence of ulcerations of both types. In addition, the score

evaluates the surface involved by disease, i.e. the fraction of the gut wall that is visibly (by endoscopy) inflamed. As this status of visible inflammation is expected to represent the level of inflammation in the LP, to represent this subscore we used a cell type of acute inflammation: neutrophils. For this, we scaled the neutrophil concentration to the subscore between 0 and 10 using an Emax model, with a maximal subscore of 10 according to the CDEIS and Km set to  $4.74 \cdot 10^7$ , giving reasonable subscores between 0 and 10 for both healthy individuals and IBD patients. The CDEIS gives extra 3 points in the cases of non-ulcerated or ulcerated stenosis. Stenosis, a constriction of the gut, is caused by fibrosis, i.e. too much proliferation of the tissue. This is in the model represented by values of tissue  $> 1$ . Therefore, we defined non-ulcerated stenosis as tissue  $> 1.1$  (assuming a small margin of fibrosis not directly leading to stenosis) and ulcerated stenosis by a combination of stenosis and a considerable level of ulceration.

Table 13: **CDEIS calculation.** Column “endoscopy” describes the scoring based on endoscopy, introduced by Mary and Modigliani (1989) [177], which is frequently used in clinical studies. Column “translation” describes our proposed calculation of the CDEIS based on the model’s state variables.

	endoscopy	translation
deep ulcerations	0 or 12	0, if tissue $> 0.90$ ; 12, if tissue $< 0.61$ ; linear in between
superficial ulcerations	0 or 6	0, if epi $> 0.80$ ; 6, if epi $< 0.37$ ; linear in between
surface involved by disease	0 to 10	$\frac{10 \cdot \text{Neut}^2}{\text{Km}^2 + \text{Neut}^2}$
ulcerated surface	0 to 10	$10 \cdot (1 - (1 - \frac{\text{deep}}{12})(1 - \frac{\text{superficial}}{6}))$
non-ulcerated stenosis	+3	+3, if tissue $> 1.1$
ulcerated stenosis	+3	+3, if non-ulcerated stenosis AND ulcerated surface $> 0.5$